



Universität Hamburg
DER FORSCHUNG | DER LEHRE | DER BILDUNG



**Functional Investigation of Unknown
Malaria Proteins in the Human Malaria
Parasite *Plasmodium falciparum***

**Dissertation with the aim of achieving a doctoral degree at the
Faculty of Mathematics, Informatics and Natural Sciences**

**Department of Biology
University Hamburg**

**submitted by
Marius Florian Schmitt**

Hamburg, 2020

Dissertationsgutachter: Dr. Tobias Spielmann

Prof. Dr. Tim Gilberger

Datum der Disputation: 24.04.2020

Eidesstattliche Versicherung

Hiermit erkläre ich an Eides statt, dass ich die vorliegende Dissertationsschrift selbst verfasst und keine anderen als die angegebenen Quellen und Hilfsmittel benutzt habe.

Hamburg, den

Marius Florian Schmitt

Language certificate

I am a native speaker, have read the present PhD thesis and hereby confirm that it complies with the rules of the English language.

A handwritten signature in blue ink, appearing to be 'PH', with a long horizontal flourish extending to the right.

Paul Hughes, Darmstadt, February 26th, 2020

Summary

The most severe form of malaria in humans is caused by the *Plasmodium falciparum* parasite that is transmitted during a blood meal of female *Anopheles* mosquitoes. The clinical symptoms of malaria are caused exclusively by the asexual replication cycle of the parasite inside erythrocytes. Within the erythrocyte, *P. falciparum* parasites ingest cytosol from the host cell as a source of amino acids and to provide space for growth. This very specialized form of endocytosis is called host cell cytosol uptake (HCCU). *P. falciparum* blood stages multiply their genome by closed mitosis before cell division leads to the generation of up to 32 daughter cells in a process termed schizogony.

The *P. falciparum* genome comprises approximately 5700 genes, with more than 2600 being annotated as ‘genes with unknown function’. Most of the unknown genes are highly adapted to the specialized life cycle of *P. falciparum* parasites and show little or no homology outside the Apicomplexa. To gain a deeper understanding of the parasite’s biology, the evaluation of parasite-specific essential genes and a subsequent functional analysis is of high interest. The processes these genes are involved in also hold a potential for therapeutic intervention, as they are specific for parasite biology, and their inhibition is not likely to harm the human host.

So far, the functional analysis of essential genes has been hampered by the lack of robust genetic modification systems. The recently published selection linked integration (SLI) method overcomes this problem. SLI allows a rapid selection of parasites with a particular genomic integration. It also enables the evaluation of gene essentiality and the subsequent functional analysis of the expressed proteins, using a conditional inactivation system known as knock sideways.

As a proof of principle for the knock sideways system intended for the candidates in this thesis, the *P. falciparum* GTPase Rab5b was selected for an in depth functional analysis. In other organisms, such as humans or yeast, Rab5b plays a function in early endocytosis together with the protein VPS45. The present study shows that conditional inactivation of *PfRab5b* leads to an endocytosis phenotype similar to the phenotype after conditional inactivation of *PfVPS45*, which was the first protein identified to be involved in host cell cytosol uptake in malaria parasites. This study presents experimental evidence that *PfRab5b* is directly involved in host cell cytosol uptake and suggests that endolysosomal transport in the parasites shows similarities to those of model systems in eukaryotes.

The present thesis also conducted a medium throughput screen of unknown *P. falciparum* genes using the SLI-method. To reduce the number of genes to a manageable size, this study focussed on the genes on chromosome 3. In order to identify the most promising candidates for functional analysis, genes were subjected to various selection steps to focus on candidates that were parasite-specific, expressed in blood stage parasites and amenable to the conditional inactivation technique intended to be used. This resulted in a list of 33 candidates that were endogenously tagged. The corresponding gene products were localized and a subset functionally analysed.

The present thesis provides the localization of 15 novel proteins, comprising proteins localized in the nucleus (1), in foci in the cytoplasm (5), in the parasite cytosol (3), foci in close proximity to the nuclei (3), one that might be located at the inner membrane complex and two that had an unclear localisation due too low GFP signals. Additionally, an evaluation of gene and protein essentiality at genomic and protein level was performed for 21 genes and 8 proteins.

A detailed functional analysis was conducted for the unknown protein candidate M7. The GFP tagged M7 was located in one or two foci close to the outer part of the nucleus, and the foci multiplied with the number of nuclei. Subsequent conditional inactivation of M7 by knock sideways showed a growth defect and impairment of the nuclear division process. To understand how M7 is positioned in relation to the parasite nucleus, confocal time lapse imaging was performed, indicating a role of M7 in the nuclear division process.

M7 showed remote homology to Ska2, a protein of the so-called Ska complex which is essential during mitosis in eukaryotes. During mitosis in *Plasmodium* parasites, the GFP tagged M7 showed a similar localisation pattern to the mitotic markers Centrin3 and α -tubulin. A co-localization of GFP tagged M7 with these markers detected α -tubulin in foci at the outer part of the nucleus, partially overlapping with foci of the GFP tagged M7 (facing the parasite plasma membrane) and the foci of mCherry tagged Centrin3.

To determine potential interaction partners of M7, the newly-established dimerization induced quantitative biotin identification (DIQ-BioID) was used. DIQ-BioID showed interaction partners which, based on homology to proteins in other organisms, might be involved in mitosis. These interaction partners included a protein with remote homology to Ska3, suggesting that this was the so far not annotated PfSka3. Taken together, these results indicate that M7 might be the *P. falciparum* orthologue of Ska2 and that the M7 protein plays an

essential role during the nuclear division in the parasite similar to the human Ska complex and the functional Ska complex equivalent (Dam/DASH complex) in yeast.

Overall, the results of this thesis provide new insights for a better understanding of the parasite's DNA replication and endocytosis and reveals targets for further investigation that might turn out to be helpful for drug development.

Zusammenfassung

Die schwerste Form der Malaria beim Menschen wird durch den Parasiten *Plasmodium falciparum* verursacht, der bei einer Blutmahlzeit der weiblichen Anopheles-Mücke übertragen wird. Die klinischen Symptome der Malaria werden ausschließlich durch den ungeschlechtlichen Replikationszyklus des Parasiten in den Erythrozyten verursacht. Innerhalb der Erythrozyten nehmen die *P. falciparum*-Parasiten Zytosol aus der Wirtszelle auf, um Aminosäuren zu gewinnen und Platz für ihr Wachstum zu schaffen. Diese sehr spezielle Form der Endozytose wird als Wirtszellen-Zytosolaufnahme (HCCU) bezeichnet. Die Blutstadien von *P. falciparum* vervielfältigen ihr Genom durch geschlossene Mitose, bevor die Zellteilung zur Bildung von bis zu 32 Tochterzellen in einem als Schizogonie bezeichneten Prozess führt.

Das Genom von *P. falciparum* umfasst etwa 5700 Gene, von denen mehr als 2600 als "Gene mit unbekannter Funktion" annotiert sind. Die meisten der unbekanntenen Gene sind stark an den spezialisierten Lebenszyklus von *P. falciparum*-Parasiten angepasst und zeigen wenig oder keine Homologie außerhalb der Apicomplexa. Um ein tieferes Verständnis der Biologie des Parasiten zu erhalten, sind die Auswertung parasitenspezifischer essentieller Gene und eine anschließende Funktionsanalyse von hohem Interesse. Die Prozesse, an denen diese Gene beteiligt sind, bergen das Potenzial für therapeutische Eingriffe, da sie spezifisch auf die Biologie des Parasiten ausgerichtet sind und ihre Hemmung den menschlichen Wirt wahrscheinlich nicht schädigt.

Bisher wurde die Funktionsanalyse wesentlicher Gene durch das Fehlen robuster genetischer Modifikationssysteme erschwert. Die kürzlich veröffentlichte Methode der selection linked integration (SLI) überwindet dieses Problem. SLI ermöglicht eine schnelle Selektion von Parasiten mit einer bestimmten genomischen Integration. Sie erlaubt auch die Bewertung der Gen-Essentialität und die anschließende funktionelle Analyse der exprimierten Proteine mit Hilfe eines konditionalen Inaktivierungssystems, das als Knock-Sideways bekannt ist.

Als "Proof of Principle" für das Knock-Sideways-System, das für die Kandidaten in dieser Arbeit vorgesehen ist, wurde die *P. falciparum* GTPase Rab5b für eine eingehende Funktionsanalyse ausgewählt. In anderen Organismen, wie dem Menschen oder Hefen, spielt Rab5b zusammen mit dem Protein VPS45 eine Funktion in der frühen Endozytose. Die vorliegende Studie zeigt, dass die bedingte Inaktivierung von *PfRab5b* zu einem Endozytose-Phänotyp führt, der dem Phänotyp nach der bedingten Inaktivierung von *PfVPS45* ähnlich ist. Dieses Protein war das erste Protein, das bei Malariaparasiten an der Zytosolaufnahme der Wirtszelle beteiligt ist. Die vorliegende Arbeit legt experimentelle Beweise dafür vor, dass auch *PfRab5b* direkt an der Zytosolaufnahme der Wirtszelle beteiligt ist, und legt nahe, dass der endolysosomale Transport in den Parasiten Ähnlichkeiten mit denen von Modellsystemen in Eukaryoten aufweist.

In der vorliegenden Arbeit wurde zusätzlich ein Medium-Durchsatz-Screening unbekannter *P. falciparum*-Gene mit der SLI-Methode durchgeführt. Dabei lag der Fokus auf den Genen von Chromosom 3, um die Anzahl der Gene auf eine überschaubare Größe zu reduzieren. Die Gene wurden verschiedenen Selektionsschritten unterzogen, um sich auf die für die funktionelle Analyse vielversprechendsten Kandidaten zu konzentrieren. Dazu gehörten jene, die parasitenspezifisch sind, in Parasiten im Blutstadium exprimiert werden und die für die vorgesehene Technik der konditionalen Inaktivierung geeignet sind. Dies führte zu einer Liste von 33 Kandidaten, die endogen markiert wurden. Die entsprechenden Genprodukte wurden lokalisiert und eine Teilmenge funktionell analysiert.

Die vorliegende Arbeit liefert die Lokalisierung 15 neuartiger Proteine, bestehend aus Proteinen, die im Zellkern (1), in Fokussen im Zytoplasma (5), im Zytosol des Parasiten (3) und in Fokussen in unmittelbarer Nähe der Zellkerne (3) lokalisiert sind. Ein Protein wies eine mögliche Lokalisierung am inneren Membrankomplex auf und zwei Proteine eine unklare Lokalisierung aufgrund eines zu niedrigen GFP-Signals. Zusätzlich wurde für 21 Gene und 8 Proteine eine Bewertung der Gen- und Proteinessentialität auf Genom- und Proteinebene durchgeführt.

Für den unbekanntem Proteinkandidaten M7 wurde eine detaillierte Funktionsanalyse durchgeführt. Das GFP-gekennzeichnete M7 befand sich in einem oder zwei Fokussen nahe dem äußeren Teil des Zellkerns. Diese Fokusse multiplizierten sich mit der Anzahl der Kerne. Die anschließende konditionale Inaktivierung von M7 durch Knock Sideways zeigte einen Wachstumsdefekt und eine Beeinträchtigung des Kernteilungsprozesses. Um zu verstehen,

wie M7 im Verhältnis zum Zellkern des Parasiten positioniert ist, wurde eine konfokale Zeitrafferaufnahme durchgeführt, die auf eine Rolle von M7 im Kernteilungsprozess hinweist. Darüber hinaus zeigte M7 eine entfernte Homologie zu Ska2, einem Protein des sogenannten Ska-Komplexes, das während der Mitose in Eukaryonten essentiell ist. Während der Mitose in *Plasmodium*-Parasiten zeigte das mit M7 markierte GFP ein ähnliches Lokalisierungsmuster wie die mitotischen Marker Centrin3 und α -Tubulin. Eine Co-Lokalisierung von GFP-gekennzeichnetem M7 mit diesen Markern zeigte α -Tubulin in Fokussen am äußeren Teil des Zellkerns, die sich teilweise mit den Fokussen des GFP-gekennzeichneten M7 (Richtung Plasmamembran des Parasiten) und den Fokussen des mCherry-gekennzeichneten Centrin3 überlappten. Zur Bestimmung potenzieller Interaktionspartner von M7 wurde die neu etablierte dimerisierungs-induzierte quantitative Biotin-Identifikation (DIQ-BioID) verwendet. Die DIQ-BioID zeigte Interaktionspartner, die aufgrund ihrer Homologie zu Proteinen in anderen Organismen an der Mitose beteiligt sein könnten. Zu diesen Interaktionspartnern gehörte ein Protein mit entfernter Homologie zu Ska3, was darauf hindeutet, dass es sich um das bisher nicht annotierte *PfSka3* handelt.

Zusammenfassend deuten die Ergebnisse darauf hin, dass M7 das *P. falciparum*-Ortholog von Ska2 darstellt und das M7 Protein eine wesentliche Rolle in der Kernteilung des Parasiten spielt, ähnlich wie der menschliche Ska-Komplex und das funktionelle Ska-Komplex-Äquivalent (Dam/DASH-Komplex) in Hefen.

Insgesamt liefern die Ergebnisse dieser Arbeit neue Erkenntnisse für ein besseres Verständnis der DNA-Replikation und Endozytose des Parasiten und zeigen Ziele für weitere Untersuchungen auf, die sich als hilfreich für die Entwicklung von Medikamenten erweisen könnten.

Table of contents

Eidesstattliche Versicherung	i
Language certificate	ii
Summary	I
Zusammenfassung	III
Table of contents	VI
List of figures	XII
List of tables	XIV
Abbreviations	XV
1 Introduction.....	1
1.1 Malaria “King of Diseases”	1
1.1.1 Epidemiology and distribution	2
1.1.2 Clinical manifestation	4
1.1.3 Control strategies and roll back malaria.....	5
1.1.4 Malaria treatment	6
1.1.5 Vaccine development	8
1.2 <i>Plasmodium</i> parasite’s biology.....	10
1.2.1 Life cycle of <i>P. falciparum</i> parasites.....	10
1.2.2 Hepatic cycle	11
1.2.3 Erythrocytic cycle.....	11
1.3 Parasite cell biology with emphasis on parasite specific aspects	14
1.3.1 Cell cycle and checkpoints	15
1.3.2 <i>P. falciparum</i> parasite’s organelles	17
1.3.3 Host cell modifications and protein export	20

1.3.4	The canonical secretory pathway	20
1.3.5	Exported proteins	21
1.3.6	Endocytosis	21
1.3.7	Host cell cytosol uptake	22
1.3.8	The lysosomal pathway	23
1.4	Methods for gene modifications	23
1.4.1	Homologous recombination	23
1.4.2	Target gene disruption.....	24
1.4.3	Selection-linked-integration	24
1.4.4	Zinc-finger nucleases	25
1.4.5	CRISPR/Cas	26
1.4.6	Cre and FLP recombinases.....	26
1.4.7	Gene-silencing by RNA interference	26
1.4.8	Tetracycline-controlled transcriptional activation	27
1.4.9	Degradation of mRNA by ribozymes.....	27
1.4.10	Aptamers and the TetR-DOZI system.....	27
1.4.11	Protein destabilization by destabilization domains	28
1.4.12	Knock sideways.....	28
1.5	<i>Plasmodium</i> ‘unknown proteins’ and their potential.....	29
1.5.1	Genome wide screens.....	30
1.5.2	Protein interactome studies	31
1.5.3	Protein evolution	32
1.6	Aims of the thesis	33
2	Materials	34
2.1	Technical devices.....	34
2.2	Chemicals	35
2.3	Labware and disposables	37
2.4	Kits.....	38

2.5	Solutions, buffers and media	38
2.5.1	Media and buffers for microbiologic culture	38
2.5.2	Solutions and buffers for cell biological experiments.....	39
2.5.3	Solutions and buffers for molecular biological experiment	42
2.6	DNA- and protein ladders.....	43
2.7	Polymerases and enzymes	43
2.8	Antibodies.....	43
2.9	Fluorescence dyes.....	43
2.10	Plasmids.....	44
2.11	Oligonucleotides	44
2.12	Bacterial and <i>Plasmodium</i> parasite strains	44
2.13	Software and bioinformatic tools.....	44
3	Methods.....	46
3.1	Molecular biology methods	46
3.1.1	Polymerase chain reaction (PCR).....	46
3.1.2	Purification of PCR-product and digested vectors.....	47
3.1.3	Restriction digest of DNA, PCR and vector products.....	47
3.1.4	Ligation of DNA	48
3.1.5	Plasmid isolation	48
3.1.6	DNA precipitation	49
3.1.7	External cloning by Life Technologies	49
3.1.8	Sequencing of plasmid DNA.....	49
3.1.9	Agarose gel electrophoresis.....	49
3.1.10	Genomic DNA isolation.....	50
3.2	Microbiological methods.....	50
3.2.1	Preparation of chemically competent <i>E. coli</i> cells	50
3.2.2	Transformation of plasmid DNA in chemically competent <i>E. coli</i> cells	50
3.3	Cell biological methods	51

3.3.1	Continuous culture of <i>P. falciparum</i> (Trager et al., 1976).....	51
3.3.2	Blood smears and Giemsa staining	51
3.3.3	Preparation of <i>P. falciparum</i> parasites cryo-stabilates and thawing procedure .	52
3.3.4	Sorbitol synchronization of <i>P. falciparum</i> parasites	52
3.3.5	Purification of <i>P. falciparum</i> infected erythrocytes with a Percoll gradient.....	52
3.3.6	Saponin lysis	53
3.3.7	<i>P. falciparum</i> transfection by electroporation.....	53
3.3.8	Selection for transgenic <i>P. falciparum</i> cell lines.....	54
3.3.9	Knock sideways induction	55
3.3.10	DiQ-BioID of <i>P. falciparum</i> proteins	55
3.3.11	Growth assay by flow cytometry (Boersema et al., 2009).	56
3.3.12	Parasite stage assay by microscopy.....	56
3.3.13	E64 bloated food vacuole assay	56
3.3.14	Vesicle accumulation assay.....	57
3.4	Microscopy	57
3.4.1	Live cell and fluorescence microscopy	57
4	Results.....	59
4.1	Selection of <i>P. falciparum</i> genes with unknown function.....	59
4.1.1	<i>PfRab5b</i> as proof of principle	60
4.1.2	Functional investigation of <i>P. falciparum</i> genes with unknown function	70
4.2	Candidate M1 (PF3D7_0303100)	73
4.3	Candidate M2 (PF3D7_0304300)	75
4.4	Candidate M3 (PF3D7_0305200)	75
4.5	Candidate M4 (PF3D7_0305400)	78
4.6	Candidate M5 (PF3D7_0305500)	78
4.7	Candidate M6 (PF3D7_0306100)	79
4.8	Candidate M7 (PF3D7_0307500)	81
4.9	Candidate M8 (PF3D7_0307600)	92

4.10	Candidate M9 (PF3D7_0307700)	94
4.11	Candidate M10 (PF3D7_0307900)	94
4.12	Candidate M11 (PF3D7_0308100)	96
4.13	Candidate M12 (PF3D7_0308300)	98
4.14	Candidate M13 (PF3D7_0308700)	99
4.15	Candidate M14 (PF3D7_0308800)	101
4.16	Candidate M15 (PF3D7_0309900)	101
4.17	Candidate M16 (PF3D7_0310900)	101
4.18	Candidate M17 (PF3D7_0312900)	106
4.19	Candidate M18 (PF3D7_0313000)	107
4.20	Candidate M19 (PF3D7_0313200)	109
4.21	Candidate M20 (PF3D7_0313400)	111
4.22	Candidate M24 (PF3D7_0314700)	112
5	Discussion	116
5.1	Role of Rab5b in host cell cytosol uptake	116
5.2	Functional investigation of <i>P. falciparum</i> proteins with unknown function.....	120
5.2.1	Selection of the unknown candidates	120
5.2.2	Localization of the candidates.....	122
5.2.3	Candidate essentiality prediction on the gene level	124
5.2.4	Candidate's essentiality prediction on protein level.....	125
5.3	Functional investigation of candidate M7	126
5.4	Functional investigation of candidate M16	130
5.5	Origin of the unknown genes.....	130
5.6	Conclusion	132
6	References.....	134
	Publications	160
	Danksagung	161
	Appendix	A
		X

Appendix 1	A
Appendix 2	B
Appendix 3	C
Appendix 4	D
Appendix 5	E
Appendix 6	H
Appendix 7	K
Appendix 8	O

List of figures

Figure 1: Malaria endemic regions.....	3
Figure 2: <i>P. falciparum</i> parasite's life cycle.	11
Figure 3: Schematic comparison of traditional views of mitosis with mitosis in blood stage <i>Plasmodium</i> parasites.....	17
Figure 4: <i>P. falciparum</i> infected red blood cell.	18
Figure 5: Schematic of selection linked integration strategy.	25
Figure 6: Schematic of the principle for knock sideways using the nucleus as site for mislocalisation.....	29
Figure 7: Frequency distribution of phenotypes among different organisms.	30
Figure 8: Blood smear preparation.....	51
Figure 9: Schematic of selection strategy of the unknown genes from chromosome 3.	60
Figure 10: Knock sideways and growth analysis of Rab5b	61
Figure 11: Rab5b is important for the survival of <i>P. falciparum</i> parasites.....	63
Figure 12: Rab5b vesicle accumulation assay.....	64
Figure 13: Rab5b vesicle accumulation assay (quantification).....	65
Figure 14: Rab5b does not co-localize with Kelch 13	66
Figure 15: Rab5b bloated food vacuole assay.....	67
Figure 16: Rab5b complementation cell lines.....	70
Figure 17: PCR diagnostics to confirm correct integration of the plasmid into the desired region of the genome.....	72
Figure 18: Localization of endogenously tagged candidate M1 (PF3D7_0303100).	74
Figure 19: Knock sideways and growth curve of endogenously tagged candidate M1 (PF3D7_0303100).....	75
Figure 20: Localization of endogenously tagged candidate M3 (PF3D7_0305200).	77
Figure 21: Knock sideways and growth curve of endogenously tagged candidate M3 (PF3D7_0305200).....	78
Figure 22: Localization of endogenously tagged candidate M6 (PF3D7_0306100).	80
Figure 23: Knock sideways and growth curve of endogenously tagged candidate M6 (PF3D7_0306100).....	81
Figure 24: Localization of endogenously tagged candidate M7 (PF3D7_0307500).	82
Figure 25: Knock sideways and growth curve of endogenously tagged candidate M7 (PF3D7_0307500).....	83

Figure 26: Candidate M7 (PF3D7_0307500) confocal time lapse imaging.	84
Figure 27: M7 (PF3D7_0307500) co-localization with Centrin3.....	85
Figure 28: Candidate M7 (PF3D7_0307500) knock sideways and co-localization with tubulin.	88
Figure 29: Dimerization of candidate M7 (PF3D7_0307500) with biotin ligase BirA*.	89
Figure 30: Scatterplots of DIQ-BioID with candidate M7 (PF3D7_0307500).....	90
Figure 31: Localization of endogenously tagged candidate M8 (PF3D7_0307600).	93
Figure 32: Knock sideways and growth curve of endogenously tagged candidate M8 (PF3D7_0307600).....	94
Figure 33: Localization of endogenously tagged candidate M10 (PF3D7_0307900).	96
Figure 34: Localization of endogenously tagged candidate M11 (PF3D7_0308100).	97
Figure 35: Localization of endogenously tagged candidate M12 (PF3D7_0308300).	99
Figure 36: Localization of endogenously tagged candidate M13 (PF3D7_0308700).	100
Figure 37: Localization of endogenously tagged candidate M16 (PF3D7_0310900).	103
Figure 38: Knock sideways and growth curve of endogenously tagged candidate M16 (PF3D7_0310900).....	104
Figure 39: Candidate M16 (PF3D7_0310900) knock sideways and co-localization with tubulin.....	106
Figure 40: Localization of endogenously tagged candidate M17 (PF3D7_0310900).	107
Figure 41: Localization of endogenously tagged candidate M18 (PF3D7_0313000).	108
Figure 42: Knock sideways and growth curve of endogenously tagged candidate M18 (PF3D7_0313000).....	109
Figure 43: Localization of endogenously tagged candidate M19 (PF3D7_0313200).	111
Figure 44: Localization of endogenously tagged candidate M20 (PF3D7_0313400).	112
Figure 45: Localization of endogenously tagged candidate M24 (PF3D7_0314700).	114
Figure 46: Knock sideways and growth curve of endogenously tagged candidate M24 (PF3D7_0314700).....	115
Figure 47: Model of Rab5b during host cell cytosol uptake.....	120
Figure 48: Model of the localization of M7 based on the results of this thesis.....	130

List of tables

Table 1: PCR mix for FirePol DNA polymerase (10 µl batch).....	46
Table 2: PCR conditions for analytical purpose.....	46
Table 3: Phusion PCR mix (50 µl batch)	47
Table 4: PCR conditions for preparative purpose	47
Table 5: T4 DNA ligation mix	48
Table 6: Gibson mix.....	48
Table 7: Candidates list for functional analysis.	70
Table 8: Top hits of M7 DIQ-BioID.	91
Table 9: Overview of analyzed candidates with localization, knock sideways and SLI-TGD	123

Abbreviations

2D	Two-dimensional
3D	Three-dimensional
ACT	Artemisinin-based combination therapies
AMA	Apical membrane antigen
ARTs	Artemisinins
BioID	Biotin identification
BSD	Blasticidin S deaminase
CRISPR	Clustered regularly interspaced short palindromic repeat
crt	Chloroquine resistance transporter
CSP	Circumsporozoite protein
C-terminal	Carboxy-terminal
DAPI	4'6-Diamino-2-phenylindol
DD	Destabilization domain
DDT	Dichloro-diphenyl-trichloroethane
DHFR	Dihydrofolat reductase
DIC	Differential interference contrast
DIQ-BioID	Dimerization induced quantitative BioID
DNA	Desoxyribonucleic acid
DSB	Double-stranded breaks
DSM1	BEI resources
EBA	Erythrocyte binding antigen
eDD	<i>E. coli</i> DHFR-DD
ER	Endoplasmic reticulum
FKBP	FK506 binding protein
FRB	FKBP rapamycin binding domain
FV	Food vacuole
GDP	Guanine diphosphate
GFP	Green fluorescence protein
GTP	Guanine triphosphate
HCCU	Host cell cytosol uptake
hDHFR	Human dihydrofolat reductase
hpi	Hours post infection

IMC	Inner membrane complex
iRBCs	Infected red blood cells
ITNs	Insecticide treated mosquito nets
KS	Knock sideways
mRNA	Messenger ribonucleic acids
MSPs	Merozoite surface proteins
neo	Neomycin phosphotransferase II
NLS	Nuclear localization signal
NPP	new permeation pathways
N-terminal	Amino-terminal
PEXEL	<i>Plasmodium</i> export element
PI3P	Phosphatidylinositol 3-phosphate
PNEPs	PEXEL negative exported proteins
PPM	Parasite plasma membrane
PTEX	<i>Plasmodium</i> translocon of exported protein
PV	Parasitophorous vacuole
PVM	Parasitophorous vacuole membrane
Rab	Ras related protein in brain
RBCs	red blood cells
siRNA	Small interfering RNA
SLI	Selection linked integration
TetO	Tetracycline operators
TetR	Tetracycline repressor protein
TGD	Targeted gene disruption
UTR	Untranslated region
vpp	Vesicles per parasite
VPS	Vacuolar protein sorting
WHO	World Health Organization
WSV	Whole Sporozoite Vaccine
yDHODH	Yeast dihydroorodotat dehydrogenase
ZFN	Zinc-finger nuclease

1 Introduction

1.1 Malaria “King of Diseases”

The first records of malaria infections, referring to the typical symptoms and the tendency to epidemic occurrence, were registered 2700 BC by the ancient Chinese Canon of Medicine. Thenceforth the disease was also noted in many other civilizations like Arabic, Assyrian, Babylonian, Chinese, Egyptian, Indian, Greek and Roman (Carter et al., 2002; Cox, 2002; Neghina et al., 2010; Retief et al., 2006). During the Vedic period (1500-800 BC), people suffered from the “king of diseases”, which was characterized by fever and enlargement of the spleen (Sherman, 1998). The first valuable information linking the malaria disease to the bite of an mosquito, appeared between 500 to 221 BC (Sallares, 2009). Also, the Greeks had known Malaria since about 500 BC. The first physician, who described the malarial paroxysm including most of the symptoms like chills, exacerbation, fever, and sweats, was also a Greek, Hippocrates (460-377 BC). He was able to differentiate the different clinical types of malaria, due to the periodicity of the fevers (Cunha et al., 2008; Sherman, 1998). In the 5th century AD, the Romans also suffered from the great epidemic fever in Rome (Sallares, 2009). In the year 1440 AD, the first attested mention of the word “mal’aria” was found, which means “bad, evil, or corrupted air”. In the 16th century, the disease was noted as far as northern Europe (Britain, Denmark and Sweden) (Dobson, 1980; Dobson, 1994; Hulden et al., 2005). After the importation of slaves from Africa in the 16th and 17th century, malaria became also endemic in North America (Russell, 1968). Finland was reached in the 17th century, followed by France and Germany during the 19th century (Davidson, 1899; Hulden et al., 2005; Sérandour et al., 2007). Over the time, the disease had many different names, like Roman fever, intermittent fever, periodical fever, autumnal fever, marsh fever, mal’aria etc. (Cunha et al., 2008; Guillemin, 2001; Nicholls, 2012; Schlagenhauf, 2004). The final word malaria was then mention in the book “Storia delle febbri intermittenti di Roma” by Francesco Puccinotti in 1838 (Guillemin, 2001; Sallares, 2009; Snowden, 2006).

In the 19th century, Alphonse Laveran (1845-1922) discovered a single-cell parasite as the causative agent for malaria (Laveran, 1881). Later on, it was demonstrated that the parasites were transmitted by mosquitoes of the genus *Anopheles* (Ross, 2002). Today, more than 200 *Plasmodium* species are known which are transmitted by the female *Anopheles* mosquito.

Plasmodium parasites are classified to the phylum Apicomplexa, and five *Plasmodium* species are known to be pathogenic for humans: *P. knowlesi*, *P. ovale*, *P. malariae*, *P. vivax* and the most virulent *P. falciparum*. In the past, but still today, malaria has influenced the demographic and socioeconomic evolution and also shortened the life expectancy of many people. Despite major research efforts, malaria is still one of the leading causes of infectious disease related deaths worldwide (Figure 1) (World-Health-Organisation, 2017).

1.1.1 Epidemiology and distribution

Malaria transmission occurs in warm and humid climate zones, which are found mainly in the tropical and subtropical regions (Figure 1). The ambient temperature in malaria occurring areas has a strong impact on transmission. Ambient temperatures below 18°C increase the time required for development in the vector, which results in a restriction of transmission tropical and subtropical regions (Figure 1) (Sachs et al., 2002; Snow et al., 2005).

1.1.1.1 Malaria cases case report

In 2017, about 3.2 billion people were at the risk of being infected with malaria (Figure 1). This resulted in an estimated 219 million cases and 435.000 deaths. Most of the cases were reported in African regions (92 %), followed by South East Asia (5 %) and the Eastern Mediterranean region (2 %) (Figure 1). Particularly at risk are children under the age of five. Although in 2017 an estimated 20 million fewer malaria cases occurred than in 2010, data from 2015-2017 show that there has been no further significant progress in reducing global malaria cases during this time period (Figure 1) (World-Health-Organisation, 2017).

1.1.1.2 Human malaria

The most virulent form of malaria is caused by *P. falciparum* parasites. *P. falciparum* parasites are responsible for the majority of deaths (99 %), although *P. vivax* parasites show a wider geographical distribution (Mendis et al., 2001). Most of the *P. falciparum* malaria cases appear in the African region, but it is also endemic in South East Asia and South America. The predominant *Plasmodium* species in South East Asia is *P. vivax*, which is also endemic in all tropical regions. Most of the African people show a mutation in the Duffy receptor (Duffy negative) which potentially limits *P. vivax* parasite transmission to Duffy positive populations (Miller et al., 1976; Miller et al., 1975). However, there is evidence that also *P. vivax* cases occur across all parts of the African continent. The wide geographical distribution of this

malaria species is due to the ability to develop at comparably low temperatures in the *Anopheles* mosquito and the capacity to persist as dormant forms in the liver of patients which permits to remain during climatic conditions preventing mosquito transmission. The ability to form dormant liver stages (hypnozoites), *P. vivax* parasites share only with *P. ovale* parasites and can cause a relapse after months or years (Greenwood et al., 2008; White, 2011; World-Health-Organisation, 2017). In comparison to *P. falciparum* malaria, *P. vivax* malaria is less deadly but also causes serious symptoms and, in some cases, severe disease (Hay et al., 2010; Sinka et al., 2011; Sinka et al., 2010).

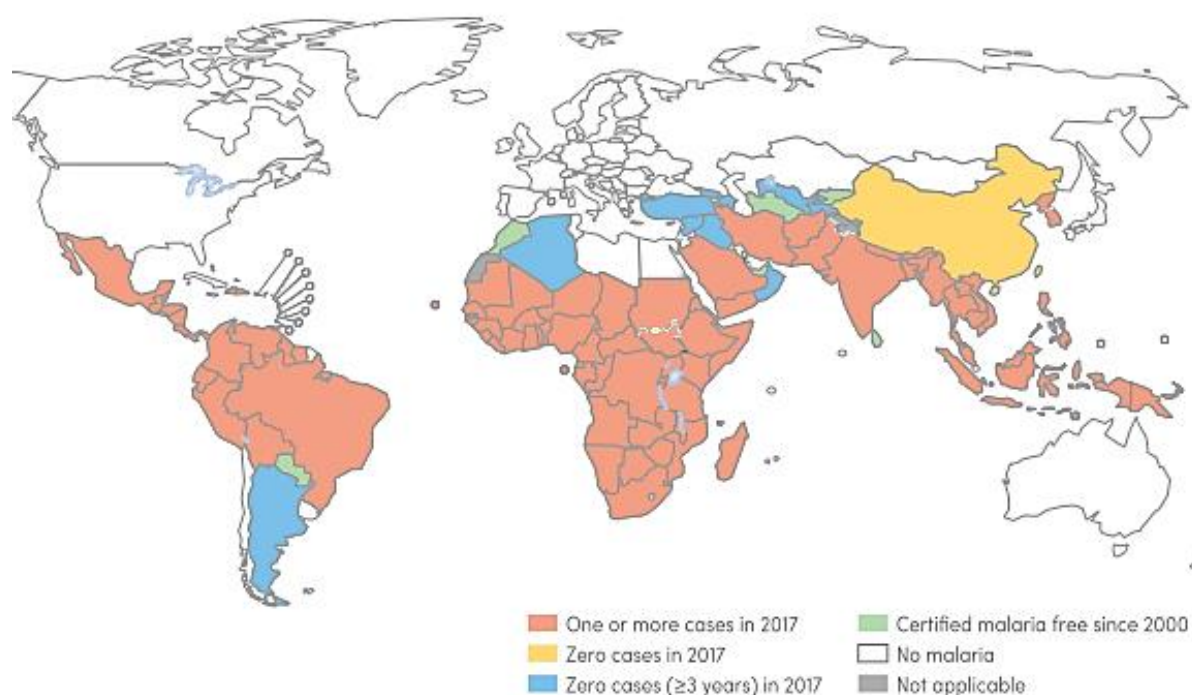


Figure 1: Malaria endemic regions.

Map of malaria endemic regions showing countries with one or more cases in 2017 (red) and zero cases in 2017 (yellow). Countries with zero cases for more than or within the three years before 2017 are shown in blue. Countries which have been certified as malaria free since 2000 are shown in green. Countries with no malaria are shown in white; grey countries are not applicable. Modified from (World-Health-Organisation, 2018c).

P. malariae parasites and *P. falciparum* parasites are usually endemic in the same regions. *P. ovale* cases were reported in Asia and in the Western Pacific, but *P. ovale* infections are mainly prevalent in sub-Saharan Africa (Collins et al., 2005). There were some reports in South East Asia of human *P. knowlesi* infections (Cooper et al., 2019; Pongvongsa et al., 2018; Zaw et al., 2019). *P. knowlesi* is the only known *Plasmodium* species postulated to be zoonotic. The natural hosts of *P. knowlesi* parasites are macaques, but transmission from macaques to humans is also possible (Knowles et al., 1932). To date it is not clear, whether

there has been human to human transmission with *P. knowlesi* parasites or the cases have been falsely identified (Kantele et al., 2011; Singh et al., 2013; Singh et al., 2004).

1.1.1.3 Malaria transmitting vectors

The *Plasmodium* parasite cannot sexually replicate without its transmitting vector, a female *Anopheles* mosquito, which is a key factor for malaria distribution. Globally, 400 *Anopheles* species are known, and 41 of these are capable of transmitting malaria. In African regions, the dominant vector species are *A. gambiae* and *A. arabiensis*, but there are also some other vectors from the *Anopheles* genus, which in some parts of Africa can even have a greater impact on malaria transmission than *A. gambiae* and *A. arabiensis* (Coetzee et al., 2004; Gillies et al., 1987; Gillies et al., 1968; Sinka et al., 2010). Compared to Africa, the Asia-Pacific region is much more diverse in its diversity of transmitting vectors. Nineteen malaria transmitting *Anopheles* species have been reported from that region (Hay et al., 2010; Sinka et al., 2011; Sinka et al., 2010).

1.1.2 Clinical manifestation

The primary symptoms are versatile and appear as vomiting, diarrhoea, chills, headaches, dizziness, abdominal pain and dry cough (Barcus et al., 2007; Trampuz et al., 2003). Those symptoms are difficult to distinguish from other parasitic, bacteria or virus caused diseases and can lead to an incorrect diagnosis (Bartoloni et al., 2012; Trampuz et al., 2003). The incubation periods vary between the different *Plasmodium* species and range from nine to 40 days (Bartoloni et al., 2012), excluding dormant stages. In addition to the incubation period, periodic fever is also specific to the species. *P. vivax*, *P. ovale*, *P. malariae* and *P. knowlesi* cause periodic fever with mostly uncomplicated symptoms, whereas *P. falciparum* causes irregular fevers, which usually occurs daily with severe disease progression. The clinical symptoms and the specific intermitted fevers are mainly caused by schizont rupture and destruction (or lysis) of the infected erythrocytes. The clinical symptoms of *P. vivax* and *P. ovale* occur in a synchronous manner every 48 hours, resulting in fever attacks every third day (tertian fever). *P. knowlesi* has a 24 hours erythrocytic cycle, which causes daily fever and symptom patterns. In a *P. malariae* infection, the fever occurs every 72 hours (quartan malaria) (Bartoloni et al., 2012; Singh et al., 2013; Sinton et al., 1932), coinciding with the three-day development cycle of this parasite.

The severity of *P. falciparum* malaria is mainly explained by the ‘sticking’ of all infected RBCs to capillaries. Therefore, infected RBCs bind to endothelial receptors, like CD36, ICAM-1, PECAM or CSA, a process known as cytoadherence (Craig et al., 2012). Adherence and blockage of the microvasculature can cause vessel collapse (Cabrales et al., 2010), pulmonary respiratory distress (Taylor et al., 2006), oedema and haemato-encephalic barrier rupture, leading to a phenomenon termed cerebral malaria (Dorovini-Zis et al., 2011; MacPherson et al., 1985). Furthermore, *P. falciparum* malaria can cause hyperparasitemia (parasitemia over 10%) prostration, anemia, renal impairment, impaired consciousness and thrombocytopenia (Craig et al., 2012).

1.1.3 Control strategies and roll back malaria

In the 1950s, a major World health organization (WHO) malaria eradication campaign started with the aim to reduce malaria transmission and the eradication of the disease. In many national malaria control programs, the insecticide dichloro-diphenyl-trichloroethane (DDT) was used for indoor residual spraying. Those programs, reduced the population at risk from approximately 77 % to approximately 50 %, between 1900 to 1975 (Enayati et al., 2010). The second tool in this campaign was the use of chloroquine for treatment and prevention. The programs for malaria eradication in the US and Europe were successful, and thus these countries became malaria free. The eradication campaign largely ignored sub-Saharan Africa; however, control interventions, using DDT before 1960, reduced malaria transmission in South Africa, Swaziland, Zimbabwe, Mauritius southern Cameroon, Liberia, the highland savanna areas in Madagascar and Uganda (Enayati et al., 2010; Kouznetsov, 1977). For these successes, the vector control with DDT was an essential component. After the end of the eradication program, malaria infections increased again overall and chloroquine-resistant parasites and DDT-resistant mosquitos were observed (Ballou et al., 1987; Hastings et al., 2000; Lines et al., 1991). Furthermore, DDT is suspected of causing cancer and was banned in Western countries in 1970 (Faroon et al., 2002; Harada et al., 2016; Harada et al., 2003). In other countries, malaria control by mosquito reduction is still conducted as before with DDT. Therefore pesticides such as Bti (Chung et al., 2001) or Pyrethroids are used for aerial spraying (van den Berg, 2009). Additionally, the use of insecticide-treated bed nets (ITNs) is one of the most powerful tools for malaria control (Binka et al., 2006). In Africa, more than half of the population at risk sleeps under an ITN. Furthermore, ITNs have shown to lower the child mortality rate significantly (Greenwood et al., 2008). In addition, malaria has been

controlled by drug combination therapies (Bloland et al., 2000; Nosten et al., 2002) and monitoring systems (Enayati et al., 2010; Nabarro, 1999).

1.1.4 Malaria treatment

Malaria is a preventable and treatable disease and does most likely not lead to death, if diagnosed early enough and treated within 24 hours after the first symptoms appeared. However, it requires the use of high-dose medications to get a rapid and full elimination of *Plasmodium* parasites. The faster the elimination, the lower is the chance for a chronic infection, a severe disease or death. Before treatment, it is very important to ensure that only confirmed malaria cases are treated with antimalarials, to avoid the potential heavy side effects of some of the treatments (World-Health-Organisation, 2018b). For malaria prevention or treatment, a comparably large number of drugs are available. These drugs are: Quinine and derivatives, such as chloroquine, halofantrine, and tafenoquine; antifolates such as pyrimethamine, chlorproguanil, and trimethoprim; artemisinin and artemisinin derivatives, the current first line treatment (in combination with either: piperazine, mefloquine, lumefantrine, amodiaquine or sulfadoxine-pyrimethamine) as well as Atovaquone, an antimalarial of its own class. Several antibacterial drugs like clindamycin and tetracycline also have antiplasmodial effects (Arrow, 2004).

1.1.4.1 Quinine

Aminoquinolines are alkaloids and were the first antimalarial drugs used. Quinine was already discovered in 1820 as an extract from the cinchona bark and is active against asexual blood stage parasites (see.1.2) (Faurant, 2011; Foley et al., 1998). Most of the 4-aminoquinoline derivatives like chloroquine target the detoxification of haemoglobin by the inhibition of the polymerization of haematin in the food vacuole (FV) (see. 1.3.2.1) Haematin is toxic for the parasite and can cause lysis and membrane damage (Foley et al., 1998; Miller et al., 2013; Pulcini et al., 2015). Whereas the aminoquinoline related mefloquine was shown to target the *P. falciparum* ribosomes to inhibit protein synthesis (Wong et al., 2017). The 8-aminoquinolines (primaquine) were used as a drug against the dormant liver stages (hypnozoites) of *P. vivax* and *P. ovale* (Campo et al., 2015).

The widespread use of chloroquine for malaria control (Gustafsson et al., 1987) led to a broad spread of resistance in *P. falciparum* parasites and hampered the use of chloroquine (Payne, 1987). The resistance mechanism has been associated with mutations in the chloroquine

resistance reporter gene (*crt*) (Fidock et al., 2000). The *crt* encodes for a FV transporter which pumps chloroquine out of the FV. A mutation leads to a faster efflux of the drug from the FV in comparison to the un-mutated protein, which results in a decreased chloroquine sensitivity (Bray et al., 1998; Durand et al., 2001; Fidock et al., 2000; Pulcini et al., 2015).

1.1.4.2 Antifolates

Antifolates such as pyrimethamine, proguanil, chlorproguanil and trimethoprim inhibit the dihydrofolate reductase (DHFR), which deprives the parasite from essential folate cofactors, that the parasite needs for its amino- and nucleic acid metabolism (Yuthavong, 2002). Also, antifolates resistant *Plasmodium* parasites were observed in South America, Southeast Asia (reviewed in: (Le Bras et al., 2003)) and Africa (reviewed in: (Venkatesan et al., 2013)). Antifolate-resistant *Plasmodium* parasites contain a single point mutation in the DHFR gene, causing the drugs to lose their affinity to their catalytic binding sites (Delves et al., 2012; Muller et al., 2010).

1.1.4.3 Atovaquone

Atovaquone is usually given with proguanil to increase the efficiency of the therapy. Atovaquone inhibits mitochondrial electron transport within the *Plasmodium* parasites (Goodman et al., 2016; McKeage et al., 2003). Resistant parasite strains show a mutation in their mitochondrial desoxyribonucleic acid (DNA)-encoded *cytochromeB* gene. This mutation is postulated to prevent the parasite from generating sporozoites in the mosquito phase (Goodman et al., 2016). This has the advantage that the resistance cannot spread and all resistances observed must have arisen *de novo* in the host.

1.1.4.4 Artemisinin

Artemisinin was identified in the early 1970s and isolated from the sweet wormwood (*Artemisia annua*). Further research led to the development of more stable derivatives (Faurant, 2011). In 2015, Youyou Tu received the Nobel Prize for making this drug available (Nobel-Media, 2015) (Tu, 2011; Tu et al., 1981). The mode of action of arteminins (ARTs) is still unclear, but it is assumed that ARTs get activated before they become active as a drug. The activator for ARTs seems to be the reduction of the Fe^{3+} from of heme to Fe^{2+} heme (Becker et al., 2004; Meunier et al., 2010). This activation is thought to lead to carbon centred radicals, by the iron catalysed reductive scission of the drug (Li et al., 2010; Meshnick et al.,

1991). The formed radicals interact with nucleophiles, like enzyme active sites, unsaturated membrane lipids, and also with heme (Bray et al., 2005; Straimer et al., 2012; Wang et al., 2015). It was postulated that the radicals' interaction damages the endoplasmic reticulum (ER), the mitochondrion and the FV, but also multiple other functional pathways and that this wide activity is the reason for the efficiency of the drug (Li et al., 2010; Meshnick et al., 1989; Meshnick et al., 1993; O'Neill et al., 2004; Posner et al., 1992). Because the main haemoglobin digestion in the parasite takes place in the trophozoite stage (see. 1.2.3) (Klonis et al., 2013), ART is most effective in this stage. It is less active in stages where less or no haemoglobin digestion occurs, like in mature gametocytes (see. 1.2.3.1) (Adjalley et al., 2011) or the liver stage (Meister et al., 2011). A recent study from Birnbaum et al. (Birnbaum et al., 2020) showed that haemoglobin digestion also takes place in early ring stage parasites which explains the activity of ART also in very early ring stage parasites (Klonis et al., 2013; Xie et al., 2016).

The WHO recommends artemisinin-based combination therapies (ACTs) for the treatment of uncomplicated malaria. ACTs combine artemisinin derivatives with at least one other compound with a different mechanism of action. For severe malaria, the WHO recommends an injectable artesunate treatment for at least 24 hours followed by a 3-day course of an ACT. The combination therapies try to avoid the development of resistance to artemisinin derivatives (World-Health-Organisation, 2018a). However, since 2008, first cases of parasites with lowered susceptibility to ART have been reported (Dondorp et al., 2009). This is increasingly leading to treatment failures in South East Asia and greatly threatens the advances in malaria control achieved in recent years.

1.1.5 Vaccine development

The complex *Plasmodium* parasite's biology and the diverse parasite genome have hampered the development of effective vaccines in recent years (reviewed in: (Mahmoudi et al., 2018)). So far, there are five different approaches for the development of malaria vaccines.

1.1.5.1 Sporozoite subunit vaccines

The most prominent and the first malaria vaccine that completed phase III trials is RTS,S/AS01 (Mosquirix®). The target of this vaccine is the circumsporozoite protein (CSP) that is believed to be needed for sporozoite motility and hepatocyte invasion (see. 1.2.1) (Coppi et al., 2005; Ouattara et al., 2015; Sinnis et al., 2002; Tewari et al., 2002).

RTS,S/AS01 consists of two components: 18 copies of the central repeat and a C-terminal domain of CSP which is fused to the hepatitis B virus surface antigen. RTS,S/AS01 is also combined with the liposomal adjuvant system AS01 in an attempt to increase the vaccine's protection (Draper et al., 2018). In phase III trials, RTS,S/AS01 protection rates up to 36,3 % for clinical malaria were observed, compared to the control (RTS, 2015). However, more recent studies showed that efficacy fades over (Olotu et al., 2013) time, and even rebound effects occur, which can lead to increasing clinical malaria cases compared to the control (Olotu et al., 2016). Nevertheless, RTS,S/AS01 is authorized for further usage in pilot areas (World-Health-Organisation, 2020) .

1.1.5.2 Whole sporozoite vaccines

Whole sporozoite vaccines (WSV) are a promising vaccine approaches, because in preclinical animal models and humans, high levels of protection against homologous human malaria infection was achieved. The WSV work with radiation attenuated sporozoites (RAS) (Nussenzweig et al., 1967; Nussenzweig et al., 1969), genetically attenuated parasites (GAP) and sporozoites administered under drug cover (CPS) (Beaudoin et al., 1980; Cochrane et al., 1980; Itsara et al., 2018; Voller et al., 1980). The first WSV which was studied in rodents (Nussenzweig et al., 1967; Nussenzweig et al., 1969) and humans were radiation attenuated sporozoites. They were arrested in the liver stage and showed a potent immunity in humans (Beaudoin et al., 1980; Cochrane et al., 1980; Voller et al., 1980). However, parasite genetic diversity is a major problem for protection against heterologous strains (Walk et al., 2017), so that it is unclear if this approach will result in a feasible vaccine.

1.1.5.3 Blood-stage vaccines

Blood stage vaccines try to cause immunity in humans, by eliciting antigen specific antibody concentrations in the human blood. Therefore, merozoite antigens, like the erythrocyte binding antigen 175 (EBA175), the merozoite surface protein 1 (MSP1), or the apical membrane antigen 1 (AMA1), were induced to the human blood, which should lead to antibody production to block erythrocyte invasion (reviewd in: (Fowkes et al., 2010). Despite decades of efforts, none of these blood stage vaccine approaches showed protection in clinical trials, whereby the main issue might be the high diversity of antigens based on genetic polymorphisms (Draper et al., 2018; Ogutu et al., 2009; Sagara et al., 2009).

1.1.5.4 Transmission-blocking vaccines

Another malaria vaccine strategy is to target the sexual stages (see. 1.2.3.1) and prevent the parasite from transmission. In preclinical studies, different antigens, like the gametocyte antigens Pfs48/45/230 and the ookinete surface protein Pfs25, performed well (Pehrson et al., 2017). However, a purely transmission blocking vaccine poses ethical problems (due to collective immunization) and further clinical studies have not been carried out with these candidates.

1.2 *Plasmodium* parasite's biology

1.2.1 Life cycle of *P. falciparum* parasites

P. falciparum parasites show a complex life cycle, which consists of two hosts: the female *Anopheles* mosquito, and the human (Figure 2). The life cycle is divided into three different parts: human liver stages (hepatic cycle), human blood stages (erythrocytic cycle) and mosquito stages (sexual development).

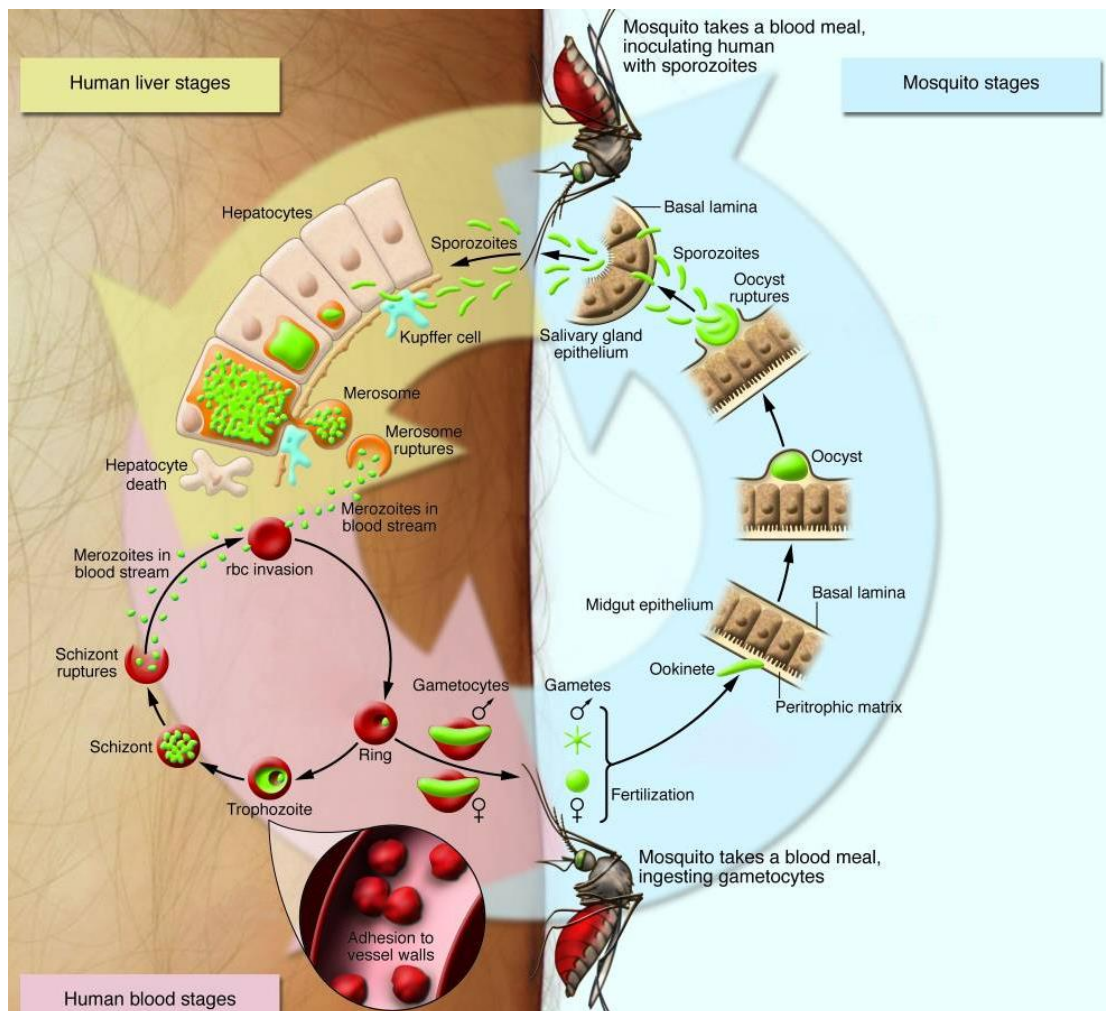


Figure 2: *P. falciparum* parasite's life cycle.

Illustration of the *P. falciparum* life cycle with human liver stages (yellow bold arrow), human blood stages (pink bold arrow) and mosquito stages (blue bold arrow). Host cells are displayed in red (red blood cells) or bright pink (hepatocytes) and parasites are shown in green. Mosquito midgut epithelium cells are shown in brown. Modified from (Greenwood et al., 2008).

1.2.2 Hepatic cycle

The hepatic cycle starts with the blood meal of the female *Anopheles* mosquito. During this meal, less than a hundred sporozoites are inoculated from the mosquito salivary glands to the human host (Figure 2) (Jin et al., 2007). Some sporozoites stay either in the skin or are eliminated by the lymph system (Yamauchi et al., 2007), but there are also sporozoites that reach the blood vessels and enter the blood stream. Despite a lack of symptoms, recent studies suggest that this phase already initiates an immune system (Liehl et al., 2014; Miller et al., 2014; Roland et al., 2006). The sporozoites are then transported to the liver where they cross the liver sinusoidal wall and migrate through the Kupffer cells or endothelial cells to the hepatocytes (cells of the main parenchymal tissue of the liver) (Figure 2) (Prudêncio et al., 2006). It is postulated that sporozoites target and enter the hepatocytes by using the circumsporozoite protein and the thrombospondin-related anonymous protein, which bind to heparan sulphate proteoglycans and the CD81 receptor on the hepatocyte surface (Pinzon-Ortiz et al., 2001; Robson et al., 1995; Silvie et al., 2003; Sultan et al., 1997). Once within a hepatocyte, the parasite transmigrates and establishes a replication competent parasitophorous vacuole (PV) (Risco-Castillo et al., 2015). Essential for PV establishment are the sporozoite proteins P36, P52 and proteins from the 6-cys family, which interact with the hepatocyte receptor EphA2 (Kaushansky et al., 2015). In the infected hepatocytes, the parasites develop to trophozoites and then in merozoites by undergoing schizogony. The final step during liver development is the rupture of the PV, whereby the merozoites are released in membrane-bound structures (merosomes) into the blood stream (Figure 2) (Vaughan et al., 2012). In *P. falciparum* parasites the development in the liver takes on average 5.5 days (Bartoloni et al., 2012; Sturm et al., 2006).

1.2.3 Erythrocytic cycle

The erythrocytic cycle is a complex multistep process and starts with the invasion of red blood cells (RBCs) by free merozoites released from the liver into the bloodstream (Figure 2). The invasion process is completed in less than two minutes after merozoites have been released (Glushakova et al., 2005; Wright et al., 2014). The primary contact of the merozoite

to the RBC can occur at any point of the merozoite surface and the binding is mediated by a low affinity interaction of merozoite surface proteins (MSPs) to the RBCs surface (Wright et al., 2014).

The attachment is followed by the re-orientation of the merozoite to bring its apical invasion machinery (apical complex) close to the RBC membrane. The apical complex consists of flattened vesicles underlying the plasma membrane, which are interconnected with the cytoskeleton, termed inner membrane complex (IMC), an actin-myosin motor and secretory organelles like micronemes, dense granules and rhoptries. The micronemes and rhoptries promote the irreversible attachment and the re-orientation by parasite ligands such as the reticulocyte-binding like homologs (stored in the rhoptries) and erythrocyte binding antigens (EBAs) (stored in the micronemes) (O'Donnell et al., 2000). Next, rhoptry neck proteins (RONs) form together with the apical membrane antigen (AMA1) a 'tight junction' at the RBC membrane (Cao et al., 2009; Srinivasan et al., 2011). Subsequently, the merozoite invades actively by pushing itself into the RBC using a parasite encoded actin-myosin motor (Baum et al., 2006; Weiss et al., 2016). Thereby, RBC membrane wrapping and local clearing of cytoskeletal elements are induced (Dasgupta et al., 2014). During invasion the parasite uses parts of the invaginated RBC membrane as well as lipids and proteins, which the rhoptries secrete to surround itself with a second membranous vacuole, termed PV. The membrane of the PV is called parasitophorous vacuole membrane (PVM) (Cowman et al., 2012; Koch et al., 2016).

Inside the RBC, the parasite is termed the ring stage (Figure 2) (0-18 hours post infection (hpi)). The ring stage is mobile in the host cell and can change in shape between a disc-shaped form and an amoeboid phenotype (Gruring et al., 2011). It is assumed that the ring stage shows low metabolically activity and represents a slowly growing "lag" phase in which the parasite establishes host cell modifications (see. 1.3.3) needed to support its development in the RBC by exporting different kinds of proteins into the RBC cytosol (Hiller et al., 2004; Maier et al., 2008; Marti et al., 2004; Spielmann et al., 2006).

After 18 hpi, the ring stage matures to the trophozoite stage (Figure 2). In this stage, the parasite arrests inside the RBC (Gruring et al., 2011). In the period from 18 until 30 hpi, the parasite grows rapidly and at the same time internalises up to 80 % of the RBC cytosol until the parasite occupies almost the entire RBC. The cytosol of the RBC consists mostly of haemoglobin, which the parasite takes up (host cell cytosol uptake (HCCU)) and then degrades to amino acids (AAs) and hemozoin inside a lysosome-like compartment of the FV. This is done for gaining space for growth and also as a feeding supply for amino acids

(Krugliak et al., 2002). However, the primary function is to gain space for rapid growth rather than the feeding purpose (Krugliak et al., 2002).

The trophozoite stage is followed by the schizont stage (Figure 2). The schizont stage starts around 30 hpi and is characterized by schizogony. During schizogony, asynchronous nuclear division takes place (see. 1.3.1.2) without parallel cell division (Arnot et al., 2011; Gladfelter, 2006; Rabinowitz, 1941). Besides the genome, mitochondria and apicoplast (see. 1.3.2) are replicated and segregated into the newly forming daughter cells termed merozoites. Additionally the parasitophorous plasma membrane (PPM) and the organelles of the apical complex are formed for each merozoite. (Francia et al., 2014; Gerald et al., 2011; Kono et al., 2012; van Dooren et al., 2005). In a process termed 'egress' the RBC and the mature schizonts (segmenters) burst and release the merozoites into the blood stream (Figure 2). It is presumed that the egress is triggered by a cascade of proteases, which leads to the formation of pores in the RBC-membrane, disintegration of the PVM and destruction of the RBC-cytoskeleton (Blackman et al., 2013; Thomas et al., 2018). With the egress of the merozoites, the parasite completes one round of the asexual life cycle, which can be continued by invading other RBCs (Figure 2).

1.2.3.1 Sexual development

1.2.3.1.1 Sexual development in the human

During the asexual life cycle in RBCs, a small number (less than 10 %) of sexual male and female precursors (termed 'gametocytes') are formed from young blood stage parasites, which look like ring stage parasites. The commitment for gametocyte development occurs in the previous cycle, before schizogony (Bruce et al., 1990) and takes place in the bone marrow (Aguilar et al., 2014; De Niz et al., 2018). Gametocyte development takes 8 to 12 days (Sinden, 2009) and is divided into five stages (I-V) (Hawking et al., 1971) which can be distinguished by morphological appearance and using molecular markers (Pradel, 2007). Crucial for this process is the transcription factor AP2-G which leads - when disrupted - to parasites that are unable to form gametocytes (Kafsack et al., 2014; Sinden et al., 1996; Sinha et al., 2014). Recent data postulate that the *P. falciparum* gametocyte development 1 (GDV1) is a sexual commitment activator, which acts as an effector protein that triggers eviction of the adapter protein Heterochromatin protein 1 (HP1). This leads to de-repression of the *ap2-g* gene and thus to sexual commitment (Filarsky et al., 2018). It is also assumed that the parasite reacts to host-derived physiological states, such as for instance in response to low serum

levels of the lipid lysophosphatidylcholine (LysoPC), which leads to activation of sexual differentiation (Brancucci et al., 2017). Furthermore, it has been shown that microvesicles deriving from infected RBCs are involved in the induction of gametocyte formation (Josling et al., 2015; Mantel et al., 2013; Regev-Rudzki et al., 2013).

1.2.3.1.2 Sexual development in the mosquitoes

During a blood meal the mosquito takes up the micro- and macrogametocytes, which developed in the human (Figure 2). The altered physiological environment in the mosquito midgut, such as the drop in temperature, a change in pH (Billker et al., 1997) and the presence of xanthurenic acid induce the maturation of gametocytes into gametes (Billker et al., 1998). During this maturation, the female gametes are released from the RBC and become permissive for sexual fertilization. The male gametes undergo three rounds of DNA replication (leading to eight nuclei) and eight flagellas are assembled. Next, the matured male gametes are released (exflagellation). Subsequently, the male and female gametes fuse and form a diploid zygote (Josling et al., 2015; Sinden, 2009). The zygote develops further into an ookinete (Figure 2) (Sinden et al., 1985). The ookinete reaches the extracellular space between the midgut epithelium and the basal lamina by traversing the midgut epithelial wall. The ookinete develops further into an oocyst. The oocyst matures and multiples by mitotic divisions for 9 – 20 days until up the 8000 sporozoites are produced and the rupture of the oocyst occurs (Sinden, 2009). Some of the released sporozoites are transported into the epithelium of the salivary glands (Korochkina et al., 2006; Rosenberg et al., 1991). During another blood meal of the *Anopheles* mosquito, the sporozoites are inoculated to humans (in case of *P. falciparum* parasites) to start the next round in the life cycle.

1.3 Parasite cell biology with emphasis on parasite specific aspects

P. falciparum is a highly adapted parasite with many specialized ‘features’ to survive inside the human and the *Anopheles* host. It has, for example, unique and modified organelles, an altered mitosis, an exoproteome that modifies the host cell to avoid the clearance by the spleen, unique apical organelles, a specialized secretory and endolysosomal pathway and cell cycle. All these properties differentiate *P. falciparum* parasites from most other eukaryotes.

1.3.1 Cell cycle and checkpoints

The cell cycle in *P. falciparum* parasites differs from the ‘classical’ cell cycle in eukaryotes (1.2.3 Erythrocytic cycle), but can still be categorised into the ‘classical’ cell cycle phases.

1.3.1.1 Cell cycle

The ‘classical’ cell cycle based on model organisms follows a series of clearly defined events which are tightly regulated and controlled by a series of checkpoints. The ‘classical’ cycle consists of two major phases: the interphase and the mitotic phase. The interphase is further subdivided into two gap phases (G1 and G2) and an S phase (Barnum et al., 2014). In *P. falciparum* parasites the merozoite can be presumed as a G0 or G1 phase (Ishiyama et al., 2008). This phase is followed by the early ring to trophozoite stage which possesses a single haploid nucleus in an inter- or G1 phase (Jacobberger et al., 1992). An S phase including DNA synthesis occurs in mid to mature trophozoite stage (Arnot et al., 2011; Chulay et al., 1983; Merckx et al., 2003) followed by a closed mitosis. A G2 phase is lacking in *P. falciparum* parasites (reviewed in: (Matthews et al., 2018) .

1.3.1.2 Mitosis

The ‘classical’ mitosis itself is divided into four different phases: prophase, metaphase, anaphase, and telophase (Heath, 1980; Mitchison et al., 2001; Pines et al., 2001). In the prophase, the chromosomes start to condense inside the nucleus and the microtubule organizing centres (MTOCs) duplicate within the cytoplasm (Fig. 3 A, Traditional View of Mitosis [Traditional]).

In *P. falciparum* parasites the prophase starts with the assembly of the microtubules inside the nucleus and the duplication of the centriolar plaques (centrosome equivalents, also called MTOCs (Fig. 3 A, *Plasmodium* Mitosis [*Plasmodium*])) (reviewed in: (Matthews et al., 2018). In contrast to the ‘classical’ mitosis, *P. falciparum* chromosomes do not appear to condense (Read et al., 1993) and the centriolar plaques duplicate asynchronous and are embedded in pores of the nuclear membrane (Bannister et al., 2000b; Gerald et al., 2011; Schrevel et al., 1977). Due to the asynchronous duplication of the centriolar plaques, the *P. falciparum* mitosis is in comparison to the ‘classical’ mitosis an asynchronous mitotic division (Arnot et al., 2011; Sampson, 1981).

Next, in the ‘classical’ metaphase, the nuclear membrane starts to dissemble, so that the MTOCs and their microtubules get access to the chromosomes (De Souza et al., 2007).

Furthermore, the microtubules connect, mainly at the kinetochores, to the chromosomes from both spindle poles and gather at the spindle centre (Fig. 3 B, Traditional) (Gerald et al., 2011). During metaphase in *P. falciparum* parasites the nuclear membrane remains intact, this is called a closed mitosis and is widespread in many organisms (reviewed in: (Boettcher et al., 2013). *P. falciparum* parasites also form a bipolar mitotic spindle inside the nucleus and connects the kinetochores (Prensier et al., 1986) (Fig. 3 B, *Plasmodium*).

The ‘classical’ metaphase is followed by an ‘classical’ anaphase, whereby the spindle extends and segregates the sister chromatids towards the opposite poles (Fig. 3 C, Traditional)(Gerald et al., 2011). Finally, in telophase, the daughter chromosomes decondense, the nuclear membrane assembles and the cell starts to divide into daughter cells (Fig. 3 D, Traditional) (Gerald et al., 2011).

During *P. falciparum* anaphase, the kinetochores also separate and move to the opposite spindle poles, similar to the anaphase in the ‘classical’ mitosis (Fig. 3 C, *Plasmodium*). In the telophase, the nuclear membrane divides and the daughter genome separates without cell division (De Souza et al., 2009; Gerald et al., 2011) (Fig. 3 D, *Plasmodium*). Thereafter, the parasite cell passes through several cycles of asynchronous mitosis. To so far unknown signals, the final round of mitosis is apparently synchronous, followed by budding into membrane-bound daughter cells (merozoites), resulting in a syncytial cell (Arnot et al., 1998; Bannister et al., 2000a; Matthews et al., 2018; Read et al., 1993).

1.3.1.2.1 Plasmodium cell cycle regulators

To date the regulation of mitosis of the parasite by checkpoints remains elusive and checkpoint proteins have not been identified (Matthews et al., 2018). Even though a G1 checkpoint (known checkpoint for cell cycle regulation in higher eukaryotes) was presumed in the related parasite *T. gondii* in response to nutrient starvation (Suvorova et al., 2013) the evidence for a similar checkpoint in *Plasmodium* parasites is still missing (Babbitt et al., 2012). Although, the *Plasmodium* genome encodes for an unusual repertoire to known regulators in eukaryotic cells, like cyclins, none of them are homologs of ‘classical’ cell cycle cyclins (Francia et al., 2014; Ganter et al., 2017; Merckx et al., 2003; Roques et al., 2015). Furthermore, there is no evidence of a G2 checkpoint and the presence of intra S and M checkpoints is unlikely due to the variation in the speed of genome replication at various life cycle stages (Arnot et al., 2011; Gray et al., 2016; Sinden, 2015).

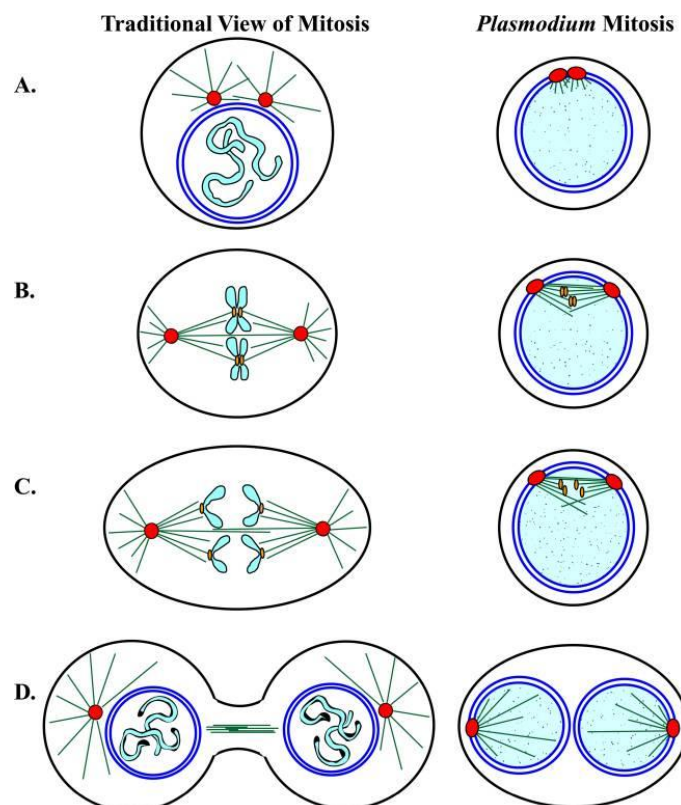


Figure 3: Schematic comparison of traditional views of mitosis with mitosis in blood stage *Plasmodium* parasites. The schematic shows the four different mitotic phases: **A**) prophase, **B**) metaphase **C**) anaphase **D**) telophase. During these phases the plasma membranes (black lines), microtubule organizing centres (MTOCs, red circles), microtubules (green lines), kinetochores (tan ovals), nuclear membranes (dark blue lines), condensed chromosomes (light blue), and uncondensed chromosomes (light blue with stipple pattern) are shown (Gerald et al., 2011).

1.3.2 *P. falciparum* parasite's organelles

An organelle is a structure or a part that is enclosed by its own membrane inside a cell and has a particular function. Organelles are typical for eukaryotic cells and are absent in prokaryotic cells, like bacterial cells (reviewed in: (Satori et al., 2013). ‘Typical’ eukaryotic organelles are the ER, the Golgi apparatus, peroxisomes, lysosomes, mitochondria, chloroplasts, and the nucleus. Compared to other eukaryotes, malaria parasites have a partially modified setup of organelles. Whereby all malaria parasites harbour an ER, a nucleus, mitochondria, an unstacked Golgi apparatus, and a lysosome-like compartment termed the vacuole food (FV) (see.1.3.2.1) (Figure 4) (Bannister et al., 2000a; Struck et al., 2005; Taraschi et al., 1998; van Dooren et al., 2005). Peroxisomes are absent in malaria parasites. Additionally, *P. falciparum* parasites possess specialized secretory organelles fundamental for the invasion process which are the micronemes, rhoptries, dense granules, and exonemes. Further structures are the IMC, the conoid (reviewd in: (Baum et al., 2008; Gubbels et al., 2012), and the apicoplast (see.1.3.2.2) (McFadden et al., 1996).

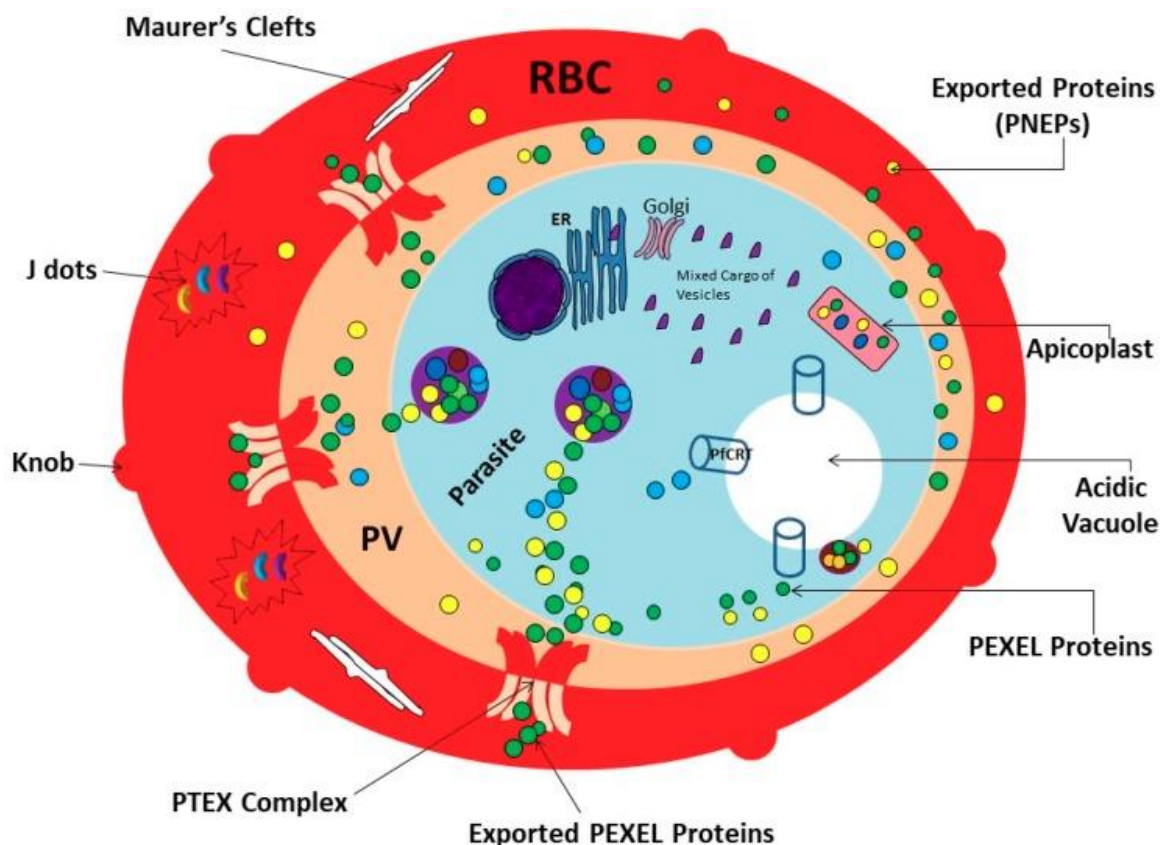


Figure 4: *P. falciparum* infected red blood cell.

The figure shows a *P. falciparum* infected red blood cell including host cell modifications and protein pathways. Acidic vacuole is a synonym for FV; ER, endoplasmic reticulum; PV, parasitophorous vacuole; PTEX, *Plasmodium* translocon of exported proteins; RBC, red blood cell; PEXEL, proteins export element; PNEPs, PEXEL-negative export proteins; PfcRT *Plasmodium falciparum* chloroquine transporter. Figure from (Daniyan et al., 2019).

1.3.2.1 The food vacuole

The FV (Figure 4) is a lysosome-like compartment for the degradation of the haemoglobin that is taken up during the parasite's development in the RBC (Francis et al., 1997; Gluzman et al., 1994; Goldberg et al., 1990; Vander Jagt et al., 1986). It additionally acts as a dynamic internal store for free Ca^{2+} . The surplus of Ca^{2+} inside the FV leads to an acidic environment in the FV compared to the parasitic cytosol (Biagini et al., 2003). At the beginning of each intra-erythrocyte cycle, the FV is newly formed and discarded during egress. This *de novo* generation distinguishes the FV from other organelles such as the apicoplast and the mitochondria (Ehlgen et al., 2012). It is assumed that the genesis of the FV starts in late ring stage with the fusion of several vesicles derived from cytostomal invaginations (Abu Bakar et al., 2010; Lazarus et al., 2008). Proteases like plasmepsin and falcipain drive the digestion of haemoglobin to AAs and α -hematin (Goldberg et al., 1991; Goldberg et al., 1990). The resulting α -hematin is toxic to the parasite, because it has the ability to form free radicals within the FV. To avoid the cell damage induced by free radicals, the parasite polymerizes the

α -hematin into the non-toxic hemozoin, which is also known as the malaria pigment. However, the polymerization process and the enzymes catalysing it are still not fully known (Francis et al., 1997; Sullivan, 2002; Sullivan et al., 1996).

1.3.2.2 The apicoplast

The apicoplast (Figure 4) is common in all apicomplexan parasites except *Cryptosporidium* (Zhu et al., 2000) and present in all stages of *P. falciparum* parasites (McFadden et al., 1996; McFadden et al., 1999). It is a four-membrane bound plastid with metabolic activity that originates from the secondary endosymbiont (reviewed in: (Foth et al., 2003; Gould et al., 2008)). Although the apicoplast is derived from a photosynthetic red alga, it has lost its photosynthetic activity (Janouskovec et al., 2010). The apicoplast and the mitochondrion cannot be formed *de novo* and must be inherited at each cell division (Janouskovec et al., 2010; van Dooren et al., 2005; van Dooren et al., 2013). Most of apicoplast encoded genes migrated to the nucleus during evolution (McFadden et al., 1999), so that most of the apicoplast proteins have to be transported into the apicoplast (McFadden et al., 1999). Thereby the proteins are guided by specific signal sequences (within the protein sequence) and cross the four apicoplast membranes, via a specific import machinery (Agrawal et al., 2013; Ralph et al., 2004; Sommer et al., 2007; Spork et al., 2009). The apicoplast's own 35kb genome encodes for tRNAs, rRNAs, translation- and transcription-related proteins and several other genes (Arisue et al., 2012; Wilson et al., 1996). Furthermore, it was shown that the apicoplast is dispensable in the blood stage, if isopentenyl pyrophosphate (IPP) is supplemented (Yeh et al., 2011). This suggests that isoprenoid biosynthesis is the only essential function in blood stage parasites, although pathways for the synthesis of iron-sulfur clusters, fatty and lipoic acids were also detected (Ralph et al., 2004; Seeber et al., 2010; van Dooren et al., 2013).

1.3.2.3 The unstacked Golgi-apparatus

In *P. falciparum* parasites, the Golgi (Figure 4) appears to be unstacked, such as e.g. in *Entamoeba histolytica* (Dacks et al., 2003; Ghosh et al., 1999). It is postulated that an unstacked Golgi significantly increases vesicles budding of the unstacked cisternae compared to stacked membranes (Wang et al., 2008). It is also assumed that the unstacked cisternae allow rapid vesiculation (for Golgi in preparation for its subsequent partitioning) at the onset of mitosis (Wang et al., 2008). Although the may appear small and simplified compared to organisms with a stacked Golgi, the *P. falciparum* Golgi contains various 'classical' Golgi proteins such as GRASP (Struck et al., 2005; Struck et al., 2008a), the TRAPP complex, Rab6

(Adisa et al., 2007; de Castro et al., 1996; Struck et al., 2008b; Van Wye et al., 1996) or the KDEL-receptor (Elmendorf et al., 1993; van Dooren et al., 2005).

1.3.3 Host cell modifications and protein export

As the RBCs do not contain organelles or any protein trafficking machinery, *P. falciparum* parasites establish host cell modifications, e.g. for nutrients and waste exchange or for the export of proteins (Figure 4) for survival (Leirião et al., 2004; Spielmann et al., 2006; Tilley et al., 2011). For nutrient uptake and the exchange of waste products, *P. falciparum* parasites increases the RBCs permeability by establishing *Plasmodium* surface anion channels (PSAC), or to small structurally unrelated solutes by inducing the so-termed new permeation pathways (NPP) (Alkhalil et al., 2004; Staines et al., 2007; Staines et al., 2006).

Host cell modifications are also needed to avoid the clearance by the spleen (Angus et al., 1997; Chotivanich et al., 2000; Chotivanich et al., 2002; Tilley et al., 2011). As part of the avoiding strategy *P. falciparum* parasites, forms electron-dense, cup-shaped structures beneath the RBC membrane (knobs) in trophozoite stages (Aikawa et al., 1967; Kilejian et al., 1991; Luse et al., 1971). To the knob's surface, *P. falciparum* parasites exports the *P. falciparum* erythrocyte membrane protein 1 (PfEMP1) family (Oberli et al., 2014). The PfEMP1 family is highly diverse and can bind to specific receptors at endothelial cells (Janes et al., 2011; Su et al., 1995). This mechanism can lead to sequestration of the infected RBC and is believed to be a response to avoid the clearance by the spleen (Berendt et al., 1990; Khoury et al., 2014). Sequestration is the reason why in *P. falciparum* infected patients only ring stage parasites can be detected in the blood circulation (David et al., 1983).

Host cell modifications such as the knob or the NPP formation depend on protein export (see.1.3.5). Exported proteins enter the secretory pathway of the parasite (see 1.3.4) before they overcome the PPM and PVM to reach the host cell.

1.3.4 The canonical secretory pathway

In model organisms proteins like bacterial lipoproteins enter the canonical secretory pathway via a signal peptide (SP) (Devillers-Thiery et al., 1975; von Heijne, 1990), which is a 15 to 20 amino acid long hydrophobic region at the proteins N-terminus. The SP is bound by signal recognition particles (SRP) which leads the protein to the SRP receptor at the ER membrane. The SP of most proteins is then cleaved by a signal peptidase (Blobel et al. 1975, Blobel et al. 1975). In *P. falciparum* parasites, there are many secreted proteins that are missing a N-

terminal SP, but probably use an internal signal to enter the canonical secretory pathway, or may be inserted post translationally into the ER (Spielmann et al. 2010, Deponete et al. 2012). Inside the ER (in model organisms as well as in *Plasmodium* parasites), the proteins are transported via the transitional ER (Lee et al., 2008; Struck et al., 2008b) to the Golgi (Lee et al., 2008; Struck et al., 2008b). Less is known about the *P. falciparum* late secretory pathway, downstream the Golgi and remains largely uncharacterised (Deponete et al., 2012).

1.3.5 Exported proteins

Exported proteins, like the PfEMP1 proteins can be identified by short amino acid motifs termed the *Plasmodium* export element (PEXEL) (Marti et al., 2004). Beside the exported proteins with a PEXEL motif, also PEXEL negative exported proteins (PNEPS) were found. Both groups include proteins with transmembrane domains and soluble proteins (Heiber et al., 2013; Spielmann et al., 2010; Spielmann et al., 2006).

During export, the proteins first enter the canonical secretory pathway (see. 1.3.4)

Thereby it is assumed that the cleaved N-terminus of the exported proteins directs the mature protein to the PV. On the way to the PV exported proteins might be transported via vesicles (reviewed in:(Deponete et al., 2012)) The N-terminus probably also mediates substrate recognition for translocation at the PVM (Spielmann et al., 2010), whereby proteins without additional export signals (to the SP) will stay in the PV (Crabb et al., 2010; Elsworth et al., 2014). Further exported proteins were transported across the PVM by the *Plasmodium* translocon of exported proteins (PTEX) (de Koning-Ward et al., 2009) into the host cell (Boddey et al., 2010; Boddey et al., 2009).

After the passage through PTEX, it is supposed that some proteins are further sorted by single membrane flattened disks located in the host cell, called Maurer's clefts (MC) (Figure4), from where the proteins are transported to the RBC membrane (Mundwiler-Pachlatko et al., 2013). How exported proteins (particularly transmembrane proteins) reach the Maurer's clefts after passage through PTEX and how they are transported on to the RBC membrane is unclear (Gruring et al., 2011).

1.3.6 Endocytosis

The general cellular process by which substances are brought into the cell is called endocytosis. During endocytosis, extracellular material is taken up via invaginations or protrusions of the plasma membrane (Schmid et al., 2007). The resulting vesicles then enter endocytic trafficking which will culminate in degradation of the endocytosed material in the

lysosome or transported back by the recycling mechanisms (Sabharanjak et al., 2002). To date, there are two general classifications of endocytic pathways: Clathrin-dependent and several Clathrin-independent pathways (Sabharanjak et al., 2002; Wieffer et al., 2009).

Clathrin-mediated endocytosis is the best characterised endocytosis pathway and serves as a model for endocytosis (Wideman et al., 2014). The first step is initiated by endocytic coat proteins which start to cluster on the inner face of the plasma membrane and is coupled to the recruitment of the cargo on the outer side of the cell. This process leads to the bending of the membrane and transforms this part of the membrane into a Clathrin coated bulge. This bulge forms into a vesicle when disconnected from the plasma membrane with the help of the protein dynamin, resulting in a Clathrin-coated and cargo-filled vesicle. The vesicles are further transported along cytoskeletal elements and are simultaneously uncoated. Downstream in the pathway the vesicles undergo sorting events and maturing processes, to release their cargo to the lysosome (Doherty et al., 2009; Kaksonen et al., 2018; Wieffer et al., 2009).

1.3.7 Host cell cytosol uptake

P. falciparum parasites use endocytosis for large scale uptake of host cell cytosol (Aikawa et al., 1966a; Rudzinska et al., 1958). During maturation of *P. falciparum* parasites, the host cell cytosol uptake is a key process for parasite growth, whereby up to 80 % of the host cell cytosol is ingested and degraded (Francis et al., 1997). HCCU is necessary for space and a source of amino acids (Krugliak et al., 2002). HCCU is still not completely understood and various theories of how HCCU might function in *P. falciparum* parasites were already postulated based on electron microscopic studies in the 1960s (Aikawa et al., 1966b). The most popular model is uptake by flask shaped invagination filled with host cell cytosol termed cytostomes. Cytostomes share some similarity to vesicles derived from membrane invaginations during endocytosis as observed in model organisms. It is believed that cytostomes bud off, like endocytic vesicles, and transported through the parasite's cytosol to the FV (Aikawa, 1966; Aikawa, 1971; Aikawa et al., 1969; Aikawa et al., 1966b; Aikawa et al., 1967; Aikawa et al., 1968; Lazarus et al., 2008; Yayon et al., 1984). Alternatively, the cytostome could also elongate and bridge the parasite's cytosol and pinch off when the FV is reached (Lazarus et al., 2008) A hybrid of these hypotheses postulates that a cytostomal elongation pinches off small vesicles for the last gap to the FV (Milani et al., 2015).

Inhibitor studies suggest some proteins that might be involved in HCCU, such as actin, dynamin, myosin, and SNAREs (Lazarus et al., 2008; Milani et al., 2015; Smythe et al., 2008; Zhou et al., 2009). Furthermore, a study from Jonscher et al. showed that inactivation of

PfVPS45 leads to an accumulation of positive host cell cytosol filled vesicles, which display the endosomal marker PI(3)P, during their transport to the FV. The inactivation of PfVPS45 also leads to parasite death, providing the first definitive evidence for a protein in HCCU (Jonscher et al., 2019).

1.3.8 The lysosomal pathway

In mammalian cells, the endosomal network comprises early, late, and recycling endosomes, which serve as hub for sorting of the initial endocytic vesicles and proteins trafficking. Early endosomes are characterized by phosphatidylinositol-3-phosphate in their outer membrane face (PI3P) (Christoforidis et al., 1999) and the small Ras related protein in brain 5 (Rab5) GTPase (Gorvel et al., 1991; Stenmark et al., 1994b). During maturation of the early to late endosome, Rab5 is exchanged with Rab7, and PI3P is converted to phosphatidylinositol-3,5-bisphosphate (Huotari et al., 2011). The late endosome fuses, including its cargo, with the lysosome as its final destination (reviewed in (Marat et al., 2016)).

The genome of *P. falciparum* parasites encode for homologs of typical lysosomal proteins, like VPS4 (Yang et al., 2004) or the three homologues of the Rab5 isoforms and one Rab7 (Quevillon et al., 2003), which were also found in yeast. In yeast, they are key determinants of endosome identity (Nagano et al., 2015). Additionally, it was shown in yeast, that the cascade of Rab5-Rab7 is important for progression from early to late endosome (Nagano et al., 2015). In *P. falciparum* parasites, the full or partial presence of this pathway is still unclear.

1.4 Methods for gene modifications

To either inactivate the gene directly or to modify it so that it can be inactivated at the transcript or protein level, various methods are possible.

1.4.1 Homologous recombination

The *P. falciparum* DNA rejoining/arranging process is termed homologous recombination. Homologous recombination is initiated by the introduction of DNA double-stranded breaks (DSB), which are concluded by strand exchange between two very similar DNA sequences (reviewed in: (Webster et al., 2014)). For gene modification, a cloned sequence on a plasmid and a single parental genomic copy are needed. Thereby *P. falciparum* parasites tolerate differences in sequence identity, between the parasite genome and the cloned sequence, up to

approximately 5 % for homologous recombination (reviewed in: (Webster et al., 2014)). The modified gene integration using homologous recombination is a random event and thus not very effective.

1.4.2 Target gene disruption

One of the first methods to study gene function in *P. falciparum* parasites was the target gene disruption (TGD). TGD uses a 250-1200 bp long homology region (HR) to target the gene in its 5' coding region. The HR is cloned into an episomal plasmid and integration into the genome via single cross-over is hoped for. The integration of the plasmid results in a truncation of the gene and leads to an unfunctional protein (reviewed in: (Webster et al., 2014)). For a long time, the TGD approach was based on passive selection of integration using drug cycling which could take weeks or months. The recent invention of selection linked integration (SLI) changed this by permitting an active selection (see.1.4.3) Disadvantages of this method can be that (i) a still functional protein fragment remains, especially in case of a short gene; (ii) integration is not achieved, e.g. if the TGD results in a fitness cost to the parasite; (iii) inability to use the system with essential genes. To date the method provided a very good indicator for essentiality of a gene when a TGD using SLI was not achieved as verified by additional methods in a set of 30 genes (Birnbaum et al., 2017; Birnbaum et al., 2020).

1.4.3 Selection-linked-integration

SLI was developed to circumvent the time consuming and often unsuccessful passive selection of homologous recombination events in *P. falciparum* parasites (Birnbaum et al., 2017). This method allows a rapid and efficient selection of parasites with a desired genomic modification. The principle of this method is shown in Figure 5, showing the strategy of a 'knock in' of a tag of interest (i.e. 2xFKBP-GFP-2xFKBP-T2A-Neo-R). The method is based on the expression of a resistance marker only after integration into the genome, but not on the episomally carried plasmid used for parasite transfection. The key player in this technique is the use of a skip peptide which allows the expression of more than one autonomous protein from a single RNA (Straimer et al., 2012; Szymczak et al., 2004).

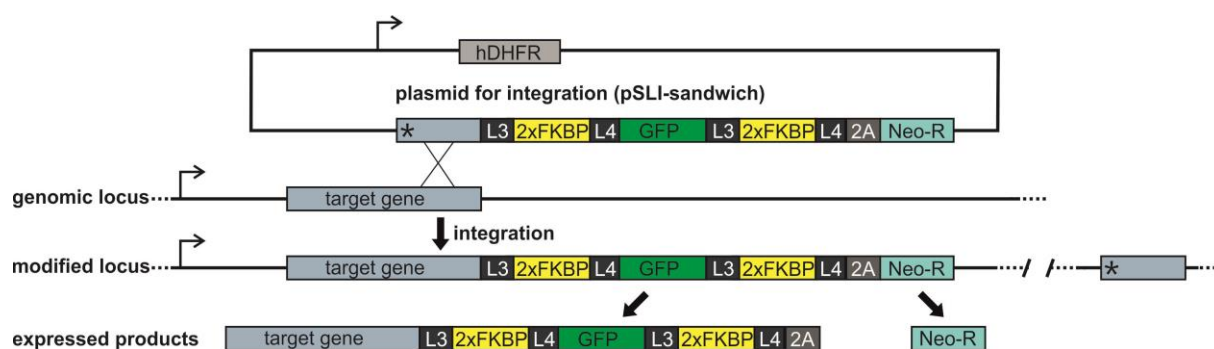


Figure 5: Schematic of selection linked integration strategy.

The figure shows the episomal plasmid (plasmid for integration (pSLI-sandwich)) including the target region (light grey square with asterisks) from the gene of interest (target gene) and a C-terminal tag. The plasmid integrated via single crossover homologous recombination (black crossed lines) of a targeting region into the genome (genomic locus → modified locus). The transgenic parasites can then be selected via the neomycin resistance, which is only expressed after integration (expressed products). L3 and L4 are linkers; 2A, T2A skip peptide; Neo-R neomycin resistance gene; asterisks, stop codon; arrows, promoters; human dehydrofolate reductase (hDHFR), episomal resistance marker. Figure modified from (Birnbbaum et al., 2017).

With this method, genes can be endogenously tagged with GFP, allowing physiological localization of the gene product. Expression from the endogenous promoter allows: localization of a physiologically active protein, the precise tracking of expression levels across different stages.

1.4.4 Zinc-finger nucleases

The Zinc-finger nucleases (ZNF) are another tool for gene modification. ZNF induce DNA DSB upon dimerization, using a zinc-finger DNA binding domain for recognizing the target sequence and the FokI nuclease for inducing the DSB during dimerization (Bitinaite et al., 1998). The cell can repair the DSB using non-homologous end joining pathways, which can result in deletions or insertions. As *P. falciparum* parasites lack the canonical non-homologous end joining, it uses an alternative homologous end joining pathway (Kirkman et al., 2014; Singer et al., 2015). Another DSB repair mechanism is the homologous recombination (see. 1.4.1), which can occur when a donor template is provided (reviewed in: (Webster et al., 2014)). For *P. falciparum* parasites gene modification, the template includes HRs for the target gene that flanks a selection marker. Upon ZFN-induced DSBs, the DSB get repaired using the template which results in the elimination of the target gene, an event that can be selected using the newly inserted marker (Lyko et al., 2012; Straimer et al., 2012). The insertion of point mutations was also shown using the HR/marker method (McNamara et al., 2013).

1.4.5 CRISPR/Cas

The clustered regularly interspaced short palindromic repeat (CRISPR)-Cas9 system can be used for all kinds of gene editing such as the generation of deletions, insertions, or introduction of mutations and for gene tagging. For this, the Cas9 endonuclease induces DSB guided to the targeted locus by RNA (Cong et al., 2013; Jinek et al., 2013; Mali et al., 2013). In *P. falciparum* parasites, the DSB can then be repaired by the repair pathways introduced above (see.1.4.4). In comparison to ZFNs, the CRISPR/Cas9 system is cheaper and also easier, because ZFNs have to be engineered for every approach whereas CRISPR/Cas9 is directed to the correct site using comparably easily designed guide RNAs (de Koning-Ward et al., 2015). In *P. falciparum* parasites, CRISPR/Cas9 was established in two proof of principle studies (Ghorbal et al., 2014; Wagner et al., 2014).

1.4.6 Cre and FLP recombinases

Cre and FLP are recombinases that can be used for gene deletion or inversion (Sauer, 1987; Zhu et al., 1995). For this, the gene of interest has to be flanked by two targeting sequences, one upstream and the other one downstream. These sequences can for example be loxP- or FRT-sites, and depending on their orientation, the gene is inverted or deleted. For the deletion of essential genes, an inducible recombinase is needed, because a permanent deletion would lead to parasite death. The inducible system for the Cre recombinase is called DiCre and consists of a split Cre recombinase which becomes activated by dimerization upon addition of the ligand rapamycin (Jullien et al., 2007; Jullien et al., 2003). DiCre was first adapted to *T. gondii* (Andenmatten et al., 2013) and later adjusted for *P. falciparum* parasites (Collins et al., 2013). In *Plasmodium* parasites also the FLP-FRT system was established for conditional mutagenesis in pre-erythrocytic stages (Lacroix et al., 2011).

1.4.7 Gene-silencing by RNA interference

In eukaryotes, RNA interference (RNAi) is used for gene silencing as a regular cellular process (Bernstein et al., 2002; Coen et al., 1988; Jorgensen, 1990). The mechanism is based on small interfering RNAs (siRNAs) which interact with messenger ribonucleic acids (mRNA). Consequently, the mRNA is degraded by activation of ribonucleases or the inhibition of translation. The siRNAs can also be artificially introduced into the cell for gene manipulation (Agrawal et al., 2003; Hamilton et al., 1999). *P. falciparum* parasites lack this mechanism and thus the opportunity of gene silencing by RNAi (Baum et al., 2009).

1.4.8 Tetracycline-controlled transcriptional activation

The Tetracycline-controlled transcriptional activation (Tet) system allows gene regulation by controlling the activity of the promoter of the gene of interest. With this system transcription of the target gene is reversibly turned off or on. To use the Tet system as a tool in gene manipulation, the original promoter has to be exchanged by a promoter that includes several tetracycline operators (TetO) (reviewed in: (Berens et al., 2003)). In order to achieve a knockdown (Tet-off), the TetO promoter responds to an antibiotic which inhibits binding of a transcriptional trans- activator domain (TRAD) to the operators, which then inactivates expression of the gene of interest. In *P. falciparum* parasites, this technique was the first successful gene regulation system (Meissner et al., 2005) that was also adopted for *P. berghei* (mouse malaria) (Pino et al., 2012). However, in *P. falciparum* parasites, the Tet-system has not been used much after its original publication.

1.4.9 Degradation of mRNA by ribozymes

Ribozymes are ribonucleic acid enzymes that cleave the mRNA in which they are incorporated. The DNA which encodes for ribozymes can be inserted in the 3' untranslated region (UTR) of an mRNA. The activation of ribozymes leads to degradation of the mRNA and consequently to a lower expression of the corresponding protein (Flores et al., 1997). In *P. falciparum* parasites the glmS ribozyme system is used, which leads to self-cleavage upon addition of glucosamine. For some targets knock down levels of over 80 % were achieved with this system (de Koning-Ward et al., 2015; Prommana et al., 2013).

1.4.10 Aptamers and the TetR-DOZI system

Aptamers are single stranded DNA and RNA oligonucleotide sequences which can bind molecules with a high specificity. Aptamers are able to bind proteins, growth factors, amino acids, virus particles or antibiotics (Ellington et al., 1990). In *Plasmodium* parasites the most recent aptamer method is termed TetR-DOZI (Belmont et al., 2010; Goldfless et al., 2014; Hunsicker et al., 2009; Niles et al., 2009). For this system a repeat of ten aptamers is targets the 3' UTR of the tetracycline repressor protein (TetR) onto the mRNA. TetR in turn binds to the mRNA decapping protein DOZI which leads to decapping of the mRNA, which results in translational repression. The addition of the drug anhydrotetracycline (ATc) leads to conformational changes of the TetR protein and prevents aptamer binding and thereby maintains protein synthesis (Ganesan et al., 2016).

1.4.11 Protein destabilization by destabilization domains

One method to conditionally deplete a protein of interest is the use of a destabilization domain (DD). DD interact with a stabilizing ligand and so stabilize the protein (Banaszynski et al., 2006). In absence of the ligand, the protein is destabilized and degraded by the ubiquitin proteasome apparatus. For *P. falciparum* parasites, two different DD are used: the FK506-binding protein DD (Banaszynski et al., 2006) which can be regulated with the ligand shield-1, and *E. coli* DHFR-DD (eDD) (Iwamoto et al., 2010) which is stabilized by trimethoprim. For the use in post-translational control, the DD is fused to the N- or the C-terminus of the protein of interest, which leads to its degradation. In *P. falciparum* parasites the DD method was successfully used for a considerable number of proteins but unfortunately may work for only about one in 10 proteins (Armstrong et al., 2007; de Azevedo et al., 2012; de Koning-Ward et al., 2015; Muralidharan et al., 2011). The eDD system appears to work mainly for chaperones and therefore has not seen wide use (Beck et al., 2014; Muralidharan et al., 2011). Another destabilization approach is the auxin inducible degron. For this system the protein of interest is fused to the auxin responsive AUX/IAA sequence which - in the presence of auxin - recruits an E3 ubiquitin ligase that in turn degrades the protein (Philip et al., 2015). Little use is seen in *P. falciparum* parasites (Kreidenweiss et al., 2013).

1.4.12 Knock sideways

To assess protein function, the ligand-induced dimerization of the FKBP and FRB proteins has been used for a broad variety of approaches (Banaszynski et al., 2006; Belshaw et al., 1996; Chen et al., 1995; Choi et al., 1996; Liang et al., 1999). Whereby the publication of Robinson et al. termed their ligand-induced dimerization of the FKBP and FRB approach ‘knock sideways’ (KS) (Robinson et al., 2010) and in a publication of Haruki et al. a similar approach was termed ‘anchor-away’ (Haruki et al., 2008). In *P. falciparum* parasites, the SLI technique (see. 1.4.3) also allows - as shown in Figure 6 - FRB dimerization to FKBP, which is already included in the primary construct for GFP tagging. The tagged protein can thus rapidly be removed from its site of action via a second protein containing FRB upon the addition of a small molecule dimerizer (rapalog). In *P. falciparum* parasites, the KS was tested for a set of 30 proteins (Birnbaum et al., 2017; Birnbaum et al., 2020) While having a good KS success rate, the speed and level of regulation can vary with the target, and in some cases the system does not work (Birnbaum et al., 2017).

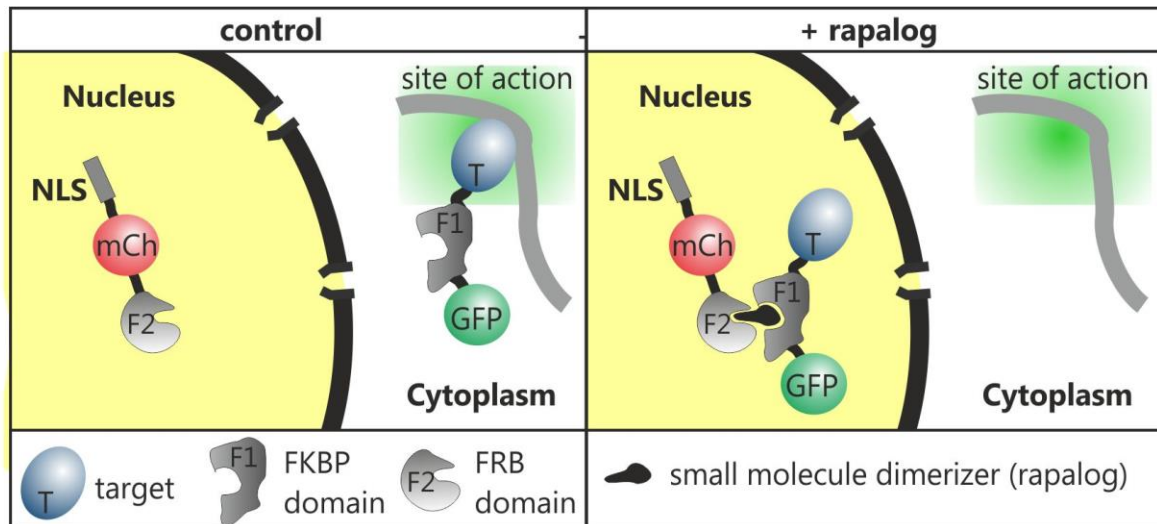


Figure 6: Schematic of the principle for knock sideways using the nucleus as site for mislocalisation.

In the figure the KS principle is shown. **Left)** The tagged protein is located at its site of action and the mislocalizer with a nuclear location signal **Right)** The tagged protein is dimerized, under the addition of rapalog, to the mislocalizer and is so removed from its site of action. NLS nuclear localisation signal; mCh, mCherry. Figure from (Bimbaum et al., 2017).

1.5 *Plasmodium* ‘unknown proteins’ and their potential

Although malaria research has made great progress, much is still unknown about this disease and especially about the specific biology of malaria parasites. This specific biology is of particular interest to drug development, as malaria parasites are eukaryotic cells, similar to the cells of the human body, and thus chemicals affecting its basic processes are likely to also negatively affect the human host. For drug development, it is therefore important to identify and investigate the parasite-specific biological processes, as these provide starting points for a specific inhibition of the pathogen without host damage. Based on the present annotation of the *P. falciparum* genome it has not been possible to assign a function to many of the encoded proteins (according to: PlasmoDB (Aurrecochea et al., 2009)). These proteins without homology to proteins in other organisms are likely to have parasite-specific functions and therefore of high interest. Recent research on parasite-specific functions focused on a few well-defined processes such as protein export, haemoglobin uptake, and red blood cell invasion of the parasite. One reason for this is that the study of unknown proteins is difficult as, until recently, robust systems for conditional gene or protein inactivation had been lacking and because the lack of homologues gives no indication for a possible function of these proteins. The unknown proteins encoded by the parasite therefore harbour a high potential to unravel novel biology of the parasite and are of interest for drug development as they may reveal the parasite's Achilles heels.

1.5.1 Genome wide screens

To identify essential genes in a first step, genome wide screening is useful. To date, two genome wide screens with this goal have been carried out with malaria blood stage parasites.

1.5.1.1 PlasmoGem (Bushell et al., 2017)

The PlasmoGem screen aimed for the identification of essential genes and pathways in *P. berghei*, a malaria parasite infecting rodents that is often used as a model for *P. falciparum* parasites due to the comparatively ease of using genetic tools and the possibility to obtain *in vivo* data. The study measured relative competitive growth rates of 2,578 barcoded *P. berghei* knockout mutants in the mouse host, by comparing the relative growth of pools of mutants by simultaneously co-transfecting multiple barcoded vectors. This resulted in data for over 50 % of the genes. From these results, the authors created a phenotype database. The study postulates that two-thirds of the *P. berghei* genes are required for relative asexual intra-erythrocytic growth *in vivo*. In comparison to any other organism, this is the highest proportion of genes essential for growth (Figure 7) (Bushell et al., 2017).

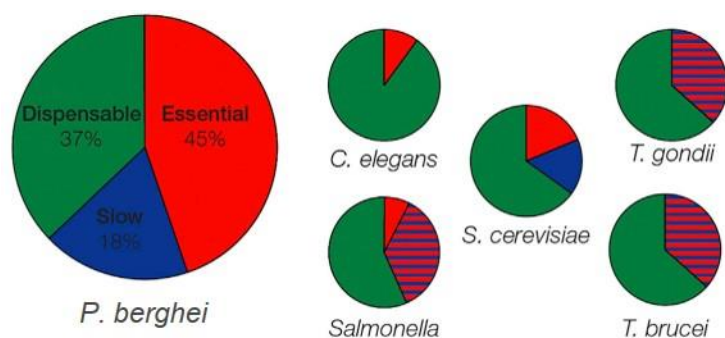


Figure 7: Frequency distribution of phenotypes among different organisms.

The schematic frequency distribution depicts genes postulated as required for normal growth (red), genes that are postulated to lead to a growth reduction (blue) and genes which are postulated to be dispensable for growth (green). Analyzed genes where it was not distinguished between lethality and reduced growth phenotypes are shown in red/blue stripes. Modified from (Bushell et al., 2017).

1.5.1.2 Saturation-based mutagenesis screen (Zhang et al., 2018)

The saturation-based mutagenesis screen targets the same questions as the PlasmoGem publication, but uses a different approach and, importantly uses the human parasite *P. falciparum*. Genome wide screens for *P. falciparum* parasites are for different reasons difficult to conduct (de Koning-Ward et al., 2015). The authors claim to overcome these difficulties using *piggybac* transposon mutagenesis. With the *piggybac* transposon

mutagenesis the authors generated over 38,000 mutants, saturating the genome. The study found that ~ 3000 blood stage expressed genes are essential for optimal parasite growth (Zhang et al., 2018).

1.5.2 Protein interactome studies

Protein interactomes reveal insights into uncharacterized proteins and their possible function on a proteome wide scale. They uncover local and global functional relationships between gene products, resulting in an interaction network.

The first approach to investigate the *P. falciparum* protein interaction network was carried out in 2005 (LaCount et al., 2005). The authors of the study used a version of the yeast two-hybrid assay (Fields et al., 1989) with *P. falciparum* protein fragments in combination with an informatic analysis of network connectivity. The authors of the study claim that they found 2846 unique protein interactions, where most of the protein interactions include at least one previously uncharacterized protein (LaCount et al., 2005). Unfortunately the results of this study are not very reliable, as easily implemented assays to confirm the results are missing (Brown et al., 2011) and the expression of *P. falciparum* genes in yeast is poor (LaCount et al., 2009; Sibley et al., 1997). Additionally, the expression of protein fragments might not confirm the interaction of full length *P. falciparum* proteins (Brown et al., 2011).

Another *P. falciparum* protein interactome study was done in 2006 wherein ~ 68 % of the parasite proteome was analysed and provided functional inferences for more than 2000 uncharacterized proteins, based on the corresponding association network (Date et al., 2006). Their method for interactome maps is based on the statistical Bayesian model where the authors incorporate continuously uniform updated, reference priors. Additionally they superimposed their data on *P. yoelii*, *T. gondii*, and *Cryptosporidium parvum* genomes, to show relationships between these parasites based on retained functional linkages (Date et al., 2006).

A protein interactome network for *Plasmodium* schizonts was conducted by Hillier et al. (Hillier et al., 2019). The authors of this study combined machine learning with blue native-polyacrylamide electrophoresis and quantitative mass spectrometry. The study spanned three species and identified over 20,000 putative protein interactions, organized into 600 protein clusters. The authors conclude that their interactome represents a high-confidence map of the native organization of core cellular processes in *Plasmodium* parasites and that the network reveals putative functions for uncharacterized proteins (Hillier et al., 2019).

1.5.3 Protein evolution

Despite proteome studies the origin of many proteins in *P. falciparum* parasites is still unknown. Especially the *P. falciparum* parasite's unknown proteins show no similarity to known proteins in other organisms outside the Apicomplexa. This circumstance leads to the question, if the unknown proteins and their function have their origin in an evolutionary ancestry (divergent evolution) or did they raised 'de novo' (convergent evolution)?

During divergent evolution, differences accumulate within one species, leading to speciation (Gross, 1967). One Example to illustrate divergent evolution in general, is the evolutionary development of 'flying' frogs originated from a common ancestor with tree frogs. In comparison to tree frogs, the 'flying' frogs developed skin flaps on the arms and legs, enlarged hands and feet with webbing in between, and they reduced their weight. This adaptation enables them a gliding flight (Emerson et al., 1990). This process might also happen on protein level, so that the term divergent evolution can be applied to proteins derived from homologous genes with independent functions. That could either happen through a speciation event (orthologous genes) or by gene duplication (paralogous genes). In both cases, the protein function derived independently from a similar origin (Fitch, 1970). An example for divergent evolution on protein level might be multi domain proteins with demanding function raised from proteins domains with primitive function (Huang et al., 2008). Divergent evolution seems also to be capable of pushing homologous proteins to achieve different folds and various sequences (Grishin, 2001; Murzin, 1998).

Convergent evolution is the presence of a similar feature which is not related to common ancestors (Tunstad, 2013). An general example of convergent evolution are the wings of birds and bats which have the same function (analogous structures) but originated from different ancestors (Machado et al., 2016). Convergent evolution might also happen within proteins, due to limited variations in which polypeptides fold for physiochemical reasons. This is for example assumed for antifreeze proteins that share similar structural attributes (Chen et al., 1997; Davies et al., 2012) and hairpin-like structures (Tomii et al., 2012).

1.6 Aims of the thesis

Malaria research has made great progress in the recent years, but many aspects of the biology of the parasite are not or only partially understood. The key players for a deeper understanding of the *P. falciparum* parasite's biology and a potential treasure for future drug development are the *P. falciparum* proteins annotated with 'unknown function'. To date, tools for analysing a large number of these proteins are still missing or have limitations, for example, genome-wide screens have so far only investigated gene essentiality without further functional analysis. This thesis aims to use the SLI method (Birnbaum et al., 2017) to systematically investigate the unknown proteins on chromosome 3 as proof of principle to uncover novel, essential and parasite-specific biology by

- (i) providing their localization
- (ii) determining which of these proteins are essential
- (iii) analysing the function of selected, essential target proteins
- (iv) generating a resource of cell lines that can also be used by the community for functional analysis.

2 Materials

2.1 Technical devices

Device	Specifications	Company
Agarose gel chamber	Sub Cell GT basic	Bio-Rad, München
Analytical Balance	870	Kern
Autoclave	V120	Systec, Wettengel
Bacterial incubator	Thermo function line	Heraeus, Hannover
Centrifuge	J2-HS	Beckmann Coulter, Krefeld
Centrifuge	Avanti J-26S XP	Beckmann Coulter, Krefeld
Centrifuge	Megafuge 1.0R	Heraeus, Hannover
Centrifuge	5415 C	Eppendorf, Hamburg
Confocal microscope	Olympus FV1000	Olympus, Hamburg
Electro blotter	Phase	Bio-Rad, Munich
Electroporator	Gene Pulser X- Cel	Bio-Rad, Munich
Electroporator	Nucleofector II AAD-1001N	Amaxa Biosystems, Germany
Flow cytometer	LSR II	BD Instruments, USA
Fluorescence microscope	Axioscope 1	Zeiss, Jena
Gel imager	ChemiDoc XRS+	Bio-Rad, Munich
Ice machine	EF 156 easy fit	Scotsmann, Venon Hills, USA
Laboratory scale	Acculab Atilon-ATL	Acculab Sartorius, Göttingen
Light microscope	Axio Lab A1	Zeiss, Jena
Microscope digital camera	Orca C4742-95	Hamamatsu Phototonics K.K.
Microwave	Micro 750W	Whirlpool, China
<i>P. falciparum</i> cell culture incubator	Heratherm IGS400	Thermo Scientific, Langensfeld
PCR mastercycler	Eppgradient	Eppendorf, Hamburg
pH-meter	SevenEasy	Mettler-Toledo, Gießen
Photometer	Bio Photometer plus	Eppendorf, Hamburg
Photometer	Nano Drop	Eppendorf, Hamburg
Pipettes	1-10/200/1000 µl	Gilson, Middleton, USA
Pipettor	Matrix Cellmate II	Thermo Scientific, Schwerte
Pipettor	Pipetboy acu	IBS, USA
Power supply	Power PAC 300	VWR, Taiwan
Roller mixer	STR6	Bio-Rad, München
Shaking Incubator	Max Q4000	Barnstead, Iowa, USA
Sterile laminar flow bench	Sterile Gard III Advance	Baker, Stanford, USA
Sterile laminar flow bench	Safe 2020	Thermo Scientific, Pinneberg
Thermoblock	Thermomixer compact	Eppendorf, Hamburg
Ultrapure water purification	Milli Q	Merck, Darmstadt
UV transilluminator	PHERolum 289	Biotec Fischer, Reiskirchen
Vacuum pump	BVC Contorl	Vacuubrand, Wertheim
Vortexer	Genie 2	Scientific Industries, USA

Waterbath	1083	GFL, Burgwedel
-----------	------	----------------

2.2 Chemicals

(4-(2-Hydroxyethyl)-1-piperazineethanesulfonic acid)

(HEPES)	Roche, Mannheim
1,4-dithiothreitol (DTT)	Biomol, Hamburg
3-(N-morpholino)propanesulfonic acid (MOPS)	Sigma, Steinheim
4',6-diamidino-2-phenylindole (DAPI)	Roche, Mannheim
Acetic acid Roth	Roth, Karlsruhe
Acrylamide/Bisacrylamide solution (40 %)	Roth, Karlsruhe
Agar LB (Lennox)	Roth, Karlsruhe
Agarose	Invitrogen, USA
AlbumaxII	Gibco, Life Technologies, USA
Albumin bovine Fraction V (BSA)	Biomol, Hamburg
Ammonium persulfate (APS)	Applichem, Darmstadt
Ampicillin	Roche, Mannheim
Bacto™ Pepton	BD, USA
Bacto™ yeast extract BD	BD, USA
Biotin Sigma	Sigma Aldrich, Steinheim
Blasticidin S	Invitrogen, USA
Bromophenol blue	Merck, Darmstadt
Calcium chloride (CaCl ₂)	Sigma Aldrich, Steinheim
Concanavalin A G-250 Sigma	Sigma Aldrich, Steinheim
Desoxynucleotides (dNTPs)	Thermo Scientific, Lithuania
D-Glucose	Merck, Darmstadt
Dihydroethidium (DHE)	Cayman, Ann Arbor, USA
Dimethyl sulfoxide (DMSO)	Sigma, USA
Dipotassium phosphate	Merck, Darmstadt
Disodium phosphate	Roth, Karlsruhe
Dulbecco's Phosphate Buffered Saline (DPBS)	PAN, Biotech, Aidenbach
Ethanol	Roth, Karlsruhe
Ethidium bromide	Sigma, Steinheim
Ethylenediaminetetraacetic acid (EDTA)	Biomol, Hamburg
Gentamycin	Ratiopharm, Ulm

Giemsa's azure, eosin, methylene blue solution	Merck, Darmstadt
Glutardialdehyd (25 %)	Roth, Karlsruhe
Glycerol	Merck, Darmstadt
Glycine	Biomol, Hamburg
	Blood bank,
Human red blood cells Sterile, concentrate	Universitätsklinikum, Eppendorf (UKE), Hamburg
Hydrochloric acid (HCl)	Merck, Darmstadt
Hypoxanthin	Sigma, Steinheim
Isopropanol	Roth, Karlsruhe
LB-Medium (Lennox)	Roth, Karlsruhe
Magnesium chloride (MgCl ₂)	Merck, Darmstadt
Methanol	Roth, Karlsruhe
Milk powder	Roth, Karlsruhe
N, N, N, N-Tetramethylethylenediamin (TEMED)	Merck, Darmstadt
Paraformaldehyde (PFA)	Polyscience, Warrington, USA
Percoll	GE Healthcare, Sweden
Phenylmethylsulfonylfluorid (PMSF)	Sigma, Steinheim
Potassium chloride	Merck, Darmstadt
Protease inhibitor cocktail ("Complete Mini")	Roche, Mannheim
Rapalog (A/C Heterodimerizer AP21967)	Clontech, Mountain View, USA
RPMI (Roswell Park Memorial Institute)-Medium	Appllichem, Darmstadt
Rubidium chloride	Sigma, Steinheim
Saponin	Sigma, Steinheim
Sodium acetate	Merck, Darmstadt
Sodium bicarbonate	Sigma, Steinheim
Sodium chloride	Gerbu, Gaiberg
Sodium dihydrogen phosphate	Roth, Karlsruhe
Sodium dodecyl sulfate (SDS)	Appllichem, Darmstadt
Sodium hydroxide	Merck, Darmstadt
Sorbitol	Sigma, Steinheim
β-Mercaptoethanol	Merck, Darmstadt
Tetanolysin	Sigma, Steinheim
Trichloroacetic acid	Roth, Karlsruhe

Tris base	Roth, Karlsruhe
Triton X-100	Biomol, Hamburg
Water for molecular biology (Ampuwa)	Fresenius Kabi, Bad Homburg

2.3 Labware and disposables

Labware and disposables	Specification	Company
Conical falcon tubes	15 ml, 50 ml	Sarstedt, Nümbrecht
Cryotubes	1.6 ml	Sarstedt, Nümbrecht
Culture bottles	50 ml	Sarstedt, Nümbrecht
Disposable pipette tips	1-10/20-200/100-1000 μ l	Sarstedt, Nümbrecht
Eppendorf reaction tubes	1.5 / 2 ml	Sarstedt, Nümbrecht; Eppendorf, Hamburg
Filter tips	1-10/20-200/100-1000 μ l	Sarstedt, Nümbrecht
Flow cytometry tubes	55.1579	Sarstedt, Nümbrecht
Glass cover slips	24x65 mm thickness 0.13-0.16 mm	R. Langenbrinck, Emmerdingen
Glass slides		Engelbrecht, Edermünde
Gloves, latex		Kimtech Science EcoShield; Braun, Melsungen
Leukosilk tape		BSN medical
Multiply- μ Strip Pro 8-Strip		Sarstedt, Nümbrecht
PCR-reaction tube		
Nitrocellulose blotting membrane Protean	Amersham 0.45 μ m	GE Healthcare
One way canulas		Braun, Melsungen
One way syringe		Braun, Melsungen
Parafilm		Bemis, USA
Pasteur pipettes		Brand, Wertheim
Petri dishes	15x60mm / 14x90 mm	Sarstedt, Nümbrecht
Plastic pipettes	5 / 10/ 25 ml	Sarstedt, Nümbrecht
Sterile filter	0.22 μ m	Sarstedt, Nümbrecht
Transfection cuvettes	0.2 cm	Bio Rad, München

2.4 Kits

NucleoSpin. Extract II	Macherey-Nagel, Düren
NucleoSpin. Plasmid	Macherey-Nagel, Düren
QIAamp DNA Mini Kit	Qiagen, Hilden
QIAGEN Plasmid Midi Kit	Qiagen, Hilden
Western Blot ECL-SuperSignal West Pico	Thermo Scientific, Schwerte

2.5 Solutions, buffers and media

2.5.1 Media and buffers for microbiologic culture

10x LB stock solution	10 % NaCl 5 % Peptone 10 % yeast extract in dH ₂ O autoclaved
Ampicillin stock solution	100 mg/ml in dH ₂ O autoclaved
Glycerol freezing solution	50 % (v/v) glycerol in 1 x LB medium
Kanamycin stock solution	Kanamycin 30 mg/ml in H ₂ O
LB Agar plate solution	1.5 % Agar-Agar in 1x LB medium
LB medium	1 % (w/v) NaCl 0,5 % (w/v) pepton 1 % (w/v) yeast extract in dH ₂ O in dH ₂ O
SOB	0.5 g NaCl 20 g tryptone deionized H ₂ O, to 950 ml 5 g yeast extract 10 ml KCL solution (250 mM) Adjust pH 7.0 5 ml MgCl ₂ (2M)
Transformation buffer	3 g/l PIPES (10 mM) 2.2 g/l CaCl ₂ -2H ₂ O (15 mM) 18.6 g/l KCl (250 mM) 10.9 g/l MnCl ₂ -4H ₂ O Adjust pH 6.7

2.5.2 Solutions and buffers for cell biological experiments

2.5.2.1 *P. falciparum* in vitro culture

60 % Percoll solution	6.7 ml Percoll stock solution 3.3 ml RPMI complete medium
Amaya transfection buffer	90 mM NaPO ₄ 5 mM KCl 0.15 mM CaCl ₂ 50 mM HEPES pH7.3 in dH ₂ O sterile filtered
Blasticidin S deaminase (CID) working solution	5 mg/ml BSD in RPMI complete medium sterile filtered
DHE stock solution (10x)	5 mg DHE in 1 ml DMSO
DHE working solution (1x)	0.5 mg DHE in 1 ml DMSO
DSM1 stock solution (50x)	187,5 mM DSM1 in DMSO
DSM1 working solution	100 µl DSM1 stock solution ad 5 ml in 95% DMSO / 5% 1xPBS solution
FACS stop solution	0.5 µl Glutaraldehyde (25%) in 40 ml RPMI complete medium
G418 working solution	50 mg/ml in RPMI complete medium sterile filtered

Ho33342 stock solution (10x)	4.5 mg Ho33342 in 1 ml DMSO
Ho33342 working solution (1x)	0.45 mg Ho33342 in 1 ml DMSO
Human red blood cells	Blood group 0+, sterile concentrate, Blood Bank Universitätsklinikum Eppendorf (UKE), Hamburg
Parasite freezing solution (PFS)	4,2 % (w/v) D-Sorbitol 0,9 % (w/v) NaCl 28 % (v/v) Glycerol in dH ₂ O sterile filtered
Parasite lysis buffer	4 % SDS 0.5 % Triton 0.5x PBS in dH ₂ O
Parasite thawing solution (PTS)	3,5 % (w/v) NaCl in dH ₂ O sterile filtered
Percoll stock solution	90 % (v/v) Percoll 10 % (v/v) 10x PBS
Rapalog (AP21967) stock solution	500 mM in ethanol
Rapalog working solution	1:20 dilution of stock solution in RPMI complete medium
RPMI complete medium	1,587 % (w/v) RMPI 1640

	12 mM NaHCO ₃ 6 mM D-Glucose 0.5 % (v/v) Albumax II 0.2 mM Hypoxanthine 0.4 mM Gentamycin pH 7.2 in dH ₂ O sterile filtered
Synchronization solution	5 % (w/v) D-Sorbitol in dH ₂ O sterile filtered
Transfection buffer (Cytomix)	120 mM KCl 150 μM CaCl ₂ 2 mM EGTA 5 mM MgCl ₂ 10 mM K ₂ HPO ₄ /KH ₂ PO ₄ 25 mM Hepes pH 7.6 in dH ₂ O sterile filtered
WR99210 stock solution	20 mM WR99210 in DMSO
WR99210 working solution	1:1000 dilution of stock solution in RPMI complete medium sterile filtered

2.5.3 Solutions and buffers for molecular biological experiment

2.5.3.1 DNA precipitation

Sodium acetate	1 M NaAc, pH 5.2
Tris-EDTA (TE) buffer	10 mM Tris-HCl pH 8,0 1 mM EDTA pH 8,0

2.5.3.2 DNA gel electrophoresis

50x TAE	2 M Tris base 1 M Pure acetic acid 0.05 M EDTA pH 8,5
6x Loading buffer	40 % Glycerol (v/v) 2.5 % (w/v) Xylene cyanol 2.5 % (w/v) Bromophenol blue in dH ₂ O

2.5.3.3 Gibson assembly buffers

5x isothermal reaction buffer (6 ml)	3 ml 1 M Tris-HCl pH 7.5 150 µl 2 M MgCl 60 µl each of 100 mM dGTP/dATP/dTTP/dCTP 300 µl 1 M DTT 1.5 g PEG-8000 300 µl 100 nM NAD ad 6 ml dH ₂ O
--------------------------------------	--

Assembly master mixture (1.2 ml)	320 μ l 5x isothermal reaction buffer 0.64 μ l 10 U / μ l T5 exonuclease 20 μ l 2 U / μ l Phusion DNA polymerase 160 μ l 40 U / μ l Taq DNA ligase ad 1.2 ml dH ₂ O
----------------------------------	--

2.6 DNA- and protein ladders

Reagent	Company
GeneRuler™1000 bp ladder	Thermo Fisher, Waltham MA, USA
PageRuler™ prestained protein ladder	Thermo Fisher, Waltham MA, USA
PageRuler™ unstained protein ladder	Thermo Fisher, Waltham MA, USA

2.7 Polymerases and enzymes

Enzyme/Polymerase	Company
FirePol. DNA Polymerase [5 U/ μ l]	Solis Biodyne, Taipei, Taiwan
Phusion. High-Fidelity DNA Polymerase [2 U/ μ l]	NEB, Ipswich, USA
Restriction enzymes	NEB, Ipswich, USA
T4 DNA-Ligase [3 U/ μ l]	NEB, Ipswich, USA
Taq DNA-ligase (40U/ μ l)	NEB, Ipswich, USA

2.8 Antibodies

Antibody coupled beads	Streptavidin Sepharose	For pulldown of proteins	GE Healthcare life science, Illinois, USA
------------------------	------------------------	--------------------------	---

2.9 Fluorescence dyes

Dihydroethidium	Cayman Chemicals, Michigan, USA
Hoechst 33342	Chemodex, Gallen, Switzerland
DAPI	Roche, Basel, Switzerland

2.10 Plasmids

Plasmid	Source
pSLI-sandwich (pARL1-2xFKBP-GFP 2xFKBP-T2A-Neo ^R)	(Birnbaum et al., 2017)
pSLI-TGD (pARL1-GFP-T2A-Neo ^R)	(Birnbaum et al., 2017)
<i>crt</i> 5'UTR_1xNLS-FRB-mCherry (BSD ^R)	(Birnbaum et al., 2017)
<i>hsp86</i> 5'UTR_3xNLS-FRB-mCherry (BSD ^R)	(Birnbaum et al., 2017)
<i>nmd3</i> 5'UTR_1xNLS-FRB-mCherry (DSM1 ^R)	(Birnbaum et al., 2017)
<i>nmd3</i> 5'UTR_mCherry-Kelch13 (DSM1 ^R)	(Birnbaum et al., 2017)
<i>crt</i> 5'UTR_1xNLS-FRB-T2A-P40-mCherry (BSD ^R)	Flemming, unpublished
<i>nmd3</i> 5'UTR_BirA*-2xGGGGS-FRB-mCherry (DSM1 ^R) (BirA-N ^L)	cloned by Kruse (Jonscher et al., 2019)
<i>nmd3</i> 5'UTR_-mCherry- FRB-2xGGGGS-BirA* (DSM1 ^R) (BirA-C ^L)	cloned by Kruse (Jonscher et al., 2019)

2.11 Oligonucleotides

All oligonucleotides were synthesized by Sigma-Aldrich (Steinheim).

2.12 Bacterial and *Plasmodium* parasite strains

<i>Escherichia coli</i> XL-10 Gold	<i>Tet^r Δ(mcrA)183 Δ(mcrCB-hsdSMRmrr) 173 endA1 supE44 thi-1 recA1 gyrA96 relA1 lac Hte [F'proAB lacI q Z ΔM15 Tn10 (Tet^r)Amy Cam^r]</i>
<i>Plasmodium falciparum</i> 3D7	Clone of NF54 isolate (MRA-1000) isolated from a malaria patient near the Amsterdam airport (Walliker et al., 1987)

2.13 Software and bioinformatic tools

Software	Company
A plasmid Editor (ApE)	Open Source (http://biologylabs.utah.edu/jorgensen/wayned/ape/)

Axio Vision 40 v4.7.0.0	Zeiss, Jena
BLAST	https://blast.ncbi.nlm.nih.gov/Blast.cgi
Corel Draw X8	Corel Corporation, Ottawa, USA
Corel Photo-Paint X8	Corel Corporation, Ottawa, USA
GraphPad Prism 6.0d	GraphPad Software, La Jolla, USA
HHpred	https://toolkit.tuebingen.mpg.de/#/tools/hhpred
ImageJ 1.48v	Open Source (http://rsbweb.nih.gov/ij/)
Imaris x64 7.8	Bitplane AG, Zürich, Schweiz
Microsoft Office 2016	Microsoft Corporations, Redmond, USA
MotifScan	http://myhits.isb-sib.ch/cgi-bin/motif_scan
PlasmoDB	Plasmodb.org
Xcellence rt v5.2.0.3554	Olympus, Hamburg

3 Methods

3.1 Molecular biology methods

3.1.1 Polymerase chain reaction (PCR)

Polymerase chain reaction is used for amplification of specific DNA fragments. To do so, a unique forward and reverse primer has to be designed which is then used for flanking the DNA target sequence. The fragment is then potentially amplified in each cycle. The cycle comprises: denaturation, annealing, and extension. The denaturation splits the DNA into single strands for the annealing of the primers. The elongation rebuilds the double strands, using a DNA polymerase which starts at the primers. The optimal annealing temperature can be calculated using the melting temperature. Elongation times depend on the used polymerase and the size of the DNA fragment. For analytical purposes (Table 1 and 2), like colony screens, integration checks, excision checks, FIREPol[®] DNA Polymerase (Solis Biodyne) was used and for preparative PCRs (Table 3 and 4) Phusion[®] High-Fidelity DNA Polymerase (NEB) was taken.

Table 1: PCR mix for FirePol DNA polymerase (10 µl batch)

Reagent	Volume [µl]
Ampuwa [®] H ₂ O	6.4
MgCl ₂ (25 mM)	0.6
dNTPs (2 mM)	1
Forward Primer (10 mM)	0.4
Reverse Primer (10 mM)	0.4
10x FirePol Buffer	1
FirePol DNA Polymerase	0.1
DNA template	0,1

Table 2: PCR conditions for analytical purpose

Cycle number	Denaturation	Annealing	Elongation
1	2 min, 95 °C	-	-
2–30	30 s, 95 °C	30 s, 45-68 °C	1 min/kb, 68-72 °C
31			10 min, 72 °C

Table 3: Phusion PCR mix (50 µl batch)

Reagent	Volume [µl]
Ampuwa® H ₂ O	30.4
dNTPs (2 mM)	5
Forward Primer (10 mM)	2
Reverse Primer (10 mM)	2
5x Phusion Buffer	10
Phusion DNA Polymerase (2 U/µl)	0.3
DNA template	0,3

Table 4: PCR conditions for preparative purpose

Cycle number	Denaturation	Annealing	Elongation
1	2 min, 95 °C	-	-
2–30	20 s, 95 °C	30 s, 45-72 °C	0.5 min/kb, 72 °C
31			5 min, 72 °C

PCR products were checked for correct size by agarose gel electrophoresis and subsequently purified (see 3.1.2).

3.1.2 Purification of PCR-product and digested vectors

For isolation and purification of DNA fragments, plasmids and digested vectors, the NucleoSpin® Gel and PCR Clean-up kit (Macherey-Nagel) were used. The kit used a column that binds the negative charged DNA to a silica membrane. The following clearance of lysate, binding, washing and elution were performed according to the protocol.

3.1.3 Restriction digest of DNA, PCR and vector products

Restriction approaches were conducted with enzymes from NEB and their restriction buffer CutSmart® according to the manufacturer's protocol. Usually 50 µl of eluted PCR product were mixed with 0.5-1 µl (1.5 U Enzyme/ µg DNA) and 5 µl buffer. Additionally, DpnI, for cutting methylated DNA of the plasmid, was added in case of plasmid as PCR template. In case of vector digestion, ~ 1 µg of vector was added to a 50 µl mix. The digestion mix was incubated at 37°C for 3 h.

3.1.4 Ligation of DNA

The insertion of DNA into a linearized vector was done either by T4 DNA ligase or the Gibson assembly.

3.1.4.1 T4 DNA ligase

T4 DNA ligase is an enzyme which repairs DNA double strength breaks by catalysing phosphodiester bonds between the 3 prime hydroxyl group at one side and the 5 prime phosphate group of the other side of the DNA fragment. In the lab, the T4 is used for fusion of templates and vectors. T4 was prepared as shown in Table 5 and incubated either 3 - 4 h at room temperature or at 4°C overnight.

Table 5: T4 DNA ligation mix

Reagent	Volume [μ l]
10x T4 ligase buffer	1
T4 ligase	1
Vector DNA	0.5
PCR product	7.5

3.1.4.2 Gibson assembly

Another method for ligation of inserts into a linearized vector is the Gibson assembly. The method is based on overlaps (~ 15 - 40 bp) of the inserts, homologue to the ends of the vector or other DNA fragments. The Gibson assembly allows fusion of up to 6 different inserts and was prepared as shown in Table 6. The ligation mix was incubated for 60 min at 50°C.

Table 6: Gibson mix

Reagent	Volume [μ l]
Assembly master mixture	7.5
Vector DNA	1
PCR product	0.5
Ampuwa® H ₂ O	Ad 10

3.1.5 Plasmid isolation

For low amount of plasmid DNA (mini-preparation) 2 ml LB medium was inoculated with a PCR positive bacterial colony and incubated overnight at 37°C / 750 rpm. The next day, the

plasmid DNA was isolated with the NucleoSpin Plasmid Kit (Machery-Nagel) according to their protocol.

For bigger amounts of plasmid DNA (midi-preparation), 100 ml LB medium was inoculated with a PCR positive bacterial colony and incubated overnight at 37°C /130 rpm. The next day, the QIAfilter Plasmid Midi Kit was performed according to the manufacturer's protocol.

3.1.6 DNA precipitation

For DNA precipitation, 50 – 100 µg plasmid DNA was mixed with 1/10 volume of sodium acetate (3 M, pH 5.0) and three volumes of pure ethanol. Subsequently, the sample was centrifuged at maximum speed for 10 min and then washed with 70 % of ethanol. For transfection, the pellet was solved in 10 µl or 20 µl TE buffer, depending on the transfection method.

3.1.7 External cloning by Life Technologies

A part of the initial gene candidates, were cloned by Life Technologies (Darmstadt). Therefore, the vectors pSLI-sandwich (pARL1-2xFKBP-GFP 2xFKBP-T2A-Neo^R) (Birnbaum et al., 2017) and pSLI-TGD (pARL1-GFP-T2A-Neo^R) (Birnbaum et al., 2017) were provided to Life Technologies (Darmstadt). Additionally, the homology regions were sent to Life Technologies (Darmstadt), which cloned these sequences in the according vectors.

3.1.8 Sequencing of plasmid DNA

To ensure that a vector or an insert was correctly amplified and inserted without mutations, every further processed clone was sent to SeqLab (Sequence Laboratories, Göttingen) for sequencing. The mixture included 200 – 800 ng plasmid DNA (usually 3 µl), 3 µl of 10 mM sequencing primer (forward or reverse) and adjusted to 15 µl Ampuwa[®] H₂O.

3.1.9 Agarose gel electrophoresis

Agarose gel electrophoresis is used for DNA fragments separation according to their length under the influence of an electric field. Usually the agarose gel concentration was adjusted to 1 % w/v in 1 x TAE buffer containing 1 µg/ml ethidium bromide. Ethidium bromide intercalates into the DNA and can be illuminated by UV-light. The sample was mixed with 6x loading dye before application to the gel. For size detection, a 1 kb Ladder (Fermentas) was added into a pocket next to the sample. The electric field was applied with 10 volts/cm for

35 min. The DNA is separated due to its negative charge and the molecular sieve originating from the gel. The UV-light DNA visualisation was done in the ChemiDoc™ XRS (Biorad) imager and also imaged with the ImageLab software.

3.1.10 Genomic DNA isolation

Genomic DNA isolation was used to confirm correct integration of plasmid into the target genomic locus or genomic DNA as templated for PCR. For isolation, 200 µl of blood from at least 1 % parasite containing (trophozoites or schizonts) culture was used and processed with the QIAamp DNA Mini Kit according the manufacturer's protocol.

3.2 Microbiological methods

3.2.1 Preparation of chemically competent *E. coli* cells

E. coli chemically competent cells were used to introduce plasmid DNA into *E. coli* for plasmid multiplication. The following protocol is based on Inoue et al. (Inoue et al., 1990).

For preparation, 10 ml LB medium containing 34 µg / ml chloramphenicol were inoculated with a fresh glycerol stock of XL-10 gold bacteria in a 50 ml falcon (lid not totally closed) and cultivated at 37°C / 130 rpm overnight. The next day, 200 ml SOB medium were inoculated with 5 ml overnight culture and incubated at 18°C / 160rpm until a OD_{600nm} of 0.45 – 0.6 (20 – 24 h) was reached. The culture was then split into four 50 ml falcons and stored for 10 min on ice. Next, the falcons were centrifuged at 3000 g for 15 min at 4°C. The supernatant was then discarded, and the pellet was resuspended in 20 ml ice cold transformation buffer. Subsequently, the falcons were chilled for 10 min on ice. Afterwards, another centrifugation (3000 g, 15 min, at 4°C) and supernatant discarding step followed. The pellets were then mixed with 16 ml ice cold transformation buffer (each pellet in 4 ml). The mixture was pooled and 1.2 ml DMSO was applied by gently swirling. The competent cells were divided into pre-chilled Eppendorf tubes (100 µl aliquots) and frozen immediately in liquid nitrogen or dry ice mixed with ethanol. The cells were stored at – 80°C.

3.2.2 Transformation of plasmid DNA in chemically competent *E. coli* cells

Transformation of plasmid DNA uses chemically competent *E. coli* cells (see. 3.2.1). For transformation, a 100 µl competent cell aliquot was gently thawed on ice and afterwards mixed with 5 µl of T4-, or 10 µl of Gibson ligated vector. The mixture was then stored on ice for 20 min. Subsequently, a heat shock (42°C) for 30 was applied, followed by chilling the

sample on ice for 5 min. The transformation mixture is plated on a LB agar plate containing an antibiotic as selection marker. The plates were incubated at 37°C overnight.

3.3 Cell biological methods

3.3.1 Continuous culture of *P. falciparum* (Trager et al., 1976)

Continuous cell culture of *P. falciparum* was conducted by the use of a special growth medium (RPMI1640 containing 0.5 % Albumax) and the addition of 0 + erythrocytes (transfusion blood, Universitätsklinikum Hamburg-Eppendorf). The haematocrit of the culture was adapted to 5 % , and in case of an introduced parasites resistance, the related drug was additionally applied. For selection after transfection, the following drugs were available: WR99210 (used concentration uc. 4 nM), Blasticidin S (used concentration 2 µg / ml) and DSM1 (used concentration 0.9 µM). For integrant selection, 400 µg / ml G418 (Neomycin) were added to the parasites cultures. The parasites were cultured in petri dishes and incubated at 37°C inside a box containing a gas mixture (5 % O₂, 5 % CO₂, and 90 % N₂). The culture was checked by Giemsa smear and microscopy every day or every second day. Based on the smear, the medium of the culture was changed or the culture was diluted 1/10,1/20,1/40 depending on parasitemia.

3.3.2 Blood smears and Giemsa staining

The calculation of parasitaemia, stage analyses and to check parasite condition, Giemsa stained thin blood smears were prepared. For preparation, 0.1 – 1 µl blood from culture was applied onto one end of a labelled microscope slide (Figure 9 top). Subsequently, the drop was brought into contact with the edge of another slide (Figure 9 middle). Next, the slide was pushed in a quick and smooth motion in a 45° angle to the other side of the labelled slide (Figure 9 bottom). Afterwards, the blood smear was fixed for 10 s in in ≥ 99 % methanol.

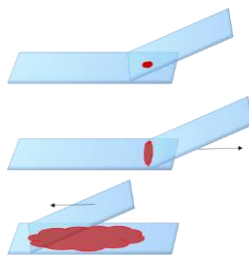


Figure 8: Blood smear preparation.

Top: A blood drop from the cell culture is applied (red) to a microscopy slide (light blue) **Middle:** Blood drop gets in contact with the pusher slide (light blue in 45° angle). **Bottom:** Smearing the blood drop in a quick and smooth motion. Black arrows indicate the direction for pulling (arrow directing to the right) and pushing (arrow directing to the left).

The fixed slide was transferred for staining into *Giemsa's azur eosin methylene blue solution* (Merck, Darmstadt, Germany) and incubated for at least 5 min. Next, the slide was washed with tap water and dried by dapping it with a tissue. Finally, the stained smears were analyzed by using a microscope (Carl Zeiss, Oberkochen, Germany) with optical magnification of 600 – 1000.

3.3.3 Preparation of *P. falciparum* parasites cryo-stabilates and thawing procedure

Freezing: *P. falciparum* parasites can be stored at – 80°C for a few years or in liquid nitrogen for long-term storage. The freezing procedure needs a culture containing at least 1 % ring stage parasites. First, the culture was centrifuged (1800 x g, 3 min, room temperature), and after centrifugation, the supernatant was discarded. Next, the pellet was resuspended in 1 ml malaria freezing solution and transferred to a 2 ml cryotube. The tube was conscientiously labelled and immediately frozen. For long time storage in liquid nitrogen, the software My Samples was used for administration.

Thawing: Cryo-stabilates were thawed in a 37°C water bath for 30 – 60 s and subsequently transferred into a 2 ml reaction tube. The tube containing the parasites were centrifuged (2000 x g, 3 min, at room temperature) and the supernatant was afterwards removed. The pellet was resuspended in 1 ml malaria thawing solution and washed once with pre-warmed RPMI medium. The washed culture was then transferred into a petri dish for cultivation.

3.3.4 Sorbitol synchronization of *P. falciparum* parasites

The sorbitol synchronization uses the new permeation pathway of the parasite for cell lysis. This pathway is built up after 18 h so that parasite from 0 to 18 h (ring stage parasites) are not affected. For ring stage synchronization, the culture was transferred into a falcon and centrifuged (3 min, 1800 x g, at room temperature). Afterwards, the supernatant was discarded, the pellet resuspended in 5 x the pellet volume of prewarmed (37°C) D-Sorbitol in dH₂O. The culture was then incubated in the water bath for at least 7 min at 37°C and centrifuged (3 min, 1800 x g, at room temperature) after incubation. Subsequently, the supernatant was discarded and the culture was washed once with RPMI medium. The culture was then cultivated further.

3.3.5 Purification of *P. falciparum* infected erythrocytes with a Percoll gradient

A Percoll gradient is able to separate trophozoites and schizonts, by their unique density, from uninfected RBCs and ring stage parasites. The Percoll gradient is composed of three different

Percoll concentrations (40 %, 60 %, 80 %). The three concentrations were carefully layered (each layer 450 – 500 μ l) in a 2 ml Eppendorf tube. The pelleted culture was resuspended in 200 μ l RPMI medium and put on top of the gradient without disturbing the Percoll phases. Next, the tube including the gradient was centrifuged (16,000 x g, 5 min, room temperature), which caused a separation into four phases. The phase on top contains merozoites and debris, the two layers below schizonts (middle top) and trophozoites (middle low). In the pellet, rings and uninfected RBCs can be found. The favoured phase was transferred to a new 2 ml Eppendorf tube and washed three times with RPMI medium.

For schizont and merozoite transfection only 4 ml of 60 % Percoll were prepared in a 15 ml falcon and carefully overlaid with 10 ml of resuspended culture. Next, the falcon including Percoll and culture was centrifuged (2000 x g, 6 min, room temperature, without break). Subsequently, the RPMI medium was discarded and the schizont layer on top of the Percoll was transferred into a new falcon and washed with RPMI medium. Afterwards, the pellet was resuspended either in RPMI medium or TE buffer for transfection.

3.3.6 Saponin lysis

Saponin is a detergent that selectively lyses the RBCs and the PVM membrane. The PPM stays at low saponin concentrations intact, due to a different lipid composition. For lysis, a parasite culture (5 – 10 % parasitemia) was centrifuged (3 min, 1800 x g, at room temperature) and the supernatant was discarded after centrifugation. Subsequently, the pellet was washed once with 1.5 x volume of sterile DPBS and then resuspended in 7 up to 20 pellet volumes of ice-cold freshly prepared DPBS containing 0.03 % saponin. The resuspension was incubated for 10 min on ice and the centrifuged (5 min, 11,000 x g, at 4°C). The pellet contained intact RBC and PV membranes. The supernatant includes soluble RBCs and PV protein. Next, the supernatant was discarded and the pellet was washed until the supernatant stayed clear of residual haemoglobin. The pellet was then mixed with lysis buffer with complete protease inhibitor cocktail. Subsequently, the lysate was stored at – 20°C. For mass-spectrometry, a special lysis buffer was used and the lysate was stored at – 80°C.

3.3.7 *P. falciparum* transfection by electroporation

P. falciparum transfection was performed with two different electroporation methods.

Ring stage transfection:

For ring stage transfection, the BioRad system was used. Therefore, 250 μ l of a ring synchronized parasite culture (parasitemia of 5 – 10 %) was mixed with 100 μ g of DNA (dissolved in 20 μ l TE buffer) and 385 μ l cytomix. Subsequently, the mixture was transferred into an electroporation cuvette (2 mm, BioRad) and then electroporated with GenePulser Xcell (350 V, 50 μ F, ∞ Ω). After electroporation, the parasites were transferred into a petri dish for cultivation. The medium was changed every day for 5 days, and after 24 h the selection drug was added.

Segmeter transfection:

Another even more efficient transfection method is the electroporation of segmenters. Therefore, a segmeter synchronized culture (parasitemia 5 – 10 %) was purified with 60 % Percoll (see 3.3.5) and the segmeter layer was transferred into an 15 ml falcon and washed with pre warmed RPMI medium and resuspended in 90 μ l transfection buffer. Additionally, 20 - 50 μ g of DNA (dissolved in 10 μ l TE buffer) was added to the segmeter mix and subsequently electroporated with the Amaxa system (Nucleofector II AAD-1001N, program U-033) in an electroporation cuvette (2 mm, BioRad). The electroporated segmenters were then transferred into a 2 ml reaction tube containing pre warmed (37°C) blood (300 μ l) and 200 μ l RPMI medium. Subsequently the reaction tube was incubated for 30 min at 750 rpm. After incubation the content of the reaction tube was transferred into a petri dish for cultivation. The medium was changed every day for 5 days in a row. Twenty-four hours past transfection the selection drug was added.

3.3.8 Selection for transgenic *P. falciparum* cell lines

The SLI system (see **Fehler! Verweisquelle konnte nicht gefunden werden.**) allows integration of episomal plasmids into the genome. Therefore, the pSLI-sandwich or the pSLI-TGD, containing the target region of the gene of interest, was transfected into the parasite (see.3.3.7) and selected by use of WR. Next, instead of WR, G418 (final concentration of 400 μ g / ml) or Dsm1 (final concentration 1.5 μ M) was added to a mixed culture with a parasitemia of 4 – 10 %. The following 7 days the medium was changed daily and after one week every second day until the parasites appeared. The culture was kept for at least 56 days in culture; in case of non-appearance after this time period the culture was discarded. During the selection process Giemsa smears were done regularly to check re-appearance of parasites and in the beginning (day one to day four) to avoid overgrowing. In case of re-appeared parasites, the genomic DNA was isolated (see.3.1.10) and a PCR to check correct integration

was performed. The PCR also showed if original locus was still present and, in that case, WR was applied for two more *P. falciparum* cycles.

3.3.9 Knock sideways induction

For KS induction, an integrated parasite (containing an episomal mislocalizer) cell line was grown and synchronized according to due to specification of the experiment. Just before the start of the experiment the culture was split into two similar volumes. One served as negative control culture without the addition of rapalog and the second as positive control containing 250 nM rapalog (AP21967, Clontech). The KS was analysed, by fluorescence microscopy or FACS assay (see. 3.3.11).

3.3.10 DiQ-BioID of *P. falciparum* proteins

The biotin labelling was performed with two times 150 ml culture of transgenic parasites (parasitemia 2 – 5 %) containing a with SLI integrated tagged gene and an the episomal BirA*-FRB-FRB-mCherry plasmid. For more accuracy also a cell line with the c-terminal construct was prepared and sent for mass-spectrometry. The two cultures were grown for 20 up to 24 h in presence of Biotin and one with the additional addition of rapalog (250 nM final concentration). The cultures were feed every eight hours to avoid overgrowing. After the incubation, the cultures were lysed with saponin (see. 3.3.6). For mass-spectrometry, the lysate was thawed twice (on ice) and frozen (at -80°C) for complete lysis. For debris sedimentation the samples were centrifuged (10 min, 16000 x g) and the supernatant was transferred into a falcon. Next, the samples were diluted in a ratio of 1:2 with a mixture of 50 nM TrisHCL pH 5,5, 2x protease inhibitor cocktail, 1 mM PMSF. Afterwards, 50 µl Streptavidin-Sepharose beads (equilibrated in 50 nM TrisHCL, pH 7.5) were added and the mixture incubated in a horizontal rolling incubator over night at 4°C. The following day, the samples were centrifuged (1 min, 16000 x g) to sediment the streptavidin beads in a 1.5 ml reaction tube and washed twice with lysis buffer, once in pre-chilled Ampuwa® H₂O, twice in cold TrisHCl (pH 7.5) and at the end three times with cold TEAB (100 mM). Each washing step consisted of an incubation period of 2 min in a horizontal rolling incubator, followed by centrifugation (2 min, 16000 x g). The sedimented streptavidin beads were re-suspended in 50 µl TEAB (100 mM) and sent on ice for mass-spectrometry analysis to the Bartfai lab (Radboud Institute, Nijmegen, Netherlands). The lab used multiplex peptide, stable-isotope dimethyl labelling for quantification.

3.3.11 Growth assay by flow cytometry (Boersema et al., 2009).

Flow cytometry was used to analyse daily growth over a time period of five days. The method is already described by (Malleret et al., 2011). For growth assay, a mixed, transgenic KS culture was measured by LSRII flow cytometer (counting 100,000 events) and analysed with FACSDiva to determine parasitaemia. Next, the culture was adjusted by splitting the culture into two petri dishes to ~ 0.1 %. For one dish KS was induced (see. 3.3.9) and the other served as negative control without rapalog. On day one, two, three, four and five an aliquot of 20 µl was stained for 20 min (with 78 µl RPMI, 1 µl Hoechst 33342, 1 µl dihydroethidium) and afterwards inactivated (with 400 µl RPMI containing 0.003 % glutaraldehyde) in a FACS tube. Afterwards, the parasitaemia was again analysed by LSRII and FACSDiva.

3.3.12 Parasite stage assay by microscopy

To analyse specific growth defects and phenotypes, a growth assay with tightly synchronized parasites was performed. Therefore, a mixed culture was synchronized with sorbitol (see. 3.3.4) and grown for ~ 36 h until it reached segmenter stage. Next, the segmenters were isolated by Percoll (see. 3.3.5) and given into a pre-warmed (37°C) mix, containing 10 ml RPMI and 500 µl blood. Subsequently, the parasites were incubated for re-invasion for 6 h at 37°C. After incubation the culture was again synchronized with sorbitol to achieve 0 – 6 hpi old parasites. The culture was then split into 4 x 2 ml petri dishes, whereby in two dishes the KS was induced and the others served as negative control. Two trays each (positive and negative KS) were incubated in one box. Every six hours until 60 h Giemsa smears and fluorescence microscopy were performed, with the box being changed at every sampling, to keep the growth as stable as possible. The stages were then analysed by microscopic counting and stage evaluation.

3.3.13 E64 bloated food vacuole assay

The E64 bloated FV assay was performed with a sorbitol treated culture synchronized to a stage window of 10 – 18 hpi, with a parasitaemia of approximately 5 %. The culture was grown for 8 h until the parasites reached young trophozoite stage (18 – 26 h). To obtain parasites size at time point zero, a sample was removed before the culture was split into two petri dishes. In both dishes E64 protease inhibitor (Sigma Aldrich) with a final concentration of 33 µM was added. In the positive sample KS was induced (see. 3.3.9). The cultures were incubated for another 8 h and subsequently stained with 4.5 µg / ml dihydroethidium for 20 min at room temperature. Next, the samples were washed, blinded and imaged by

fluorescence microscopy. The analysis was done with ImageJ by scoring bloated FVs and measuring parasites size. Statistics are described in the figure's legend.

3.3.14 Vesicle accumulation assay

For vesicle accumulation assay a transgenic parasite culture containing the KS plasmid was synchronized with sorbitol (see. 3.3.4) to a stage window of 0 – 18 hpi. The culture was then grown for 16 h until it reached trophozoite stage and split into eight different petri dishes. In four dishes KS was induced (see. 3.3.9); the others served as negative controls. Four individual boxes were equipped with pairs of treated and untreated dishes and incubated at 37°C. After 2, 4, 6 and 8 hours a box with one pair was removed and the samples were analysed by microscopy. The samples were blinded and the vesicles counted in the DIC image.

3.4 Microscopy

3.4.1 Live cell and fluorescence microscopy

Many experiments, like live cell and fluorescence samples, were analysed by microscopy with microscopes from Zeiss (AxioImager M1 or M2) containing a filter sets (49, 44 and 64) also from Zeiss, a LQ-HXP 120, a camera (Hamamatsu Orca C4742 95), two numerical aperture lenses (100 × / 1.4 and 63 × / 1.4) and the Axio Vision 40 v 4.7.0.0 software. The imaging was performed as described by Gruring et al. (Gruring et al., 2012). Further image editing was done with Corel Photo-Paint X 8. If the experiment required it, the parasites were stained with DAPI (1 µg / µl) and / or Tubulin Tracker™ deep red (0.5 µg / µl).

3.4.1.1 Confocal imaging

Confocal imaging allows 3D reconstruction and time lapse imaging of fluorescent parasites. The imaging process, especially the time lapse imaging, required a special preparation. On the day before the experiment, the parasite culture was checked for sufficient parasitemia and, if required, KS was induced. Additionally, 14 ml RPMI medium was mixed with 0.5 – 1 ml of blood (overnight medium) and incubated at 4°C. The next day, the medium blood mix was transferred into 2 ml reaction tubes and incubated at 37°C, 750 rpm until it was used. Two hours before the experiment ~ 200 µl conA (cell culture grade Sigma C0412, 0.5 mg / ml final concentration) were added to the bottom of an ibidi dish (uncoated; #81151). The lid was closed and the dish was incubated for 10 – 20 min at room temperature. In the meantime, 500 µl of parasite culture was transferred into a 1.5 ml reaction tube and centrifuged (1 min, 1000

x g). After centrifugation, the supernatant was removed and carefully washed (three times) with dTPBS. Finally, the pellet was resuspended in 500 μ l dTPBS. Next, the conA was removed from the ibidi dish by washing it three times with 1 ml dTPBS and the parasites were added. The ibidi dish lid was closed and the dish was incubated for 10 min at room temperature. During incubation the overnight medium was centrifuged two times with keeping the supernatant (3 min, full speed) to get rid of the RBCs. After the dish was incubated, unbound parasites were removed by washing the bottom of the ibidi dish with dTPBS until the dTPBS stayed clear. The dTPBS was then exchanged for 8.5 ml supernatant of the overnight medium and sealed with parafilm. Finally, the bound parasite culture was transferred to the incubation chamber of the confocal microscope (Olympus FluoView 1000). The imaging was adjusted and controlled by the FluoView software. For image processing, Imaris and Corel Photo-Paint software was used.

4 Results

4.1 Selection of *P. falciparum* genes with unknown function

For functional investigation of *P. falciparum* genes with unknown function, a defined number of genes had to be selected (Figure 9). Because a subset of genes with unknown function on chromosome one and two were already analysed by two lab members of the Spielmann group (Master Thesis, Sabine Schmidt) and Jakob Birnbaum (Birnbaum et al., 2017), for this project, genes of chromosome 3 (249 genes) from *P. falciparum* strain 3D7 were selected (Figure 9) using the malaria gene database PlasmoDB (release 31 (Aurrecochea et al., 2009)). Due to the use of knock sideways (see. 1.4.12) genes with a signal peptide (55 genes) and afterwards genes with a transmembrane domain (49 genes) were removed (Figure 9; using PlasmoDB). For the investigation of only unknown genes, all genes annotated with unknown function (according to: PlasmoDB (Aurrecochea et al., 2009)) were chosen (39 genes), informed by an additional BLAST search (Altschul et al., 1990), where genes with homology (e value < 1e-50 and percent identity \geq 55 %) outside the Apicomplexa were excluded (106 genes; Figure 9). The functional investigation of *P. falciparum* genes in this project is based on in vitro culturing (see. 2.5.2.1), wherefore in the last selection step, only those genes were chosen (33 genes) which were expressed in erythrocytic stages (Le Roch supplement table S1 (Le Roch et al., 2003), expression level for the erythrocytic cycles \geq 13.7). Finally, the selection resulted in 33 genes for further investigation. Therefore the individual homology regions (Table 7; 1.4.3). of the selected genes were cloned into the pSLI-sandwich (pARL1-2xFKBP-GFP-2xFKBP-T2A-Neo^R) vector for knock-in and endogenous tagging and the pSLI-TGD (pARL1-GFP-T2A-Neo^R) for target gene disruption (Birnbaum et al., 2017).

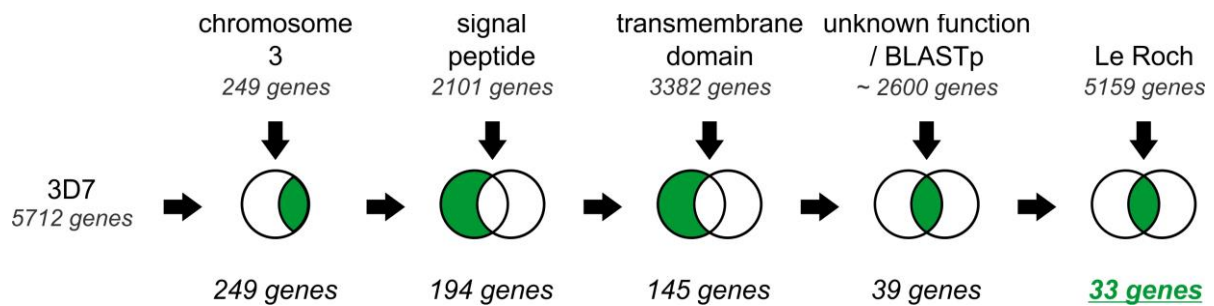


Figure 9: Schematic of selection strategy of the unknown genes from chromosome 3.

The selection steps are depicted in venn diagrams (black circles); the selected genes (green filling, bottom gene numbers) were chosen for the next selection step, resulting in a final set of chosen genes (underlined green genes). The selection steps (top row) are shown from left to right (black arrows). The amount of genes within each selection criteria is shown beneath the criteria description. The gene selection until 145 genes was performed using PlasmoDB; BLASTp, basic local alignment search tool for protein sequences; Le Roch, expression level for the erythrocytic cycles (supplement table S1 from (Le Roch et al., 2003)); Final set of selected candidates are shown in 3D7, *P. falciparum* strain.

4.1.1 *PfRab5b* as proof of principle

During selection and cloning of the candidates, the *PfRab5b* (Rab5b) (Quevillon et al., 2003) protein was chosen as proof of principle to carry out a thorough functional analysis intended with the selected candidates. For this Rab5b was endogenously tagged with 2xFKBP-GFP, using SLI (Birnbaum et al., 2017) and co-transfected with an episomally expressed 1xNLS-FRB-mCherry (BSD^R) (Birnbaum et al., 2017) mislocalizer expressed under the *crt* promoter (Flemming, 2015). This cell line was further analyzed in this project. Firstly, the kinetics of mislocalisation after induction of the knock sideways experiments was analyzed. Efficient mislocalization to the nucleus was evident already 15 min after addition of rapalog (to induce the knock sideways), which stayed stable during the following hours (Figure 10 A). Examination of the culture after overnight inactivation (21 h) of Rab5b by knock sideways revealed the accumulation of vesicle-like structures within the parasite (Figure 10 A, black arrow heads). Next, a growth analysis was performed to assess the importance of Rab5b for parasite development. The analyses revealed a reduction in growth, when *PfRab5b*-2xFKBP-GFP-2xFKBP was inactivated (Figure 10 B and Appendix 4).

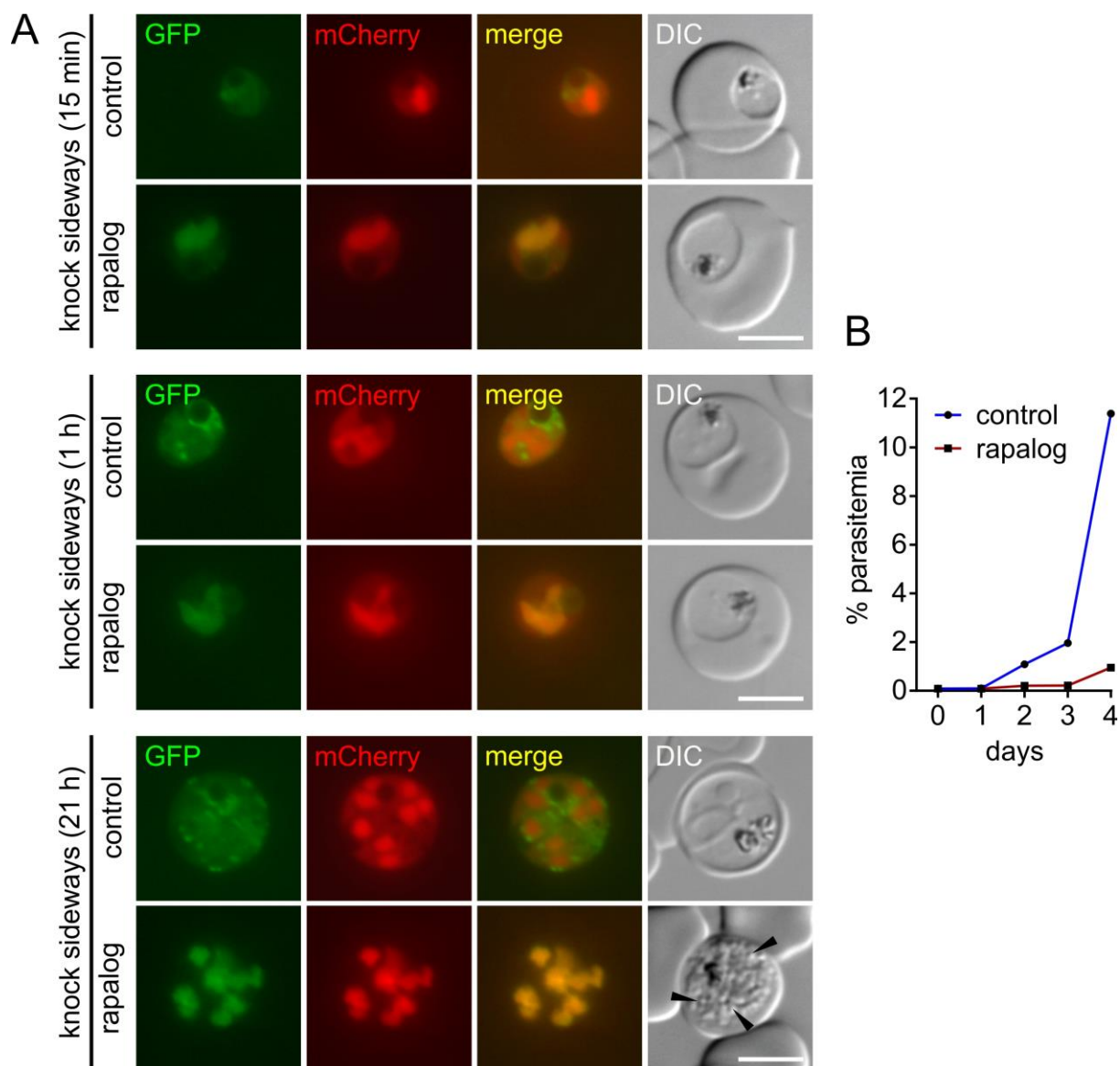


Figure 10: Knock sideways and growth analysis of Rab5b

A) Representative live cell images of cell line expressing endogenous PfRab5b fused to 2xFKBP-GFP-2xFKBP ('GFP') with an episomally expressed 1xNLS-FRB-mCherry mislocalizer ('mCherry'). The cell culture was split into two dishes: one served as control (control) without rapalog, and the second was grown in presence of 250 nM rapalog ('rapalog'). The samples for live cell imaging were taken after 15 min, 1 h, and 21 h. Black arrow heads point to vesicles inside the parasite. Scale bars 5 μ m, DIC (differential interference contrast), merge (merged green and red channel). **B)** Parasite growth as determined by flow cytometry of PfRab5b-2xFKBP-GFP-2xFKBP knock sideways parasites grown in the presence of rapalog (inactivated) and rapalog untreated parasites (control). One representative of three independent experiments (replicas shown in Appendix 4).

In order to determine the stage during asexual blood stage development in which the growth defect after inactivation of *PfRab5b* took effect, a more detailed growth analysis using synchronous parasites was conducted. The parasites were monitored for 62 hours after the induction of the knock sideways to gain insights into stage specific effects. The inactivation of *PfRab5b* showed no effect on ring stage parasites, but revealed a delay in growth and an arrest in trophozoite and schizont stages, compared to the control (Figure 11 A, B). Parasites grown in presence of rapalog for more than 42 h revealed an abnormal morphology, as judged by Giemsa smear (Figure 11 B rapalog 48 h and 60 h), indicating an arrest of *PfRab5b* inactivated parasites. After 42 h, parasites (grown in presence of rapalog) displayed a reduction in growth (of 5.5 % parasitemia) compared to the control (Figure 11 A). Starting from 18 hpi, clear circular areas became apparent in the body of the parasites in Giemsa smears (Figure 11 B black arrow heads). Such a phenotype was previously seen after inactivation of *PfVPS45*, which indicated the presence of what appeared to be multiple vesicles in the parasite cytoplasm (Jonscher et al., 2019). This suggests the presence of such vesicles also in *PfRab5b* inactivated parasites. These probable vesicles increased over time (Figure 11 B).

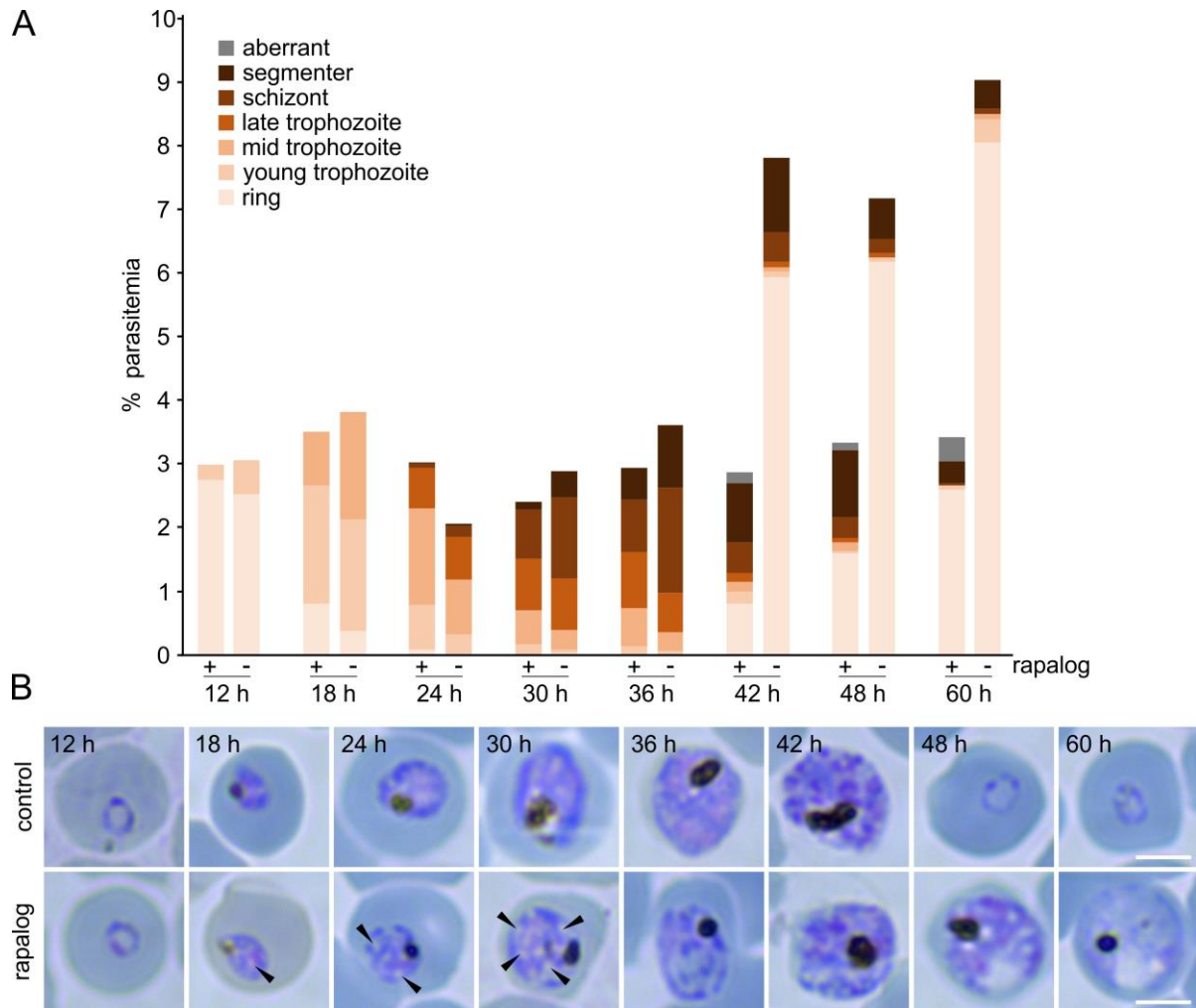


Figure 11: Rab5b is important for the survival of *P. falciparum* parasites.

A) One single experiment of synchronized parasite cell line expressing endogenous *PfRab5b* fused to 2xFKBP-GFP-2xFKBP with an episomally expressed 1xNLS-FRB-mCherry mislocalizer. Parasites were grown in the presence of 250 nM rapalog for inactivation of *PfRab5b* (+) and without rapalog (-) over 60 h. Samples were taken after 12 hpi, 18 hpi, 24 hpi, 30 hpi, 36 hpi, 42 hpi, 48 hpi and 60 hpi. The samples were smeared and stained with Giemsa for stage and parasitemia counting. **B)** Shows representative Giemsa smears of grown in presence of rapalog (rapalog) and rapalog untreated (control) parasites at the specified time points, from the stage experiment shown in A. Scale bar 5 μ m, black arrow heads point to clear circular areas in the body of the parasites (suggesting vesicles).

The Rab5b vesicle like phenotype was then further analyzed and quantified over time in a vesicle accumulation assay (Jonscher et al., 2019). For this assay, the inactivation of Rab5b via knock sideways was induced, in parasites synchronized to an 8 hour time window. Effective mislocalization in rapalog-treated cells and a steadily increasing accumulation of vesicles were observed ranging from 2.3 (S.D +/- 1.2) vesicles per parasite (vpp) at 2 h post induction to 6.3 (S.D +/- 4.7) vpp at 8 h post induction (Figure 12, Figure 13 and Appendix 1). Compared to the control with 1.3 (S.D +/- 1.4) vpp after 2 h post induction to 2.2 (S.D +/- 1.4) vpp after 8 h post induction. 1.3 (S.D +/- 1.0) vpp were observed for parasites before induction of the knock sideways (Figure 13).

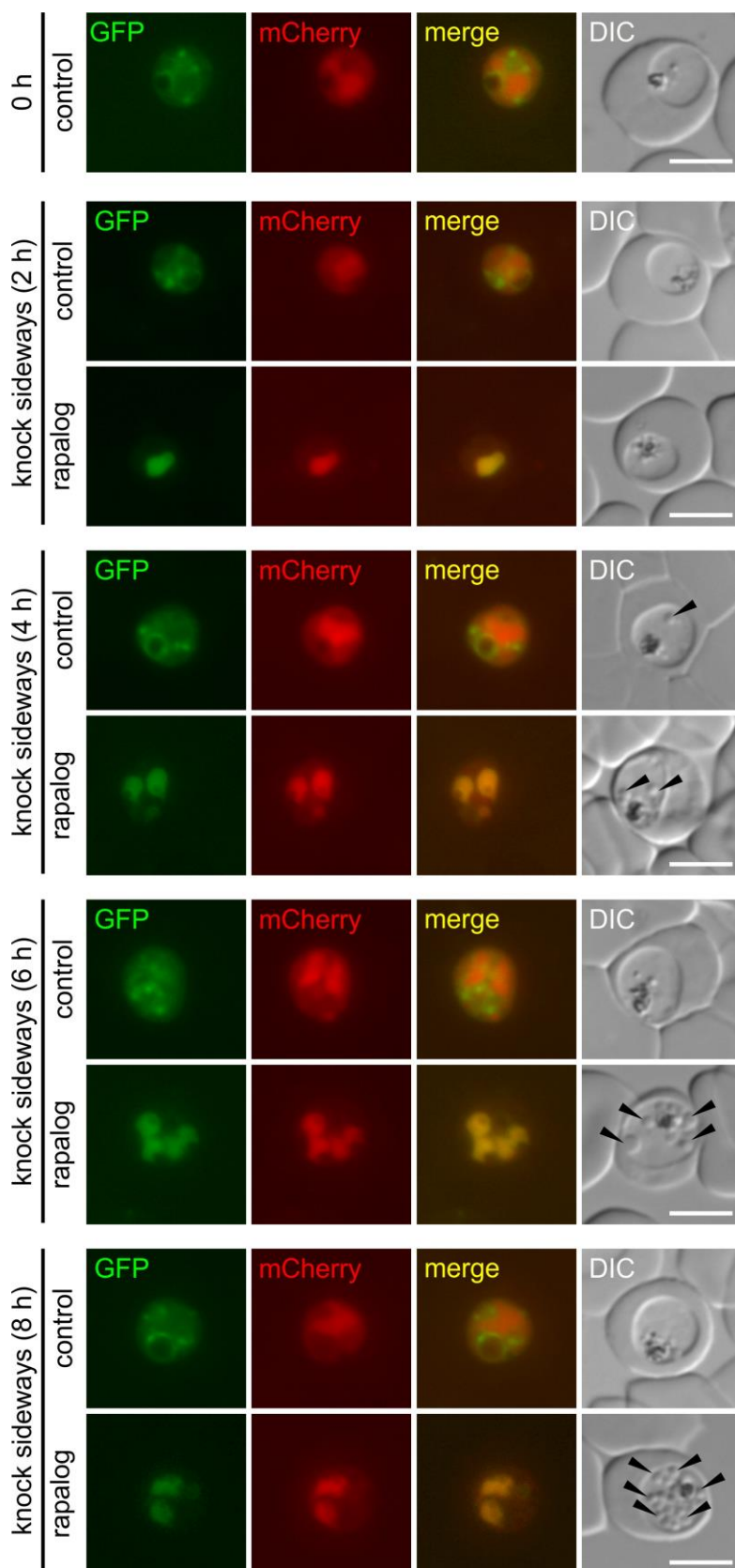


Figure 12: Rab5b vesicle accumulation assay.

Representative live cell images of cell line expressing endogenous *Pf*Rab5b fused to 2xFKBP-GFP-2xFKBP ('GFP') with an episomally expressed 1xNLS-FRB-mCherry mislocalizer ('mCherry'). The cell culture was split into two dishes: one served as control (control) without rapalog, and the second was grown in the presence of 250 nM rapalog (rapalog). The samples for live cell imaging were taken at the time points indicated. Black arrow heads indicate vesicles accumulating inside the parasite. Scale bars 5 μ m, DIC (differential interference contrast), merge (merged green and red channel).

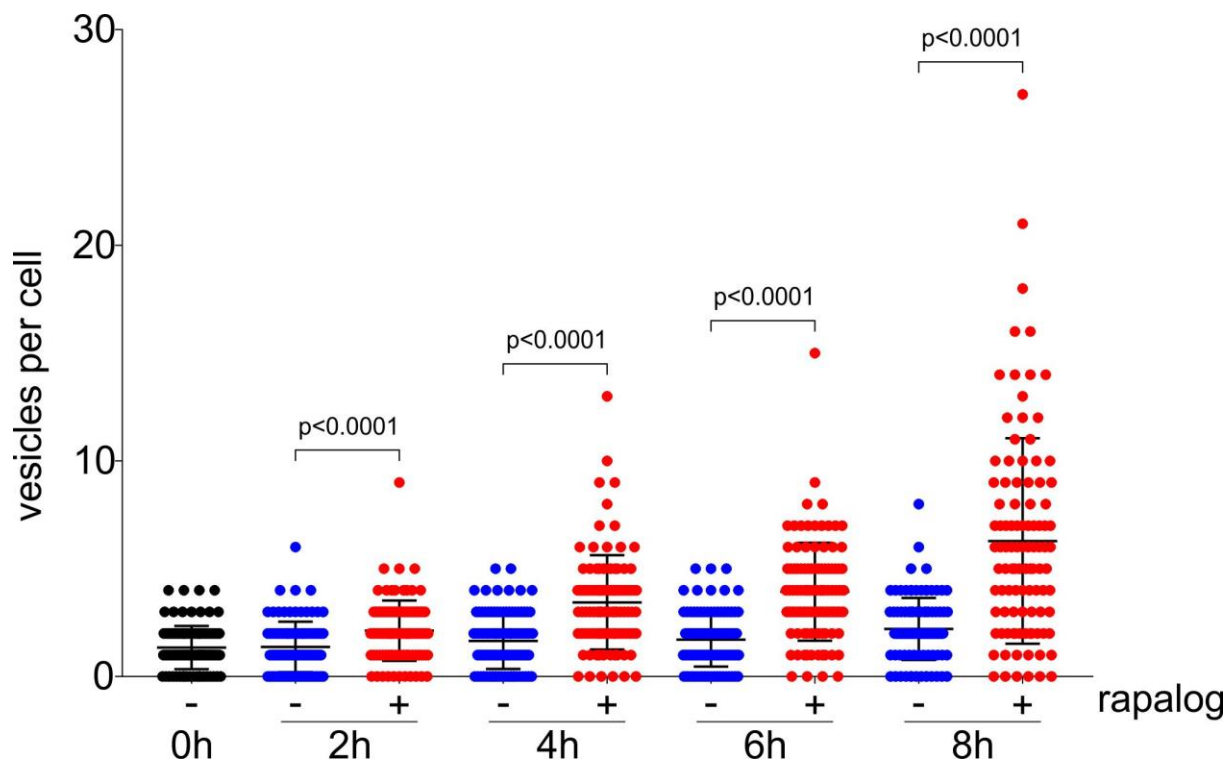


Figure 13: Rab5b vesicle accumulation assay (quantification).

The assay was performed with tightly (parasites synchronized to an 8 h time window) synchronized (trophozoite), parasite cell line expressing endogenous *PfRab5b* fused to 2xFKBP-GFP-2xFKBP with an episomally expressed 1xNLS-FRB-mCherry mislocalizer. Starting culture was split into two cultures, one grown in the presence of 250 nM rapalog (rapalog) and the other remained without rapalog (control). Samples were taken at the indicated time points (after KS induction) and the vesicle count was performed based on DIC images. The figure displays data from three pooled individual experiments with a total of 102 cells per time point and condition (individual replicas shown in Appendix 1). The rapalog and control conditions of every time point were significantly different from each other ($p < 0.001$, paired t-test). Error bars show S.D. and p stands for p-value.

Subsequently, it was investigated if Rab5b co-localizes with Kelch13. Kelch13 has recently been shown to be involved in endocytosis (Birnbaum et al., 2020) and Flemming co-localized *PfRab5b*-2xFKBP-GFP with an endosomal marker PI3P (P40-mCherry) (Flemming, 2015). For co-localization, Kelch13 was C-terminally tagged with mCherry and episomally expressed in the *PfRab5b*-2xFKBP-GFP-2xFKBP knock in cell line. In agreement with previous results (Birnbaum et al., 2017; Birnbaum et al., 2020), Kelch13-mCherry was localized at foci in close proximity to the parasite's FV (Figure 14, K13-mCherry). The co-localization experiment revealed that *PfRab5b*-2xFKBP-GFP-2xFKBP was present in foci within the cytosol and at the FV that did not co-localize with Kelch13-mCherry foci (Figure 14).

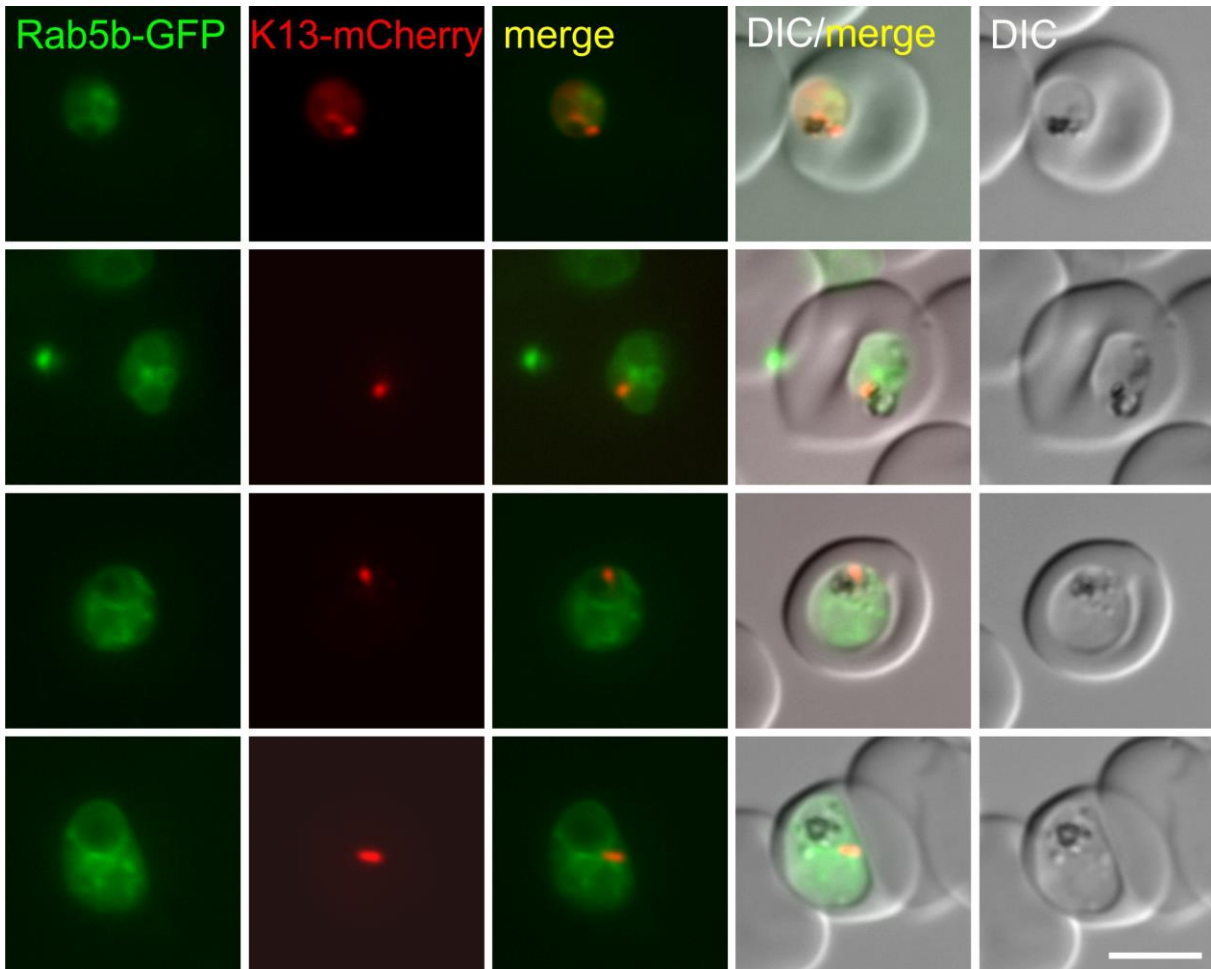


Figure 14: Rab5b does not co-localize with Kelch 13

Representative live cell images of cell line expressing endogenous PfRab5b fused to 2xFKBP-GFP-2xFKBP ('GFP') with an episomally expressed 1xNLS-FRB-mCherry mislocalizer ('mCherry'). PfRab5b-2xFKBP-GFP-2xFKBP does not co-localize with Kelch13-mCherry. Scale bar 5 μm , DIC (differential interference contrast), merge (merged green and red channel).

To show that *Pf*Rab5b is involved in endocytosis and the suspected vesicular-like structures in *Pf*Rab5b inactivated parasites, are intermediates of host cell cytosol uptake, derived from endocytosis, a bloated FV assay with E64 (Jonscher et al., 2019) was performed. E64 inhibits hemoglobin digestion inside the FV (Bailly et al., 1992; Sijwali et al., 2004). The addition of E64 led to bloated FVs in control cells after 8 h post induction (Figure 15 A, C and Appendix 2). In *Pf*Rab5b inactivated parasites, 79.4 % of parasites had no bloated FV (Figure 15 A, C and Appendix 2). Hence an inactivation of *Pf*Rab5b prevented the arrival of new host cell cytosol in the FV. Additionally, the cell size was determined to confirm that the absence of hemoglobin uptake and digestion does not arrest parasite development within the 8 h of the assay (Figure 15 B and Appendix 2). Even though parasites (grown in presence of rapalog) are slightly smaller, these parasites still grew over the 8 h assay time, demonstrating that parasite death is not the reason for the lack of transport of HCCU to the FV (Figure 15 B and Appendix 2).

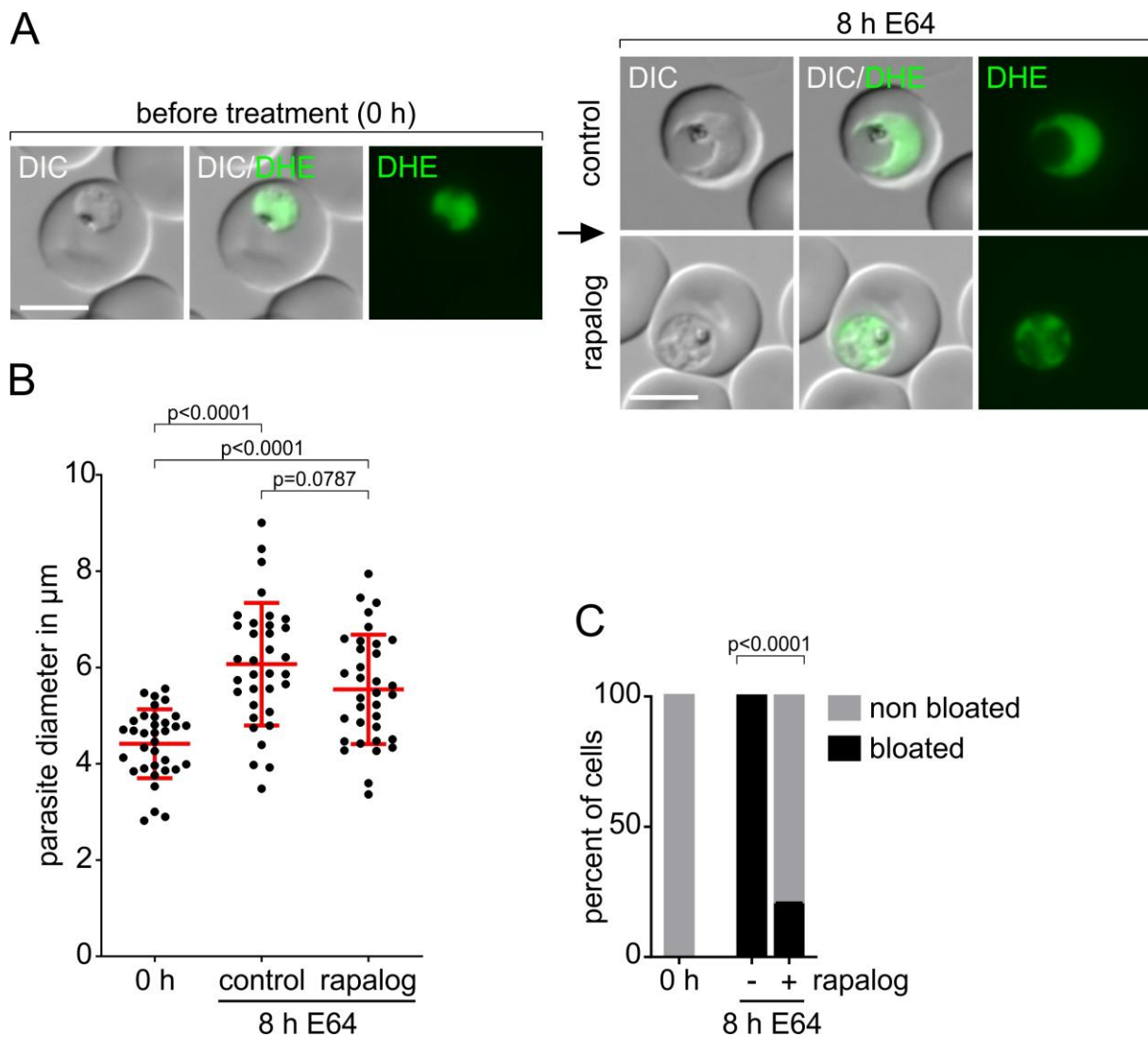


Figure 15: Rab5b bloated food vacuole assay.

A left) Representative live cell images of cell line expressing endogenous *PfRab5b* fused to 2xFKBP-GFP-2xFKBP ('GFP'), with an episomally expressed 1xNLS-FRB-mCherry mislocalizer, before treatment with E64 and rapalog. **A right)** Representative live cell images after 8 h knock sideways induced Rab5b cultures. For the experiment, a starting culture was treated with 33 μM E64 and split into two dishes. One culture stayed without rapalog (control), the other grown in the presence of 250 nM rapalog (rapalog). The cultures were incubated for 8 h. After incubation, the cytoplasm was stained with dihydroethidium (DHE) for live cell imaging. Scale bar 5 μm , DIC (differential interference contrast). **B)** Statistics of parasite diameter from the experiment shown in A). **C)** Quantification of bloated and non-bloated FVs from experiment shown in A). The figure shows one representative experiments of three independent experiments (replicas shown in Appendix 2). For all conditions, 34 cells were assessed per one experiment and significands were calculated using Fisher's exact test. Cell size was measured with ImageJ software, and p stands for p-value.

In order to determine that the *PfRab5b* knock sideways growth phenotype is specific and not caused by the presence of *PfRab5b*-2xFKBP-GFP-2xFKBP in the nucleus rather than its loss of function, the *PfRab5b*-2xFKBP-GFP-2xFKBP knock sideways cell line was complemented with an episomally expressed functional copy of *PfRab5b* (a codon adjusted *PfRab5b* fused to 2xmyc and expressed by virtue of a T2A skip peptide with 1xNLS-FRB-mCherry under the control of the *crt* promoter and selected with BSD -named plasmid *crt-PfRab5b* codonadjusted-2xmyc-T2A-1xNLS-FRB-mCherry-BSD^R). In a knock sideways growth

experiment the complementation construct restored parasite growth (Figure 16 A and Appendix 4). Additionally, the experiment revealed that rapalog had no effect on parasites, confirming what was previously shown (Birnbaum et al., 2017; Jonscher et al., 2019).

4.1.1.1 Single point mutations in Rab5b-GTPases

Rab5 GTPases have been shown to be involved in regulation of vesicular transport and component of intercellular membranes (Pfeffer, 1992). Several studies revealed that the cycling between GTP- and GDP bound forms are critical in Rab protein function (Becker et al., 1991; Tisdale et al., 1992; Walworth et al., 1992; Walworth et al., 1989). Mutations that introduced a strongly decreased (Q79L, GTP-bound) GTPase activity revealed unusual large early endosomal structures. Mutations that had a preferential affinity for GDP (S34N, p21 inhibitor) revealed accumulation of very small endocytic vesicles for S34N (Stenmark et al., 1994a). In order to further probe into the function of Rab5 GTPases in *P. falciparum* parasites, three different mutations were introduced into the *PfRab5b* complementation constructs (*crt-PfRab5b* codonadjusted-2xmyc-T2A-1xNLS-FRB-mCherry-BSD^R) resulting in three complementing *PfRab5b* versions containing the single point mutations S48N, N148I or Q94L. S48N and N148I should have a preferential affinity for GDP and Q94L should decrease GTP activity. The positions of the known GTPase- regulating single point mutations (Stenmark et al., 1994a) in humans were aligned to the genome of *P. falciparum* parasites and inserted to the predicted position (Appendix 3). The mutated constructs were co-transfected into the *PfRab5b*-2xFKBP-GFP-2xFKBP cell line resulting in three different complementation cell lines. Unexpectedly, all three mutated Rab5b versions were able to fully rescue the growth phenotype upon inactivation of the endogenous FKBP-tagged wild type Rab5b via knock sideways and no phenotype was detected by microscopy (Figure 16 B – D and Appendix 4). As the mislocalizer, which was co-expressed with the complementing *PfRab5b*, was efficiently expressed, a lack of expression of the complementing construct cannot explain this finding and it is also expected that this would have led to a growth phenotype.

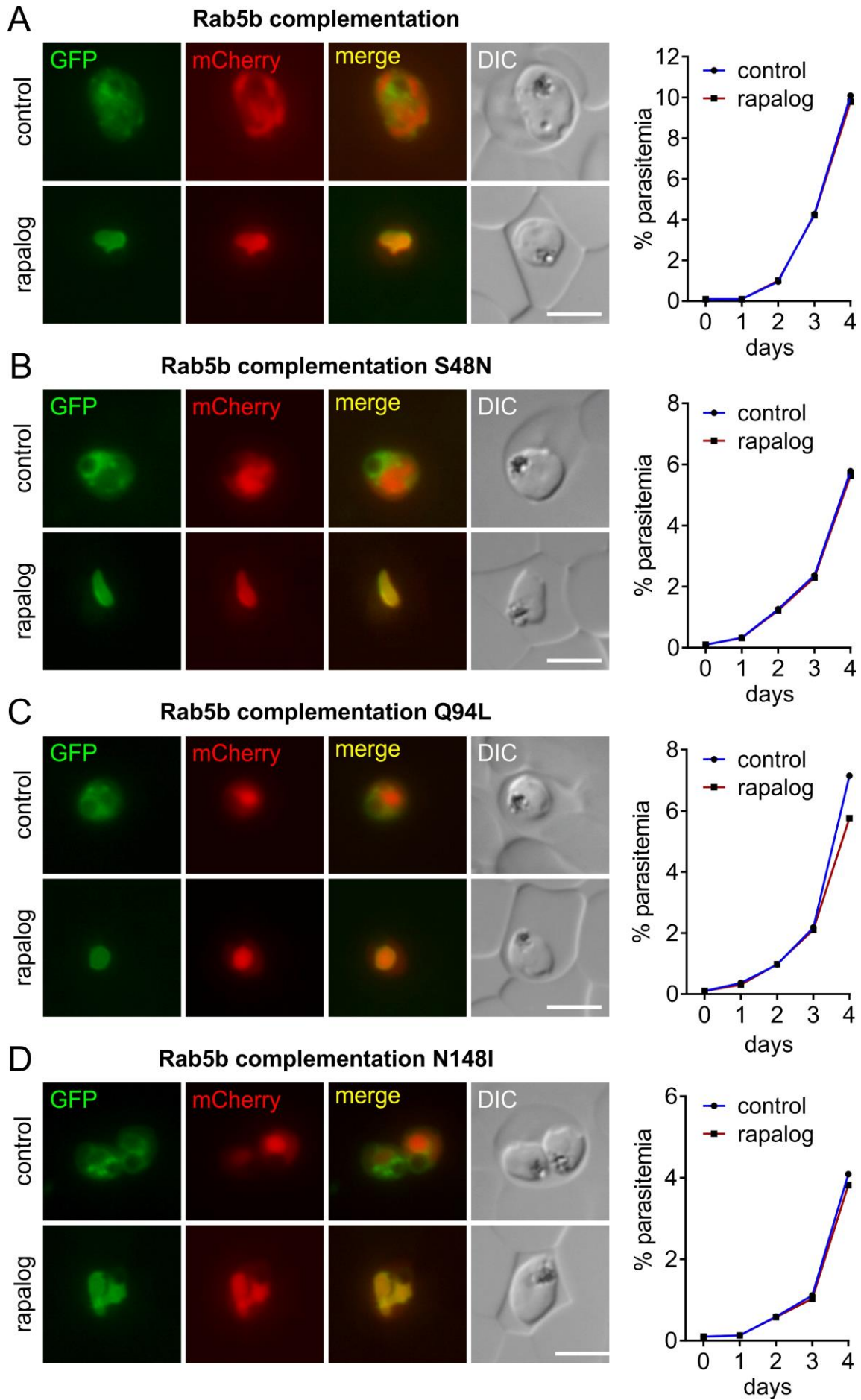


Figure 16: Rab5b complementation cell lines.

Representative live cell images of cell line expressing endogenous *Pf*Rab5b fused to 2xFKBP-GFP-2xFKBP ('GFP') with an episomally expressed copy of: A crt-Rab5b codonadjusted-2xmyc-T2A-1xNLS-FRB-mCherry-BSDR ('mCherry'), B) crt-Rab5b(S48N) codonadjusted-2xmyc-T2A-1xNLS-FRB-mCherry-BSDR ('mCherry'), C) crt-Rab5b(Q94L) codonadjusted-2xmyc-T2A-1xNLS-FRB-mCherry-BSDR ('mCherry') D) crt-Rab5b(N148I)codonadjusted-2xmyc-T2A-1xNLS-FRB-mCherry-BSDR ('mCherry'). The cell cultures were split into two dishes: one served as control (control) without rapalog, and the other was grown in the presence of 250 nM rapalog (rapalog). The samples for live cell imaging were taken after 21 h after induction of KS. Scale bars 5 μ m, DIC (differential interference contrast), merge (merged green and red channel). The graph to the right of the image panels shows parasite growth as determined by flow cytometry of the respective cell lines, showing parasite development grown in presence of rapalog (red line, rapalog) and rapalog untreated parasites (blue line, control) over five days (one representative experiment of three independent experiments (replicas shown in Appendix 3)).

4.1.2 Functional investigation of *P. falciparum* genes with unknown function

Beside the proof of principle analysis of *Pf*Rab5b, the 33 genes selected from chromosome 3 were endogenously tagged with 2xFKBP-GFP-2xFKBP by SLI using pSLI-sandwich (Birnbaum et al., 2017) for localization and functional analysis. In this work, 21 proteins of the 33 candidates were analyzed. The homology region (HR) for the genome knock-in using pSLI-sandwich varied from 437 to 957 bp in length for the analyzed target genes. To attempt gene disruptions, the pSLI-TGD plasmid was used (Birnbaum et al., 2017) and HR in the N-terminal part of the target gene was chosen that comprised between 273 up to 393 bp (Table 7).

Table 7: Candidates list for functional analysis.

The table shows the candidates which were selected for functional investigation. HR, homology region; bp, base pairs.

Protein ID	Assigned as	HR (bp)	Assigned as	HR (bp)	Gene length (bp)
PF3D7_0303100	M1 loc	723	M1 TGD	333	4326
PF3D7_0304300	M2 loc	747	M2 TGD	369	4290
PF3D7_0305200	M3 loc	957	M3 TGD	357	3420
PF3D7_0305400	M4 loc	573	M4 TGD	288	754
PF3D7_0305500	M5 loc	939	M5 TGD	372	11802
PF3D7_0306100	M6 loc	908	M6 TGD	348	2111
PF3D7_0307500	M7 loc	861	M7 TGD	359	1904
PF3D7_0307600	M8 loc	930	M8 TGD	362	2462
PF3D7_0307700	M9 loc	935	M9 TGD	300	6483
PF3D7_0307900	M10 loc	927	M10 TGD	342	11625
PF3D7_0308100	M11 loc	939	M11 TGD	393	5136
PF3D7_0308300	M12 loc	651	M12 TGD	273	1014
PF3D7_0308700	M13 loc	900	M13 TGD	291	1632

PF3D7_0308800	M14 loc	437	M14 TGD	332	473
PF3D7_0309900	M15 loc	909	M15 TGD	351	5440
PF3D7_0310900	M16 loc	618	M16 TGD	354	2361
PF3D7_0312900	M17 loc	648	M17 TGD	275	1232
PF3D7_0313000	M18 loc	632	M18 TGD	375	1184
PF3D7_0313200	M19 loc	684	M19 TGD	297	702
PF3D7_0313400	M20 loc	741	M20 TGD	300	2355
PF3D7_0314700	M24 loc	894	M24 TGD	321	3546

For pSLI-TGD six and for pSLI-sandwich, four individual integration attempts were performed respectively. Attempts were scored as failed, if no correct integration was achieved after 8 weeks of selection with G418 (selection for integrands). Correct integration was confirmed by PCR for 15 candidates for the pSLI-sandwich construct to localize the candidates and for subsequent functional studies. M2, M4, M5, M9, M14 and M15 were refractory to C-terminal tagging with 2xFKBP-GFP-2xFKBP-T2A-Neo^R, which might represent essential proteins that are inactivated by a C-terminal tag, even though this proportion was somewhat higher than reported previously (Birnbbaum et al., 2017). For the pSLI-TGD, knock-ins only M12 was confirmed by PCR (Figure 17). In case of correct integration by pSLI-TGD, the gene was considered as dispensable for parasite growth. For one candidate, an intermediate culture, with parasites expressing endogenous M3 fused to pSLI-TGD and parasites with wild type ('original') locus was observed (Figure 17, M3_TGD).

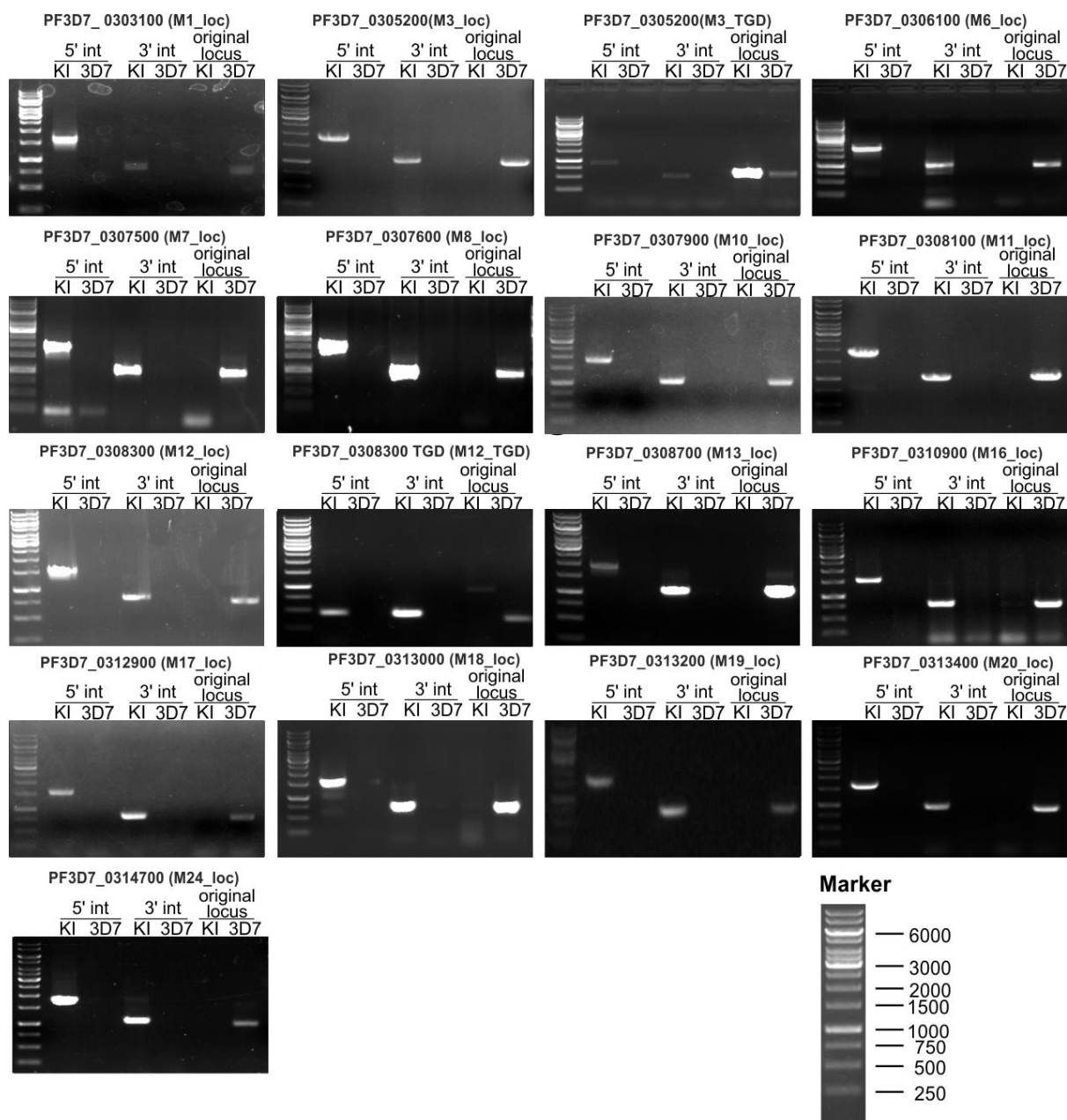


Figure 17: PCR diagnostics to confirm correct integration of the plasmid into the desired region of the genome.

PCR products from genomic parasite DNA of the cell lines (indicated by candidates-IDs are shown above the agarose gels) were applied and separated using agarose gel electrophoresis. Primers used are as postulated for the SLI method (depicted in Figure 1 from (Birnbbaum et al., 2017)), demonstrating a PCR product across 5' and 3' integration junction indicated by bands in lanes labelled 5' int and 3' int, as well as quantitative absence of original locus ('original locus'). No band at the lane labeled with 'original locus' confirms that no parasites with wild type locus remained in the cell culture. The band at original locus 3D7 serves as control. Shown right at the bottom (**Marker**), shows marker bands which are indicated in bp of the 1kb DNA ladder and can be used as guide for the markers in the gel images with the PCR products; knock-in cell line (KI), wild type parasite line (3D7), target gene disruption using pSLI-TGD vector (TGD), gene tagging using pSLI-sandwich (loc).

4.2 Candidate M1 (PF3D7_0303100)

M1 (PF3D7_0303100) is a protein predicted as a putative CLP1 P-loop domain-containing protein, and consists of 1441 AA (according to: PlasmoDB (Aurrecochea et al., 2009)). BLAST search (Altschul et al., 1990) revealed no significant similarity (e-value ≥ 9.9) outside Apicomplexa, and a motif scan with MyHits (Pagni et al., 2004) showed no significant hit. Using the HHPred server for protein remote homology detection and 3D structure prediction (HHPred) to identify more remote relationships to known proteins or domains (Zimmermann et al., 2018) the best hit, with a putative similarity (HHPred probability score $\geq 95\%$) to M1 was a ribonuclease, polynucleotide kinase domain in *Chaetomium thermophilum*. In a saturation-based mutagenesis screen (Zhang et al., 2018) M1 was classified as dispensable for growth similarly the orthologue protein in *P. berghei* parasites was identified as non-essential for growth (Bushell et al., 2017).

To analyze M1, the corresponding gene product was tagged with 2xFKBP-GFP-2xFKBP by modification of the endogenous locus using SLI. Correct integration of the pSLI plasmid resulting in the M1-2xFKBP-GFP-2xFKBP knock-in was confirmed by PCR (Figure 17), whereas no correct integration could be achieved for the corresponding pSLI-TGD plasmid. Microscopy with the M1-2xFKBP-GFP-2xFKBP cell line revealed detectable fluorescence signal from early trophozoite to schizont stage on, whereas no fluorescence was detectable in ring stage parasites. M1-2xFKBP-GFP-2xFKBP was found distributed in the cytoplasm of the parasite with additional non-uniform foci and accumulations that in some parasites localized at the parasite plasma membrane (PPM) or the FV (Figure 18).

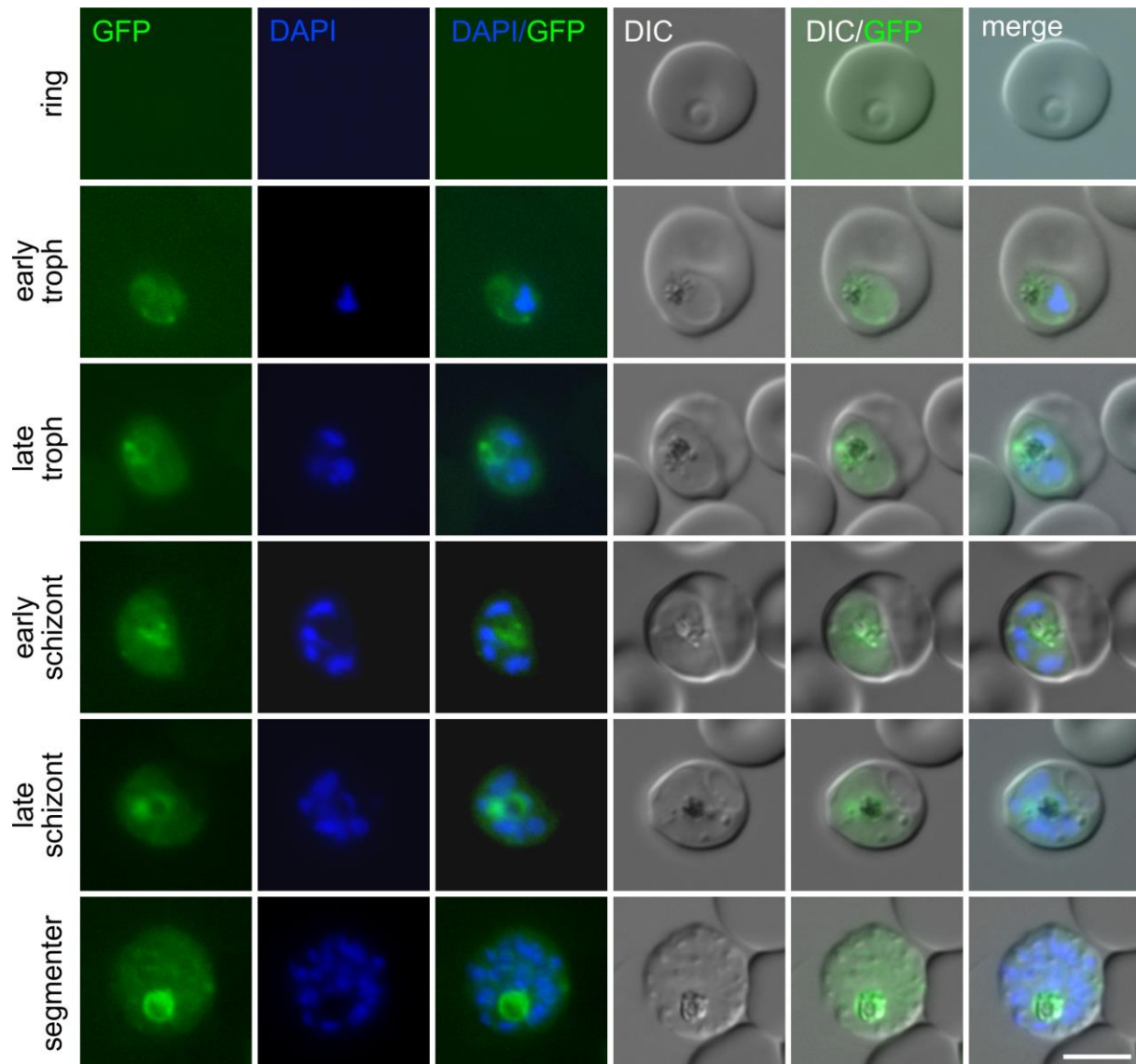


Figure 18: Localization of endogenously tagged candidate M1 (PF3D7_0303100).

Representative live cell images ($n \geq 3$ fluorescence microscopy sessions, with at least 20 inspected cells per session) of knock-in cell line M1-2xFKBP-GFP-2xFKBP ('GFP'). The stages are indicated on the left of the panel. Parasite nuclei were stained with DAPI. Scale bar 5 μm , DIC (differential interference contrast).

To functionally analyze M1, the M1-2xFKBP-GFP-2xFKBP cell line was co-transfected with an episomally expressed 1xNLS-FRB-mCherry mislocalizer (Birnbaum et al., 2017) (Figure 19 panel) and knock sideways was carried out. This revealed that M1 was efficiently mislocalized to the nucleus 24 h after addition of rapalog to induce the knock sideways (Figure 19 panel). However, growth analysis over five days showed no effect on parasite growth in the parasites with the inactivated M1 compared to the control (Figure 19 growth curve, and Appendix 5). In conclusion the knock sideways reveals that M1 is dispensable for growth of asexual blood stage parasites.

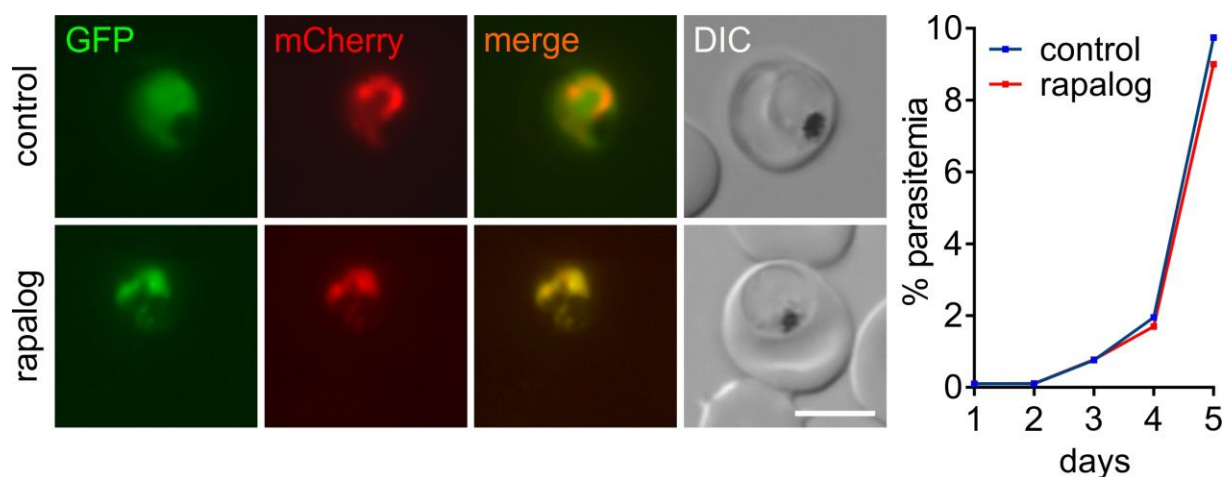


Figure 19: Knock sideways and growth curve of endogenously tagged candidate M1 (PF3D7_0303100).

Panel) Representative live cell images ($n \geq 3$ fluorescence microscopy sessions, with at least 20 inspected cells per session) of knock-in cell line M1-2xFKBP-GFP-2xFKBP (“GFP”) with an episomally expressed 1xNLS-FRB-mCherry mislocalizer. The cell culture was split into two dishes: one served as control without rapalog (control), and the other grown in the presence of 250 nM rapalog (rapalog). The samples for live cell imaging were taken 24 h post addition of rapalog. Scale bar 5 μm , DIC (differential interference contrast). **The graph to the right of the image panels** shows parasite growth as determined by flow cytometry of the M1-2xFKBP-GFP-2xFKBP knock sideways parasites grown in the presence of rapalog (inactivated) and without rapalog (control). One representative of three independent experiments (replicas shown in Appendix 5).

4.3 Candidate M2 (PF3D7_0304300)

The M2 (PF3D7_0304300) protein comprises 1429 AA and is annotated as conserved *Plasmodium* protein, with unknown function (according to: PlasmoDB (Aurrecochea et al., 2009)). BLAST search (Altschul et al., 1990) revealed no significant similarity outside Apicomplexa, and a motif scan with MyHits (Pagni et al., 2004) showed no significant hit. Using HHPred to identify more remote relationships to known proteins or domains (Zimmermann et al., 2018), only hits over short stretches or to common structural domains, such as coiled coils were found. In the saturation-based mutagenesis screen (Zhang et al., 2018) M2 was classified as dispensable for parasite growth. In contrast the orthologue protein in *P. berghei* parasites (Bushell et al., 2017) was annotated as essential for parasite growth. Attempts to disrupt the gene, using pSLI-TGD were not successful. Also, endogenous C-terminal tagging with 2xFKBP-GFP-2xFKBP was unsuccessful in four independent attempts, indicating that C-terminal tagging of M2 might interfere with correct protein function or localization. This protein was therefore not further analyzed.

4.4 Candidate M3 (PF3D7_0305200)

M3 (PF3D7_0305200) is annotated as conserved *Plasmodium* protein with unknown function (according to: PlasmoDB (Aurrecochea et al., 2009)). The protein consists of 1139 AA, and BLAST search (Altschul et al., 1990) revealed no significant similarity with any protein

outside Apicomplexa. A motif scan with MyHits (Pagni et al., 2004) showed a GRIP domain in position 1084 - 1135 (e-value: 0.00042) which plays a role in Golgi trafficking (Barr, 1999; Munro et al., 1999). The best hit using HHPred (Zimmermann et al., 2018) with a putative similarity to M3 was a myosin domain in *Gallus gallus*. In the saturation-based mutagenesis screen (Zhang et al., 2018) M3 was classified as dispensable for parasite growth, whereas the orthologue protein in *P. berghei* parasites (Bushell et al., 2017) was annotated as essential for growth.

To analyze M3, the corresponding gene product was tagged with 2xFKBP-GFP-2xFKBP by modification of the endogenous locus using SLI. Correct integration of the pSLI plasmid resulting in the M3-2xFKBP-GFP-2xFKBP knock-in was confirmed by PCR (Figure 17). Parasites with a successful disruption of the gene coding for M3 were obtained, but verification of correct integration of the plasmid in these parasites revealed that some parasites in the population still contained the intact locus (Figure 17 M3_TGD). As judged by PCR, the parasites with the disrupted locus disappeared after repeated selection on WR99210 and G418 (neomycin), a procedure typically leading to the opposite effect and employed to obtain clean disruption lines (Figure 17).

Microscopy with the M3-2xFKBP-GFP-2xFKBP cell line revealed fluorescence detectable levels from ring to segmenter stages. In ring stages, M3-2xFKBP-GFP-2xFKBP was visible uniformly distributed in the cytoplasm with a single accumulation (Figure 20). From trophozoite to the segmented schizont stage the cytoplasmic localization remained together with several foci that increase steadily in number with continued development in the asexual cycle were observed. The foci were frequently, but not always, in proximity but not overlapping with the nuclei (Figure 20). Nuclei typically had one or two foci of M3-2xFKBP-GFP-2xFKBP associated, potentially indicating a Golgi or secretory pathway location.

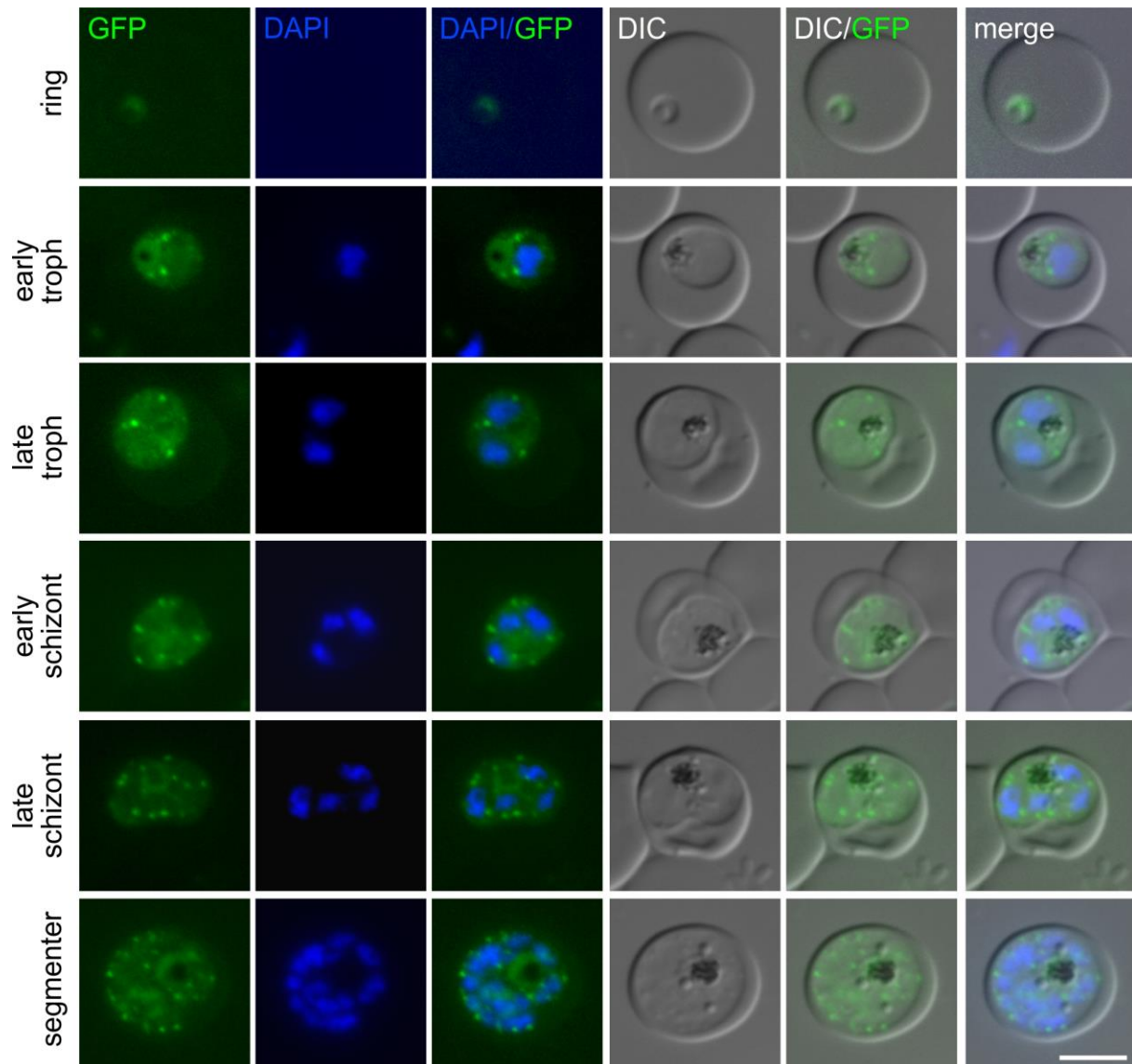


Figure 20: Localization of endogenously tagged candidate M3 (PF3D7_0305200).

Representative live cell images ($n \geq 3$ fluorescence microscopy sessions, with at least 20 inspected cells per session) of knock-in cell line M3-2xFKBP-GFP-2xFKBP ('GFP'). The stages are indicated on the left of the panel. Parasite nuclei were stained with DAPI. Scale bar 5 μm , DIC (differential interference contrast).

To functionally analyze M3, the M3-2xFKBP-GFP-2xFKBP cell line was co-transfected with an episomally expressed 1xNLS-FRB-mCherry mislocalizer (Birnbaum et al., 2017) (Figure 21 panel) and knock sideways was carried out. This revealed that M3 was efficiently mislocalised to the nucleus 24 h after addition of rapalog to induce the knock sideways (Figure 22 panel). Growth analysis over five days showed growth defect on parasite growth in the parasites with the inactivated M3 compared to the control (Figure 21 growth curve, and Appendix 5). Together with the failure to obtain a clean SLI-TGD line for M3, this suggests that M3 has some importance for efficient parasite growth in the asexual blood stage.

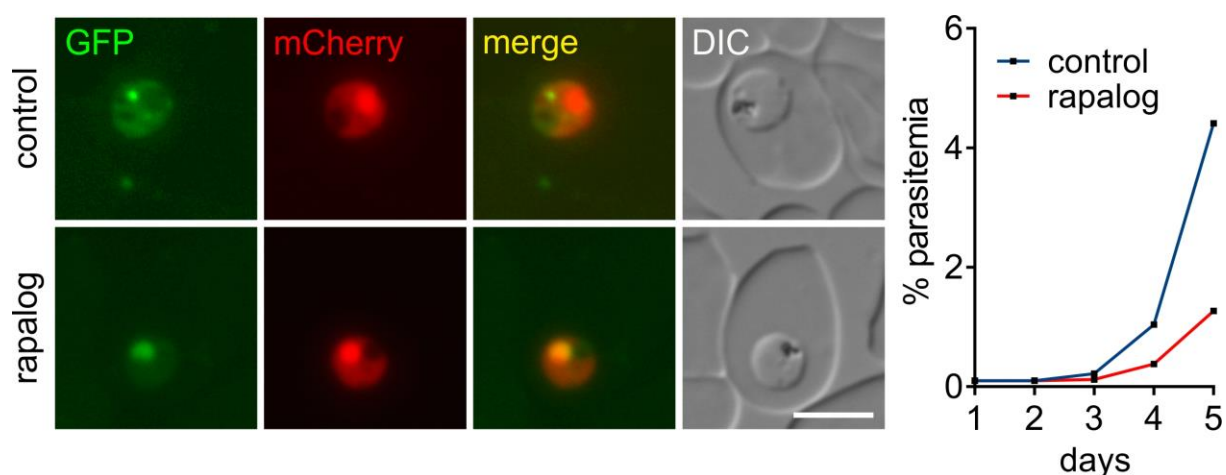


Figure 21: Knock sideways and growth curve of endogenously tagged candidate M3 (PF3D7_0305200).

Panel) Representative live cell images ($n \geq 3$ fluorescence microscopy sessions, with at least 20 inspected cells per session) of knock-in cell line M3-2xFKBP-GFP-2xFKBP (“GFP”) with an episomally expressed 1xNLS-FRB-mCherry mislocalizer. The cell culture was split into two dishes: one served as control without rapalog (control), and the other grown in the presence of 250 nM rapalog (rapalog). The samples for live cell imaging were taken 24 h post addition of rapalog. Scale bar 5 μm , DIC (differential interference contrast). **The graph to the right of the image panels** shows parasite growth as determined by flow cytometry of the M3-2xFKBP-GFP-2xFKBP knock sideways parasites grown in the presence of rapalog (inactivated) and without rapalog (control). One representative of three independent experiments (replicas shown in Appendix 5).

4.5 Candidate M4 (PF3D7_0305400)

M4 (PF3D7_0305400) is annotated as conserved protein with unknown function and is composed of 145 AA (according to: PlasmoDB (Aurrecochea et al., 2009)). BLAST search (Altschul et al., 1990) revealed a homology to an insulinase family protein (e-value: $3e-14$, percent identity: 26 %) in *Desulfovibrio hydrothermalis*. A motif scan with MyHits (Pagni et al., 2004) showed no significant homology. Using HHPred (Zimmermann et al., 2018), only hits over short stretches or to common structural domains, such as coiled coils were found. In the saturation-based mutagenesis screen (Zhang et al., 2018), M4 was classified as essential for parasite growth, similarly the orthologue protein in *P. berghei* parasites was identified as essential for parasite growth (Bushell et al., 2017). Attempts to disrupt the gene, using pSLI-TGD were not successful. Also, endogenously C-terminal tagging with 2xFKBP-GFP-2xFKBP was unsuccessful in four independent attempts, indicating that C-terminal tagging of M4 might interfere with correct protein function or localization. This protein was therefore not further analysed.

4.6 Candidate M5 (PF3D7_0305500)

M5 (PF3D7_0305500) comprises 3933 AA and is annotated as conserved *Plasmodium* protein with unknown function (according to: PlasmoDB (Aurrecochea et al., 2009)). BLAST search (Altschul et al., 1990) revealed no significant similarity outside the

Apicomplexa, and a motif scan with MyHits (Pagni et al., 2004) showed no significant hit. Using HHPred (Zimmermann et al., 2018), only hits over short stretches or to common structural domains, such as coiled coils were found. In the saturation-based mutagenesis screen (Zhang et al., 2018) M5 was classified as essential for parasite growth. Similarly the orthologue protein in *P. berghei* parasites was identified as essential for parasite growth (Bushell et al., 2017). Attempts to disrupt the gene, using pSLI-TGD were not successful. Also, endogenously C-terminal tagging with 2xFKBP-GFP-2xFKBP was unsuccessful in four independent attempts indicating that C-terminal tagging of M5 might interfere with correct protein function or localization. This protein was therefore not further analyzed.

4.7 Candidate M6 (PF3D7_0306100)

M6 (PF3D7_0306100) is annotated as conserved protein with unknown function and comprises 628 AA (according to: PlasmoDB (Aurrecochea et al., 2009)). BLAST search (Altschul et al., 1990) revealed no significant similarity to other organisms outside Apicomplexa, and a motif scan with MyHits (Pagni et al., 2004) showed no significant hit. Using HHPred (Zimmermann et al., 2018), only hits over short stretches or to common structural domains, such as coiled coils were found. In the saturation-based mutagenesis screen (Zhang et al., 2018), M6 was classified as essential for parasite growth, similarly the orthologue protein in *P. berghei* parasites was identified as essential for parasite growth (Bushell et al., 2017).

To analyze M6, the corresponding gene product was tagged with 2xFKBP-GFP-2xFKBP by modification of the endogenous locus using SLI. Correct integration of the pSLI plasmid resulting in the M6-2xFKBP-GFP-2xFKBP knock-in was confirmed by PCR (Figure 17), whereas no correct integration could be achieved for the corresponding pSLI-TGD plasmid. Microscopy with the M6-2xFKBP-GFP-2xFKBP cell line revealed detectable fluorescence signal of M6-2xFKBP-GFP-2xFKBP in all asexual parasite stages. The protein located to the nucleus where it was uniformly distributed (Figure 22).

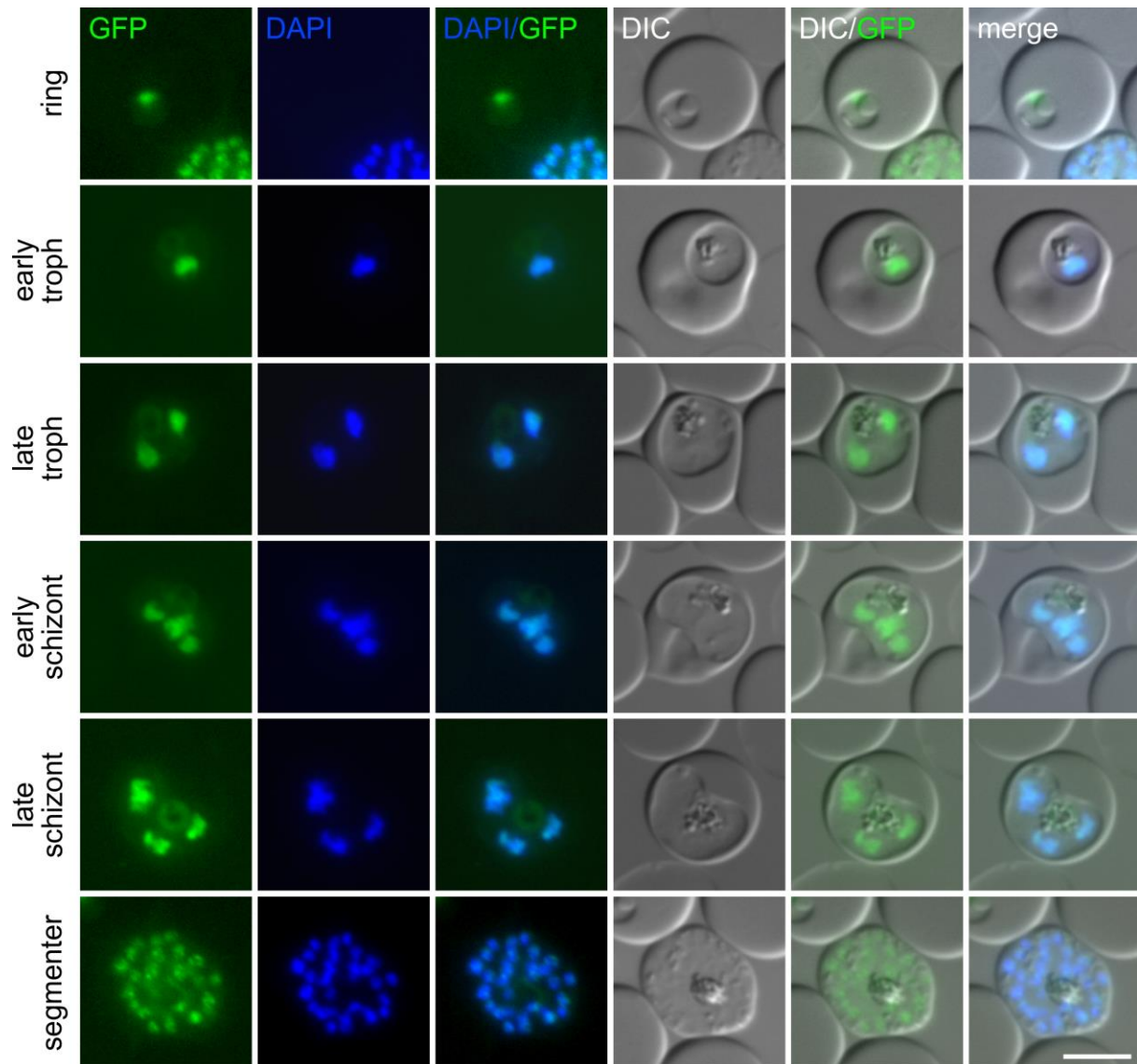


Figure 22: Localization of endogenously tagged candidate M6 (PF3D7_0306100).

Representative live cell images ($n \geq 3$ fluorescence microscopy sessions, with at least 20 inspected cells per session) of knock-in cell line M6-2xFKBP-GFP-2xFKBP ('GFP'). The stages are indicated on the left of the panel. Parasite nuclei were stained with DAPI. Scale bar 5 μm , DIC (differential interference contrast).

To functionally analyze M6, the M6-2xFKBP-GFP-2xFKBP cell line was co-transfected with an episomally expressed lyn-FRB-mCherry mislocalizer for mislocalization to the PPM (Birnbaum et al., 2017) (Figure 23 panel) and knock sideways was carried out. Inspection of the cells after induction of the knock sideways revealed that the mislocalization was incomplete 24 h after inducing in the parasites with the inactivated M6. In addition, reverse localization from mislocalizer into the nucleus was also observed (Figure 23 panel). Hence, the knock sideways achieved only a partial inactivation. Growth analysis over five days showed no effect on parasite growth in the parasites with the inactivated M6 compared to the control which may be due to the insufficient mislocalization (Figure 23 growth curve, and

Appendix 5). In conclusion it is unclear if the M6 protein is important for growth of asexual blood stage parasites.

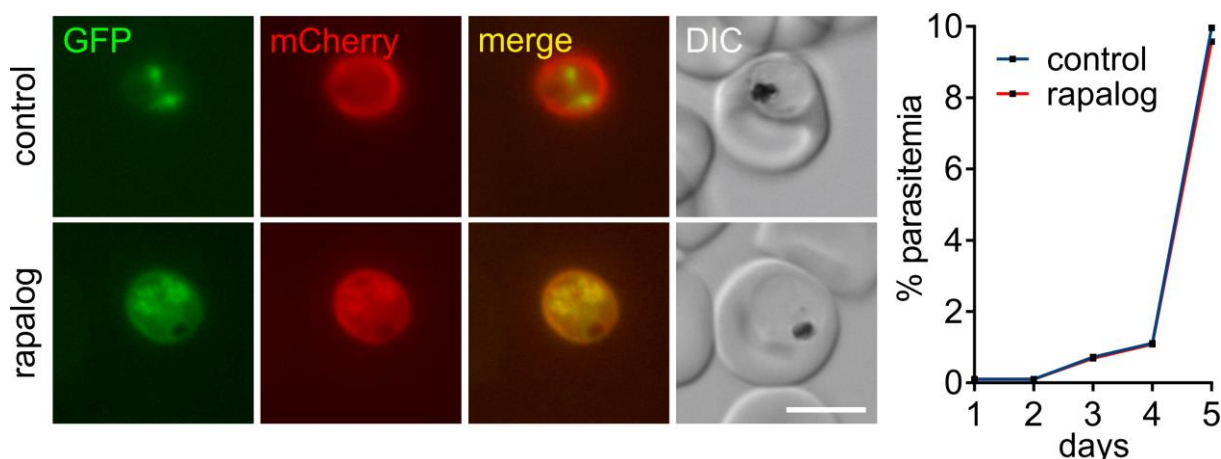


Figure 23: Knock sideways and growth curve of endogenously tagged candidate M6 (PF3D7_0306100).

Panel) Representative live cell images ($n \geq 3$ fluorescence microscopy sessions, with at least 20 inspected cells per session) of knock-in cell line M6-2xFKBP-GFP-2xFKBP ('GFP') with an episomally expressed lyn-FRB-mCherry mislocalizer. The cell culture was split into two dishes: one served as control without rapalog (control), and the other grown in the presence of 250 nM rapalog (rapalog). The samples for live cell imaging were taken 24 h post addition of rapalog. Scale bar 5 μ m, DIC (differential interference contrast). **The graph to the right of the image panels** shows parasite growth as determined by flow cytometry of the M6-2xFKBP-GFP-2xFKBP knock sideways parasites grown in the presence of rapalog (inactivated) and without rapalog (control). One representative of three independent experiments (replicas shown in Appendix 5).

4.8 Candidate M7 (PF3D7_0307500)

M7 (PF3D7_0307500) was annotated as conserved protein with unknown function (according to: PlasmoDB, release 31 (Aurrecochea et al., 2009)). During the analysis of this protein the name was changed to spindle and kinetochore-associated protein 2, putative (according to: PlasmoDB, release 46 (Aurrecochea et al., 2009)). The protein comprises 389 AA and a BLAST search (Altschul et al., 1990) revealed a similarity to an uncharacterized protein DBB from 1 – 346 AA in *Piliocolobus tephosceles* (e-value $3e-80$, percent identity: 49 %). A motif scan with MyHits (Pagni et al., 2004) showed no significant hit. The top hits using HHpred (Zimmermann et al., 2018), revealed putative similarities of M7 to the *Homo sapiens* spindle and kinetochore-associated protein 3 and spindle and kinetochore-associated protein 1. The saturation-based mutagenesis screen (Zhang et al., 2018), classified M7 as essential for parasite growth. Similarly the orthologue protein in *P. berghei* parasites was identified as essential for parasite growth.

To analyze M7, the corresponding gene product was tagged with 2xFKBP-GFP-2xFKBP by modification of the endogenous locus using SLI. Correct integration of the pSLI plasmid resulting in the M7-2xFKBP-GFP-2xFKBP knock-in was confirmed by PCR (Figure 17), whereas no correct integration could be achieved for the corresponding pSLI-TGD plasmid. Microscopy with the M7-2xFKBP-GFP-2xFKBP cell line revealed detectable expression of

M7-2xFKBP-GFP-2xFKBP from young trophozoites to segmenter stages at the end of the cycle (Figure 24). The protein was uniform, located in one (Figure 24) or two foci (Figure 24 arrow head) close to the outer part of the nucleus more often towards the PPM. The M7-2xFKBP-GFP-2xFLBP foci multiplied with the number of nuclei. The outer part of the nuclei typically had one and sometimes two foci (Figure 24 arrow head) of M7-2xFKBP-GFP-2xFKBP associated, might indicating a nuclear membrane location.

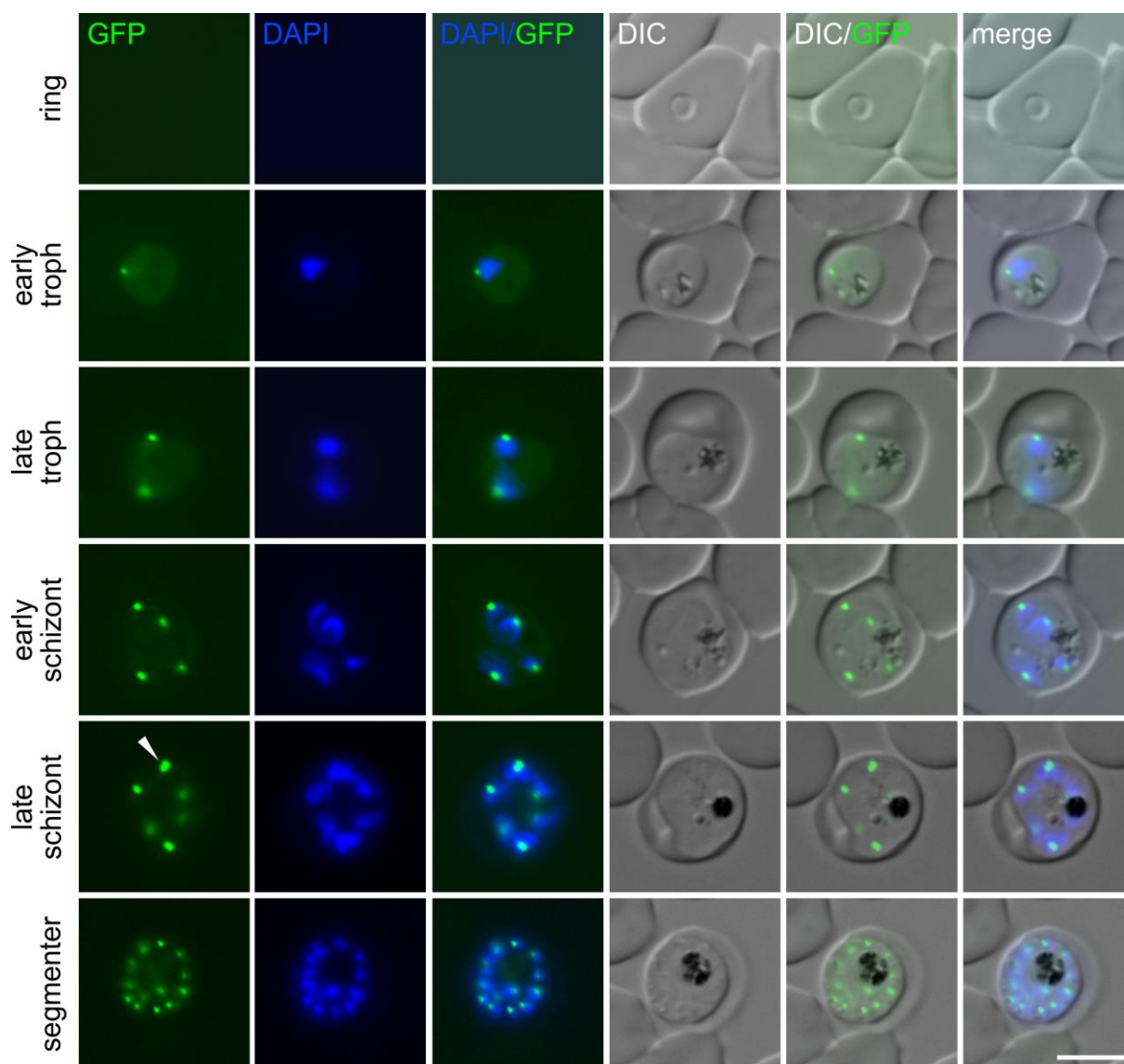


Figure 24: Localization of endogenously tagged candidate M7 (PF3D7_0307500).

Representative live cell images ($n \geq 3$ fluorescence microscopy sessions, with at least 20 inspected cells per session) of knock-in cell line M7-2xFKBP-GFP-2xFKBP ('GFP'). The stages are indicated on the left of the panel. Parasite nuclei were stained with DAPI. Scale bar 5 μm , DIC (differential interference contrast).

To functionally analyse M7, the M7-2xFKBP-GFP-2xFKBP cell line was co-transfected with an episomally expressed lyn-FRB-mCherry mislocalizer (Birnbbaum et al., 2017) (Figure 26 panel) and knock sideways was carried out. This revealed that M7 was efficiently mislocalised 24 h after addition of rapalog to induce the knock sideways (Figure 25 panel). Growth analysis over five days showed severe growth defect on parasite growth in the parasites with the inactivated M7 compared to the control (Figure 25 growth curve, and Appendix 5). Together with the failure to obtain a SLI-TGD line for M7, this suggests that M7 has importance for efficient parasite growth in the asexual blood stage.

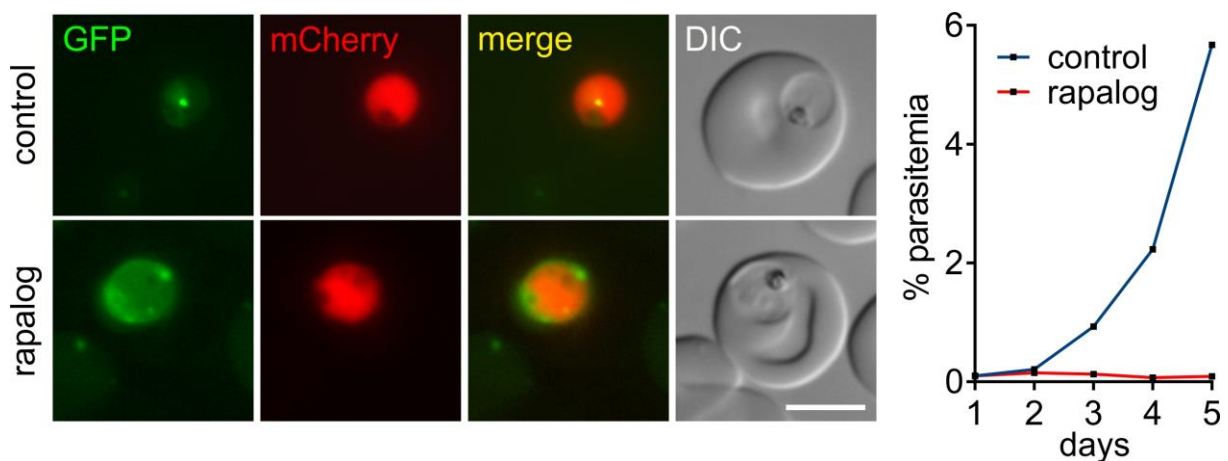


Figure 25: Knock sideways and growth curve of endogenously tagged candidate M7 (PF3D7_0307500).

Panel) Representative live cell images ($n \geq 3$ fluorescence microscopy sessions, with at least 20 inspected cells per session) of knock-in cell line M7-2xFKBP-GFP-2xFKBP ('GFP') with an episomally expressed lyn-FRB-mCherry mislocalizer. The cell culture was split into two dishes: one served as control without rapalog (control), and the other grown in the presence of 250 nM rapalog (rapalog). The samples for live cell imaging were taken 24 h post addition of rapalog. Scale bar 5 μ m, DIC (differential interference contrast). **The graph to the right of the image panels** shows parasite growth as determined by flow cytometry of the M7-2xFKBP-GFP-2xFKBP knock sideways parasites grown in the presence of rapalog (inactivated) and without rapalog (control). One representative of three independent experiments (replicas shown in Appendix 5).

Initial localization of M7-2xFKBP-GFP-2xFKBP indicated close localization at the outer part of the nucleus often facing PPM. To understand how M7 behaved in relation to the parasite nucleus, confocal time lapse imaging was performed to get spatio-temporal information. The M7-2xFKBP-GFP-2xFKBP cell line therefore was co-transfected with an episomally expressed 3xNLS-FRB-mcherry plasmid (Birnbbaum et al., 2017) to see the nucleus during time lapse imaging. For confocal time lapse imaging The M7-2xFKBP-GFP-2xFKBP with an episomally expressed 3xNLS-FRB-mcherry parasites were synchronized with sorbitol to a time window of 8 h, coated on an Ibidi dish with a bottom suitable for microscopy and imaged at the confocal microscope under culture conditions as described (Grüring et al., 2011). Parasites were imaged every 20 min using the 488 nM and 559 nM laser lines. M7-2xFKBP-GFP-2xFKBP is displayed in green and the nucleus in red (Figure 26). Time lapse imaging of M7-2xFKBP-GFP-2xFKBP with an episomally expressed 3xNLS-FRB-mcherry

plasmid over a time frame of 100 min, showed M7-2xFKBP-GFP-2xFKBP from 0 min to 40 min, in a focus at the outer part of the nucleus (Figure 26, 20 min to 40 min). From 20 min to 40 min M7-2xFKBP-GFP-2xFKBP fluorescence signal seemed to be brighter in comparison to the M7-2xFKBP-GFP-2xFKBP fluorescence signal at the 0 min time point (Figure 26, 0 min, 20 min, 40 min). After 60 min one nucleus was seen with two M7-2xFKBP-GFP-2xFKBP foci (Figure 26, 60 min). The M7-2xFKBP-GFP-2xFKBP foci seemed to have migrated to opposite directions at the outer part of the nucleus (Figure 26, 60 min to 100 min). At time point 100 min two individual nuclei were seen with each one M7-2xFKBP-GFP-2xFKBP foci at the outer part of the nucleus (Figure 26, 100 min). These experiments might indicate an association of M7 separation with the division of the nucleus.

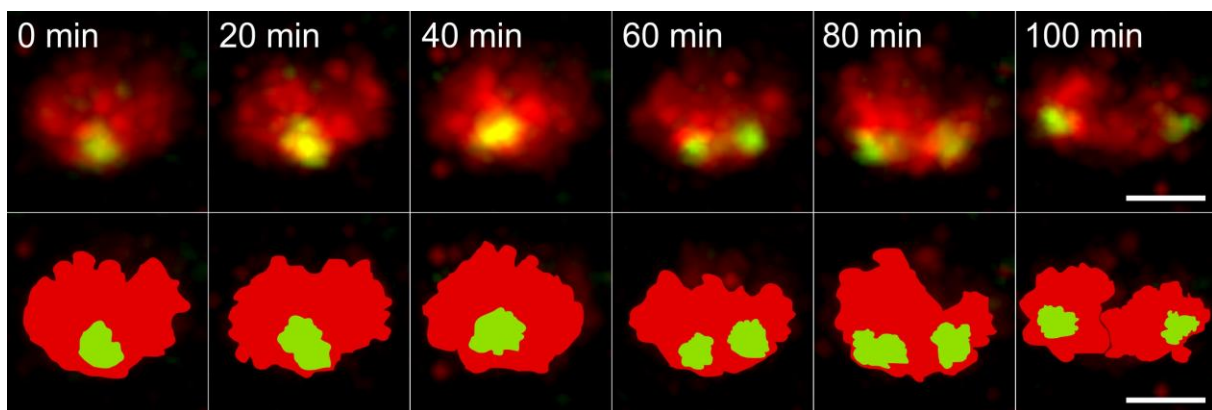


Figure 26: Candidate M7 (PF3D7_0307500) confocal time lapse imaging.

Top row) Representative confocal live cell images ($n \geq 3$ confocal time lapse imaging sessions, with at least 8 inspected cells per session) of M7-2xFKBP-GFP-2xFKBP cell line (green) with an episomally expressed 3xNLS-FRB-mCherry plasmid (red). The images show maximum intensity projections of 3D reconstructions of the merged green and red signal. Additionally, the Gaussian filter of the Imaris software was applied for image processing. The images were taken every 20 min (time points labeled above the pictures) over a time frame of 100 min. **Bottom row**) Schematic model (not representative results) of top row confocal images. The images are color codes of the 3D max projection transferred to 2D schematics. Scale bars 5 μm .

Due to the localization of M7-2xFKBP-GFP-2xFKBP, the apparent separation of M7 foci with nuclear division in the confocal time lapse imaging and the predicted homology to the human protein SKA2 (according to: HHPred (Zimmermann et al., 2018)), it is possible that M7 is the parasite orthologue of SKA2. To better assess this, appropriate co-localization markers were selected. Because microtubules are associated with SKA2 in eukaryotes (Helgeson et al., 2018; Jeyaprakash et al., 2012) and centrins might play an essential role in microtubule serving (Sanders et al., 1994; Wolfrum, 1995) the centrins marker Centrin3, which was already used in *P. falciparum* parasites, (Mahajan et al., 2008) was chosen as co-localization marker. Therefore *PfCentrin3* was C-terminally tagged with mCherry and co-transfected (kindly performed by Jessica Kimmel) into the M7-2xFKBP-GFP-2xFKBP integration cell line. The Centrin3 foci appeared to be positioned more towards the PPM

while M7-2xFKBP-GFP-2xFKBP foci appeared to be more closely facing the nuclei (Figure 27). Centrin3-mCherry and M7-2xFKBP-GFP-2xFKBP were located very closely together and partially overlapped (Figure 27).

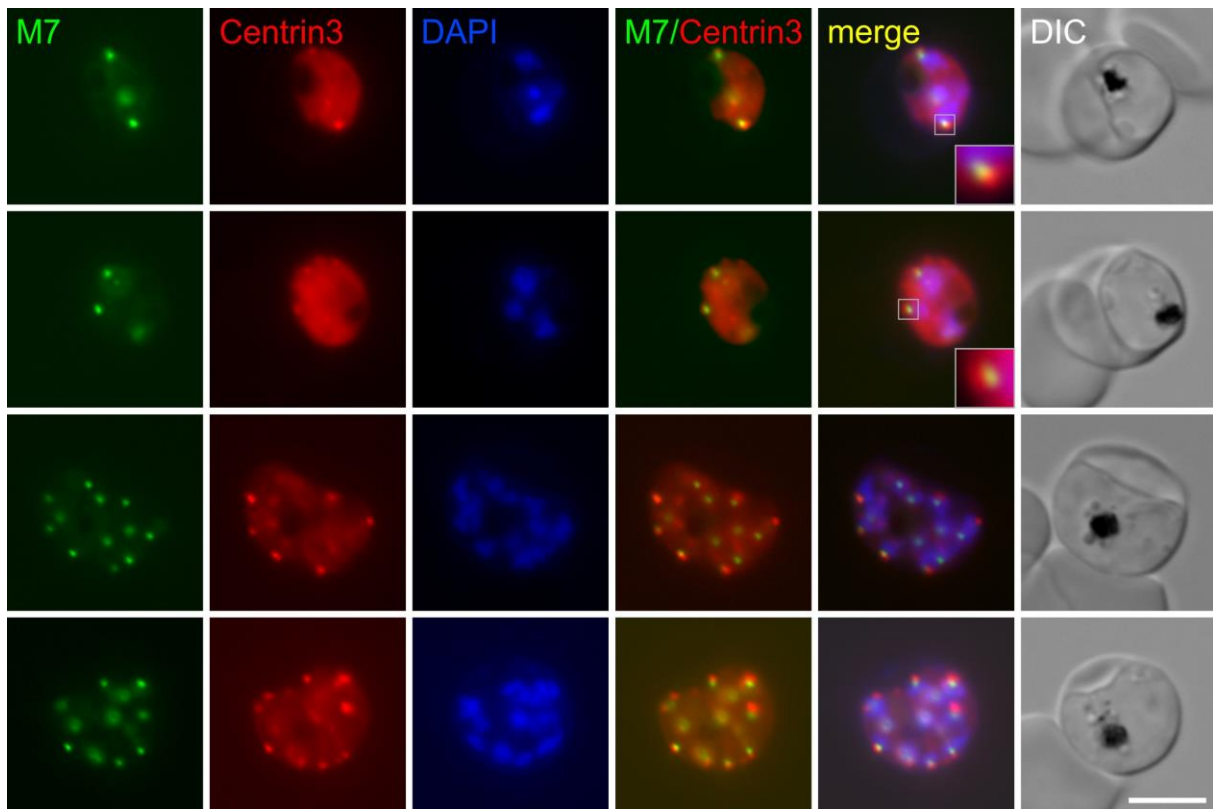


Figure 27: M7 (PF3D7_0307500) co-localization with Centrin3.

Representative live cell images ($n \geq 3$ fluorescence microscopy sessions, with at least 15 inspected cells per session) of knock-in cell line of M7-2xFKBP-GFP-2xFKBP (green) with episomally expressed Centrin3-mCherry (Centrin3, red). Parasite nuclei were stained with DAPI (blue). Zoom pictures are displayed with a 3x magnification (grey square). Scale bar 5 μm , DIC (differential interference contrast).

Next, M7-2xFKBP-GFP-2xFKBP was co-localized with tubulin to determine the involvement of M7-2xFKBP-GFP-2xFKBP in nuclear division. Alpha and beta-tubulins polymerize into microtubules (Gunning et al., 2015) and are essential for mitosis and other cellular processes (reviewed in: (Verhey et al., 2007; Westermann et al., 2003)). The tubulin staining was performed with Tubulin Tracker™ Deep Red (Invitrogen, USA) in the M7-2xFKBP-GFP-2xFKBP cell line. Tubulin appeared in a bright focus, at the nuclei with two filaments to the left and right originating from the centre towards the nucleus. The bright central tubulin foci was situated between the nuclei and the M7-2xFKBP-GFP-2xFKBP foci, whereby the M7-2xFKBP-GFP-2xFKBP foci were facing the PPM. M7-2xFKBP-GFP-2xFKBP touched the tubulin, but did not fully co-localize with it (Figure 28 control).

To get more detailed information about the role of M7 in mitosis, knock sideways was induced to inactivate M7 in a mixed parasite culture followed by staining with DAPI and

Tubulin Tracker™. The control cell line without rapalog appeared as expected with normal looking nuclei and correctly located M7-2xFKBP-GFP-2xFKBP foci and tubulin (Figure 28 control). In contrast, the cell line where M7 had been inactivated (Figure 28 rapalog) showed blurry and lumpy nuclei. Additionally, the nuclei were not correctly divided (Figure 28 rapalog, DAPI). In contrast to the control, the tubulin filaments appeared in long filaments without a clearly defined centre. In the control, the tubulin filaments multiplied with the number of nuclei. This was not seen in the parasites where M7 was inactivated (Figure 28 rapalog, tubulin).

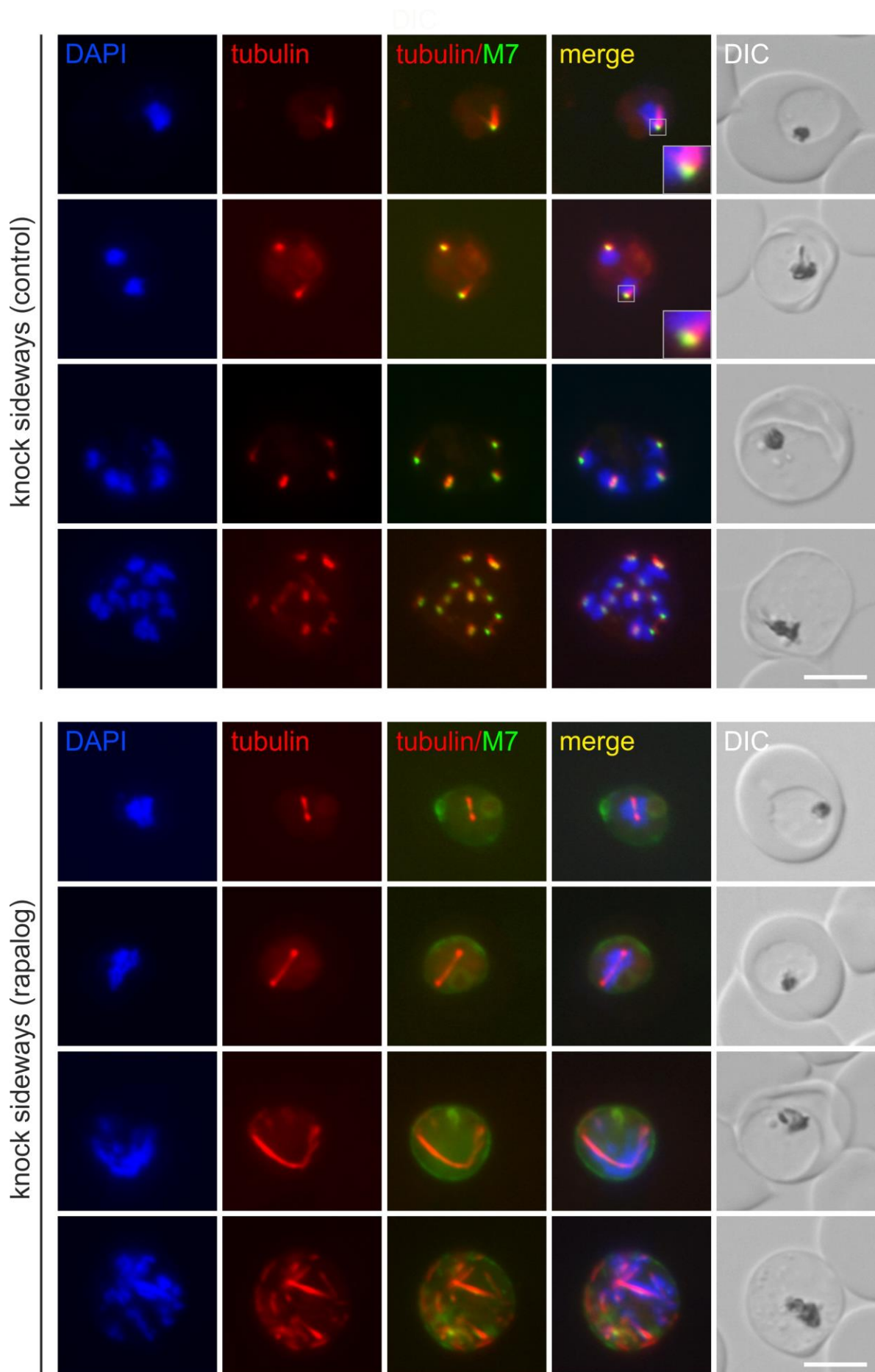


Figure 28: Candidate M7 (PF3D7_0307500) knock sideways and co-localization with tubulin.

Representative live cell images ($n \geq 3$ fluorescence microscopy sessions, with at least 15 inspected cells per session) of knock-in cell line of M7-2xFKBP-GFP-2xFKBP (green) with an episomally expressed lyn-FRB-mCherry mislocalizer. The cell culture was split into two dishes: one served as control without rapalog (control), and the other was grown in the presence of 250 nM rapalog (rapalog). The samples for live cell imaging were taken 8 h post addition of rapalog. Parasite nuclei were stained with DAPI (blue) and TubulinTracker™ deep red (tubulin, red). Zoom pictures are displayed with a 3x magnification (grey square). Scale bar 5 μm , DIC (differential interference contrast).

To identify potential interaction partners and to get more indications regarding the function of M7, DIQ-BioID was performed (Birnbaum et al., 2020) with the M7 protein. DIQ-BioID is based on a heterodimerization which makes it easier to distinguish between background and real interactors of target proteins by using the same starting culture in similar way to a knock sideways experiment. But instead of inactivating the protein, the hetero dimerization brings the Biotin ligase BirA* in close proximity to the FKBP tagged target protein, when rapalog is added.(Birnbaum et al., 2020) If biotin is added to the cell culture, the proteins in a range of ~ 10 nm around the ligase are labeled with biotin (biotinylation) (Choi-Rhee et al., 2004; Cronan, 2005; Kim et al., 2016). The labeled proteins can then be purified by streptavidin beads and analyzed by mass spectrometry (Birnbaum et al., 2020). To enable biotinylation of potential M7 interaction partners from the M7 C- and N-terminal side, two different BirA* constructs, BirA*-CL (Birnbaum et al., 2020) and BirA*-NL (Birnbaum et al., 2020) were co-transfected into the M7-2xFKBP-GFP-2xFKBP cell line. To demonstrate that BirA*-CL and BirA*-NL dimerize to M7-2xFKBP-GFP-2xFKBP, a mixed parasite culture was incubated in and without the presence of rapalog for 21 h and analyzed by fluorescence microscopy. The dimerization was confirmed by the overlap of BirA*-CL and BirA*-NL with M7-2xFKBP-GFP-2xFKBP foci (Figure 29 A, B rapalog). As expected, the control cell lines showed no overlap and only cytoplasmic staining BirA*-CL and BirA*-NL (Figure 29 A, B control).

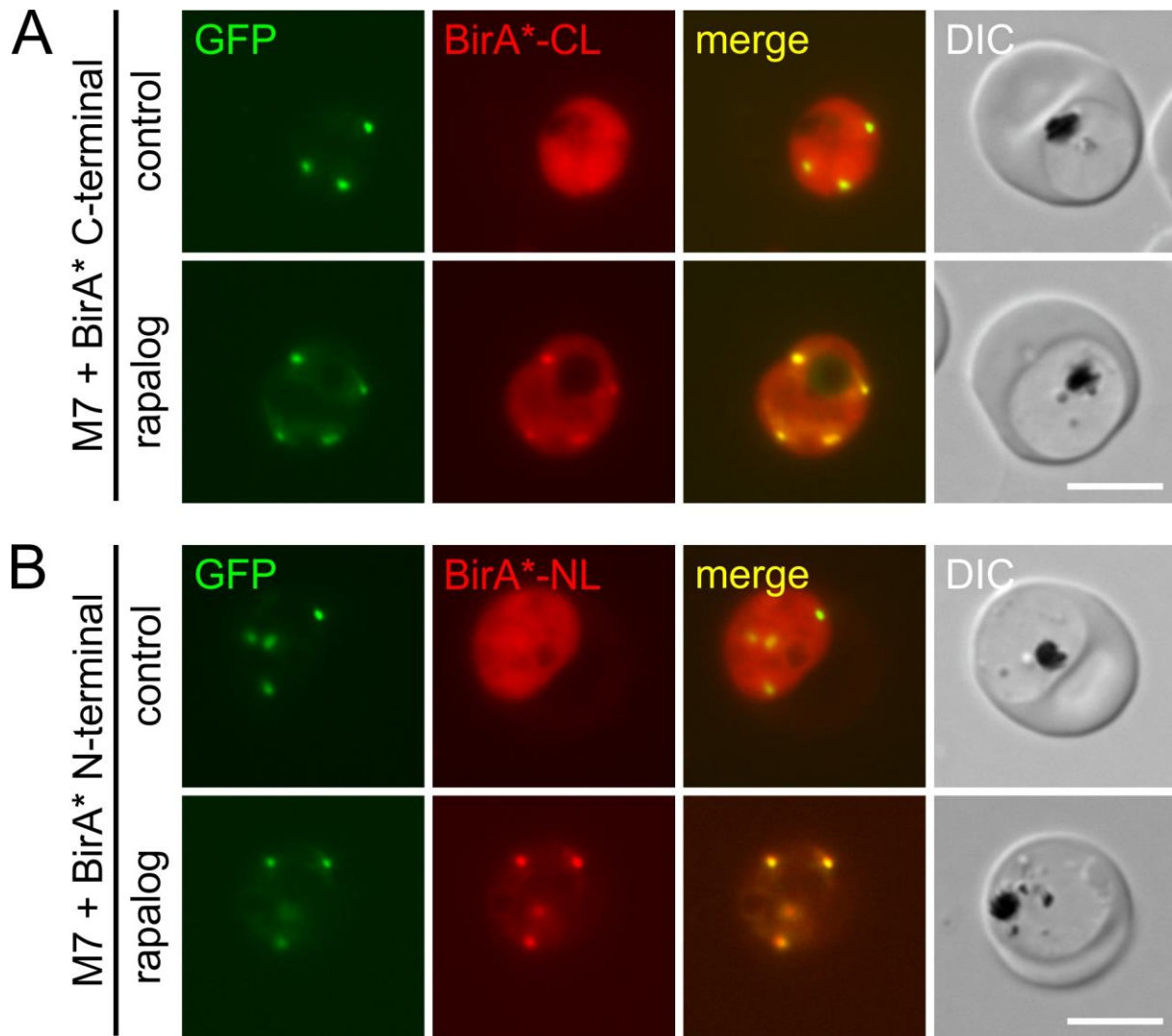


Figure 29: Dimerization of candidate M7 (PF3D7_0307500) with biotin ligase BirA*.

Representative live cell images ($n \geq 3$ fluorescence microscopy sessions, with at least 10 inspected cells per session) of knock-in cell line of M7-2xFKBP-GFP-2xFKBP (green) with an episomally expressed BirA*-CL (**A**) or an episomally expressed BirA*-NL (**B**). Both cell cultures were split into two dishes: one served as control without rapalog (control), and the other was grown in the presence of 250 nM rapalog (rapalog). The samples for live cell imaging were taken 21 h post addition of rapalog. Scale bar 5 μm , DIC (differential interference contrast).

The DIQ-BioID experiments were performed as described in 3.3.10 with two individual replicates. The quantitative mass spectrometry (MS) using dimethyl labeling (Birnbaum et al., 2020; Boersema et al., 2009) and protein enrichment analysis were kindly conducted by the Bartfai Lab (Radboud University, Netherlands).

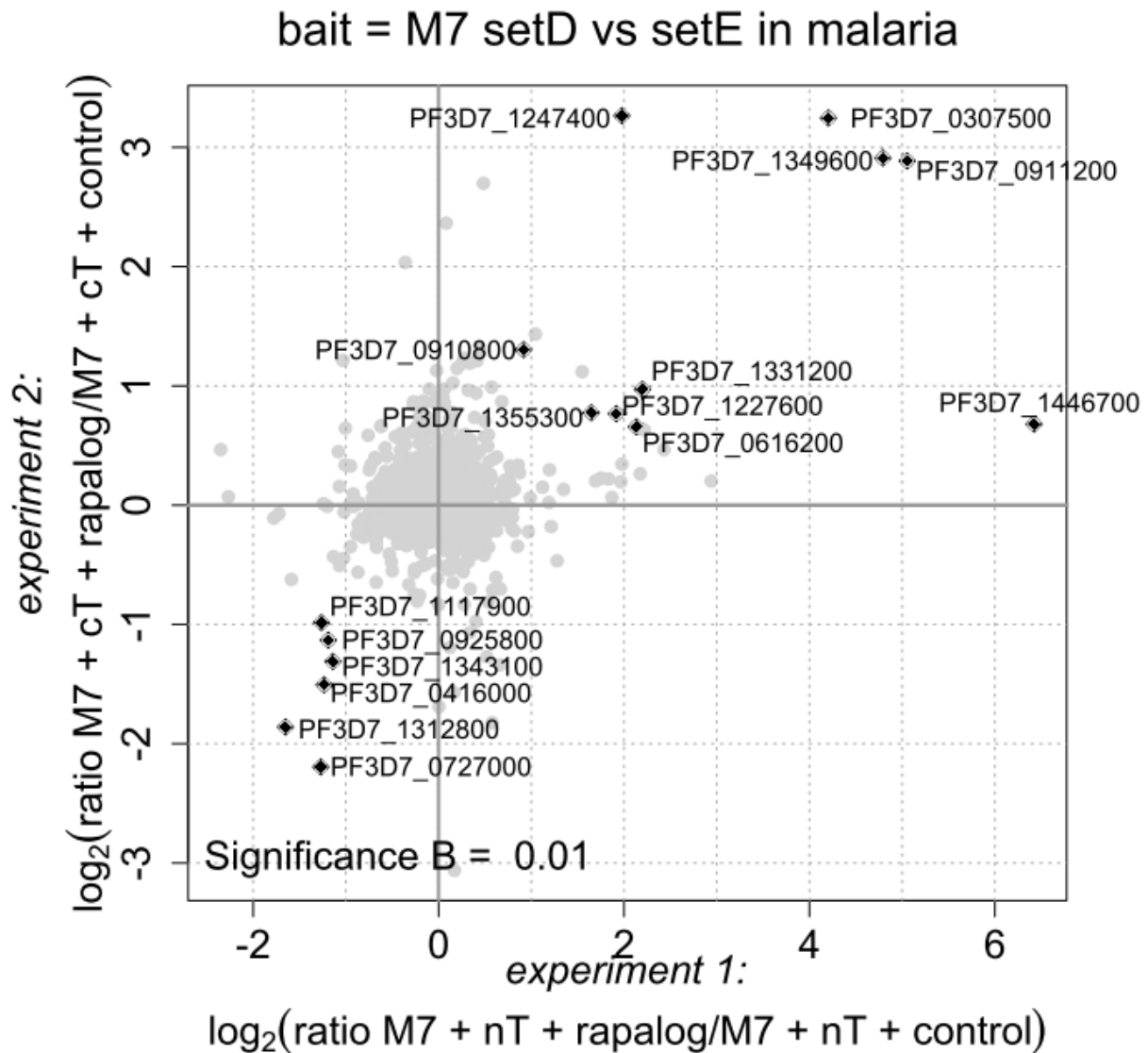


Figure 30: Scatterplots of DIQ-BioID with candidate M7 (PF3D7_0307500).

Plotted are the \log_2 -ratios of 21 h grown in presence of rapalog cultures over the control (untreated culture) obtained from two individual experiments. Experiment 1 was conducted with M7-2xFKBP-GFP-2xFKBP with an episomally expressed BirA*-NL biotinyler and experiment 2 was performed with M7-2xFKBP-GFP-2xFKBP with an episomally expressed BirA*-CL biotinyler. The upper right quarter of the scatter plot showing enriched proteins (\log_2 ratio) with their ID (PlasmoDB identifiers) indicating potential interactors of M7-2xFKBP-GFP-2xFKBP, on rapalog (biotinyler on target), compared with control (biotinyler cytoplasmic). The lower left quarter shows the unenriched proteins (\log_2 ratio) on rapalog (biotinyler on target), compared with control (biotinyler cytoplasmic) with their protein ID.

The two experiments of the mass spectrometry are displayed in scatterplots, indicating the enrichment of proteins grown in the presence of rapalog (biotinyler on target) over control (biotinyler cytoplasmic). The experiments were plotted as \log_2 -normalized ratio on both axes (Figure 30). The significance was defined as the false discovery rate for experiment 1 and experiment 2 (Appendix 7) that describes the expected proportion of false hits among all hits. The hits were sorted according to their significance from top (most significant) downwards to the bottom of Table 8. Ten significant enriched proteins were found, and the most significant hit in both experiments was M7 (Figure 30, Table 8 top hit), confirming the

correct dimerization and biotinylation of M7-2xFKBP-GFP-2xFKBP using BirA*-NL and BirA*-CL. Appendix 7 shows the individually DIQ-BioID hits for BirA*-NL and BirA*-CL experiments.

Table 8: Top hits of M7 DIQ-BioID.

The table shows the top hits of the DIQ-BioID experiments according to their significant from top (most significant) to the bottom, their protein ID, product description and the top hit of the HHPred server for protein remote homology detection and 3D structure prediction.

Protein ID	Product description	HHPred
PF3D7_0307500	M7 protein	SKA 2
PF3D7_0911200	conserved, unknown	SKA 3
PF3D7_1349600	conserved, unknown	E3 ubiquitin-protein ligase
PF3D7_1247400	FKBP35	FKBP35
PF3D7_1331200	conserved, unknown	RNA polymerase II-associated factor 1
PF3D7_0910800	NBP35, putative	cytosolic Fe-S cluster assembly factor
PF3D7_1446700	conserved, unknown	nuclear pore complex protein Nup155
PF3D7_0616200	kinetochore protein, NDC80	kinetochore protein NDC80
PF3D7_1227600	conserved, unknown	kinetochore protein NDC80
PF3D7_1355300	histone-lysine N-methyltransferase, putative	histone lysine methyltransferase

Five of the ten significant DIQ-BioID hits of M7 are annotated as proteins with unknown function (according to: PlasmoDB (Aurrecochea et al., 2009)). The most significant hit besides M7 itself (Figure 30, Table 8, PF3D7_0911200), revealed a putative similarity to the SKA 3 protein, using HHPred (Zimmermann et al., 2018) SKA3 is in humans part of a heterotrimeric SKA complex together with SKA 2 and SKA 1 (Helgeson et al., 2018). Also, the proteins PF3D7_0616200 and PF3D7_1227600 (Figure 30, Table 8) revealed a putative

similarity to homologue proteins (Table 8) linked to the SKA complex in humans as they showed homology to NDC80 (Helgeson et al., 2018). PF3D7_0910800 (Figure 30, Table 8) annotated as NBP35 can be linked to RNA processing and ribosome export (Balk et al., 2005; Hausmann et al., 2005; Netz et al., 2012; Netz et al., 2007; Yarunin et al., 2005). Also, proteins with homologies to an RNA polymerase II-associated factor 1 and a nuclear pore complex protein Nup155 were identified (Figure 30, Table 8), suggesting that they are also associated with the nucleus and its machinery. Overall, these hits validate M7 as a likely orthologue of SKA2 and link it with the same biological process where the SKA complex is involved in humans.

4.9 Candidate M8 (PF3D7_0307600)

M8 (PF3D7_0307600) comprises 746 AA and is annotated as conserved *Plasmodium* protein with unknown function (according to: PlasmoDB (Aurrecochea et al., 2009)). BLAST search (Altschul et al., 1990) revealed no similarity outside the Apicomplexa, and also the motif scan with MyHits (Pagni et al., 2004) showed no similarity to domains in other organisms. The best hit using HHPred (Zimmermann et al., 2018), with a putative similarity to M8 was a DNA repair and recombination protein in *Sulfolobus solfataricus*. In the saturation-based mutagenesis screen (Zhang et al., 2018) M8 was classified as dispensable for parasite growth similarly the orthologue protein in *P. berghei* parasites was identified as non-essential for growth (Bushell et al., 2017).

To analyze M8, the corresponding gene product was tagged with 2xFKBP-GFP-2xFKBP by modification of the endogenous locus using SLI. Correct integration of the pSLI plasmid resulting in the M8-2xFKBP-GFP-2xFKBP knock-in was confirmed by PCR (Figure 17), whereas no correct integration could be achieved for the corresponding pSLI-TGD plasmid. Microscopy with the M8-2xFKBP-GFP-2xFKBP cell line revealed detectable fluorescence signal from late trophozoite to segmenter stage. Microscopy with live cells failed to detect M8-2xFKBP-GFP-2xFKBP in rings. In a couple of trophozoites a uniform cytoplasmic pool of M8 was evident and a small number of foci in the parasite periphery became apparent in late trophozoites and early schizonts. During the segmenter stage, the M8-2xFKBP-GFP-2xFKBP was visible in accumulations forming elongated structures and disks (Figure 31).

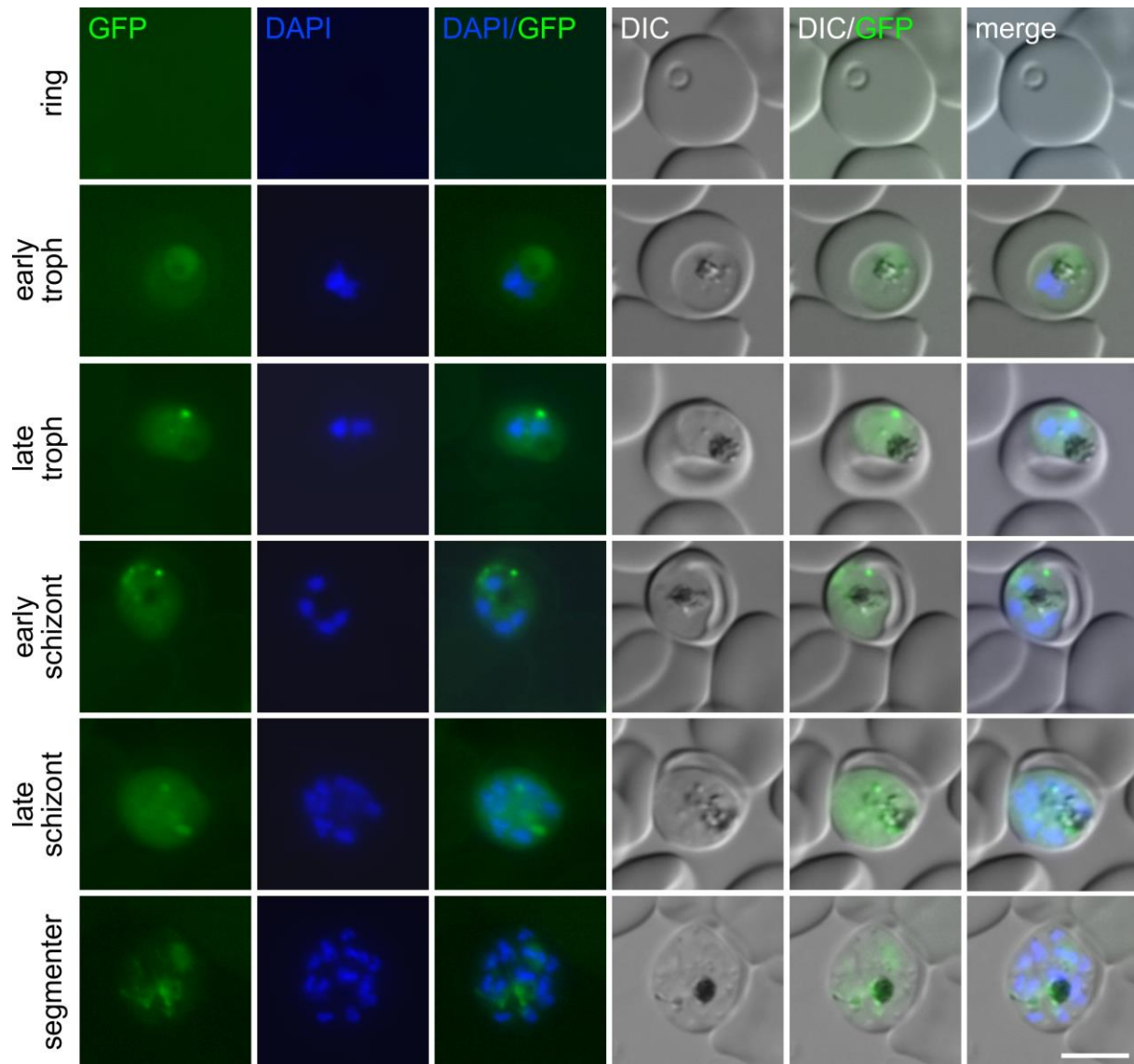


Figure 31: Localization of endogenously tagged candidate M8 (PF3D7_0307600).

Representative live cell images ($n \geq 3$ fluorescence microscopy sessions, with at least 20 inspected cells per session) of knock-in cell line M8-2xFKBP-GFP-2xFKBP ('GFP'). The stages are indicated on the left of the panel. Parasite nuclei were stained with DAPI. Scale bar 5 μm , DIC (differential interference contrast).

To functionally analyse M8, the M8-2xFKBP-GFP-2xFKBP cell line was co-transfected with an episomally expressed 1xNLS-FRB-mCherry mislocalizer (Birnbaum et al., 2017) (Figure 32 panel) and knock sideways was carried out. While the foci appeared to have fully disappeared after induction of the knock sideways, left over of M8 at the membrane and evenly distributed in the cytoplasm could not be excluded due to the low expression of the protein and low signal above background (Figure 32 left panel). Growth analysis over five days showed no effect on parasite growth in the parasites with the inactivated M8 compared to the control which may be due to the insufficient mislocalization (Figure 32 growth curve, and Appendix 5). In conclusion it is unclear if the M8 protein is important for growth of asexual blood stage parasites.

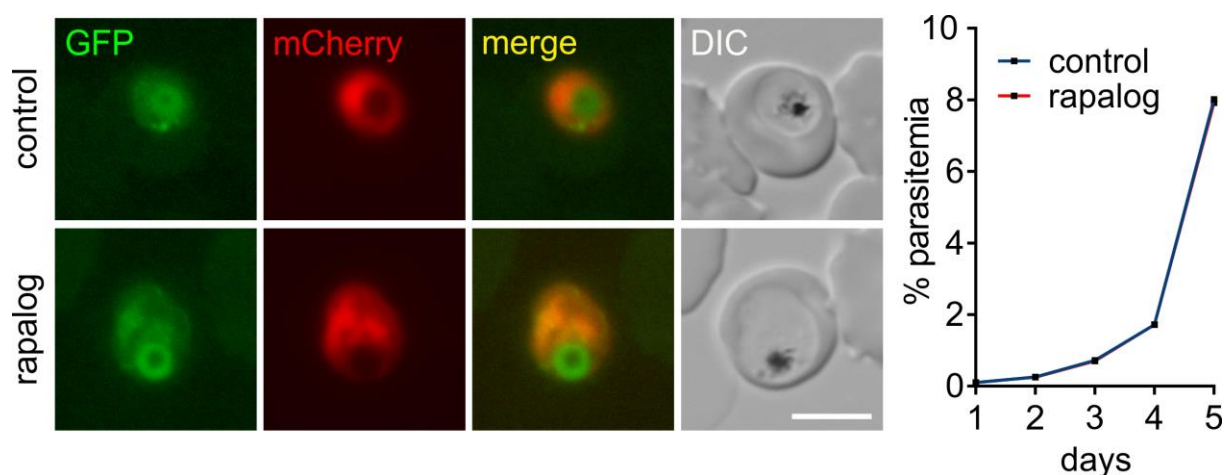


Figure 32: Knock sideways and growth curve of endogenously tagged candidate M8 (PF3D7_0307600).

Panel) Representative live cell images ($n \geq 3$ fluorescence microscopy sessions, with at least 20 inspected cells per session) of knock-in cell line M8-2xFKBP-GFP-2xFKBP ('GFP') with an episomally expressed 1xNLS-FRB-mCherry mislocalizer. The cell culture was split into two dishes: one served as control without rapalog (control), and the other grown in the presence of 250 nM rapalog (rapalog). The samples for live cell imaging were taken 24 h post addition of rapalog. Scale bar 5 μm , DIC (differential interference contrast). **The graph to the right of the image panels** shows parasite growth as determined by flow cytometry of the M8-2xFKBP-GFP-2xFKBP knock sideways parasites grown in the presence of rapalog (inactivated) and without rapalog (control). One representative of three independent experiments (replicas shown in Appendix 5).

4.10 Candidate M9 (PF3D7_0307700)

The M9 (PF3D7_0307700) is annotated as conserved protein with unknown function and comprises 1826 AA (according to: PlasmoDB (Aurrecochea et al., 2009)). BLAST search (Altschul et al., 1990) showed one hit to another uncharacterized protein from *Carassius auratus* (e-value: $1e-12$, percent identity: 25 %). An additional motif scan with MyHits (Pagni et al., 2004) showed no significant similarity. Using HHPred (Zimmermann et al., 2018), only hits over short stretches or to common structural domains, such as coiled coils were found. In the saturation-based mutagenesis screen (Zhang et al., 2018) M9 was classified as dispensable for parasite growth. In contrast the orthologue protein in *P. berghei* parasites (Bushell et al., 2017) was annotated as essential for parasite growth. Attempts to disrupt the gene, using pSLI-TGD were not successful. Also, endogenous C-terminal tagging with 2xFKBP-GFP-2xFKBP was unsuccessful in four independent attempts, indicating that C-terminal tagging of M2 might interfere with correct protein function or localization. This protein was therefore not further analyzed.

4.11 Candidate M10 (PF3D7_0307900)

M10 (PF3D7_0307900) is annotated as conserved *Plasmodium* protein with unknown function and is composed of 3724 AA (according to: PlasmoDB (Aurrecochea et al., 2009)). BLAST search (Altschul et al., 1990) revealed no similarity outside the Apicomplexa. Also a

motif scan with MyHits (Pagni et al., 2004) showed no significant hit. The best hit using HHPred (Zimmermann et al., 2018) with a putative similarity to M10 was a ribosome assembly protein in *Saccharomyces cerevisiae*. In the saturation-based mutagenesis screen (Zhang et al., 2018) M10 was classified as dispensable for parasite growth. Similarly the orthologue protein in *P. berghei* parasites was identified as essential for parasite growth (Bushell et al., 2017).

To analyze M10, the corresponding gene product was tagged with 2xFKBP-GFP-2xFKBP by modification of the endogenous locus using SLI. Correct integration of the pSLI plasmid resulting in the M10-2xFKBP-GFP-2xFKBP knock-in was confirmed by PCR (Figure 17), whereas no correct integration could be achieved for the corresponding pSLI-TGD plasmid. Microscopy with the M10-2xFKBP-GFP-2xFKBP cell line revealed no detectable fluorescence signal in rings, late schizonts and segmenters. In trophozoites and early schizonts M10-2xFKBP-GFP-2xFKBP was usually found in accumulations always close to vesicle like DIC structures (Figure 33).

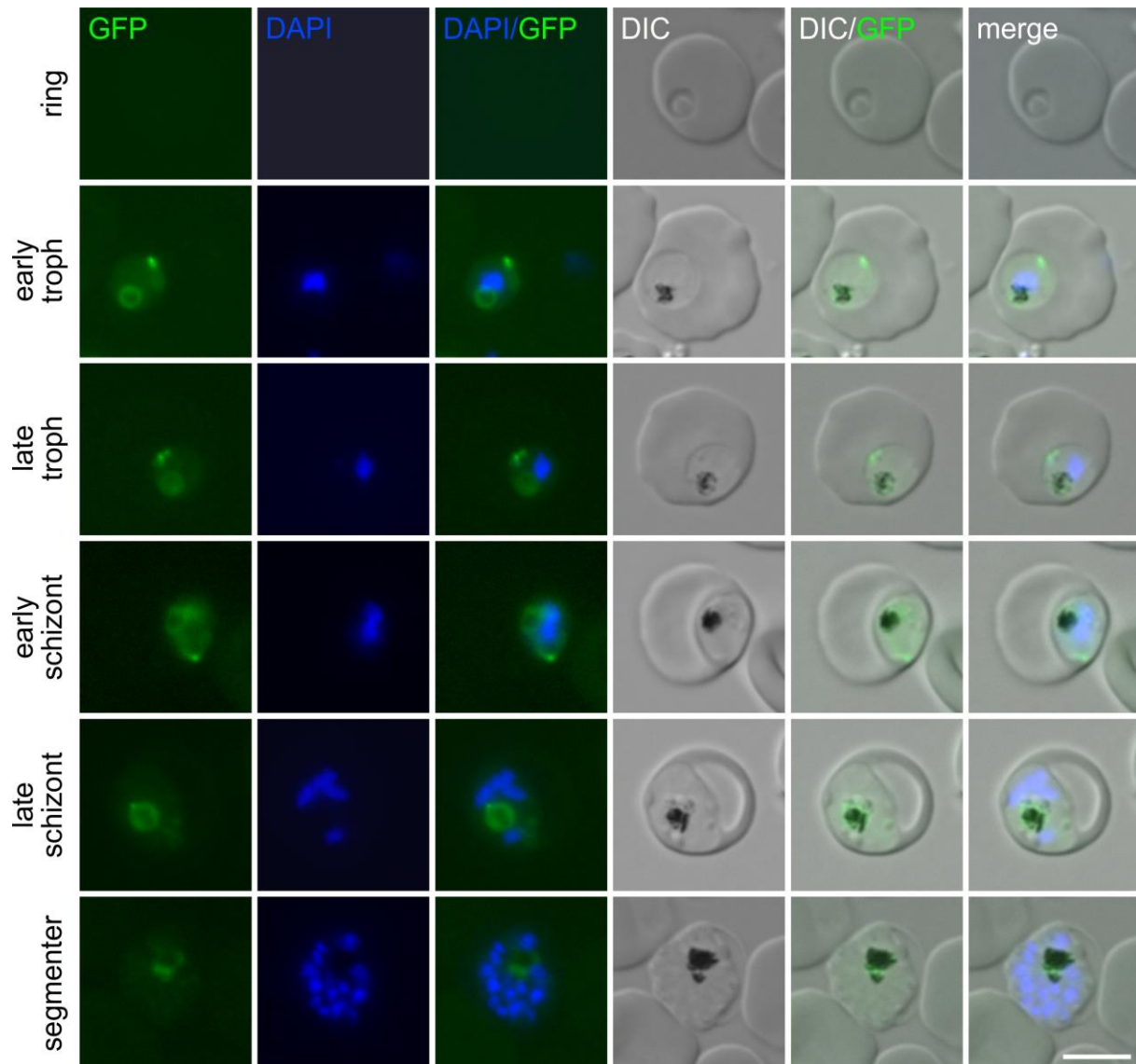


Figure 33: Localization of endogenously tagged candidate M10 (PF3D7_0307900).

Representative live cell images ($n \geq 3$ fluorescence microscopy sessions, with at least 20 inspected cells per session) of knock-in cell line M10-2xFKBP-GFP-2xFKBP (*GFP*). The stages are indicated on the left of the panel. Parasite nuclei were stained with DAPI. Scale bar 5 μm , DIC (differential interference contrast).

4.12 Candidate M11 (PF3D7_0308100)

M11 (PF3D7_0308100) consists of 1711 AA and was at the beginning of this work annotated as *Plasmodium* conserved protein with unknown function (according to: PlasmoDB, release 31 (Aurrecochea et al., 2009)) and later changed to putative zinc finger protein (according to PlasmoDB, release 46 (Aurrecochea et al., 2009)). A motif scan with MyHits (Pagni et al., 2004) showed no significant hit. BLAST search (Altschul et al., 1990) did not show a significant similarity to other organisms outside the Apicomplexa. The best hit using HHPred (Zimmermann et al., 2018) with a putative similarity to M11 was a transcription intermediary factor domain in *Homo sapiens*. In the saturation-based mutagenesis screen (Zhang et al., 2018) M11 was classified as dispensable for parasite growth. In contrast the orthologue

protein in *P. berghei* parasites (Bushell et al., 2017) was annotated as essential for parasite growth.

To analyze M11, the corresponding gene product was tagged with 2xFKBP-GFP-2xFKBP by modification of the endogenous locus using SLI. Correct integration of the pSLI plasmid resulting in the M11-2xFKBP-GFP-2xFKBP knock-in was confirmed by PCR (Figure 17), whereas no correct integration could be achieved for the corresponding pSLI-TGD plasmid. Microscopy with the M11-2xFKBP-GFP-2xFKBP cell line revealed no detectable signal, beside background fluorescence in rings and trophozoites. In early schizonts to late schizonts, the tagged protein was frequently but not always located in foci at the nuclei. In segmenters the foci increased in number and some foci were also visible, more centered than foci in schizonts (Figure 34).

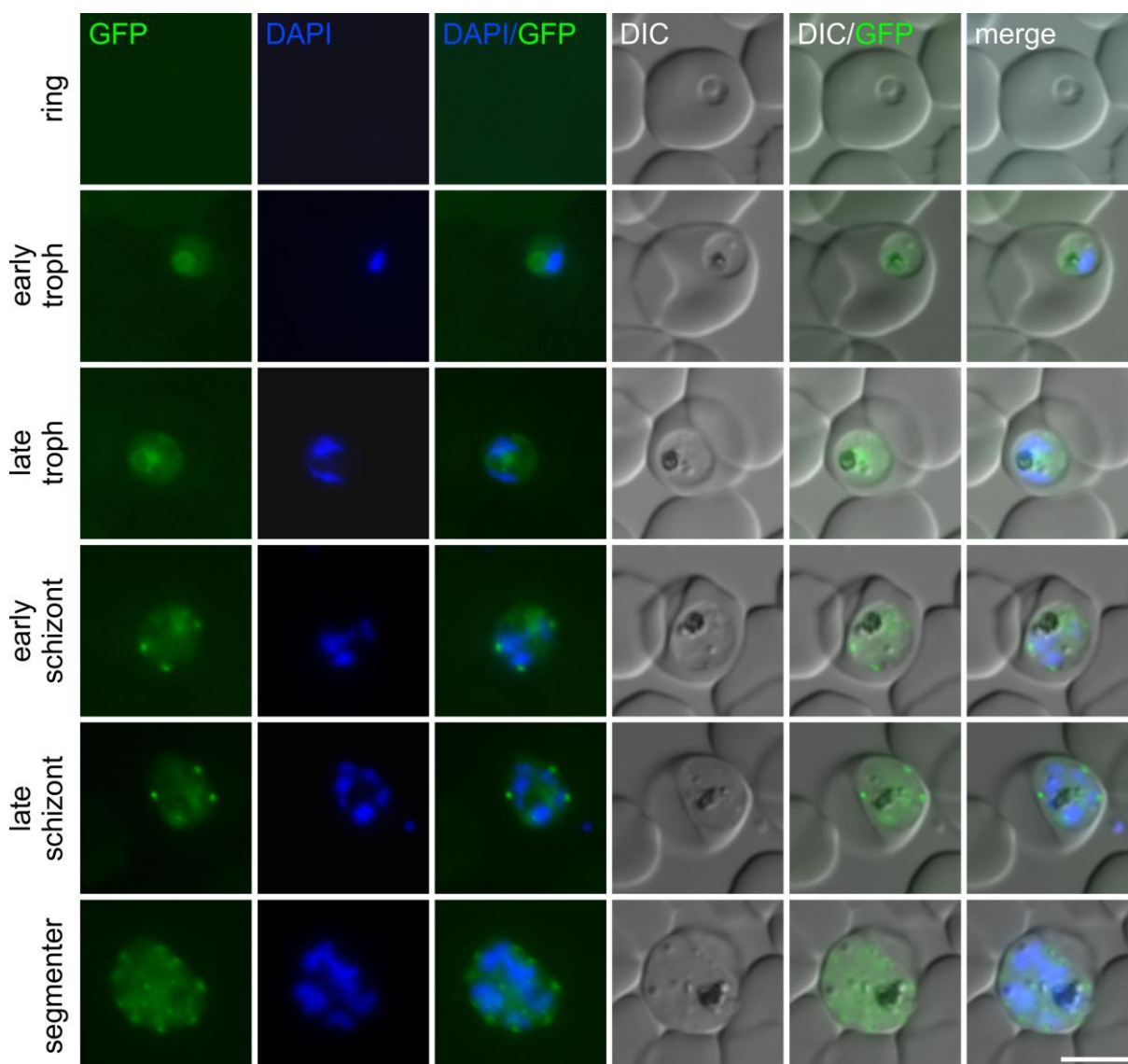


Figure 34: Localization of endogenously tagged candidate M11 (PF3D7_0308100).

Representative live cell images ($n \geq 3$ fluorescence microscopy sessions, with at least 20 inspected cells per session) of knock-in cell line M11-2xFKBP-GFP-2xFKBP ('GFP'). The stages are indicated on the left of the panel. Parasite nuclei were stained with DAPI. Scale bar 5 μm , DIC (differential interference contrast).

4.13 Candidate M12 (PF3D7_0308300)

The 337 AA comprising M12 (PF3D7_0308300) protein is annotated as *Plasmodium* conserved protein with unknown function (according: to PlasmoDB (Aurrecochea et al., 2009)). A BLAST search (Altschul et al., 1990) and the motif scan MyHits (Pagni et al., 2004) revealed no similarities to other organisms outside the Apicomplexa. Using HHPred (Zimmermann et al., 2018) no similarity to other proteins or domains was found. In the saturation-based mutagenesis screen (Zhang et al., 2018), M12 was classified as essential protein for parasite growth. In the *P. berghei* genome screen (Bushell et al., 2017) the M12 orthologue was not listed.

To analyze M12, the corresponding gene product was tagged with 2xFKBP-GFP-2xFKBP by modification of the endogenous locus using SLI. Correct integration of the pSLI plasmid resulting in the M12-2xFKBP-GFP-2xFKBP knock-in was confirmed by PCR (Figure 17). Correct integration was also achieved for the corresponding pSLI-TGD plasmid (Figure 17), indicating that M12 is dispensable for growth of asexual blood stage parasites. Microscopy with the M12-2xFKBP-GFP-2xFKBP cell line revealed no signal from ring to late trophozoite stage (Figure 36). In schizonts, the protein was diffusely distributed at the PPM, whereas in segments the nuclei were surrounded by fluorescence signals (Figure 35).

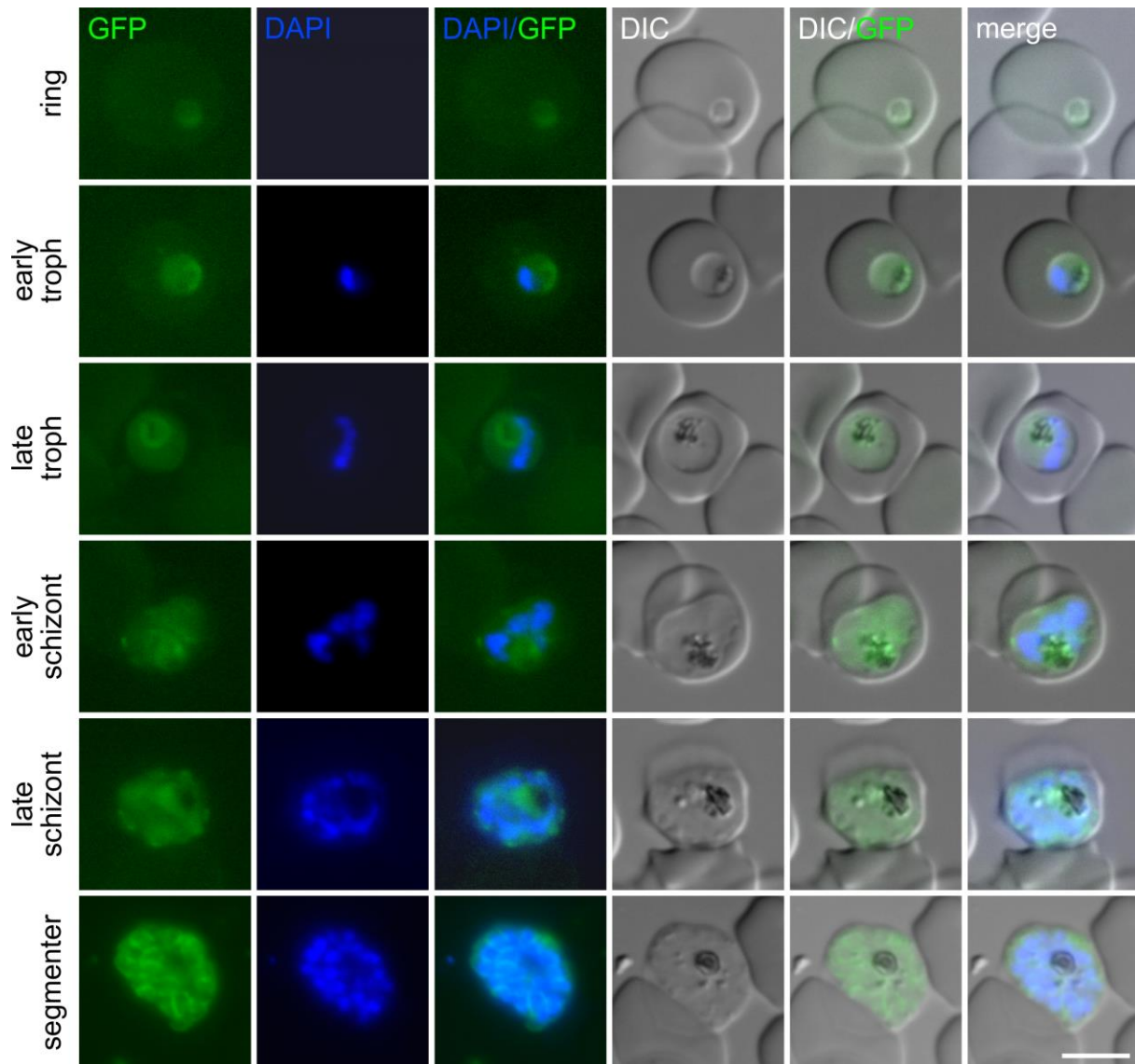


Figure 35: Localization of endogenously tagged candidate M12 (PF3D7_0308300).

Representative live cell images ($n \geq 3$ fluorescence microscopy sessions, with at least 20 inspected cells per session) of knock-in cell line M12-2xFKBP-GFP-2xFKBP (*GFP*). The stages are indicated on the left of the panel. Parasite nuclei were stained with DAPI. Scale bar 5 μm , DIC (differential interference contrast).

4.14 Candidate M13 (PF3D7_0308700)

M13 (PF3D7_0308700) comprises 492 AA and is annotated as conserved *Plasmodium* protein with unknown function (according to: PlasmoDB (Aurrecochea et al., 2009)). BLAST search (Altschul et al., 1990) showed a hit to an also uncharacterized protein of *Piliocolobus tephrosceles* (e-value: $4e-74$, percent identity: 42.8 %). The MyHits motif scan (Pagni et al., 2004) did not show significant hits. The best hit using HHPred (Zimmermann et al., 2018) with a putative similarity to M13 was a nucleoporin protein in *Homo sapiens*. In the saturation-based mutagenesis screen (Zhang et al., 2018) M13 was classified as essential for parasite growth. Similarly the orthologue protein in *P. berghei* parasites was annotated as essential for growth (Bushell et al., 2017).

To analyze M13, the corresponding gene product was tagged with 2xFKBP-GFP-2xFKBP by modification of the endogenous locus using SLI. Correct integration of the pSLI plasmid resulting in the M13-2xFKBP-GFP-2xFKBP knock-in was confirmed by PCR (Figure 17), whereas no correct integration could be achieved for the corresponding pSLI-TGD plasmid. Microscopy with the GFP tagged M13 cell line showed no detectable signal in ring and early trophozoite stages. Late trophozoites and early schizonts displayed a faint cytoplasmic staining with some roundish accumulations. In late schizonts and segmenters, M13-2xFKBP-GFP-2xFKBP was visible in clear foci in close proximity to the nuclei (Figure 36). The localization might be similar to the AIP-FKBP-GFP rhoptry protein shown by (Geiger et al., 2019), this could suggest M13 as an apical protein.

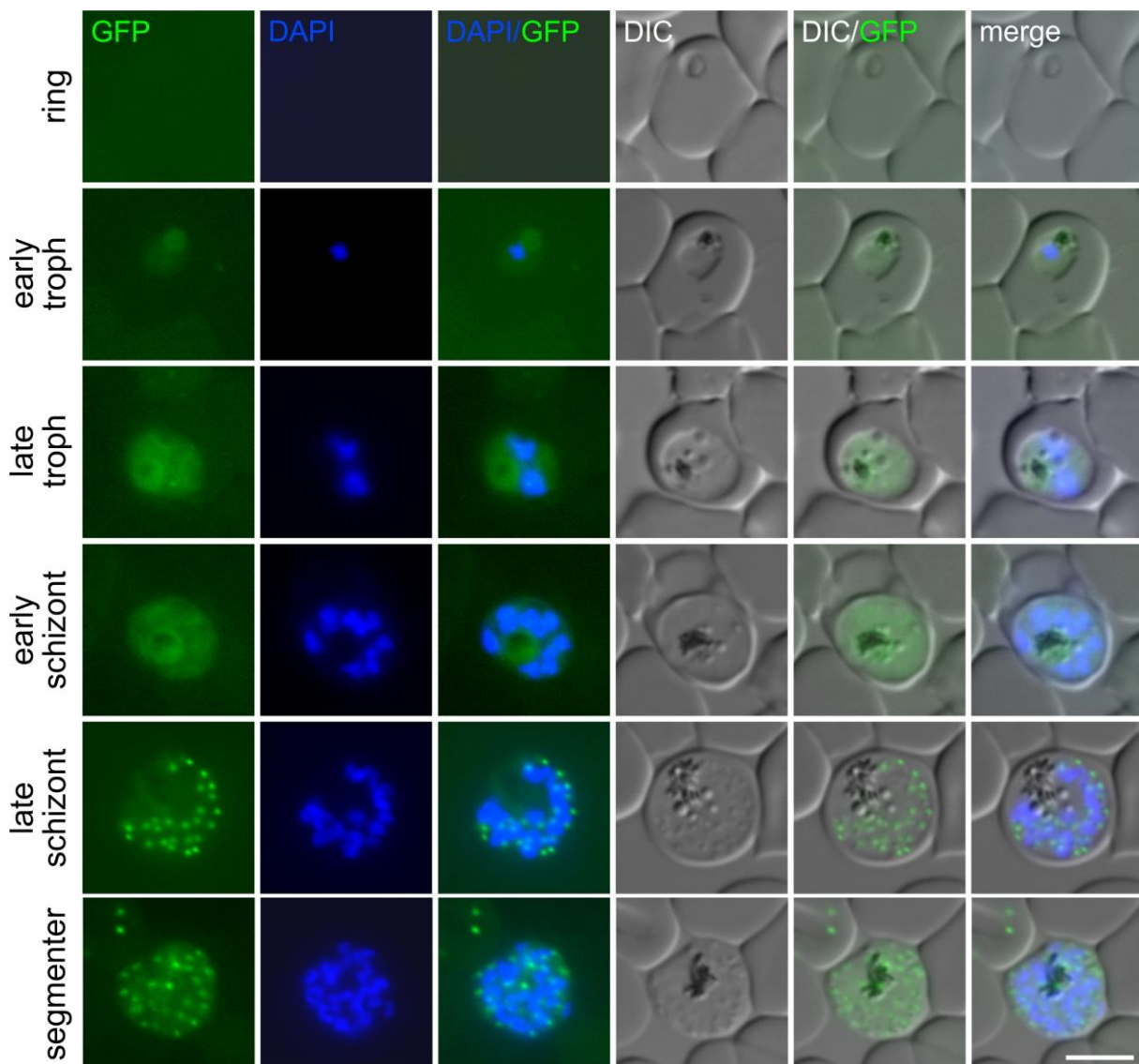


Figure 36: Localization of endogenously tagged candidate M13 (PF3D7_0308700).

Representative live cell images ($n \geq 3$ fluorescence microscopy sessions, with at least 20 inspected cells per session) of knock-in cell line M13-2xFKBP-GFP-2xFKBP ('GFP'). The stages are indicated on the left of the panel. Parasite nuclei were stained with DAPI. Scale bar 5 μm , DIC (differential interference contrast).

4.15 Candidate M14 (PF3D7_0308800)

The protein sequence of M14 (PF3D7_0308800) comprises 108 AA. M14 is annotated as conserved *Plasmodium* protein with unknown function (according to: PlasmoDB (Aurrecochea et al., 2009)). A BLAST search revealed similarity with an identity of 59 % and a cover query of 37 % to Sodium-coupled neutral amino acid transporter in *Symbiodinium microadriaticum*. No significant hit was shown with the motif scan MyHits (Pagni et al., 2004). Using HHPred (Zimmermann et al., 2018) only hits over short stretches or to common structural domains, such as coiled coils were found. The saturation-based mutagenesis screen (Zhang et al., 2018), classified M14 as intermediate phenotype between essential and dispensable for parasite growth. In the *P. berghei* genome screen (Bushell et al., 2017) the M14 orthologue was not listed. Attempts to disrupt the gene, using pSLI-TGD were not successful. Also, endogenous C-terminal tagging with 2xFKBP-GFP-2xFKBP was unsuccessful in four independent attempts, indicating that C-terminal tagging of M14 might interfere with correct protein function or localization. This protein was therefore not further analyzed.

4.16 Candidate M15 (PF3D7_0309900)

M15 (PF3D7_0309900) is annotated as conserved *Plasmodium* protein with unknown function and comprises 1673 AA (according to: PlasmoDB (Aurrecochea et al., 2009)). BLAST search (Altschul et al., 1990) revealed 13 hypothetical, predicted and uncharacterized proteins (e-values $\leq 3e-14$, percent identities ≤ 49.3 %) A motif scan performed with MyHits (Pagni et al., 2004) showed no significant hits. Using HHPred (Zimmermann et al., 2018), only hits over short stretches or to common structural domains, such as coiled coils were found. The saturation-based mutagenesis screen (Zhang et al., 2018), classified M15 as not essential for parasite growth. . In the *P. berghei* genome screen (Bushell et al., 2017) the orthologue M15 protein was not listed. Attempts to disrupt the gene, using pSLI-TGD were not successful. Also, endogenous C-terminal tagging with 2xFKBP-GFP-2xFKBP was unsuccessful in four independent attempts, indicating that C-terminal tagging of M14 might interfere with correct protein function or localization. This protein was therefore not further analyzed.

4.17 Candidate M16 (PF3D7_0310900)

The protein sequence of M16 (PF3D7_0310900) comprises 786 AA. M16 is annotated as conserved *Plasmodium* protein with unknown function (according to: PlasmoDB

(Aurrecochea et al., 2009)). BLAST search (Altschul et al., 1990), the motif scan with MyHits (Pagni et al., 2004) and HHPred (Zimmermann et al., 2018) showed no similarities to other organisms outside the Apicomplexa. The saturation-based mutagenesis screen (Zhang et al., 2018), classified M16 as an essential protein for parasite growth. In the *P. berghei* genome screen (Bushell et al., 2017) the M16 orthologue was not listed.

To analyze M16, the corresponding gene product was tagged with 2xFKBP-GFP-2xFKBP by modification of the endogenous locus using SLI. Correct integration of the pSLI plasmid resulting in the M16-2xFKBP-GFP-2xFKBP knock-in was confirmed by PCR (Figure 17), whereas no correct integration could be achieved for the corresponding pSLI-TGD plasmid. Based on live cell microscopy expression of M16-2xFKBP-GFP-2xFKBP was detectable from early trophozoites to segmenters but not in ring stages and young trophozoites. M16-2xFKBP-GFP-2xFKBP was in one or occasionally two foci in the periphery of every nucleus, often facing the PPM (Figure 37), reminiscent of the pattern observed with M7-2xFKBP-GFP-2xFKBP. During nuclear division (when the nucleus stretches), generally two foci were visible, one each at the narrow side of the stretched nucleus (Figure 37 late troph), similar to the observed phenotype of M7-2xFKBP-GFP-2xFKBP.

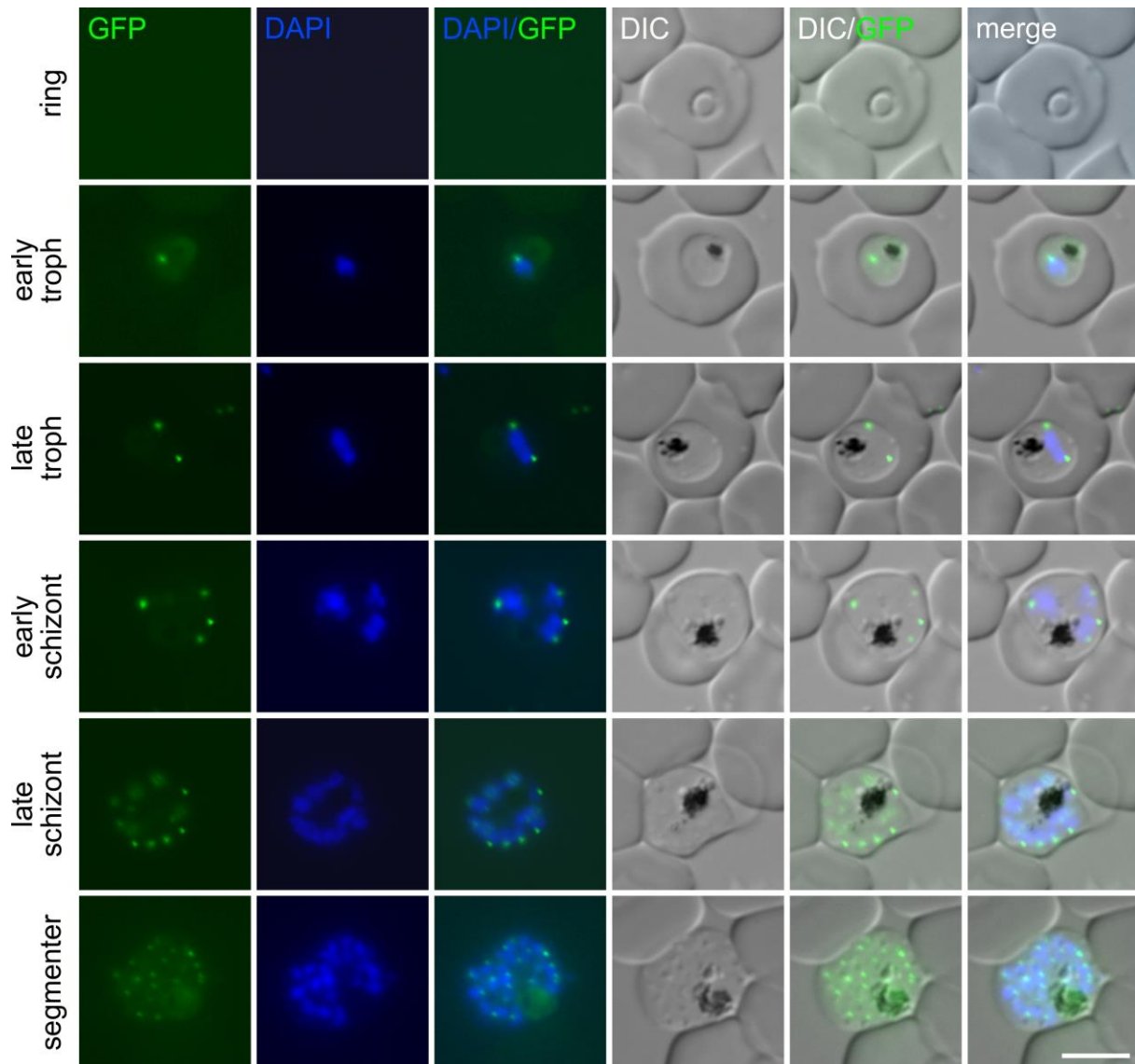


Figure 37: Localization of endogenously tagged candidate M16 (PF3D7_0310900).

Representative live cell images ($n \geq 3$ fluorescence microscopy sessions, with at least 20 inspected cells per session) of knock-in cell line M16-2xFKBP-GFP-2xFKBP (*GFP*). The stages are indicated on the left of the panel. Parasite nuclei were stained with DAPI. Scale bar 5 μm , DIC (differential interference contrast).

To functionally analyse M16, the M16-2xFKBP-GFP-2xFKBP cell line was co-transfected with an episomally expressed lyn-FRB-mCherry mislocalizer (Birnbbaum et al., 2017) (Figure 38 panel) and knock sideways was carried out. This revealed that M16 was efficiently mislocalised 24 h after addition of rapalog to induce the knock sideways (Figure 38 panel). Growth analysis over five days showed severe growth defect on parasite growth in the parasites with the inactivated M16 compared to the control (Figure 38 growth curve, and Appendix 5). Together with the failure to obtain a SLI-TGD line for M16, this suggests that M16 has importance for efficient parasite growth in the asexual blood stage.

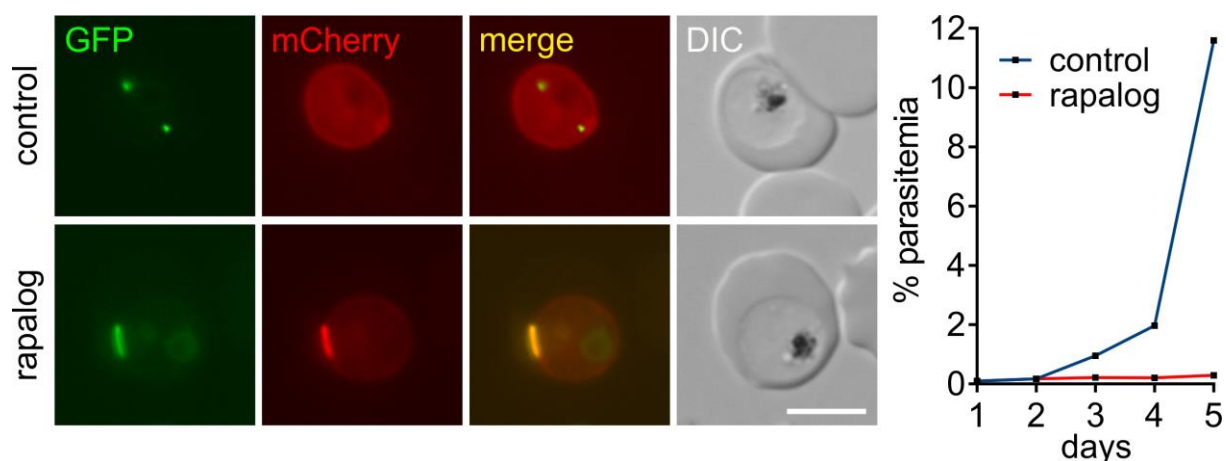


Figure 38: Knock sideways and growth curve of endogenously tagged candidate M16 (PF3D7_0310900).

Panel) Representative live cell images ($n \geq 3$ fluorescence microscopy sessions, with at least 20 inspected cells per session) of knock-in cell line M16-2xFKBP-GFP-2xFKBP ('GFP') with an episomally expressed lyn-FRB-mCherry mislocalizer. The cell culture was split into two dishes: one served as control without rapalog (control), and the other grown in the presence of 250 nM rapalog (rapalog). The samples for live cell imaging were taken 24 h post addition of rapalog. Scale bar 5 μm , DIC (differential interference contrast). **The graph to the right of the image panels** shows parasite growth as determined by flow cytometry of the M16-2xFKBP-GFP-2xFKBP knock sideways parasites grown in the presence of rapalog (inactivated) and without rapalog (control). One representative of three independent experiments (replicas shown in Appendix 5).

Due to the close proximity of M16 to the nuclei and the similarity to the localisation pattern of candidate M7, a co-localization with tubulin (TubulinTracker™) was performed. Tubulin was visible as expected in one focus at the outer part of the nuclei with two outgoing strings (Figure 39 control, tubulin, merge). M16-2xFKBP-GFP-2xFKBP partially co-localized with the center of tubulin facing the PPM (Figure 39 control). When knock sideways of M16 was induced, tubulin stayed at the nuclei (Figure 40 rapalog). While this suggested a different function of M16 compared to M7, there was nevertheless an effect on nuclear division apparent in some parasites that displayed nuclei that were not correctly divided and showed a blurry shape without clear boundaries (Figure 39 rapalog, yellow arrows heads) in the parasites with the inactivated M16 compared to the control (Figure 39 control, DAPI). However, other parasites with the inactivated M16 displayed normal looking nuclei (Figure 39 rapalog, white arrow heads). Further studies are therefore needed to clarify the function of M16 in nuclear division.

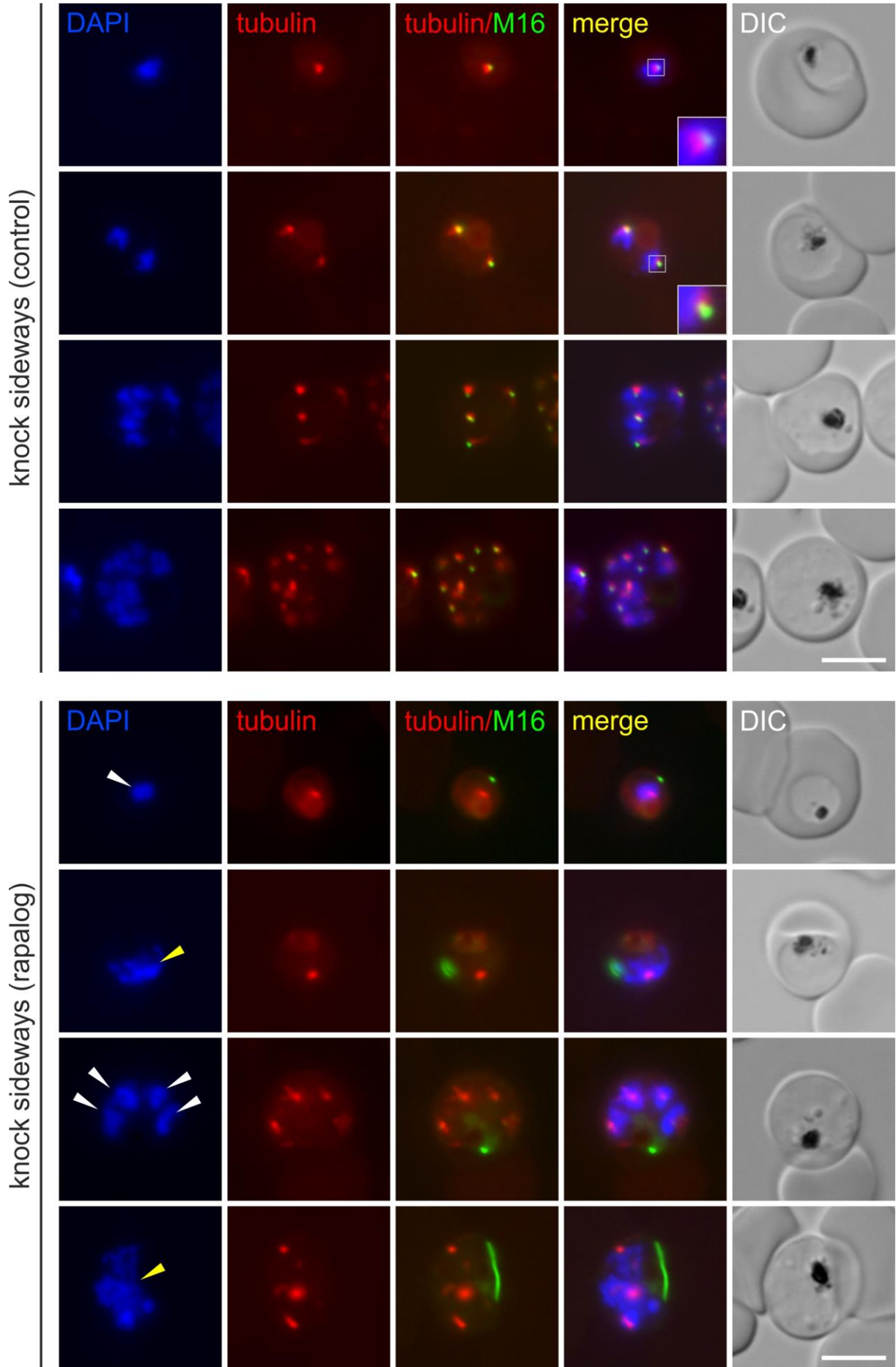


Figure 39: Candidate M16 (PF3D7_0310900) knock sideways and co-localization with tubulin.

Representative live cell images ($n \geq 3$ fluorescence microscopy sessions, with at least 15 inspected cells per session) of knock-in cell line of M16-2xFKBP-GFP-2xFKBP (green) with an episomally expressed lyn-FRB-mCherry mislocalizer. The cell culture was split into two dishes: one served as control without rapalog (control), and the other was grown in the presence of 250 nM rapalog (rapalog). The samples for live cell imaging were taken 8 h post addition of rapalog. Parasite nuclei were stained with DAPI (blue) and TubulinTracker™ deep red (tubulin, red). Zoom pictures are displayed with a 3x magnification (grey square). Yellow arrow heads pointing to ‘unusual’ nuclei, white arrowheads indicating ‘normal’ looking nuclei. Scale bars 5 μm .

4.18 Candidate M17 (PF3D7_0312900)

M17 (PF3D7_0312900) is annotated as hypothetical protein and comprises 273 AA (according to: PlasmoDB (Aurrecochea et al., 2009)). BLAST search (Altschul et al., 1990) revealed no significant similarity outside the Apicomplexa. A motif scan with MyHits (Pagni et al., 2004) showed no significant hit. Using in HHPred (Zimmermann et al., 2018), no significant hit found. The saturation-based mutagenesis screen classified the protein as dispensable for parasite growth (Zhang et al., 2018). In the *P. berghei* genome screen (Bushell et al., 2017) the M17 orthologue was not analyzed.

To analyze M17, the corresponding gene product was tagged with 2xFKBP-GFP-2xFKBP by modification of the endogenous locus using SLI. Correct integration of the pSLI plasmid resulting in the M17-2xFKBP-GFP-2xFKBP knock-in was confirmed by PCR (Figure 17), whereas no correct integration could be achieved for the corresponding pSLI-TGD plasmid. The M17-2xFKBP-GFP-2xFKBP cell line was analyzed by live fluorescence microscopy and no signal was detected in parasite ring stages of the asexual development of the parasite in RBCs (Figure 40). In trophozoites and schizonts a very low fluorescence signal was detected at the PPM (Figure 40) and in segmenter the signal was diffuse visible inside the parasites (Figure 40).

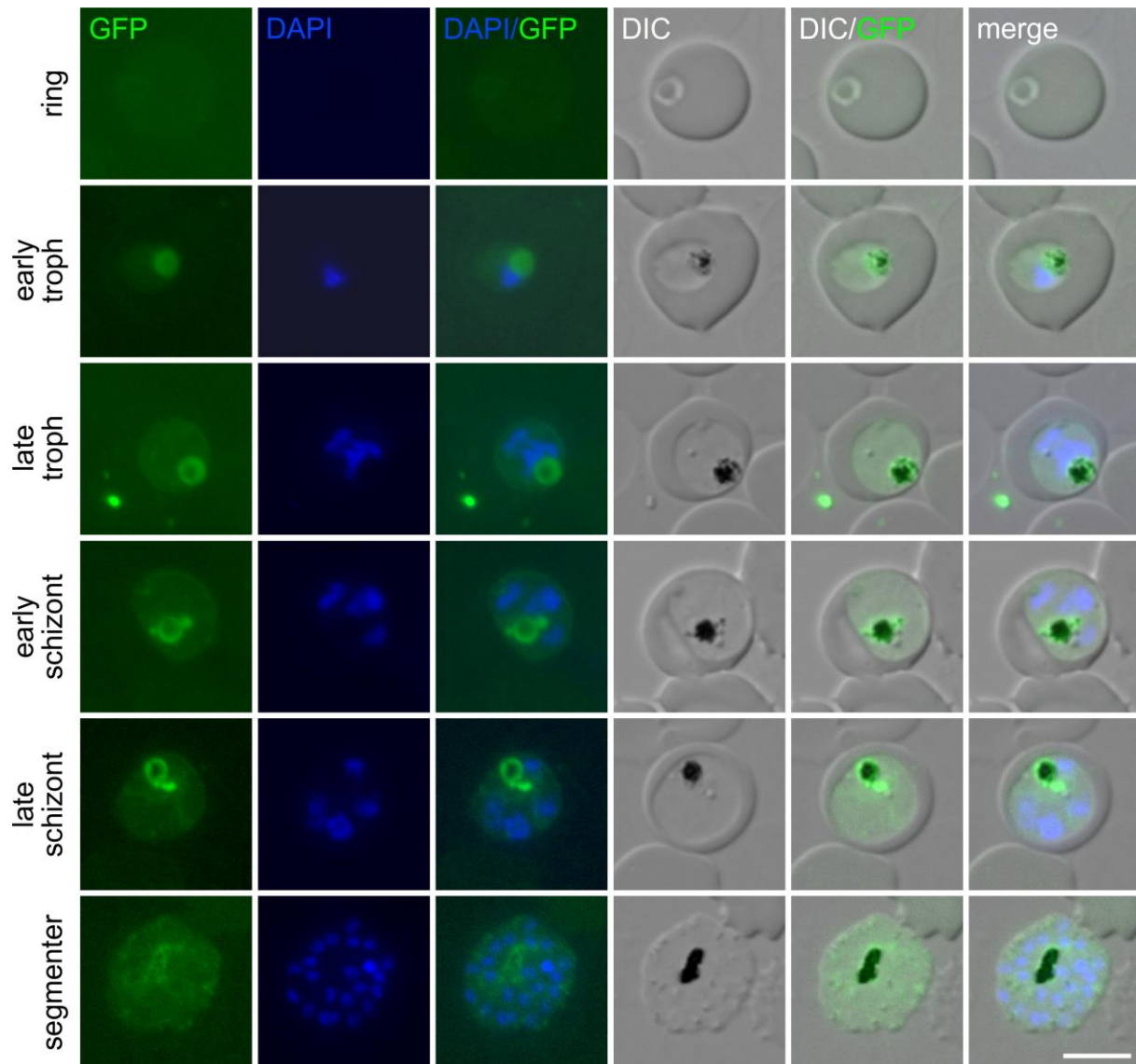


Figure 40: Localization of endogenously tagged candidate M17 (PF3D7_0310900).

Representative live cell images ($n \geq 3$ fluorescence microscopy sessions, with at least 20 inspected cells per session) of knock-in cell line M17-2xFKBP-GFP-2xFKBP ('GFP'). The stages are indicated on the left of the panel. Parasite nuclei were stained with DAPI. Scale bar 5 μm , DIC (differential interference contrast).

4.19 Candidate M18 (PF3D7_0313000)

PF3D7_0313000 (M18) is annotated as conserved *Plasmodium* protein with unknown function and the AA sequence comprises 346 AA (according to: PlasmoDB (Aurrecochea et al., 2009)). BLAST search (Altschul et al., 1990) revealed similarity (to a probable serine/threonine-protein kinase in *Piliocolobus tephrosceles* (e-value: $3e-08$, percent probability: 36.2 %)). A motif scan with MyHits (Pagni et al., 2004) showed no significant hits. Using HHPred (Zimmermann et al., 2018), only hits over short stretches or to common structural domains, such as coiled coils were found. The saturation-based mutagenesis screen (Zhang et al., 2018) revealed a dispensable function of this protein for parasite growth. The orthologue *P. berghei* protein was not analyzed (Bushell et al., 2017).

To analyze M18, the corresponding gene product was tagged with 2xFKBP-GFP-2xFKBP by modification of the endogenous locus using SLI. Correct integration of the pSLI plasmid resulting in the M18-2xFKBP-GFP-2xFKBP knock-in was confirmed by PCR (Figure 17), whereas no correct integration could be achieved for the corresponding pSLI-TGD plasmid. Microscopy revealed detectable fluorescence signal expression for M18-2xFKBP-GFP-2xFKBP in the cytoplasm over all asexual erythrocyte stages (Figure 41). In addition to the cytoplasmic distribution of M18-2xFKBP-GFP-2xFKBP, one focus was seen in early trophozoites, and from late trophozoites to segmenters multiple foci were observed that often were in proximity to the nucleus (Figure. 41). This fluorescence pattern could indicate a Golgi location but a co-localisation analysis would be needed to confirm this hypothesis.

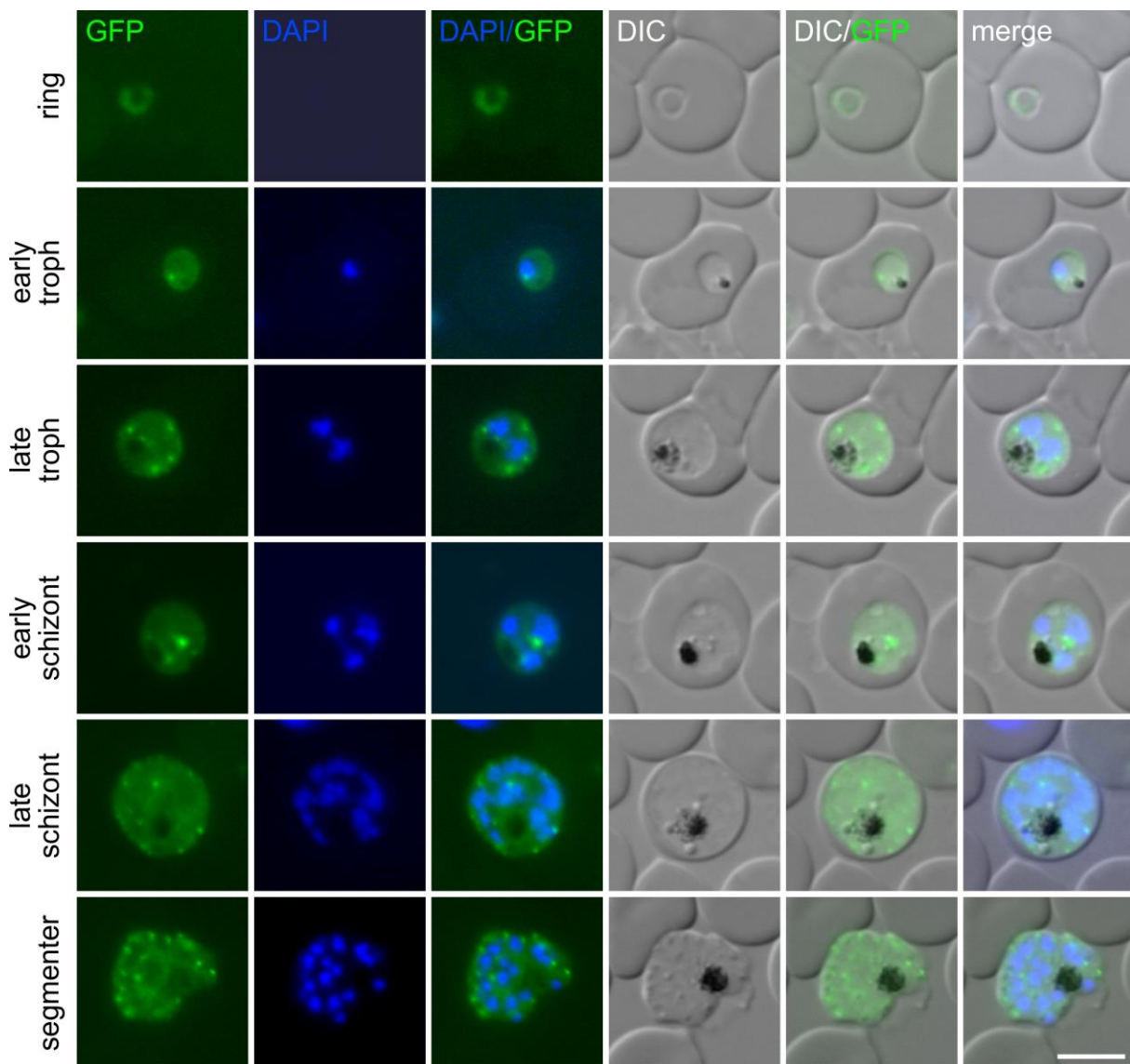


Figure 41: Localization of endogenously tagged candidate M18 (PF3D7_0313000).

Representative live cell images ($n \geq 3$ fluorescence microscopy sessions, with at least 20 inspected cells per session) of knock-in cell line M18-2xFKBP-GFP-2xFKBP ('GFP'). The stages are indicated on the left of the panel. Parasite nuclei were stained with DAPI. Scale bar 5 μm , DIC (differential interference contrast).

To functionally analyse M18, the M18-2xFKBP-GFP-2xFKBP cell line was co-transfected with an episomally expressed 1xNLS-FRB-mCherry mislocalizer (Birnbaum et al., 2017) (Figure 43 panel) and knock sideways was carried out. While most of the M18 protein was mislocalized some foci were seen outside the nucleus in the parasites with the inactivated M18, potentially indicating that some of the M18 protein population remained at its site of action (Figure 42 panel). Growth analysis over five days showed no effect on parasite growth in the parasites with the inactivated M18 compared to the control which may be due to the insufficient mislocalization (Figure 42 growth curve, and Appendix 5). In conclusion it is unclear if this protein is important for growth of asexual blood stage parasites.

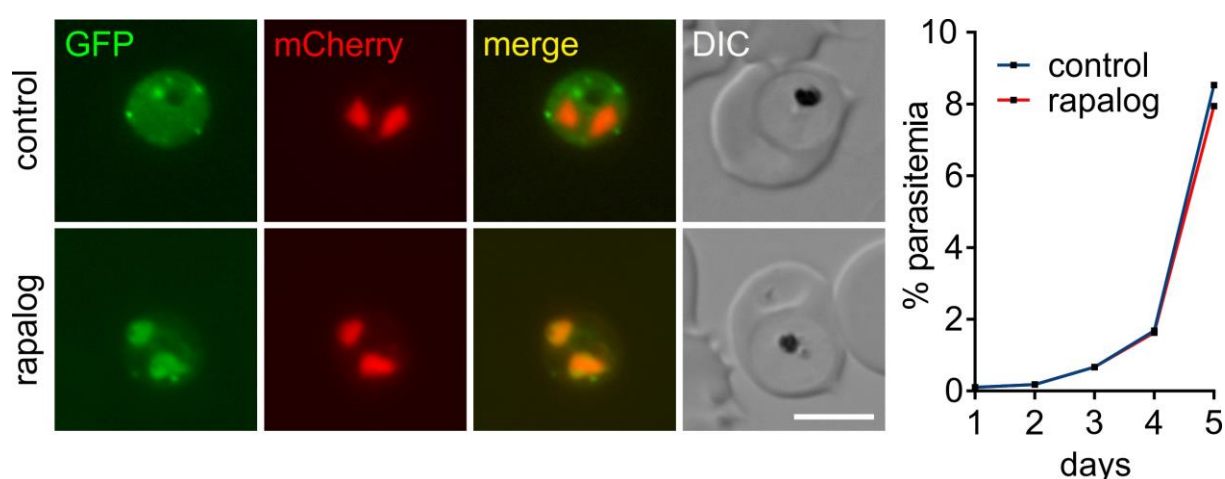


Figure 42: Knock sideways and growth curve of endogenously tagged candidate M18 (PF3D7_0313000).

Representative live cell images ($n \geq 3$ fluorescence microscopy sessions, with at least 20 inspected cells per session) of knock-in cell line M18-2xFKBP-GFP-2xFKBP ('GFP') with an episomally expressed 1xNLS-FRB-mCherry mislocalizer. The cell culture was split into two dishes: one served as control without rapalog (control), and the other grown in the presence of 250 nM rapalog (rapalog). The samples for live cell imaging were taken 24 h post addition of rapalog. Scale bar 5 μm , DIC (differential interference contrast). **The graph to the right of the image panels** shows parasite growth as determined by flow cytometry of the M18-2xFKBP-GFP-2xFKBP knock sideways parasites grown in the presence of rapalog (inactivated) and without rapalog (control). One representative of three independent experiments (replicas shown in Appendix 5).

4.20 Candidate M19 (PF3D7_0313200)

M19 (PF3D7_0313200) is annotated as conserved protein with unknown function and comprises 233 AA (according to: PlasmoDB (Aurrecochea et al., 2009)). A motif scan with MyHits (Pagni et al., 2004) showed no similarity to other domains. BLAST search (Altschul et al., 1990) showed a similarity to an unnamed protein product of *Vitrella brassicaformis* (e-value: $1e-10$, percent identity 26.1 %). Using HHPred (Zimmermann et al., 2018), only hits over short stretches or to common structural domains, such as coiled coils were found. The saturation-based mutagenesis screen (Zhang et al., 2018), classified M19 as an intermediate

phenotype between essential and dispensable for parasite growth. In the *P. berghei* genome screen (Bushell et al., 2017) the orthologue protein was not listed.

To analyze M19, the corresponding gene product was tagged with 2xFKBP-GFP-2xFKBP by modification of the endogenous locus using SLI. Correct integration of the pSLI plasmid resulting in the M19-2xFKBP-GFP-2xFKBP knock-in was confirmed by PCR (Figure 17), whereas no correct integration could be achieved for the corresponding pSLI-TGD plasmid. Microscopy of the M19-2xFKBP-GFP-2xFKBP cell line revealed no detectable fluorescence signal expression in ring stages and a faint uniform cytosolic location in young trophozoites (Figure 43). From late trophozoites to segmenters M19-2xFKBP-GFP-2xFKBP was visible in irregular accumulations in the parasite cytoplasm that did not overlap with nuclei with some additional isolated foci (Figure 43).

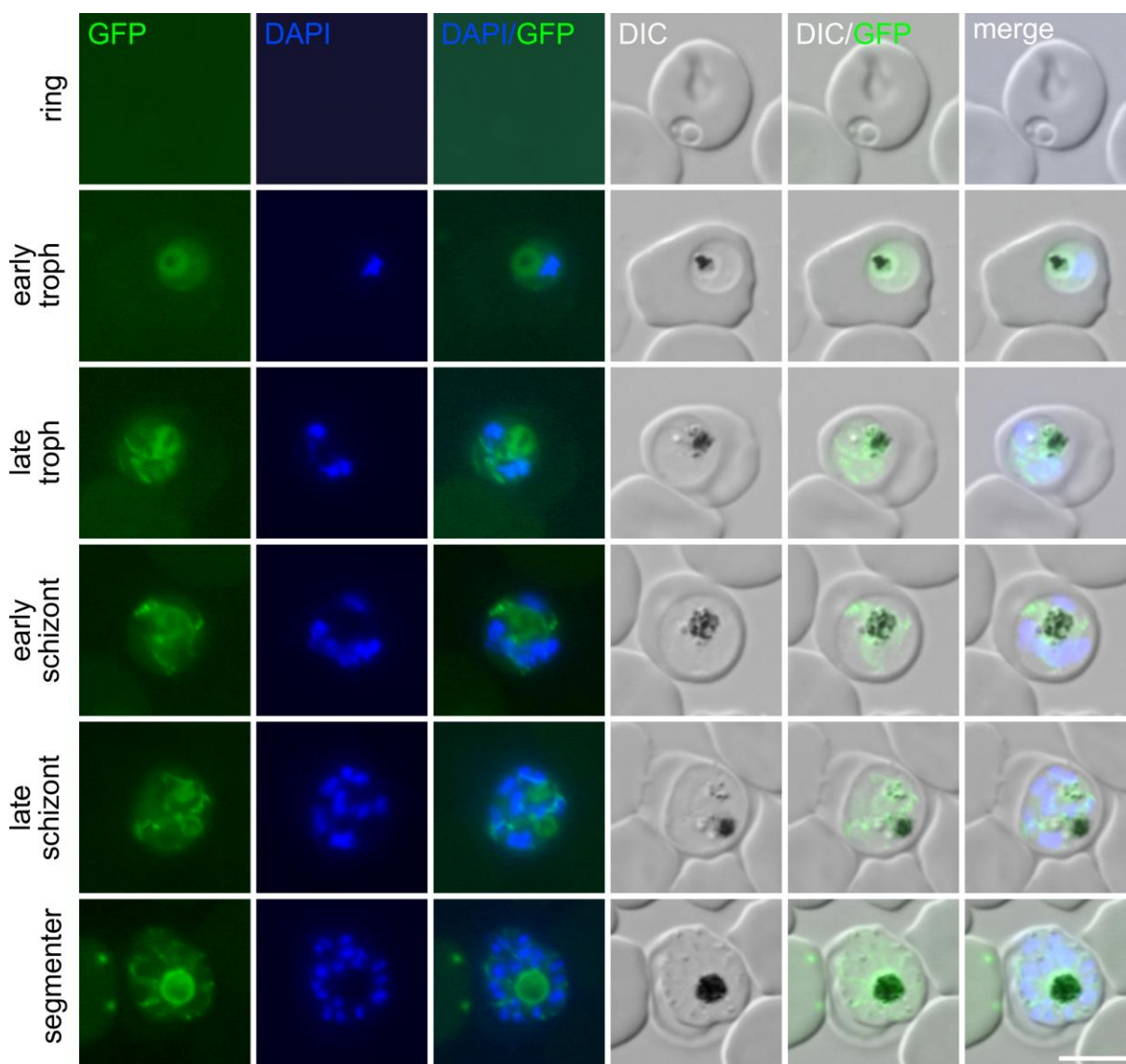


Figure 43: Localization of endogenously tagged candidate M19 (PF3D7_0313200).

Representative live cell images ($n \geq 3$ fluorescence microscopy sessions, with at least 20 inspected cells per session) of knock-in cell line M20-2xFKBP-GFP-2xFKBP ('GFP'). The stages are indicated on the left of the panel. Parasite nuclei were stained with DAPI. Scale bar 5 μm , DIC (differential interference contrast).

4.21 Candidate M20 (PF3D7_0313400)

M20 (PF3D7_0313400) is annotated as conserved *Plasmodium* protein with unknown function and comprises 784 AA (according to: PlasmoDB (Aurrecochea et al., 2009)). A BLAST search (Altschul et al., 1990) revealed a similarity to a ribonuclease E in *Tatumella saanichensis* (e-value: 0.007, percent identity: 35 %) and additional seven hypothetical proteins (e-values $\geq 1\text{e-}04$, percent identities ≤ 47.9 %). In a motif scan with MyHits (Pagni et al., 2004), no significant hit was shown. Using HHPred (Zimmermann et al., 2018), only hits over short stretches or to common structural domains, such as coiled coils were found. The saturation-based mutagenesis screen (Zhang et al., 2018), classified M20 as essential for parasite growth. In the *P. berghei* genome screen (Bushell et al., 2017) the M20 orthologue protein was not listed.

To analyze M20, the corresponding gene product was tagged with 2xFKBP-GFP-2xFKBP by modification of the endogenous locus using SLI. Correct integration of the pSLI plasmid resulting in the M20-2xFKBP-GFP-2xFKBP knock-in was confirmed by PCR (Figure 17), whereas no correct integration could be achieved for the corresponding pSLI-TGD plasmid. Fluorescence microscopy with the cell line M20-2xFKBP-GFP-2xFKBP revealed only a mostly uniform cytosolic GFP signal, indicating that M20-2xFKBP-GFP-2xFKBP was only poorly expressed in all asexual blood stages (Figure 44). As typically non-specific background shows a signal in the FV (like described for 3D7 (Birnbaum et al., 2017)), not the parasite cytosol, it is most likely that M20 is present evenly distributed in the parasite cytoplasm (Figure 44).

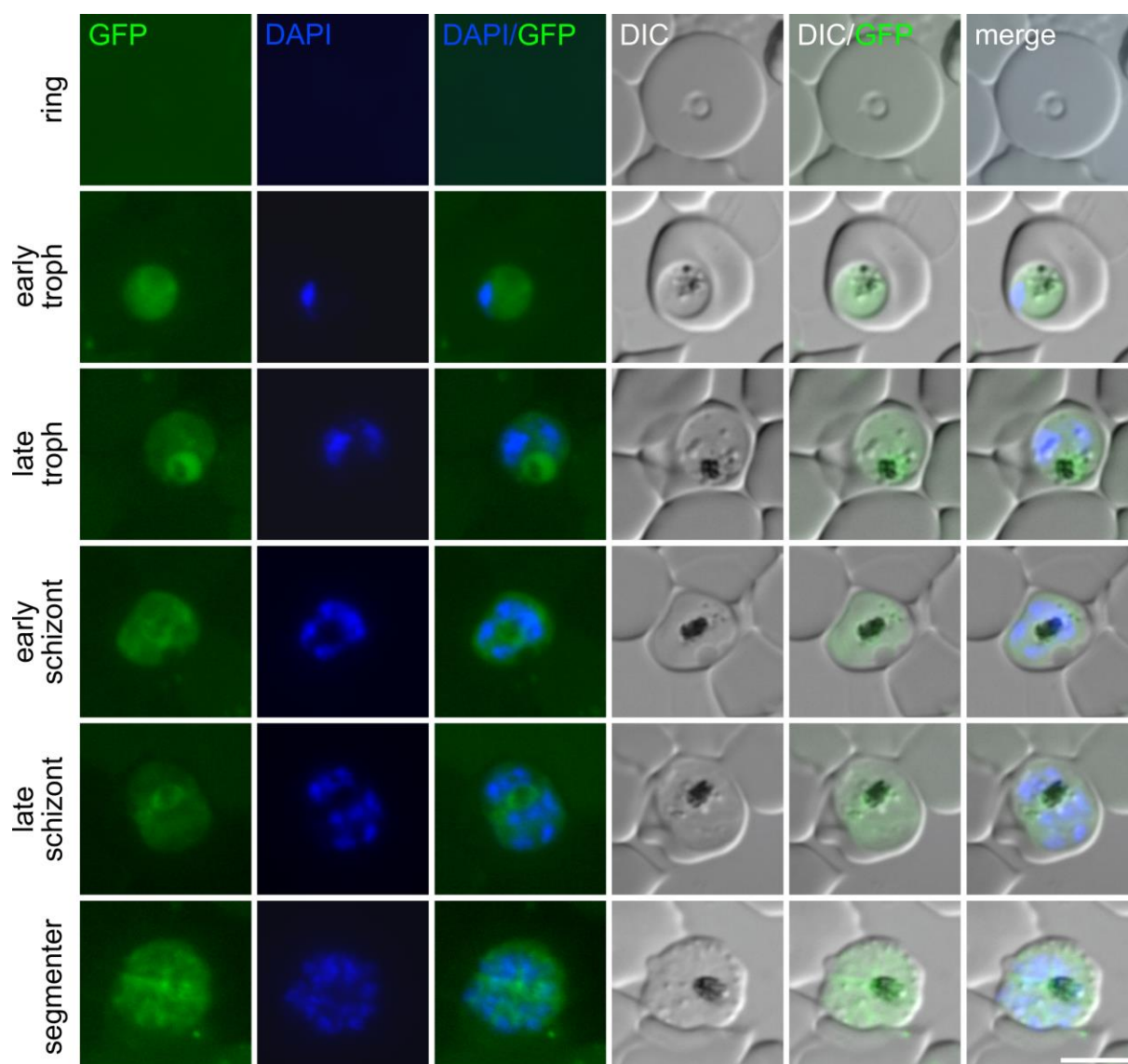


Figure 44: Localization of endogenously tagged candidate M20 (PF3D7_0313400).

Representative live cell images ($n \geq 3$ fluorescence microscopy sessions, with at least 20 inspected cells per session) of knock-in cell line M20-2xFKBP-GFP-2xFKBP (*GFP*). The stages are indicated on the left of the panel. Parasite nuclei were stained with DAPI. Scale bar 5 μm , DIC (differential interference contrast).

4.22 Candidate M24 (PF3D7_0314700)

At the time this work was started, PF3D7_0314700 (M24) was annotated as conserved *Plasmodium* protein with unknown function (according to: PlasmoDB, release 31 (Aurrecochea et al., 2009)). During the course of this work, the annotation changed to ring finger protein RNF1 (according to: PlasmoDB, release 46 (Aurrecochea et al., 2009)). The protein comprises 1181 AA, and a BLAST search (Altschul et al., 1990) showed no significant similarity to other organisms outside the Apicomplexa. A motif scan with MyHits (Pagni et al., 2004) also displayed a Zinc finger (RING finger) domain at position 1131-1171. The best hit using HHPred (Zimmermann et al., 2018), with a putative similarity to M24 was an ERAD-associated E3 ubiquitin-protein ligase HRD1 from *Saccharomyces cerevisiae*. The

saturation-based mutagenesis screen (Zhang et al., 2018), classified M24 as dispensable for parasite growth. Similarly the orthologue protein in *P. berghei* parasites was annotated as non-essential for parasite growth.

To analyze M24, the corresponding gene product was tagged with 2xFKBP-GFP-2xFKBP by modification of the endogenous locus using SLI. Correct integration of the pSLI plasmid resulting in the M24-2xFKBP-GFP-2xFKBP knock-in was confirmed by PCR (Figure 17), whereas no correct integration could be achieved for the corresponding pSLI-TGD plasmid. Fluorescence microscopy with the cell line M24-2xFKBP-GFP-2xFKBP revealed only a mostly uniform cytosolic GFP signal, indicating that M24-2xFKBP-GFP-2xFKBP was only poorly expressed in all asexual blood stages (Figure 45). As typically non-specific background shows a signal in the FV (like described for 3D7 (Birnbaum et al., 2017), not the parasite cytosol, it is most likely that M24 is present evenly distributed in the parasite cytoplasm (Figure 45).

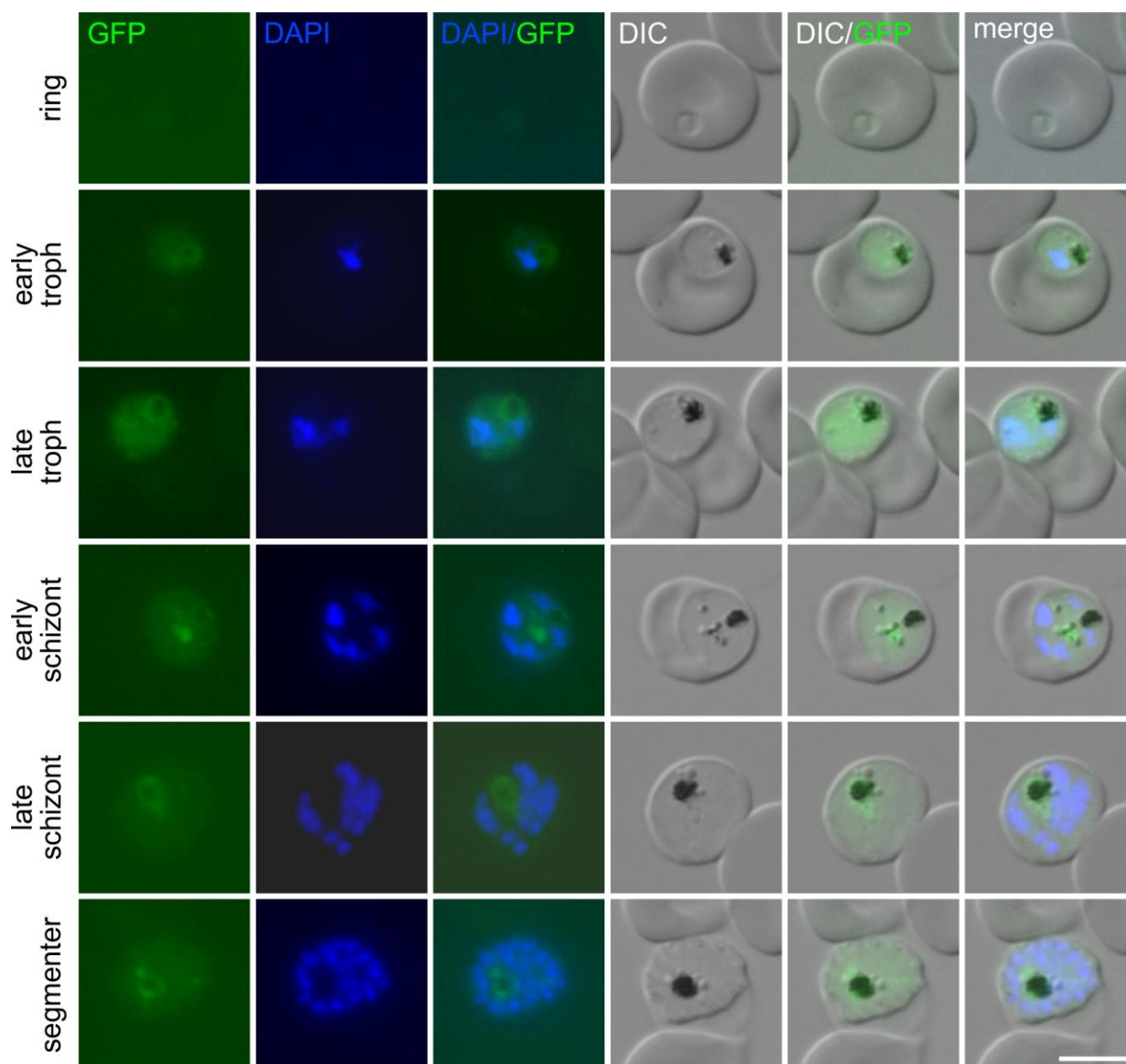


Figure 45: Localization of endogenously tagged candidate M24 (PF3D7_0314700).

Representative live cell images ($n \geq 3$ fluorescence microscopy sessions, with at least 20 inspected cells per session) of knock-in cell line M24-2xFKBP-GFP-2xFKBP (*GFP*). The stages are indicated on the left of the panel. Parasite nuclei were stained with DAPI. Scale bar 5 μm , DIC (differential interference contrast).

To functionally analyse M24, the M24-2xFKBP-GFP-2xFKBP cell line was co-transfected with an episomally expressed 1xNLS-FRB-mCherry mislocalizer (Birnbaum et al., 2017) (Figure 46 panel) and knock sideways was carried out. This revealed that M24 was efficiently mislocalised to the nucleus 24 h after addition of rapalog to induce the knock sideways (Figure 46 panel). However, growth analysis over five days showed no effect on parasite growth in the parasites with the inactivated M24 compared to the control (Figure 46 growth curve, and Appendix 5). In conclusion the knock sideways reveals that M24 dispensable for growth of asexual blood stage parasites.

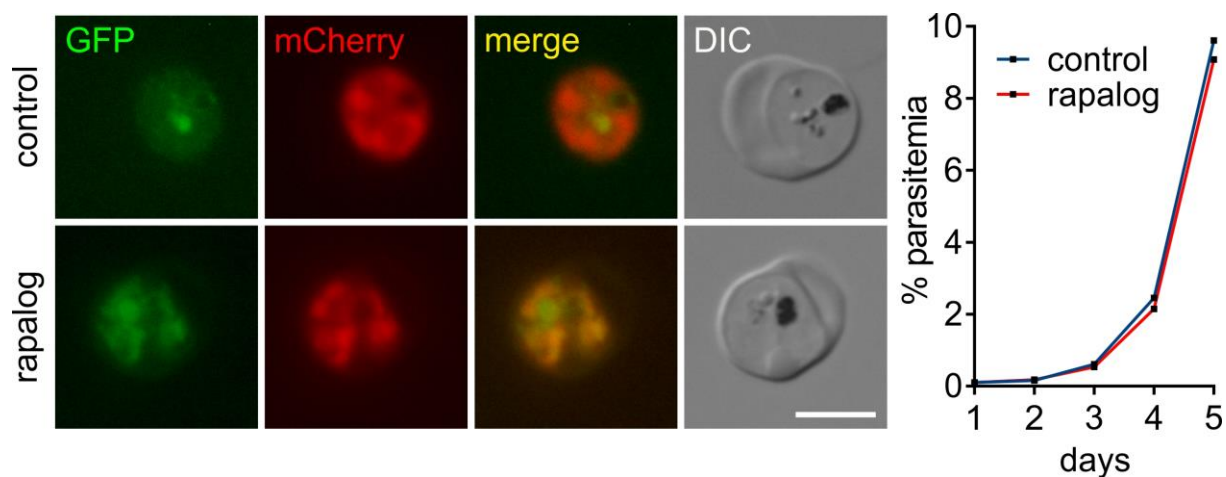


Figure 46: Knock sideways and growth curve of endogenously tagged candidate M24 (PF3D7_0314700).

Panel) Representative live cell images ($n \geq 3$ fluorescence microscopy sessions, with at least 20 inspected cells per session) of knock-in cell line M24-2xFKBP-GFP-2xFKBP ('GFP') with an episomally expressed Δ NLS-FRB-mCherry mislocalizer. The cell culture was split into two dishes: one served as control without rapalog (control), and the other grown in the presence of 250 nM rapalog (rapalog). The samples for live cell imaging were taken 24 h post addition of rapalog. Scale bar 5 μ m, DIC (differential interference contrast). **The graph to the right of the image panels** shows parasite growth as determined by flow cytometry of the M24-2xFKBP-GFP-2xFKBP knock sideways parasites grown in the presence of rapalog (inactivated) and without rapalog (control). One representative of three independent experiments (replicas shown in Appendix 5).

5 Discussion

More than one third (according to: PlasmoDB(Aurrecochea et al., 2009)) of the approximately 5700 *P. falciparum* genes (Gardner et al., 2002) are annotated to be of ‘unknown function’. Most of these genes are probably highly adapted to the parasite’s life cycle, and their investigation will lead to a better understanding of the parasite’s biology. The understanding of the parasite’s biology is essential to find parasite specific drug targets. This work specifically deals with genes with unknown function and a medium throughput screen of the genes of the third *P. falciparum* chromosome was carried out. To achieve this, the SLI-system was used to obtain endogenously tagged versions of the corresponding gene products, permitting the localisation of the physiological protein in living cells, its functional analysis using the knock sideways technique and for selected cases, an interaction analysis using DiQ-BioID (Birnbaum et al., 2017; Birnbaum et al., 2020). Additionally, a functional analysis of *PfRab5b* was carried out which served as proof of principle for the knock sideways method and subsequent functional assays while the cell lines for the analysis of the candidates from chromosome 3 were generated.

5.1 Role of Rab5b in host cell cytosol uptake

In humans, the Rab-GTPases and Rab like-GTPases comprise more than 70 proteins (Bock et al., 2001; Stenmark et al., 2001) and are members of the Ras superfamily (Colicelli, 2004). Rab-GTPases were identified as essential regulators for membrane trafficking (Bucci et al., 2006; Salminen et al., 1987; Schmitt et al., 1986; Touchot et al., 1987) and vesicular / tubular transport (Pfeffer, 1992). Thereby, they can switch between an active GTP- or an inactive GDP-bound conformation (Becker et al., 1991; Tisdale et al., 1992; Walworth et al., 1992; Walworth et al., 1989), catalyzed by a guanine nucleotide exchange factor (GEF) (Delprato et al., 2004). In recent years it was shown that Rab-GTPases are important for several events, including vesicle budding from donor membranes, coat assembly, cargo selection and physical budding (reviewed in: (Stenmark, 2009)).

In mammalian cells the Rab5 GTPase was localized to early endosomes and on the cytoplasmic surface of the plasma membrane (Chavrier et al., 1990a; Chavrier et al., 1990b) and has been shown to be involved in early endocytosis (Bucci et al., 1992; Gorvel et al., 1991). It was also postulated that Rab5, forming a complex with GDP dissociation inhibitor (GDI), is an essential factor for Clathrin coated pit formation at the plasma membrane and during Clathrin mediated endocytosis for transferrin receptors (McLauchlan et al., 1998). Rab5 was renamed to Rab5a as two additional isoforms (Rab5b and Rab5c) were found

(Chavrier et al., 1992; Wilson et al., 1992). It was shown that the isoforms share all the structural features and cooperate in the regulation of endocytosis (Bucci et al., 1995).

In *P. falciparum* parasites, a gene with a significant similarity to *rab5* was identified (Gardner et al., 1998). Later on, also two other *rab5* homologs (*Pfrab5b* and *Pfrab5c*) were identified, whereby *Pfrab5b* does not encode a classical Rab C-terminus but is N-terminally modified (Quevillon et al., 2003). Recently, it was shown that *PfRab5a* is not involved in endocytosis (Birnbaum et al., 2017). The function of *Rab5b* and *Rab5c* is still unclear (Ebine et al., 2016; Ezougou et al., 2014). Sven Flemming could show that *Rab5b* co-localizes with the endosomal marker PI(3)P at the FV and its extension and proposed *PfRab5b* as a protein putatively involved in endocytosis (Flemming, 2015).

In order to validate that *Rab5b* is involved in endocytosis, the *Rab5b-2xFKBP-GFP-FKBP* cell line (kindly provided by Sven Flemming) was used for further analysis in this thesis.

By functional analysis and quantification experiments, *Rab5b* revealed an essential role in host cell cytosol uptake like the recently postulated VPS45 protein (Jonscher et al., 2019). VPS45 was the first protein shown to be involved in HCCU, whereby the inactivation of VPS45 led to the formation of PI(3)P positive vesicles in the parasite and a lethal phenotype. VPS45 was localized near the FV and Golgi (Jonscher et al., 2019). *Rab5b* inactivation revealed a similar growth defect in addition to vesicle accumulation, as observed for parasites where VPS45 was inactivated. However, a lower number of accumulated vesicles over time were observed in parasites, where *Rab5b* was inactivated compared to parasites where VPS45 was inactivated, and the growth phenotype for *Rab5b* inactivated parasites was not as pronounced. A possible explanation for this could be a partial compensation by one of the other *PfRab5* proteins. In mammalian cells, the three *Rab5* isoforms cooperate in endocytosis regulation, suggesting functional redundancy (Bucci et al., 1995; Su et al., 2006). However, there is also evidence that different *Rab5* isoforms have different functions in different cell types or species (Barbieri et al., 2000; Birnbaum et al., 2017; Chen et al., 2009; Chiariello et al., 1999; Rastogi et al., 2016; Rosenfeld et al., 2001). Because in *P. falciparum* parasites *Rab5a* was not linked to endocytosis (Birnbaum et al., 2017), only *Rab5c* can be considered to partially compensate the loss of *Rab5b*. Another option could be an incomplete knock sideways, whereby a small amount of the protein might remain functional and ensure the parasites' survival. While no *Rab5b* was apparent outside of the nucleus after the knock sideways it cannot be fully excluded that a small fraction of the *Rab5b* population remained at its physiological site of action.

In agreement with the growth phenotype, Rab5b inactivation revealed an arrest of the parasites. However, the arrest of Rab5b was mainly seen in schizonts, whereas VPS45 inactivation leads to an arrest in trophozoites and schizonts (Jonscher et al., 2019). An explanation for this is the less profound effect of the Rab5b phenotype that likely permitted the cells to progress further in the cycle or potentially a mild difference in scoring of trophozoites and schizonts which is done based on Giemsa smears, not a defined marker, and therefore is subject to some level of variation.

To further assess a similarity of the Rab5b and the VPS45 phenotype, electron microscopy experiments of parasites with inactivated *Pf*Rab5b could characterize vesicle membranes composition to compare it to those published in the parasites where VPS45 was inactivated. Electron microscopy images of parasites with inactivated VPS45 displayed vesicles with double membranes (could indicate early endocytosis) as well as vesicles with only one membrane (Jonscher et al., 2019), which might suggest matured vesicles in later endocytosis. In other organisms Rab5b, functions together with VPS45 and a third protein, rabenosyn-5 in endocytosis (Deneka et al., 2002; Eathiraj et al., 2005; Gengyo-Ando et al., 2007; Nielsen et al., 2000; Rahajeng et al., 2010; Tall et al., 1999). The results in this thesis therefore support the assumption that Rab5b and VPS45 participate in the same endocytic intermediate step with similar function and maybe even in the same complex, suggesting an at least partially canonical endolysosomal pathway in malaria parasites. A co-localization with VPS45 and subcellular analysis with a Golgi marker, like GRASP, would give additional information about this interaction. A good method to show protein complexes is the DiQ-BioID (Birnbaum et al., 2020). Unfortunately, the dimerization of Rab5b with an episomally co-transfected BirA* ligase seems to displace Rab5b from its site of action and resulted in a lethal, vesicle accumulating phenotype. This was also observed when in a similar attempt the biotin ligase BirA* was recruited to VPS45 in an attempt to carry out DiQ-BioID (unpublished: Jonscher and Spielmann). To overcome this problem, the BirA* ligase was endogenously fused to Rab5b (Rab5b-7xGS-BirA*) but due to time reasons no BioID was yet carried out with this cell line. The resulting mass spectrometry may show the interactors of Rab5b and might validate the interaction with VPS45. However, it should be considered that this would be a regular BioID (Roux et al., 2012) which likely would show more background than DiQ-BioID. Another method to demonstrate interaction could be the SLI2 system (unpublished: Naranjo-Prado, Mesen-Ramirez, Stäcker), whereby both proteins can be endogenously tagged in the same cell line. Also fluorescence resonance energy transfer

(FRET) (Sekar et al., 2003) and co-immunoprecipitation assays (Simon et al., 2009) would be suitable methods to validate interaction partners.

Interestingly, the most prominent artemisinin resistance marker Kelch13, as well as an EPS15-like protein and AP2 μ were shown to be involved in *P. falciparum* endocytosis (Birnbaum et al., 2020) Rab5b showed no co-localization with the Kelch13 complex, and parasites deficient for certain Kelch13 complex proteins did not show a vesicle accumulation phenotypes, although they reduced endocytosis in *P. falciparum* parasites. This reveals different protein complexes, one characterized by Kelch13 and Eps15, and another one as VPS45 and Rab5b in different intermediate steps during HCCU. Due to the missing Kelch13 vesicle phenotype and the co-localization of VPS45 with the Golgi marker Grasp, Kelch13 and EPS15 could be involved in an early - and Rab5b with VPS45 in a late - HCCU (Figure 47).

For Rab5b, an additional functional analysis was conducted, by performing gene-complementation studies using mutated versions of Rab5b, which should lead to a Rab5b GTP- and Rab5b GDP-bound conformation. In human cells these resulted in different phenotypes, either unusually large early endosomal structures, or accumulation of very small endocytic vesicles (Stenmark et al., 1994a). Functional analysis did not reveal a phenotype when Rab5b-2xFKBP-GFP-2xFKBP was inactivated and episomally complemented with a Rab5b codon adjusted copy, including these mutations. This could be due to the overexpression of the episomal mutated Rab5b protein. This can lead to surplus amounts of the protein which might have complemented even though they contained the mutation (reviewed in: (Rosano et al., 2014)). If this is the case, complementing with a construct leading to a more moderate expression of the complementing Rab5b variant could be a solution. Furthermore, Rab5b-2xFKBP-GFP-2xFKBP remaining at its site of action during the knock sideways could compensate the effect of the episomally expressed Rab5b mutated copy, although it is unclear why this should have happened when it did not in the uncomplemented cell line. Using the DiCre system instead of the knock sideways to excise the genomic *rab5b* gene might be a solution for this. It is also possible that the position of the mutations did not affect the GTP/GDP binding in *P. falciparum* Rab5b.

In summary, the results indicate that Rab5b is involved in *P. falciparum* HCCU, probably located in the same complex as VPS45 (Figure 47). Amongst the eleven Rab proteins in the *P. falciparum* parasite's genome (Quevillon et al., 2003), Rab5b is the first linked to endocytosis and represents the second *P. falciparum* protein identified to be involved in HCCU.

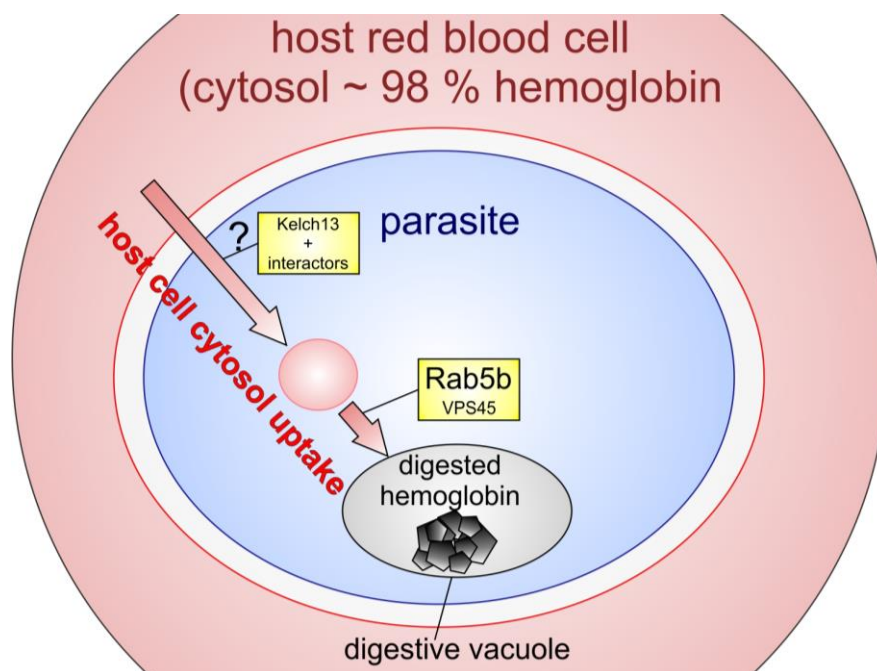


Figure 47: Model of Rab5b during host cell cytosol uptake.

Based on the results of this thesis and results from previous work (Birnbbaum et al., 2020; Jonscher et al., 2019) the figure shows a model of the molecules known to be involved in HCCU. The RBC is displayed in light red, the PVM in red, the PV is shown in white, the PPM in dark blue. The parasite is depicted in light blue, including the FV (light grey, digestive vacuole) with accumulated haemozoin (dark grey). The HCCU pathway is indicated by an arrow (light red) and proteins involved are shown in yellow boxes, circular light red structure, HCCU intermediate on the way to the FV). The model is based on: (Jonscher et al., 2019).

5.2 Functional investigation of *P. falciparum* proteins with unknown function

The genome of *P. falciparum* parasite's (strain 3D7) comprises approximately 2600 genes annotated with 'unknown function' (according to: PlasmoDB (Aurrecochea et al., 2009)) distributed on 14 chromosomes (Gardner et al., 2002). This project continued the functional investigation of chromosomes (chromosome 3), based on to the work of Sabine Schmidt (Master thesis, Sabine Schmidt), who partly analyzed chromosome 1, and Jakob Birnbbaum, who was focusing on chromosome 2 (Birnbbaum, 2017; Birnbbaum et al., 2017)

5.2.1 Selection of the unknown candidates

The third chromosome contains 249 predicted gene products (proteins) (according to: PlasmoDB (Aurrecochea et al., 2009)). Fifty-five proteins with a signal peptide and 49 proteins containing transmembrane domain(s) were excluded. This was done because these proteins are not suitable for functional analysis using the knock sideways method (Birnbbaum et al., 2017), because they are either inserted into a membrane or enter the secretory system

where they are unavailable for current mislocalisers. The 55 proteins which included a signal peptide among others included: rifin proteins (like: PF3D7_0300500, PF3D7_0300700) stevor proteins (like: PF3D7_0300400, PF3D7_0324600) a putative ER membrane subunit complex protein (PF3D7_0306700) a putative membrane transporter protein (PF3D7_0302600). Also, 13 conserved unknown proteins contained a signal peptide and were excluded. Of the removed transmembrane proteins, almost one half (24 proteins) was annotated as proteins with unknown function. The other half was annotated among others as PfEMP1, pseudogene (PF3D7_0300200), v-SNARE protein, putative (PF3D7_0314100) or as ubiquitin ligase protein (PF3D7_0312100). In view of the potential of unknown proteins (see. 1.5), the total of 37 unknown proteins which were removed highlight to develop a knock sideways system suitable for such proteins.

A suitable solution for the SP and TMs containing proteins would be the mislocalization before proteins with a signal peptide or transmembrane domain(s) reach their side of action. A mislocalizer for the secretory pathway potentially could inactivate proteins during passage through the ER or Golgi. A suitable system would be the RUSH system (retention using selective hooks). This system is based on streptavidin-binding peptide (SBP) interacting with streptavidin and was already used in other systems to control the release of proteins from the ER (Boncompain et al., 2012). To use a specific signal in ER, e.g. SDEL (Kulzer et al., 2009) as mislocalizer, and to make it inducible using FKBP-FRB, Melissa Kosh-Naucke constructed an *frb-mScarlet-sdel* vector which was transfected to a knock-in cell line. The results showed no or very little mislocalization, and it was concluded that the construct needs further optimization for large scale analysis (Kosh-Naucke, 2018).

Another conditional approach to control the trafficking destination of secretory proteins in *P. falciparum* parasites was recently published for apicoplast proteins (Roberts et al., 2019). The approach is based on unique structural requirements of apicoplast transit peptides, which the authors replaced with a conditional localization domain (CDL). In the presence of the effector ligand Shield, Shield1 binds to the CDL and causes secretion from the cell to the PV (Roberts et al., 2019). The use of CDL domains might also be possible for other secreted proteins.

Currently, the best alternative method for the excluded SP and TM proteins of the present screen might be the conditional gene excision using DiCre (Birnbaum et al., 2017; Mesén-Ramírez et al., 2019) which is independent of the properties of the protein.

5.2.2 Localization of the candidates

During the present study, 21 proteins of the third *P. falciparum* chromosome were analyzed using the SLI-method. Of these, 15 proteins were successfully endogenously tagged with GFP. These proteins were found to be located at various locations within the parasite (Table 9). One protein of the 15 GFP tagged proteins (Table 9, M6) was found, having a nuclear localization. This amounts to 6.7 % and is a lower percentage of nuclear proteins compared to other studies, such as the study of Oehring et al., where in a total of 1518 proteins distributed on all the 14 *P. falciparum* chromosomes (present in *P. falciparum* asexual blood stage parasites, using mass spectrometry and bioinformatic approaches), 48 % were determined as nuclear proteins (Oehring et al., 2012), as well as an earlier SLI study, where in a total of 18 proteins of chromosome two, 46 % had a nuclear localization (Birnbaum et al., 2017). The present screen also revealed a cytosolic localization (cytosolic and cytosolic/foci) (Table 9) for 6 of the 15 GFP tagged proteins (40 %). This is a higher number of proteins located in the cytosol, compared to the study of Oehring et al., where 16 % of the proteins were found in the cytoplasm (includes cytosol and cytoplasm proteins, excludes nuclear proteins) (Oehring et al., 2012), as well as the earlier SLI study, where 33 % of the proteins had a cytosolic localization (Birnbaum et al., 2017). The comparison of nuclear and cytosolic protein localizations in *P. falciparum* parasites shows a varying distribution among the different chromosomes and might also differ due to the method used. In conclusion, *P. falciparum* chromosome 3 reveals less nuclear proteins but more cytosolic proteins, compared to the *P. falciparum* chromosome two (Birnbaum et al., 2017) and the more general localizations of all the 14 *P. falciparum* chromosomes.

The former SLI study also revealed IMC localization for one protein (Birnbaum et al., 2017). A possible IMC localization was also considered for M12 of the present study. The localization of M12-2xFKBP-GFP-2xFKBP might be similar to IMC proteins as it was shown for BTP1 (Kono et al., 2016). Additionally, PF3D7_0308300 (M12) was found as a significant enriched hit within mass spectrometry analysis performed by Stephan Wichers (unpublished) for Phil1-BirA, an IMC protein, indicating M12 as protein within these structures.

A special localization was observed for the GFP tagged candidates M7, M11 and M16, located in foci at the nucleus. This localization might indicate a role in nuclear division (see 5.3 and 5.4).

Among these 15 proteins, two proteins showed an unclear localization due to a weak GFP signal (Table 9).

Table 9: Overview of analyzed candidates with localization, knock sideways and SLI-TGD

In the knock sideways column check marks indicate efficient KS; red check marks indicate essentiality of target by KS analysis; check mark in parenthesis indicate inefficient KS; n.d., not done; in localization column question mark indicates unclear localization due to low expression levels; in SLI-TGD column check marks indicate successful disruption of gene, x marks unsuccessful integration.

Candidate	Protein ID	Localization	Knock sideways	SLI-TGD
M1	PF3D7_0303100	cytosolic/some foci PPM	✓	x
M2	PF3D7_0304300	-	-	x
M3	PF3D7_0305200	cytosolic/foci	✓	x
M4	PF3D7_0305400	-	-	x
M5	PF3D7_0305500	-	-	x
M6	PF3D7_0306100	nuclear	(✓)	x
M7	PF3D7_0307500	foci at the nucleus	✓	x
M8	PF3D7_0307600	cytosolic/foci	(✓)	x
M9	PF3D7_0307700	-	-	x
M10	PF3D7_0307900	foci in cytosol	n.d.	x
M11	PF3D7_0308100	foci near the nucleus	n.d.	x
M12	PF3D7_0308300	PPM/IMC/cytosolic	n.d.	✓
M13	PF3D7_0308700	cytosolic/foci	n.d.	x
M14	PF3D7_0308800	-	-	x
M15	PF3D7_0309900	-	-	x
M16	PF3D7_0310900	foci at the nucleus	✓	x
M17	PF3D7_0312900	?	n.d.	x
M18	PF3D7_0313000	foci in cytosol	(✓)	x
M19	PF3D7_0313200	accumulation in cytosol	n.d.	x
M20	PF3D7_0313400	cytosolic	n.d.	x
M24	PF3D7_0314700	?	✓	x

5.2.2.1 Factors to consider for non-essential proteins

For non-essential proteins a factor to consider regarding localization is protein degradation, which might result in a cell line with a correct integration on genomic level, but without presence of full length tagged protein. Also partially degraded protein might result in a GFP signal being present at a false location, or additional staining at other subcellular locations. To exclude a degradation issue, western blot analysis could be performed in order to detect the full length tagged protein.

For essential proteins, these possibilities are much more unlikely than an incorrect localization, or protein degradation would affect parasite fitness. However, it cannot be excluded that little amounts of the protein are still at the correct location and sufficient for the parasite's survival.

5.2.2.2 Influencing factors of C-terminal tagging

Of the 21 proteins tagged with pSLI-sandwich (*2xfkbp-gfp-2xfkbp*), 6 did not show integration cell lines. As it was shown that many proteins depend on their C-terminal sequences and C-terminal modifications (Chavier et al., 1991; Hori et al., 1991; Hrycyna et al., 1993; Quevillon et al., 2003; Vorburger et al., 1989; Zhang et al., 2009), this could also be the case for the 6 candidates and C-terminal tagging by SLI might be detrimental for proteins depending on their C-terminal sequence (Birnbaum et al., 2017). Thus it is likely that the non-C-terminal taggable proteins are essential for parasite growth, as the tag hinders protein function, which is highlighting them as worthwhile targets for future studies.

A solution which permits live cell imaging and KS analysis might be N-terminal tagging, whereby the gene is destroyed and at the same time complemented with an N-terminal tagged copy that is expressed under the physiological promoter from the original locus. In addition, this new gene copy is also floxed (flanked by loxP sites), which can then be excised via a diCre recombinase for an alternative method for the functional analysis. This is also possible with the SLI-system and has already been established (Birnbaum et al., 2017).

5.2.3 Candidate essentiality prediction on the gene level

The essentiality of the proteins was tested on the genomic level as well as on the protein level. For the candidate's essentiality prediction on the gene level, SLI-TGD was used, with a homology region of 273 up to 393 bp. In the present screen, the TGD was only possible for one gene (*m12*). For another gene (*m3*), the TGD integration bands were observed, but some parasites with an original locus remained. Furthermore, the integration bands for M3 disappeared after additional WR99210 and G418 treatment, and only the original locus remained. As the knock sideways results suggested that this candidate was needed for efficient parasite growth (3.1 % reduction in growth over 5 days), it suggests that truncation of M3 incurred a negative selection pressure, explaining this result.

As no further TGDs were obtained (Table 9), this would mean that, judged on gene level, the remaining 19 candidates and thus ~ 90 % of the tested genes have to be classified as essential for parasite growth. In other genome wide screens, approximately 62 - 63 % of the genes were classified as genes which are required for normal parasites' growth (Bushell et al., 2017; Zhang et al., 2018), whereby the genome screen of Bushell et al. was conducted in vivo with the closely *P. falciparum* related parasite *P. berghei* (Bushell et al., 2017). In a former pSLI-TGD study (Birnbaum et al., 2017) 18 genes were tested, whereby 7 could not be disrupted, suggesting that ~ 39 % of the analyzed genes are essential for parasite growth. Thus a

proportion of 90 % essential genes as suggested by the present SLI-TGD screen is probably an overestimation. The possibility of a corrupted pSLI-TGD vector was considered during this work but full-length sequencing of the vector (Appendix 6) excluded this possibility. It is also possible that the skipping of the neomycin-resistance was inefficient or missing, leading to parasites that were not resistant. This scenario, however, is very unlikely as the knock-in cell lines with pSLI-sandwich vector contained the same skip and neomycin-resistance cassette, and the correct skipping was shown for both constructs (Birnbaum et al., 2017). Furthermore, previous SLT-TGD studies would have suffered the same problem. Therefore, a technical error has to be considered, such as for instance a start of G418 selection of the cultures containing the episomal SLI-TGD for integration at a parasitemia that was too low or too high. However, the procedure was carried out according to previously established standard procedures and was successful for the C-terminal tagging with the sandwich tag, indicating that a general error was unlikely. Possibly, fine details of this procedure might have reduced the efficiency of integration. This could be relevant, as much shorter homology regions were chosen for the SLI-TGD approach than for the sandwich tagging. Homology region length is the most important known parameter affecting integration efficiency (Birnbaum et al., 2017). Thus, the rather short homology regions used could be a reason for the low number of correct TGD integrations. The reason for shorter homology regions in the SLI-TGD is that for this approach, longer homology regions could lead to a gene that retains partial or fully functional. Nevertheless, it was also shown that even shorter HR (less than 200 bp) integration was successful with SLI, although the efficiency is often lower and takes more attempts (Jakob Cronshagenand (Master thesis 2020) Thuy Tuyen Tran (Master thesis 2018), (Mesén-Ramírez et al., 2019)). In conclusion, more integration attempts or a longer HR might lead to a higher integration rate of the chosen candidates using SLI-TGD.

5.2.4 Candidate's essentiality prediction on protein level

For testing candidate essentiality on the protein level, the knock sideways approach was used. To do this the 2xFKBP-GFP-2xFKBP tagged protein is pulled to an episomally expressed mislocalizer containing a FRB domain, by dimerizing the FKBP domain of the protein tag, with a small dimerizer to the FRB domain. Using knock sideways, the parasites were analyzed in a growth assay. This was performed for a total of eight proteins, whereby five proteins showed an efficient mislocalization and three only revealed a partial mislocalization (Table 9). From the eight proteins three showed a defect on parasite growth in the parasites where the protein was inactivated compared to the control (Table 9). These results suggest

that, judged on protein level, ~ 38 % of the tested proteins can be classified as important for parasite growth and is similar to the observed ~ 39 % essential genes in the former SLI study. Compared to the genome wide screens in *P. berghei* (in vivo) (Bushell et al., 2017) and *P. falciparum* (Zhang et al., 2018) were ~ 62 - 63 % of the genes were classified as required for normal parasite growth the rate for the candidates tested on protein level using KS is reduced by ~ 24 percent. This might be due to the much smaller number of tested proteins, but it is also possible that some of the partially mislocalized proteins might also be essential for parasite growth, as the remaining (not mislocalized) protein could be sufficient for parasite survival. It is also possible that some parasites were missing the mislocalizer, or did not express the mislocalizer in a sufficient amount. Another option could be that the mislocalized protein is an enzyme that can also fulfill its function at the mislocalized location. These possibilities would all result in a false ‘dispensable for growth’ assumption. In contrast to a false ‘dispensable for parasite growth’ assumption a false ‘essential for parasite growth’ assumption can arise is if the tagged protein would induce a lethal effect in the mislocalized compartment. Complementation of the KS would reveal this negative effect. However, recent studies (Birnbaum et al., 2017; Jonscher et al., 2019) and also the Rab5b cell lines analyzed in the present thesis was successfully complemented, excluding detrimental effects of the mislocalized proteins in the nucleus.

5.3 Functional investigation of candidate M7

Candidate M7 showed a localization at the nuclear membrane. The foci multiplied with every nuclear division. Images of dividing nuclei revealed two foci at one stretched nucleus. This observation was a first hint for M7 could be a protein that might be involved in nuclear division during schizogony. M7 was, at the date of the analysis, annotated as conserved protein with unknown function (according to: PlasmoDB, release 31 (Aurrecochea et al., 2009)). The HHpred server for protein remote homology detection and 3D structure prediction (Zimmermann et al., 2018) also linked the candidate to nuclear division, as it revealed a SKA2 (spindle and kinetochore associated 2) domain in its AA sequence. The human Ska complex comprises Ska1, Ska2 and Ska3 and was shown to be essential for correct kinetochore-microtubule interaction (Daum et al., 2009; Gaitanos et al., 2009; Hanisch et al., 2006; Ohta et al., 2010; Raaijmakers et al., 2009; Welburn et al., 2009). Like the Ska complex in humans, knock sideways experiments revealed M7 as an essential protein during nuclear division. The nuclear division prophase and metaphase of the parasite take place in early trophozoites. The foci of M7-2xFKBP-GFP-2xFKBP appeared in this stage, and the

fluorescence signal was increasing until the focus was separated. In pro- to metaphase conversion, the human Ska complex also starts to accumulate and peaked in metaphase (Auckland et al., 2017; Hanisch et al., 2006). The separation of foci during nuclear division was also confirmed by time lapse imaging, using confocal microscopy. A similar localization in foci at the nucleus was seen in a study from Mahajan et al., in which the *P. falciparum* Centrin3 were characterized (Mahajan et al., 2008). Centrin3 are calcium binding proteins that are associated with centrosomes, centrioles and mitotic spindle poles (Baron et al., 1991). Like candidate M7, Centrin3 play a critical role in the cell cycle. Their knockout leads to failures during basal body and centrosome duplication (Baum et al., 1986; Baum et al., 1988; Koblenz et al., 2003; Salisbury et al., 2002). A comparable phenotype was observed during the M7-2xFKBP-GFP-2xFKBP knock sideways experiments, in which the nuclei failed to divide correctly. Due to the similarities in localization and function, M7 was co-localized with overexpressed Centrin3-mCherry. The images revealed an in partial, co-localization of M7-2xFKBP-GFP-2xFKBP with Centrin3-mCherry, whereby M7-2xFKBP-GFP-2xFKBP foci, localizing between Centrin3 and the nuclei.

Another protein critical for nuclear division is tubulin, whereby it forms an intra nuclear spindle (Byers, 1981). To classify M7 in the mitotic (nuclear division) process, M7-2xFKBP-GFP-2xFKBP was also co-localized with a tubulin marker. In parasites with inactivated M7 the tubulin was mislocalized and long tubulin filaments were seen from trophozoite to schizonts, indicating a connection between M7-2xFKBP-GFP-2xFKBP and the function of tubulin in nuclear division. This also showed that parasites where M7 was inactivated are viable until the schizont stage. In the control, tubulin was located between the nucleus and M7-2xFKBP-GFP-2xFKBP foci. Taking the localizations of the nucleus, Centrin3-mCherry, tubulin and M7-2xFKBP-GFP-2xFKBP all together, we developed the following model: The chromosome is attached to tubulin and M7 might be bound to tubulin of the tubulin center. The partial overlap of Centrin3-mCherry and M7-2xFKBP-GFP-2xFKBP might indicate an interaction or at least a close localization of M7 and Centrin (Figure 49). In order to validate M7 as a *P. falciparum* Ska protein, two cell lines (M7-2xFKBP-GFP-2xFKBP with episomally expressed BirA*-NL and M7-2xFKBP-GFP-2xFKBP with episomally expressed BirA*-CL) were used for two individual DiQ-BioID experiments. This was done to enrich interacting proteins from the C- and N-terminal part of M7-2xFKBP-GFP-2xFKBP. The individual DIQ-BioID experiments showed a very different quality (Appendix 7). To increase the significance of identifying putative interaction partners, the results were combined, as it

was shown that the biotinylation from the C- and N-terminal showed similar hits (Birnbaum et al., 2020).

The combined DIQ-BioID revealed ten significantly enriched proteins, whereby the most enriched protein was M7 itself. This verified the correct dimerization of the BirA* constructs (BirA*-CL or BirA*-NL) to M7 and a successful biotinylation (Birnbaum et al., 2020) of the M7 protein. The second most significant hit of the DIQ-BioID showed a potential homology with Ska 3 using HHPred, indicating M7 as part of a Ska like complex, as it was shown in humans, that the Ska complex comprises Ska1, Ska2 and Ska3 (Gaitanos et al., 2009). The potential function of M7 in a Ska like complex was also indicated by two significantly enriched hits; one was annotated as kinetochore protein 80 (Ndc80), and another one revealed a predicted homology to Ndc80 using HHPred. The NDC80 protein has been shown to be present in other organisms during nuclear division and is assumed to be part of the receptor for Ska, the nuclear kinetochore complex Ndc80c, which comprises four subunits (Ndc80, Nuf2, Spc24 and Spc25) (Chan et al., 2012; Gaitanos et al., 2009; Raaijmakers et al., 2009; Welburn et al., 2009; Zhang et al., 2012). The interaction between Ndc80c and Ska has been shown to be essential for Ska function (Zhang et al., 2012; Zhang et al., 2017). It was also shown that Ndc80c contains microtubule-binding domains (D'Archivio et al., 2017).

The DIQ-BioID of M7 also revealed a protein with a predicted similarity (according to HHPred) to a nuclear pore protein. The nuclear pore is embedded between the mitotic nuclear envelope and the intra nuclear and is critical for the exchange of molecules (Kehrer et al., 2018; Kiseleva et al., 2001; Makhnevych et al., 2003; Weiner et al., 2011). It is also assumed that nuclear pores might give access to spindle regulating factors (Kehrer et al., 2018; Makhnevych et al., 2003). The nuclear pore complex is probably not directly part of the Ska/Ndc80 complexes, but might be in a close localization with a potentially supporting function for nuclear division. The potential interaction partners Ska3, Ndc80 and the nuclear pore complex protein support the function of M7 as Ska2 like protein in *P. falciparum* parasites.

As the M7 DIQ-BioID showed no hit with a similarity to a Ska1 protein, which is for example the case in the human part of the Ska complex (Hanisch et al., 2006; Jeyaprakash et al., 2012; Raaijmakers et al., 2009), more DIQ-BioID replicates from the C- and N- terminal part could potentially reveal a Ska1 protein. This could especially be the case because the combined DIQ-BioID used for individual cell lines showed a varying quality of the results. The varying quality of the two experiments also decreased the overall quality of the combined results, leading to a loss of significant enriched proteins only from the C- or N-terminus, like Tubulin

alpha-1A chain or kinesins (see. Appendix 7) which is probably both involved in the nuclear division process (reviewed in: (Goldstein, 2001; Hirokawa, 1998; Vale, 2003). Nevertheless, a putative Ska1 or a protein (annotated as unknown) with a remote homology was neither significantly enriched in the C- nor N-terminal M7 DIQ-BioID, which may be due to the quality of the experiments (Appendix 7). Also the absence of Ska1 in *P. falciparum* parasites is possible as PlasmoDB showed no protein annotated as Ska1.

In addition to the results for M7 shown in the present thesis, the role of M7 during nuclear division was further confirmed by the work of Jessica Kimmel (Master thesis 2020). Electron microscopy images with parasite where M7 was inactivated revealed mature parasites with morphologically changed nuclei. Additionally, a detailed stage experiment was performed, in which the growth effect was linked to schizogony by showing an arrest in schizonts. Considering all the results together, we assume that the parasites where M7 was inactivated are able to mature until late schizont stage, but the parasite is not able to form merozoites due to a failure in correct division of nuclei. This phenotype could be due to the *P. falciparum* schizogony which is characterized by nuclear division without cell division and without dissolving the nuclear membrane (closed mitosis) (Gerald et al., 2011; Schrevel et al., 1977). During closed mitosis, as e.g. observed in yeast (Ding et al., 1997) which also contain a functional homologue (DASH/DAM complex) of the human Ska complex (Chan et al., 2012; Varma et al., 2012), the chromosomes condense, and in this phase no transcription of genes takes place (Cooper, 2000). An explanation for the late arrest in schizonts after inactivation of M7 might be that although the nuclear division is impaired, the un-condensed chromosomes might still duplicate their DNA. This hypothesis is supported by fluorescence images of arrested schizonts, with a DNA amount comparable to the control. Additionally, also the tubulin filaments still increased in number from trophozoites to schizonts after inactivation of M7. In order to show normal DNA replication after inactivation of M7 quantification of the DNA amount could be performed. Further experiments will now need to confirm the M7 interaction partners identified here by DiQ-BioID. Validation of these candidates can be carried out by taking advantage of the SLI system for localization studies and functional analysis.

In summary, the results indicate that candidate M7 might be the orthologue of human Ska2 or a Ska2-like protein in *P. falciparum* parasites. The data of this thesis supports the hypothesis that M7 is part of a complex between the microtubule and the centrosomes of the mitotic spindle poles during schizogony (Figure 48). This would be the first time that a Ska-

like protein was experimentally linked within the mitotic process during schizogony in *P. falciparum* parasites.

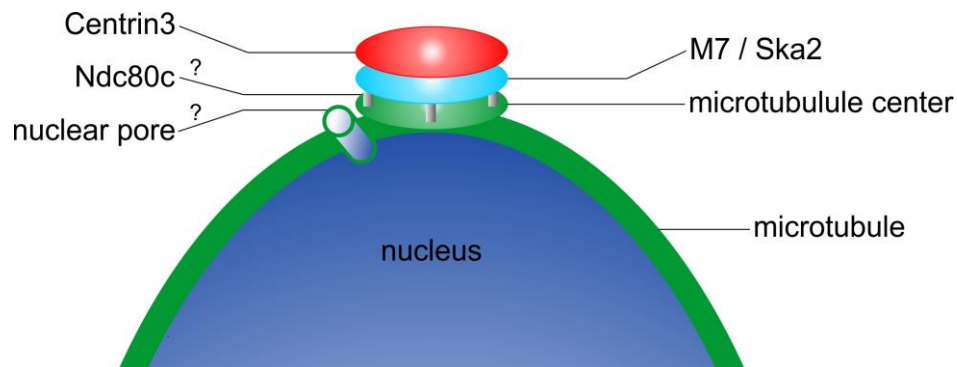


Figure 48: Model of the localization of M7 based on the results of this thesis.

The nucleus (blue) is attached during nuclear division by the microtubules (green). On top of the microtubules (mitotic spindle) the Ska complex (turquoise (including Ska2 / M7)) connects the microtubules with the centrosomes (red) of the mitotic spindle. The receptor for the Ska complex might be Ndc80c (grey tubes). Next to the binding complexes nuclear pores might be enriched (light blue tube).

5.4 Functional investigation of candidate M16

M16-2xFKBP-GFP-2xFKBP showed a similar localization and a similar growth phenotype as M7 during knock sideways experiments. To investigate a possible role of M16 in mitosis during schizogony, the M16-2xFKBP-GFP-2xFKBP expressing parasites were stained with a tubulin marker, and knock sideways was induced. In comparison to inactivating M7, tubulin was not affected when M16 was inactivated, indicating that M16 is not directly connected with tubulin. Also, the mass spectrometry results in the M7 DiQ-BioID did not show M16 as putative interactor of M7. However, some nuclei, after inactivation of M16 in parasites with inactivated M16, showed an incomplete division as observed after inactivation of M7 in M7 inactivated parasites, indicating a role of M16 during nuclear division. To confirm this assumption, further experiments are planned, such as the identification of potential interaction partners using DIQ-BioID, co-localization studies with Centrin3 and M7, detailed stage experiments and time lapse imaging using confocal microscopy.

5.5 Origin of the unknown genes

It is likely that M7 plays a role during nuclear division, which takes place in many organisms (reviewed in: (Lubischer, 2007; Sullivan et al., 2007)). However, the protein sequence revealed no relation to other proteins outside of the Apicomplexans, similar to the other unknown proteins that were analyzed. Only a very sensitive server for protein remote homology detection (HHPred) and the analysis of the M7 interactors linked M7 to the Ska

complex, which is also known in other species (Chan et al., 2012; Daum et al., 2009; Gaitanos et al., 2009; Helgeson et al., 2018; Welburn et al., 2009; Zhang et al., 2012; Zhang et al., 2017). This raises the question if two proteins with a related function have a common ancestor (divergent evolution, see. 1.5.3), or are of independent origin (convergent evolution, see. 1.5.3)

Divergent evolution might be possible for the Rab family, as Rab proteins are present in *Plasmodium* (11 *rab* genes) (Quevillon et al., 2003) and its relatives, like *Toxoplasma* (15 *rab* genes), *Neospora* (15 *rab* genes), *Theileria* (9 *rab* genes), *Babesia* (9 *rab* genes) and *Cryptosporidia* (8 *rab* genes) (reviewed in: (Langsley et al., 2008)). The different numbers of *rab* genes indicate an adaptation of the single *rab* genes regarding their host. Thus, the genus of *Neospora* and *Toxoplasma* express the highest numbers of *rab* genes and have the largest host ranges (Di Genova et al., 2019; Dubey et al., 1996; Dubey et al., 1970). The presence in these organisms and the high genetic similarity reveal a common ancestor. In addition to the different number of *rab* genes, some of the comparable *rabs* like *rab5* have different functions and expression profiles within the different species (Langsley et al., 2008). Looking at the *PfRab5* and the interactor VPS35, known from other species regarding the function in early endocytosis, *rab5a* and *rab5c* expression profiles cluster with *vps34* but not with *rab5b* (Langsley et al., 2008). Additionally, *rab5b* is lacking the C-terminal prenylation motif which is postulated to be important for its membrane attachment (Chavrier et al., 1991; Quevillon et al., 2003). The results of this thesis also support the assumption that *PfRab5b* has a different function than *PfRab5a*, as *PfRab5b* was shown to be involved in HCCU, likely during a similar step as VPS45, whereas *Rab5a* has a schizont phenotype (Birnbaum et al., 2017; Jonscher et al., 2019). In *Cryptosporidia*, *Rab5b* is missing entirely; this seems fitting, as these parasites do not need HCCU. The various functions of the conserved *rab* gene sequences in related species suggest a common ancestor and thus a divergent evolution of the Rab proteins. This assumption is also supported by the sequence similarity of Rab proteins in not so closely related organisms (reviewed in: (Stenmark, 2009)).

In comparison to the Rab family the unknown genes which were found and analyzed during this work appeared to be the result of convergent evolution, as there was no indication to a common ancestor or sequence similarity. In general this seems possible for proteins as this was postulated for antifreeze proteins that share similar structural attributes (Chen et al., 1997; Davies et al., 2012) and hairpin-like structures (Tomii et al., 2012). Another example for a probably newly raised function, originating from convergent evolution, might be true for most interactors of the artemisinin resistance marker Kelch13, as they have no homologies to

other known proteins and play a role in the HCCU (Birnbaum et al., 2020). Nevertheless, also two annotated proteins (Eps15 and AP2) with a known and similar function to proteins in other organisms were found (Birnbaum et al., 2020). Also for the unknown proteins it seems more likely that they are only divergent in sequence, particularly because a potential related protein in the human (Ska2) was found also for the unknown protein M7.

In summary, it can be said that many of the apparently unique proteins might in fact derive from divergent evolution, whereby the protein sequence that has been changed extensively in a homology is no longer detectable.

5.6 Conclusion

The aim of the screen carried out in this thesis was the functional analysis of *P. falciparum* proteins with unknown function. In order to do this, the SLI system was applied to analyse a selected set of genes on chromosome 3 of the parasite. In this study, 15 newly established SLI cell lines of previously uncharacterized genes were generated, followed by their localisation under physiological conditions. In other systems, localisation of proteins alone has proved to be a decisive advance in understanding the organism's biology (Huh et al., 2003). The proteins were located in the nucleus, at the nuclear membrane, the cytoplasm, in foci in the cytoplasm, and the PPM (Table 9). For all of the proteins, six independent target gene disruption attempts (on gene level) were performed for essentiality prediction, whereby the observed rate for essential proteins of 90 % might be an overestimation compared to other studies dealing with essentiality prediction for *Plasmodium* genes and their products. For eight cell lines, the essentiality was additionally tested on the protein level using knock sideways, whereby the observed rate of ~ 38 % of essential proteins was similar to an earlier SLI study (Birnbaum et al., 2017) and ~ 25 % lower compared to the genome wide *Plasmodium* screens (Bushell et al., 2017; Zhang et al., 2018), which might be due to inefficient KS mislocalization. In comparison to the two high throughput genome screens, the screen in this thesis included only a chosen amount of unknown proteins, but provides locations and functional data to investigate the *P. falciparum* parasite's biology.

A detailed functional analysis was performed for Rab5b, in which a role in HCCU was revealed, providing evidence for a canonical function of Rab5b together with VPS45 in endolysosomal transport of the parasite. A further protein analysed in detail was candidate M7, which might be the *P. falciparum* orthologue of Ska2, with an essential function in *P. falciparum* mitosis during schizogony. In addition, all the cell lines serve as a resource for the community for further analysis.

For further screens using the SLI-method an increase of the candidates' throughput would support the investigation of more unknown proteins and the *P. falciparum* parasite's biology. Therefore the SLI method could be combined with CRISPR/Cas9 to mediate more efficient genomic modification and hence, a larger number of parasites with the genomic change to permit immediate selection using SLI. These methods would also save the limited resistance markers. One disadvantage would be the absence of episomal cell lines, so that in case of missing integrands, the transfection has to be repeated.

Another possibility to increase the number of functional analysed proteins is the investigation of the not C-terminal taggable proteins using N-terminal gene tagging and the already established SLI-DiCre combination (Birnbaum et al., 2017).

By means of the research done by the lab members of the Spielmann group, including this thesis, it was possible to analyse the unknown genes (with some limitations as to which genes could not be analysed) from three of the 14 chromosomes of *P. falciparum* parasites using the current SLI method. This permitted to investigate the role of many unknown essential genes and linking them to parasite-specific processes in *P. falciparum* parasites. These candidates are milestones to elucidate novel parts of the parasite's biology, which pave the way for new drug targets. In the future, the SLI-system will be useful to continue the analysis of unknown *P. falciparum* genes, potentially in order to improve the system for increasing throughput, to identify more essential candidates to understand and combat malaria parasites.

6 References

- Abu Bakar, N., Klonis, N., Hanssen, E., Chan, C., & Tilley, L. (2010). Digestive-vacuole genesis and endocytic processes in the early intraerythrocytic stages of *Plasmodium falciparum*. *J Cell Sci*, *123*(Pt 3), 441-450. doi:10.1242/jcs.061499
- Adisa, A., Frankland, S., Rug, M., Jackson, K., Maier, A. G., Walsh, P., . . . Tilley, L. (2007). Re-assessing the locations of components of the classical vesicle-mediated trafficking machinery in transfected *Plasmodium falciparum*. *Int J Parasitol*, *37*(10), 1127-1141. doi:10.1016/j.ijpara.2007.02.009
- Adjalley, S. H., Johnston, G. L., Li, T., Eastman, R. T., Ekland, E. H., Eappen, A. G., . . . Fidock, D. A. (2011). Quantitative assessment of *Plasmodium falciparum* sexual development reveals potent transmission-blocking activity by methylene blue. *Proc Natl Acad Sci U S A*, *108*(47), E1214-1223. doi:10.1073/pnas.1112037108
- Agrawal, N., Dasaradhi, P. V., Mohammed, A., Malhotra, P., Bhatnagar, R. K., & Mukherjee, S. K. (2003). RNA interference: biology, mechanism, and applications. *Microbiol Mol Biol Rev*, *67*(4), 657-685. doi:10.1128/mmbr.67.4.657-685.2003
- Agrawal, S., Chung, D. W., Ponts, N., van Dooren, G. G., Prudhomme, J., Brooks, C. F., . . . Le Roch, K. G. (2013). An apicoplast localized ubiquitylation system is required for the import of nuclear-encoded plastid proteins. *PLoS Pathog*, *9*(6), e1003426. doi:10.1371/journal.ppat.1003426
- Aguilar, R., Magallon-Tejada, A., Achtman, A. H., Moraleta, C., Joice, R., Cistero, P., . . . Mayor, A. (2014). Molecular evidence for the localization of *Plasmodium falciparum* immature gametocytes in bone marrow. *Blood*, *123*(7), 959-966. doi:10.1182/blood-2013-08-520767
- Aikawa, M. (1966). The fine structure of the erythrocytic stages of three avian malarial parasites, *Plasmodium fallax*, *P. lophurae*, and *P. cathemerium*. *Am J Trop Med Hyg*, *15*(4), 449-471. doi:10.4269/ajtmh.1966.15.449
- Aikawa, M. (1971). Parasitological review. *Plasmodium*: the fine structure of malarial parasites. *Exp Parasitol*, *30*(2), 284-320. doi:10.1016/0014-4894(71)90094-4
- Aikawa, M., Cook, R. T., Sakoda, J. J., & Sprinz, H. (1969). Fine structure of the erythrocytic stages of *Plasmodium knowlesi*. A comparison between intracellular and free forms. *Z Zellforsch Mikrosk Anat*, *100*(2), 271-284. doi:10.1007/bf00343883
- Aikawa, M., Hepler, P. K., Huff, C. G., & Sprinz, H. (1966a). The feeding mechanism of avian malarial parasites. *The Journal of cell biology*, *28*(2), 355-373. doi:10.1083/jcb.28.2.355
- Aikawa, M., Huff, C. G., & Sprinz, H. (1966b). Comparative feeding mechanisms of avian and primate malarial parasites. *Mil Med*, *131*(9), Suppl:969-983.
- Aikawa, M., Huff, C. G., & Sprinz, H. (1967). Fine structure of the asexual stages of *Plasmodium elongatum*. *J Cell Biol*, *34*(1), 229-249. doi:10.1083/jcb.34.1.229
- Aikawa, M., & Jordan, H. B. (1968). Fine structure of a reptilian malarial parasite. *J Parasitol*, *54*(5), 1023-1033.
- Alkhalil, A., Cohn, J. V., Wagner, M. A., Cabrera, J. S., Rajapandi, T., & Desai, S. A. (2004). *Plasmodium falciparum* likely encodes the principal anion channel on infected human erythrocytes. *Blood*, *104*(13), 4279-4286. doi:10.1182/blood-2004-05-2047
- Altschul, S. F., Gish, W., Miller, W., Myers, E. W., & Lipman, D. J. (1990). Basic local alignment search tool. *J Mol Biol*, *215*(3), 403-410. doi:10.1016/s0022-2836(05)80360-2
- Andenmatten, N., Egarter, S., Jackson, A. J., Jullien, N., Herman, J.-P., & Meissner, M. (2013). Conditional genome engineering in *Toxoplasma gondii* uncovers alternative invasion mechanisms. *Nature methods*, *10*(2), 125-127. doi:10.1038/nmeth.2301
- Angus, B. J., Chotivanich, K., Udomsangpetch, R., & White, N. J. (1997). In vivo removal of malaria parasites from red blood cells without their destruction in acute *falciparum* malaria. *Blood*, *90*(5), 2037-2040.
- Arisue, N., Hashimoto, T., Mitsui, H., Palacpac, N. M., Kaneko, A., Kawai, S., . . . Horii, T. (2012). The *Plasmodium* apicoplast genome: conserved structure and close relationship of *P. ovale* to rodent malaria parasites. *Mol Biol Evol*, *29*(9), 2095-2099. doi:10.1093/molbev/mss082

- Armstrong, C. M., & Goldberg, D. E. (2007). An FKBP destabilization domain modulates protein levels in *Plasmodium falciparum*. *Nat Methods*, *4*(12), 1007-1009. doi:10.1038/nmeth1132
- Arnot, D. E., & Gull, K. (1998). The *Plasmodium* cell-cycle: facts and questions. *Ann Trop Med Parasitol*, *92*(4), 361-365. doi:10.1080/00034989859357
- Arnot, D. E., Ronander, E., & Bengtsson, D. C. (2011). The progression of the intra-erythrocytic cell cycle of *Plasmodium falciparum* and the role of the centriolar plaques in asynchronous mitotic division during schizogony. *Int J Parasitol*, *41*(1), 71-80. doi:10.1016/j.ijpara.2010.07.012
- Arrow, K. J. (2004). Saving Lives, Buying Time: Economics of Malaria Drugs in an Age of Resistance. In K. J. Arrow, C. Panosian, & H. Gelband (Eds.), *Saving Lives, Buying Time: Economics of Malaria Drugs in an Age of Resistance*. Washington (DC).
- Auckland, P., Clarke, N. I., Royle, S. J., & McAinsh, A. D. (2017). Congressing kinetochores progressively load Ska complexes to prevent force-dependent detachment. *J Cell Biol*, *216*(6), 1623-1639. doi:10.1083/jcb.201607096
- Aurrecoechea, C., Brestelli, J., Brunk, B. P., Dommer, J., Fischer, S., Gajria, B., . . . Wang, H. (2009). PlasmoDB: a functional genomic database for malaria parasites. *Nucleic Acids Res*, *37*(Database issue), D539-543. doi:10.1093/nar/gkn814
- Babbitt, S. E., Altenhofen, L., Cobbold, S. A., Istvan, E. S., Fennell, C., Doerig, C., . . . Goldberg, D. E. (2012). *Plasmodium falciparum* responds to amino acid starvation by entering into a hibernatory state. *Proceedings of the National Academy of Sciences*, *109*(47), E3278-E3287. doi:10.1073/pnas.1209823109
- Bailly, E., Jambou, R., Savel, J., & Jaureguiberry, G. (1992). *Plasmodium falciparum*: differential sensitivity in vitro to E-64 (cysteine protease inhibitor) and Pepstatin A (aspartyl protease inhibitor). *J Protozool*, *39*(5), 593-599. doi:10.1111/j.1550-7408.1992.tb04856.x
- Balk, J., Pierik, A. J., Aguilar Netz, D. J., Muhlenhoff, U., & Lill, R. (2005). Nar1p, a conserved eukaryotic protein with similarity to Fe-only hydrogenases, functions in cytosolic iron-sulphur protein biogenesis. *Biochem Soc Trans*, *33*(Pt 1), 86-89. doi:10.1042/bst0330086
- Ballou, W. R., Hoffman, S. L., Sherwood, J. A., Hollingdale, M. R., Neva, F. A., Hockmeyer, W. T., . . . et al. (1987). Safety and efficacy of a recombinant DNA *Plasmodium falciparum* sporozoite vaccine. *Lancet*, *1*(8545), 1277-1281. doi:10.1016/s0140-6736(87)90540-x
- Banaszynski, L. A., Chen, L. C., Maynard-Smith, L. A., Ooi, A. G., & Wandless, T. J. (2006). A rapid, reversible, and tunable method to regulate protein function in living cells using synthetic small molecules. *Cell*, *126*(5), 995-1004. doi:10.1016/j.cell.2006.07.025
- Bannister, L. H., Hopkins, J. M., Fowler, R. E., Krishna, S., & Mitchell, G. H. (2000a). A brief illustrated guide to the ultrastructure of *Plasmodium falciparum* asexual blood stages. *Parasitol Today*, *16*(10), 427-433.
- Bannister, L. H., Hopkins, J. M., Fowler, R. E., Krishna, S., & Mitchell, G. H. (2000b). Ultrastructure of rhoptry development in *Plasmodium falciparum* erythrocytic schizonts. *Parasitology*, *121* (Pt 3), 273-287. doi:10.1017/s0031182099006320
- Barbieri, M. A., Roberts, R. L., Gumusboga, A., Highfield, H., Alvarez-Dominguez, C., Wells, A., & Stahl, P. D. (2000). Epidermal growth factor and membrane trafficking. EGF receptor activation of endocytosis requires Rab5a. *J Cell Biol*, *151*(3), 539-550. doi:10.1083/jcb.151.3.539
- Barcus, M. J., Basri, H., Picarima, H., Manyakori, C., Sekartuti, Elyazar, I., . . . Baird, J. K. (2007). Demographic risk factors for severe and fatal vivax and falciparum malaria among hospital admissions in northeastern Indonesian Papua. *Am J Trop Med Hyg*, *77*(5), 984-991.
- Barnum, K. J., & O'Connell, M. J. (2014). Cell cycle regulation by checkpoints. *Methods in molecular biology (Clifton, N.J.)*, *1170*, 29-40. doi:10.1007/978-1-4939-0888-2_2
- Baron, A., Greenwood, T., & Salisbury, J. (1991). Localization of the centrin-related 165,000-Mr protein of PtK2 cells during the cell cycle. *Cell motility and the cytoskeleton*, *18*, 1-14. doi:10.1002/cm.970180102
- Barr, F. A. (1999). A novel Rab6-interacting domain defines a family of Golgi-targeted coiled-coil proteins. *Curr Biol*, *9*(7), 381-384. doi:10.1016/s0960-9822(99)80167-5
- Bartoloni, A., & Zammarchi, L. (2012). Clinical aspects of uncomplicated and severe malaria. *Mediterr J Hematol Infect Dis*, *4*(1), e2012026. doi:10.4084/MJHID.2012.026

- Baum, J., Gilberger, T. W., Frischknecht, F., & Meissner, M. (2008). Host-cell invasion by malaria parasites: insights from Plasmodium and Toxoplasma. *Trends Parasitol*, 24(12), 557-563. doi:10.1016/j.pt.2008.08.006
- Baum, J., Papenfuss, A. T., Mair, G. R., Janse, C. J., Vlachou, D., Waters, A. P., . . . de Koning-Ward, T. F. (2009). Molecular genetics and comparative genomics reveal RNAi is not functional in malaria parasites. *Nucleic Acids Res*, 37(11), 3788-3798. doi:10.1093/nar/gkp239
- Baum, J., Richard, D., Healer, J., Rug, M., Krnjanski, Z., Gilberger, T. W., . . . Cowman, A. F. (2006). A conserved molecular motor drives cell invasion and gliding motility across malaria life cycle stages and other apicomplexan parasites. *J Biol Chem*, 281(8), 5197-5208. doi:10.1074/jbc.M509807200
- Baum, P., Furlong, C., & Byers, B. (1986). Yeast gene required for spindle pole body duplication: homology of its product with Ca²⁺-binding proteins. *Proc Natl Acad Sci U S A*, 83(15), 5512-5516. doi:10.1073/pnas.83.15.5512
- Baum, P., Yip, C., Goetsch, L., & Byers, B. (1988). A yeast gene essential for regulation of spindle pole duplication. *Mol Cell Biol*, 8(12), 5386-5397. doi:10.1128/mcb.8.12.5386
- Beaudoin, R. L., Armstrong, J. C., & Vannier, W. E. (1980). Production of radiation-attenuated vaccines against malaria and schistosomiasis. *International Journal of Nuclear Medicine and Biology*, 7(2), 113-124. doi:https://doi.org/10.1016/0047-0740(80)90029-7
- Beck, J. R., Muralidharan, V., Oksman, A., & Goldberg, D. E. (2014). PTEX component HSP101 mediates export of diverse malaria effectors into host erythrocytes. *Nature*, 511(7511), 592-595. doi:10.1038/nature13574
- Becker, J., Tan, T. J., Trepte, H. H., & Gallwitz, D. (1991). Mutational analysis of the putative effector domain of the GTP-binding Ypt1 protein in yeast suggests specific regulation by a novel GAP activity. *EMBO J*, 10(4), 785-792.
- Becker, K., Tilley, L., Vennerstrom, J. L., Roberts, D., Rogerson, S., & Ginsburg, H. (2004). Oxidative stress in malaria parasite-infected erythrocytes: host-parasite interactions. *Int J Parasitol*, 34(2), 163-189. doi:10.1016/j.ijpara.2003.09.011
- Belmont, B. J., & Niles, J. C. (2010). Engineering a Direct and Inducible Protein-RNA Interaction To Regulate RNA Biology. *ACS Chemical Biology*, 5(9), 851-861. doi:10.1021/cb100070j
- Belshaw, P. J., Ho, S. N., Crabtree, G. R., & Schreiber, S. L. (1996). Controlling protein association and subcellular localization with a synthetic ligand that induces heterodimerization of proteins. *Proc Natl Acad Sci U S A*, 93(10), 4604-4607. doi:10.1073/pnas.93.10.4604
- Berendt, A. R., Ferguson, D. J., & Newbold, C. I. (1990). Sequestration in Plasmodium falciparum malaria: sticky cells and sticky problems. *Parasitol Today*, 6(8), 247-254. doi:10.1016/0169-4758(90)90184-6
- Berens, C., & Hillen, W. (2003). Gene regulation by tetracyclines. Constraints of resistance regulation in bacteria shape TetR for application in eukaryotes. *Eur J Biochem*, 270(15), 3109-3121. doi:10.1046/j.1432-1033.2003.03694.x
- Bernstein, E., Denli, A. M., & Hannon, G. J. (2002). The rest is silence. *RNA*, 7(11), 1509-1521. doi:undefined
- Biagini, G. A., Bray, P. G., Spiller, D. G., White, M. R., & Ward, S. A. (2003). The digestive food vacuole of the malaria parasite is a dynamic intracellular Ca²⁺ store. *J Biol Chem*, 278(30), 27910-27915. doi:10.1074/jbc.M304193200
- Billker, O., Lindo, V., Panico, M., Etienne, A. E., Paxton, T., Dell, A., . . . Morris, H. R. (1998). Identification of xanthurenic acid as the putative inducer of malaria development in the mosquito. *Nature*, 392(6673), 289-292. doi:10.1038/32667
- Billker, O., Shaw, M. K., Margos, G., & Sinden, R. E. (1997). The roles of temperature, pH and mosquito factors as triggers of male and female gametogenesis of Plasmodium berghei in vitro. *Parasitology*, 115 (Pt 1), 1-7. doi:10.1017/s0031182097008895
- Binka, F., & Akweongo, P. (2006). Prevention of malaria using ITNs: potential for achieving the millennium development goals. *Curr Mol Med*, 6(2), 261-267. doi:10.2174/156652406776055203
- Birnbaum, J. (2017). A novel genetic system for the functional analysis of essential proteins of the human malaria parasite Plasmodium falciparum universität Hamburg.

- Birnbaum, J., Flemming, S., Reichard, N., Soares, A. B., Mesen-Ramirez, P., Jonscher, E., . . . Spielmann, T. (2017). A genetic system to study *Plasmodium falciparum* protein function. *Nat Methods*, *14*(4), 450-456. doi:10.1038/nmeth.4223
- Birnbaum, J., Scharf, S., Schmidt, S., Jonscher, E., Hoeijmakers, W. A. M., Flemming, S., . . . Spielmann, T. (2020). A Kelch13-defined endocytosis pathway mediates artemisinin resistance in malaria parasites. *Science*, *367*(6473), 51-59. doi:10.1126/science.aax4735
- Bitinaite, J., Wah, D. A., Aggarwal, A. K., & Schildkraut, I. (1998). FokI dimerization is required for DNA cleavage. *Proc Natl Acad Sci U S A*, *95*(18), 10570-10575. doi:10.1073/pnas.95.18.10570
- Blackman, M. J., & Carruthers, V. B. (2013). Recent insights into apicomplexan parasite egress provide new views to a kill. *Curr Opin Microbiol*, *16*(4), 459-464. doi:10.1016/j.mib.2013.04.008
- Bloland, P. B., Ettlign, M., & Meek, S. (2000). Combination therapy for malaria in Africa: hype or hope? *Bulletin of the World Health Organization*, *78*(12), 1378-1388.
- Bock, J. B., Matern, H. T., Peden, A. A., & Scheller, R. H. (2001). A genomic perspective on membrane compartment organization. *Nature*, *409*(6822), 839-841. doi:10.1038/35057024
- Boddey, J. A., Hodder, A. N., Gunther, S., Gilson, P. R., Patsiouras, H., Kapp, E. A., . . . Cowman, A. F. (2010). An aspartyl protease directs malaria effector proteins to the host cell. *Nature*, *463*(7281), 627-631. doi:10.1038/nature08728
- Boddey, J. A., Moritz, R. L., Simpson, R. J., & Cowman, A. F. (2009). Role of the *Plasmodium* export element in trafficking parasite proteins to the infected erythrocyte. *Traffic*, *10*(3), 285-299. doi:10.1111/j.1600-0854.2008.00864.x
- Boersema, P. J., Raijmakers, R., Lemeer, S., Mohammed, S., & Heck, A. J. (2009). Multiplex peptide stable isotope dimethyl labeling for quantitative proteomics. *Nat Protoc*, *4*(4), 484-494. doi:10.1038/nprot.2009.21
- Boettcher, B., & Barral, Y. (2013). The cell biology of open and closed mitosis. *Nucleus (Austin, Tex.)*, *4*(3), 160-165. doi:10.4161/nucl.24676
- Boncompain, G., Divoux, S., Gareil, N., de Forges, H., Lescure, A., Latreche, L., . . . Perez, F. (2012). Synchronization of secretory protein traffic in populations of cells. *Nature Methods*, *9*(5), 493-498. doi:10.1038/nmeth.1928
- Brancucci, N. M. B., Gerdt, J. P., Wang, C., De Niz, M., Philip, N., Adapa, S. R., . . . Marti, M. (2017). Lysophosphatidylcholine Regulates Sexual Stage Differentiation in the Human Malaria Parasite *Plasmodium falciparum*. *Cell*, *171*(7), 1532-1544 e1515. doi:10.1016/j.cell.2017.10.020
- Bray, P. G., Mungthin, M., Ridley, R. G., & Ward, S. A. (1998). Access to hemozoin: the basis of chloroquine resistance. *Mol Pharmacol*, *54*(1), 170-179.
- Bray, P. G., Ward, S. A., & O'Neill, P. M. (2005). Quinolines and artemisinin: chemistry, biology and history. *Curr Top Microbiol Immunol*, *295*, 3-38. doi:10.1007/3-540-29088-5_1
- Brown, H. F., Wang, L., Khadka, S., Fields, S., & LaCount, D. J. (2011). A densely overlapping gene fragmentation approach improves yeast two-hybrid screens for *Plasmodium falciparum* proteins. *Molecular and biochemical parasitology*, *178*(1-2), 56-59. doi:10.1016/j.molbiopara.2011.04.005
- Bruce, M. C., Alano, P., Duthie, S., & Carter, R. (1990). Commitment of the malaria parasite *Plasmodium falciparum* to sexual and asexual development. *Parasitology*, *100 Pt 2*, 191-200.
- Bucci, C., & Chiariello, M. (2006). Signal transduction gRABs attention. *Cell Signal*, *18*(1), 1-8. doi:10.1016/j.cellsig.2005.07.001
- Bucci, C., Lütcke, A., Steele-Mortimer, O., Olkkonen, V. M., Dupree, P., Chiariello, M., . . . Zerial, M. (1995). Co-operative regulation of endocytosis by three RAB5 isoforms. *FEBS Letters*, *366*(1), 65-71. doi:https://doi.org/10.1016/0014-5793(95)00477-Q
- Bucci, C., Parton, R. G., Mather, I. H., Stunnenberg, H., Simons, K., Hoflack, B., & Zerial, M. (1992). The small GTPase rab5 functions as a regulatory factor in the early endocytic pathway. *Cell*, *70*(5), 715-728. doi:10.1016/0092-8674(92)90306-w
- Bushell, E., Gomes, A. R., Sanderson, T., Anar, B., Girling, G., Herd, C., . . . Billker, O. (2017). Functional Profiling of a *Plasmodium* Genome Reveals an Abundance of Essential Genes. *Cell*, *170*(2), 260-272 e268. doi:10.1016/j.cell.2017.06.030

- Byers, B. (1981). The molecular biology of the yeast *Saccharomyces* *Life cycle and inheritance* (pp. 59): Cold Spring Harbor NY.
- Cabrales, P., Zanini, G. M., Meays, D., Frangos, J. A., & Carvalho, L. J. M. (2010). Murine cerebral malaria is associated with a vasospasm-like microcirculatory dysfunction, and survival upon rescue treatment is markedly increased by nimodipine. *Am J Pathol*, *176*(3), 1306-1315. doi:10.2353/ajpath.2010.090691
- Campo, B., Vandal, O., Wesche, D. L., & Burrows, J. N. (2015). Killing the hypnozoite--drug discovery approaches to prevent relapse in *Plasmodium vivax*. *Pathogens and global health*, *109*(3), 107-122. doi:10.1179/2047773215Y.0000000013
- Cao, J., Kaneko, O., Thongkuiatkul, A., Tachibana, M., Otsuki, H., Gao, Q., . . . Torii, M. (2009). Rhoptry neck protein RON2 forms a complex with microneme protein AMA1 in *Plasmodium falciparum* merozoites. *Parasitol Int*, *58*(1), 29-35. doi:10.1016/j.parint.2008.09.005
- Carter, R., & Mendis, K. N. (2002). Evolutionary and historical aspects of the burden of malaria. *Clin Microbiol Rev*, *15*(4), 564-594.
- Chan, Y. W., Jeyaprakash, A. A., Nigg, E. A., & Santamaria, A. (2012). Aurora B controls kinetochore-microtubule attachments by inhibiting Ska complex-KMN network interaction. *J Cell Biol*, *196*(5), 563-571. doi:10.1083/jcb.201109001
- Chavrier, P., Gorvel, J. P., Stelzer, E., Simons, K., Gruenberg, J., & Zerial, M. (1991). Hypervariable C-terminal domain of rab proteins acts as a targeting signal. *Nature*, *353*(6346), 769-772. doi:10.1038/353769a0
- Chavrier, P., Parton, R. G., Hauri, H. P., Simons, K., & Zerial, M. (1990a). Localization of low molecular weight GTP binding proteins to exocytic and endocytic compartments. *Cell*, *62*(2), 317-329. doi:10.1016/0092-8674(90)90369-p
- Chavrier, P., Simons, K., & Zerial, M. (1992). The complexity of the Rab and Rho GTP-binding protein subfamilies revealed by a PCR cloning approach. *Gene*, *112*(2), 261-264. doi:10.1016/0378-1119(92)90387-5
- Chavrier, P., Vingron, M., Sander, C., Simons, K., & Zerial, M. (1990b). Molecular cloning of YPT1/SEC4-related cDNAs from an epithelial cell line. *Molecular and Cellular Biology*, *10*(12), 6578-6585. doi:10.1128/mcb.10.12.6578
- Chen, J., Zheng, X. F., Brown, E. J., & Schreiber, S. L. (1995). Identification of an 11-kDa FKBP12-rapamycin-binding domain within the 289-kDa FKBP12-rapamycin-associated protein and characterization of a critical serine residue. *Proceedings of the National Academy of Sciences of the United States of America*, *92*(11), 4947-4951. doi:10.1073/pnas.92.11.4947
- Chen, L., DeVries, A. L., & Cheng, C. H. (1997). Convergent evolution of antifreeze glycoproteins in Antarctic notothenioid fish and Arctic cod. *Proc Natl Acad Sci U S A*, *94*(8), 3817-3822. doi:10.1073/pnas.94.8.3817
- Chen, P. I., Kong, C., Su, X., & Stahl, P. D. (2009). Rab5 isoforms differentially regulate the trafficking and degradation of epidermal growth factor receptors. *J Biol Chem*, *284*(44), 30328-30338. doi:10.1074/jbc.M109.034546
- Chiariello, M., Bruni, C. B., & Bucci, C. (1999). The small GTPases Rab5a, Rab5b and Rab5c are differentially phosphorylated in vitro. *FEBS Letters*, *453*(1), 20-24. doi:https://doi.org/10.1016/S0014-5793(99)00686-9
- Choi-Rhee, E., Schulman, H., & Cronan, J. E. (2004). Promiscuous protein biotinylation by *Escherichia coli* biotin protein ligase. *Protein Sci*, *13*(11), 3043-3050. doi:10.1110/ps.04911804
- Choi, J., Chen, J., Schreiber, S. L., & Clardy, J. (1996). Structure of the FKBP12-rapamycin complex interacting with the binding domain of human FRAP. *Science*, *273*(5272), 239-242. doi:10.1126/science.273.5272.239
- Chotivanich, K., Udomsangpetch, R., Dondorp, A., Williams, T., Angus, B., Simpson, J. A., . . . White, N. J. (2000). The mechanisms of parasite clearance after antimalarial treatment of *Plasmodium falciparum* malaria. *J Infect Dis*, *182*(2), 629-633. doi:10.1086/315718
- Chotivanich, K., Udomsangpetch, R., McGready, R., Proux, S., Newton, P., Pukrittayakamee, S., . . . White, N. J. (2002). Central Role of the Spleen in Malaria Parasite Clearance. *J Infect Dis*, *185*(10), 1538-1541. doi:10.1086/340213

- Christoforidis, S., Miaczynska, M., Ashman, K., Wilm, M., Zhao, L., Yip, S.-C., . . . Zerial, M. (1999). Phosphatidylinositol-3-OH kinases are Rab5 effectors. *Nat Cell Biol*, 1(4), 249-252. doi:10.1038/12075
- Chulay, J. D., Haynes, J. D., & Diggs, C. L. (1983). Plasmodium falciparum: assessment of in vitro growth by [3H]hypoxanthine incorporation. *Exp Parasitol*, 55(1), 138-146. doi:10.1016/0014-4894(83)90007-3
- Chung, Y. K., Lam-Phua, S. G., Chua, Y. T., & Yatiman, R. (2001). Evaluation of biological and chemical insecticide mixture against Aedes aegypti larvae and adults by thermal fogging in Singapore. *Med Vet Entomol*, 15(3), 321-327. doi:10.1046/j.0269-283x.2001.00311.x
- Cochrane, A. H., Nussenzweig, R. S., & Nardin, E. H. (1980). 4 - Immunization against Sporozoites. In J. P. Kreier (Ed.), *Malaria* (pp. 163-202): Academic Press.
- Coen, E. S., & Carpenter, R. (1988). A semi-dominant allele, niv-525, acts in trans to inhibit expression of its wild-type homologue in Antirrhinum majus. *EMBO J*, 7(4), 877-883.
- Coetzee, M., & Fontenille, D. (2004). Advances in the study of Anopheles funestus, a major vector of malaria in Africa. *Insect Biochem Mol Biol*, 34(7), 599-605. doi:10.1016/j.ibmb.2004.03.012
- Colicelli, J. (2004). Human RAS superfamily proteins and related GTPases. *Sci STKE*, 2004(250), Re13. doi:10.1126/stke.2502004re13
- Collins, C. R., Das, S., Wong, E. H., Andenmatten, N., Stallmach, R., Hackett, F., . . . Blackman, M. J. (2013). Robust inducible Cre recombinase activity in the human malaria parasite Plasmodium falciparum enables efficient gene deletion within a single asexual erythrocytic growth cycle. *Mol Microbiol*, 88(4), 687-701. doi:10.1111/mmi.12206
- Collins, W. E., & Jeffery, G. M. (2005). Plasmodium ovale: parasite and disease. *Clin Microbiol Rev*, 18(3), 570-581. doi:10.1128/CMR.18.3.570-581.2005
- Cong, L., Ran, F. A., Cox, D., Lin, S., Barretto, R., Habib, N., . . . Zhang, F. (2013). Multiplex genome engineering using CRISPR/Cas systems. *Science*, 339(6121), 819-823. doi:10.1126/science.1231143
- Cooper, D. J., Rajahram, G. S., William, T., Jelip, J., Mohammad, R., Benedict, J., . . . Barber, B. E. (2019). Plasmodium knowlesi Malaria in Sabah, Malaysia, 2015–2017: Ongoing Increase in Incidence Despite Near-elimination of the Human-only Plasmodium Species. *Clinical Infectious Diseases*. doi:10.1093/cid/ciz237
- Cooper, G. M. (2000). *The cell : a molecular approach*. Washington, D.C.; Sunderland, Mass.: ASM Press ; Sinauer Associates.
- Coppi, A., Pinzon-Ortiz, C., Hutter, C., & Sinnis, P. (2005). The Plasmodium circumsporozoite protein is proteolytically processed during cell invasion. *The Journal of Experimental Medicine*, 201(1), 27-33. doi:10.1084/jem.20040989
- Cowman, A. F., Berry, D., & Baum, J. (2012). The cellular and molecular basis for malaria parasite invasion of the human red blood cell. *J Cell Biol*, 198(6), 961-971. doi:10.1083/jcb.201206112
- Cox, F. E. (2002). History of human parasitology. *Clin Microbiol Rev*, 15(4), 595-612.
- Crabb, B. S., de Koning-Ward, T. F., & Gilson, P. R. (2010). Protein export in Plasmodium parasites: from the endoplasmic reticulum to the vacuolar export machine. *Int J Parasitol*, 40(5), 509-513. doi:10.1016/j.ijpara.2010.02.002
- Craig, A. G., Khairul, M. F., & Patil, P. R. (2012). Cytoadherence and severe malaria. *Malays J Med Sci*, 19(2), 5-18.
- Cronan, J. E. (2005). Targeted and proximity-dependent promiscuous protein biotinylation by a mutant Escherichia coli biotin protein ligase. *J Nutr Biochem*, 16(7), 416-418. doi:10.1016/j.jnutbio.2005.03.017
- Cunha, C. B., & Cunha, B. A. (2008). Brief history of the clinical diagnosis of malaria: from Hippocrates to Osler. *J Vector Borne Dis*, 45(3), 194-199.
- D'Archivio, S., & Wickstead, B. (2017). Trypanosome outer kinetochore proteins suggest conservation of chromosome segregation machinery across eukaryotes. *The Journal of cell biology*, 216(2), 379-391. doi:10.1083/jcb.201608043
- Dacks, J. B., Davis, L. A., Sjogren, A. M., Andersson, J. O., Roger, A. J., & Doolittle, W. F. (2003). Evidence for Golgi bodies in proposed 'Golgi-lacking' lineages. *Proc Biol Sci*, 270 Suppl 2, S168-171. doi:10.1098/rsbl.2003.0058

- Daniyan, M. O., Przyborski, J. M., & Shonhai, A. (2019). Partners in Mischief: Functional Networks of Heat Shock Proteins of *Plasmodium falciparum* and Their Influence on Parasite Virulence. *Biomolecules*, *9*(7). doi:10.3390/biom9070295
- Dasgupta, S., Auth, T., Gov, N. S., Satchwell, T. J., Hanssen, E., Zuccala, E. S., . . . Gompper, G. (2014). Membrane-wrapping contributions to malaria parasite invasion of the human erythrocyte. *Biophys J*, *107*(1), 43-54. doi:10.1016/j.bpj.2014.05.024
- Date, S. V., & Stoeckert, C. J., Jr. (2006). Computational modeling of the *Plasmodium falciparum* interactome reveals protein function on a genome-wide scale. *Genome research*, *16*(4), 542-549. doi:10.1101/gr.4573206
- Daum, J. R., Wren, J. D., Daniel, J. J., Sivakumar, S., McAvoy, J. N., Potapova, T. A., & Gorbsky, G. J. (2009). Ska3 is required for spindle checkpoint silencing and the maintenance of chromosome cohesion in mitosis. *Curr Biol*, *19*(17), 1467-1472. doi:10.1016/j.cub.2009.07.017
- David, P. H., Hommel, M., Miller, L. H., Udeinya, I. J., & Oligino, L. D. (1983). Parasite sequestration in *Plasmodium falciparum* malaria: spleen and antibody modulation of cytoadherence of infected erythrocytes. *Proceedings of the National Academy of Sciences of the United States of America*, *80*(16), 5075-5079. doi:10.1073/pnas.80.16.5075
- Davidson, A. (1899). Ueber Malaria—und andere Blutparasiten, nebst Anhang eine wirksame Methode der Chromatin — und Blutfärbung. *Edinburgh Medical Journal*, *5*(1), 65-67.
- Davies, K. T., Cotton, J. A., Kirwan, J. D., Teeling, E. C., & Rossiter, S. J. (2012). Parallel signatures of sequence evolution among hearing genes in echolocating mammals: an emerging model of genetic convergence. *Heredity (Edinb)*, *108*(5), 480-489. doi:10.1038/hdy.2011.119
- de Azevedo, M. F., Gilson, P. R., Gabriel, H. B., Simões, R. F., Angrisano, F., Baum, J., . . . Wunderlich, G. (2012). Systematic analysis of FKBP inducible degradation domain tagging strategies for the human malaria parasite *Plasmodium falciparum*. *PLOS ONE*, *7*(7), e40981-e40981. doi:10.1371/journal.pone.0040981
- de Castro, F. A., Ward, G. E., Jambou, R., Attal, G., Mayau, V., Jaureguiberry, G., . . . Langsley, G. (1996). Identification of a family of Rab G-proteins in *Plasmodium falciparum* and a detailed characterisation of pfrab6. *Mol Biochem Parasitol*, *80*(1), 77-88. doi:10.1016/0166-6851(96)02670-9
- de Koning-Ward, T. F., Gilson, P. R., Boddey, J. A., Rug, M., Smith, B. J., Papenfuss, A. T., . . . Crabb, B. S. (2009). A newly discovered protein export machine in malaria parasites. *Nature*, *459*(7249), 945-949. doi:10.1038/nature08104
- de Koning-Ward, T. F., Gilson, P. R., & Crabb, B. S. (2015). Advances in molecular genetic systems in malaria. *Nature Reviews Microbiology*, *13*, 373. doi:10.1038/nrmicro3450
- De Niz, M., Meibalan, E., Mejia, P., Ma, S., Brancucci, N. M. B., Agop-Nersesian, C., . . . Marti, M. (2018). *Plasmodium* gametocytes display homing and vascular transmigration in the host bone marrow. *Sci Adv*, *4*(5), eaat3775. doi:10.1126/sciadv.aat3775
- De Souza, C. P., & Osmani, S. A. (2007). Mitosis, not just open or closed. *Eukaryot Cell*, *6*(9), 1521-1527. doi:10.1128/ec.00178-07
- De Souza, C. P., & Osmani, S. A. (2009). Double duty for nuclear proteins--the price of more open forms of mitosis. *Trends Genet*, *25*(12), 545-554. doi:10.1016/j.tig.2009.10.005
- Delprato, A., Merithew, E., & Lambright, D. G. (2004). Structure, exchange determinants, and family-wide rab specificity of the tandem helical bundle and Vps9 domains of Rabex-5. *Cell*, *118*(5), 607-617. doi:10.1016/j.cell.2004.08.009
- Delves, M., Plouffe, D., Scheurer, C., Meister, S., Wittlin, S., Winzeler, E. A., . . . Leroy, D. (2012). The activities of current antimalarial drugs on the life cycle stages of *Plasmodium*: a comparative study with human and rodent parasites. *PLoS Med*, *9*(2), e1001169. doi:10.1371/journal.pmed.1001169
- Deneka, M., & van der Sluijs, P. (2002). 'Rab'ing up endosomal membrane transport. *Nat Cell Biol*, *4*(2), E33-35. doi:10.1038/ncb0202-e33
- Deponte, M., Hoppe, H. C., Lee, M. C., Maier, A. G., Richard, D., Rug, M., . . . Przyborski, J. M. (2012). Wherever I may roam: protein and membrane trafficking in *P. falciparum*-infected red blood cells. *Mol Biochem Parasitol*, *186*(2), 95-116. doi:10.1016/j.molbiopara.2012.09.007

- Devillers-Thierry, A., Kindt, T., Scheele, G., & Blobel, G. (1975). Homology in amino-terminal sequence of precursors to pancreatic secretory proteins. *Proceedings of the National Academy of Sciences*, 72(12), 5016-5020. doi:10.1073/pnas.72.12.5016
- Di Genova, B. M., Wilson, S. K., Dubey, J. P., & Knoll, L. J. (2019). Intestinal delta-6-desaturase activity determines host range for *Toxoplasma* sexual reproduction. *bioRxiv*, 688580. doi:10.1101/688580
- Ding, R., West, R. R., Morphew, D. M., Oakley, B. R., & McIntosh, J. R. (1997). The spindle pole body of *Schizosaccharomyces pombe* enters and leaves the nuclear envelope as the cell cycle proceeds. *Mol Biol Cell*, 8(8), 1461-1479. doi:10.1091/mbc.8.8.1461
- Dobson, M. (1980). Marsh fever: the geography of malaria in England. *J Hist Geogr*, 6(4), 357-389.
- Dobson, M. J. (1994). Malaria in England: a geographical and historical perspective. *Parassitologia*, 36(1-2), 35-60.
- Doherty, G. J., & McMahon, H. T. (2009). Mechanisms of endocytosis. *Annu Rev Biochem*, 78, 857-902. doi:10.1146/annurev.biochem.78.081307.110540
- Dondorp, A. M., Nosten, F., Yi, P., Das, D., Phyto, A. P., Tarning, J., . . . White, N. J. (2009). Artemisinin resistance in *Plasmodium falciparum* malaria. *N Engl J Med*, 361(5), 455-467. doi:10.1056/NEJMoa0808859
- Dorovini-Zis, K., Schmidt, K., Huynh, H., Fu, W., Whitten, R. O., Milner, D., . . . Taylor, T. E. (2011). The neuropathology of fatal cerebral malaria in Malawian children. *Am J Pathol*, 178(5), 2146-2158. doi:10.1016/j.ajpath.2011.01.016
- Draper, S. J., Sack, B. K., King, C. R., Nielsen, C. M., Rayner, J. C., Higgins, M. K., . . . Seder, R. A. (2018). Malaria Vaccines: Recent Advances and New Horizons. *Cell Host Microbe*, 24(1), 43-56. doi:10.1016/j.chom.2018.06.008
- Dubey, J. P., & Lindsay, D. S. (1996). A review of *Neospora caninum* and neosporosis. *Veterinary Parasitology*, 67(1), 1-59. doi:https://doi.org/10.1016/S0304-4017(96)01035-7
- Dubey, J. P., Miller, N. L., & Frenkel, J. K. (1970). THE *TOXOPLASMA GONDII* OOCYST FROM CAT FECES. *The Journal of Experimental Medicine*, 132(4), 636-662. doi:10.1084/jem.132.4.636
- Durand, R., Jafari, S., Vauzelle, J., Delabre, J. F., Jesic, Z., & Le Bras, J. (2001). Analysis of pfcrt point mutations and chloroquine susceptibility in isolates of *Plasmodium falciparum*. *Mol Biochem Parasitol*, 114(1), 95-102.
- Eathiraj, S., Pan, X., Ritacco, C., & Lambright, D. G. (2005). Structural basis of family-wide Rab GTPase recognition by rabenosyn-5. *Nature*, 436(7049), 415-419. doi:10.1038/nature03798
- Ebine, K., Hirai, M., Sakaguchi, M., Yahata, K., Kaneko, O., & Saito-Nakano, Y. (2016). *Plasmodium* Rab5b is secreted to the cytoplasmic face of the tubovesicular network in infected red blood cells together with N-acylated adenylate kinase 2. *Malaria journal*, 15(1), 323. doi:10.1186/s12936-016-1377-4
- Ehlgen, F., Pham, J. S., de Koning-Ward, T., Cowman, A. F., & Ralph, S. A. (2012). Investigation of the *Plasmodium falciparum* food vacuole through inducible expression of the chloroquine resistance transporter (PfCRT). *PLOS ONE*, 7(6), e38781. doi:10.1371/journal.pone.0038781
- Ellington, A. D., & Szostak, J. W. (1990). In vitro selection of RNA molecules that bind specific ligands. *Nature*, 346(6287), 818-822. doi:10.1038/346818a0
- Elmendorf, H. G., & Haldar, K. (1993). Identification and localization of ERD2 in the malaria parasite *Plasmodium falciparum*: separation from sites of sphingomyelin synthesis and implications for organization of the Golgi. *EMBO J*, 12(12), 4763-4773.
- Elsworth, B., Crabb, B. S., & Gilson, P. R. (2014). Protein export in malaria parasites: an update. *Cell Microbiol*, 16(3), 355-363. doi:10.1111/cmi.12261
- Emerson, S. B., & Koehl, M. A. R. (1990). The Interaction of Behavioral and Morphological Change in the Evolution of a Novel Locomotor Type: "Flying" Frogs. *Evolution*, 44(8), 1931-1946. doi:10.2307/2409604
- Enayati, A., & Hemingway, J. (2010). Malaria management: past, present, and future. *Annu Rev Entomol*, 55, 569-591. doi:10.1146/annurev-ento-112408-085423
- Ezougou, C. N., Ben-Rached, F., Moss, D. K., Lin, J.-w., Black, S., Knuepfer, E., . . . Langsley, G. (2014). *Plasmodium falciparum* Rab5B Is an N-Terminally Myristoylated Rab GTPase That Is

- Targeted to the Parasite's Plasma and Food Vacuole Membranes. *PLOS ONE*, 9(2), e87695. doi:10.1371/journal.pone.0087695
- Faroon, O., & Harris, M. O. (2002). Toxicological profile for DDT, DDE, and DDD.
- Faurant, C. (2011). From bark to weed: the history of artemisinin. *Parasite (Paris, France)*, 18(3), 215-218. doi:10.1051/parasite/2011183215
- Fidock, D. A., Nomura, T., Talley, A. K., Cooper, R. A., Dzekunov, S. M., Ferdig, M. T., . . . Wellems, T. E. (2000). Mutations in the *P. falciparum* digestive vacuole transmembrane protein PfCRT and evidence for their role in chloroquine resistance. *Mol Cell*, 6(4), 861-871. doi:10.1016/s1097-2765(05)00077-8
- Fields, S., & Song, O. (1989). A novel genetic system to detect protein-protein interactions. *Nature*, 340(6230), 245-246. doi:10.1038/340245a0
- Filarsky, M., Frasncka, S. A., Niederwieser, I., Brancucci, N. M. B., Carrington, E., Carrió, E., . . . Voss, T. S. (2018). GDV1 induces sexual commitment of malaria parasites by antagonizing HP1-dependent gene silencing. *Science (New York, N.Y.)*, 359(6381), 1259-1263. doi:10.1126/science.aan6042
- Fitch, W. M. (1970). Distinguishing Homologous from Analogous Proteins. *Systematic Biology*, 19(2), 99-113. doi:10.2307/2412448
- Flemming, S. (2015). Visualization and characterization of endocytic processes in the human Malaria parasite *P. falciparum* (Welch, 1897). .
- Flores, M. V., Atkins, D., Wade, D., O'Sullivan, W. J., & Stewart, T. S. (1997). Inhibition of *Plasmodium falciparum* proliferation in vitro by ribozymes. *J Biol Chem*, 272(27), 16940-16945. doi:10.1074/jbc.272.27.16940
- Foley, M., & Tilley, L. (1998). Quinoline antimalarials: mechanisms of action and resistance and prospects for new agents. *Pharmacol Ther*, 79(1), 55-87. doi:10.1016/s0163-7258(98)00012-6
- Foth, B. J., & McFadden, G. I. (2003). The apicoplast: a plastid in *Plasmodium falciparum* and other Apicomplexan parasites. *Int Rev Cytol*, 224, 57-110. doi:10.1016/s0074-7696(05)24003-2
- Fowkes, F. J., Richards, J. S., Simpson, J. A., & Beeson, J. G. (2010). The relationship between anti-merozoite antibodies and incidence of *Plasmodium falciparum* malaria: A systematic review and meta-analysis. *PLoS Med*, 7(1), e1000218. doi:10.1371/journal.pmed.1000218
- Francia, M. E., & Striepen, B. (2014). Cell division in apicomplexan parasites. *Nat Rev Microbiol*, 12(2), 125-136. doi:10.1038/nrmicro3184
- Francis, S. E., Sullivan, D. J., Jr., & Goldberg, D. E. (1997). Hemoglobin metabolism in the malaria parasite *Plasmodium falciparum*. *Annu Rev Microbiol*, 51, 97-123. doi:10.1146/annurev.micro.51.1.97
- Gaitanos, T. N., Santamaria, A., Jeyaprakash, A. A., Wang, B., Conti, E., & Nigg, E. A. (2009). Stable kinetochore-microtubule interactions depend on the Ska complex and its new component Ska3/C13Orf3. *EMBO J*, 28(10), 1442-1452. doi:10.1038/emboj.2009.96
- Ganesan, S. M., Falla, A., Goldfless, S. J., Nasamu, A. S., & Niles, J. C. (2016). Synthetic RNA-protein modules integrated with native translation mechanisms to control gene expression in malaria parasites. *Nat Commun*, 7, 10727. doi:10.1038/ncomms10727
- Ganter, M., Goldberg, J. M., Dvorin, J. D., Paulo, J. A., King, J. G., Tripathi, A. K., . . . Duraisingh, M. T. (2017). *Plasmodium falciparum* CRK4 directs continuous rounds of DNA replication during schizogony. *Nat Microbiol*, 2, 17017. doi:10.1038/nmicrobiol.2017.17
- Gardner, M. J., Hall, N., Fung, E., White, O., Berriman, M., Hyman, R. W., . . . Barrell, B. (2002). Genome sequence of the human malaria parasite *Plasmodium falciparum*. *Nature*, 419(6906), 498-511. doi:10.1038/nature01097
- Gardner, M. J., Tettelin, H., Carucci, D. J., Cummings, L. M., Aravind, L., Koonin, E. V., . . . Hoffman, S. L. (1998). Chromosome 2 sequence of the human malaria parasite *Plasmodium falciparum*. *Science*, 282(5391), 1126-1132. doi:10.1126/science.282.5391.1126
- Geiger, M., Brown, C., Wichers, J. S., Strauss, J., Lill, A., Thuenauer, R., . . . Gilberger, T. W. (2019). Structural Insights Into PfARO and Characterization of its Interaction With PfAIP. *J Mol Biol*. doi:https://doi.org/10.1016/j.jmb.2019.12.024
- Gengyo-Ando, K., Kuroyanagi, H., Kobayashi, T., Murate, M., Fujimoto, K., Okabe, S., & Mitani, S. (2007). The SM protein VPS-45 is required for RAB-5-dependent endocytic transport in *Caenorhabditis elegans*. *EMBO Rep*, 8(2), 152-157. doi:10.1038/sj.embor.7400882

- Gerald, N., Mahajan, B., & Kumar, S. (2011). Mitosis in the human malaria parasite *Plasmodium falciparum*. *Eukaryot Cell*, *10*(4), 474-482. doi:10.1128/EC.00314-10
- Ghorbal, M., Gorman, M., Macpherson, C. R., Martins, R. M., Scherf, A., & Lopez-Rubio, J. J. (2014). Genome editing in the human malaria parasite *Plasmodium falciparum* using the CRISPR-Cas9 system. *Nat Biotechnol*, *32*(8), 819-821. doi:10.1038/nbt.2925
- Ghosh, S. K., Field, J., Frisardi, M., Rosenthal, B., Mai, Z., Rogers, R., & Samuelson, J. (1999). Chitinase secretion by encysting *Entamoeba invadens* and transfected *Entamoeba histolytica* trophozoites: localization of secretory vesicles, endoplasmic reticulum, and Golgi apparatus. *Infect Immun*, *67*(6), 3073-3081.
- Gillies, M. T., & Coetzee, M. (1987). *A Supplement to the Anophelinae of Africa South of the Sahara (Afrotropical Region)*: South African Institute for Medical Research.
- Gillies, M. T., & De Meillon, B. (1968). *The Anophelinae of Africa South of the Sahara: Ethiopian Zoogeographical Region*: South African Institute for Medical Research.
- Gladfelter, A. S. (2006). Nuclear anarchy: asynchronous mitosis in multinucleated fungal hyphae. *Curr Opin Microbiol*, *9*(6), 547-552. doi:10.1016/j.mib.2006.09.002
- Glushakova, S., Yin, D., Li, T., & Zimmerberg, J. (2005). Membrane transformation during malaria parasite release from human red blood cells. *Curr Biol*, *15*(18), 1645-1650. doi:10.1016/j.cub.2005.07.067
- Gluzman, I. Y., Francis, S. E., Oksman, A., Smith, C. E., Duffin, K. L., & Goldberg, D. E. (1994). Order and specificity of the *Plasmodium falciparum* hemoglobin degradation pathway. *J Clin Invest*, *93*(4), 1602-1608. doi:10.1172/jci117140
- Goldberg, D. E., Slater, A. F., Beavis, R., Chait, B., Cerami, A., & Henderson, G. B. (1991). Hemoglobin degradation in the human malaria pathogen *Plasmodium falciparum*: a catabolic pathway initiated by a specific aspartic protease. *J Exp Med*, *173*(4), 961-969. doi:10.1084/jem.173.4.961
- Goldberg, D. E., Slater, A. F., Cerami, A., & Henderson, G. B. (1990). Hemoglobin degradation in the malaria parasite *Plasmodium falciparum*: an ordered process in a unique organelle. *Proc Natl Acad Sci U S A*, *87*(8), 2931-2935. doi:10.1073/pnas.87.8.2931
- Goldfless, S. J., Wagner, J. C., & Niles, J. C. (2014). Versatile control of *Plasmodium falciparum* gene expression with an inducible protein-RNA interaction. *Nat Commun*, *5*, 5329-5329. doi:10.1038/ncomms6329
- Goldstein, L. S. (2001). Molecular motors: from one motor many tails to one motor many tales. *Trends Cell Biol*, *11*(12), 477-482. doi:10.1016/s0962-8924(01)02143-2
- Goodman, C. D., Siregar, J. E., Mollard, V., Vega-Rodriguez, J., Syafruddin, D., Matsuoka, H., . . . McFadden, G. I. (2016). Parasites resistant to the antimalarial atovaquone fail to transmit by mosquitoes. *Science*, *352*(6283), 349-353. doi:10.1126/science.aad9279
- Gorvel, J. P., Chavier, P., Zerial, M., & Gruenberg, J. (1991). rab5 controls early endosome fusion in vitro. *Cell*, *64*(5), 915-925. doi:10.1016/0092-8674(91)90316-q
- Gould, S. B., Waller, R. F., & McFadden, G. I. (2008). Plastid evolution. *Annu Rev Plant Biol*, *59*, 491-517. doi:10.1146/annurev.arplant.59.032607.092915
- Gray, K. A., Gresty, K. J., Chen, N., Zhang, V., Gutteridge, C. E., Peatey, C. L., . . . Cheng, Q. (2016). Correlation between Cyclin Dependent Kinases and Artemisinin-Induced Dormancy in *Plasmodium falciparum* In Vitro. *PLOS ONE*, *11*(6), e0157906. doi:10.1371/journal.pone.0157906
- Greenwood, B. M., Fidock, D. A., Kyle, D. E., Kappe, S. H., Alonso, P. L., Collins, F. H., & Duffy, P. E. (2008). Malaria: progress, perils, and prospects for eradication. *J Clin Invest*, *118*(4), 1266-1276. doi:10.1172/JCI33996
- Grishin, N. V. (2001). Fold change in evolution of protein structures. *J Struct Biol*, *134*(2-3), 167-185. doi:10.1006/jsbi.2001.4335
- Gross, W. (1967). Über das Gebiss der Acanthodier und Placodermen. *Journal of the Linnean Society of London, Zoology*, *47*(311), 121-130. doi:10.1111/j.1096-3642.1967.tb01399.x
- Gruring, C., Heiber, A., Kruse, F., Ungefehr, J., Gilberger, T. W., & Spielmann, T. (2011). Development and host cell modifications of *Plasmodium falciparum* blood stages in four dimensions. *Nat Commun*, *2*, 165. doi:10.1038/ncomms1169

- Gruring, C., & Spielmann, T. (2012). Imaging of live malaria blood stage parasites. *Methods Enzymol*, 506, 81-92. doi:10.1016/b978-0-12-391856-7.00029-9
- Gubbels, M. J., & Duraisingh, M. T. (2012). Evolution of apicomplexan secretory organelles. *Int J Parasitol*, 42(12), 1071-1081. doi:10.1016/j.ijpara.2012.09.009
- Guillemin, J. (2001). Miasma, malaria, and method. *Mol Interv*, 1(5), 246-249.
- Gunning, P. W., Ghoshdastider, U., Whitaker, S., Popp, D., & Robinson, R. C. (2015). The evolution of compositionally and functionally distinct actin filaments. *J Cell Sci*, 128(11), 2009-2019. doi:10.1242/jcs.165563
- Gustafsson, L. L., Beermann, B., & Abdi, Y. A. (1987). *Handbook of drugs for tropical parasitic infections*. London: Taylor and Francis Ltd.
- Hamilton, A. J., & Baulcombe, D. C. (1999). A species of small antisense RNA in posttranscriptional gene silencing in plants. *Science*, 286(5441), 950-952. doi:10.1126/science.286.5441.950
- Hanisch, A., Sillje, H. H., & Nigg, E. A. (2006). Timely anaphase onset requires a novel spindle and kinetochore complex comprising Skal and Ska2. *EMBO J*, 25(23), 5504-5515. doi:10.1038/sj.emboj.7601426
- Harada, T., Takeda, M., Kojima, S., & Tomiyama, N. (2016). Toxicity and Carcinogenicity of Dichlorodiphenyltrichloroethane (DDT). *Toxicological research*, 32(1), 21-33. doi:10.5487/TR.2016.32.1.021
- Harada, T., Yamaguchi, S., Ohtsuka, R., Takeda, M., Fujisawa, H., Yoshida, T., . . . Maita, K. (2003). Mechanisms of promotion and progression of preneoplastic lesions in hepatocarcinogenesis by DDT in F344 rats. *Toxicol Pathol*, 31(1), 87-98. doi:10.1080/01926230390173941
- Haruki, H., Nishikawa, J., & Laemmli, U. K. (2008). The anchor-away technique: rapid, conditional establishment of yeast mutant phenotypes. *Mol Cell*, 31(6), 925-932. doi:10.1016/j.molcel.2008.07.020
- Hastings, I. M., & D'Alessandro, U. (2000). Modelling a predictable disaster: the rise and spread of drug-resistant malaria. *Parasitol Today*, 16(8), 340-347. doi:10.1016/s0169-4758(00)01707-5
- Hausmann, A., Aguilar Netz, D. J., Balk, J., Pierik, A. J., Muhlenhoff, U., & Lill, R. (2005). The eukaryotic P loop NTPase Nbp35: an essential component of the cytosolic and nuclear iron-sulfur protein assembly machinery. *Proc Natl Acad Sci U S A*, 102(9), 3266-3271. doi:10.1073/pnas.0406447102
- Hawking, F., Wilson, M. E., & Gammage, K. (1971). Evidence for cyclic development and short-lived maturity in the gametocytes of *Plasmodium falciparum*. *Trans R Soc Trop Med Hyg*, 65(5), 549-559. doi:10.1016/0035-9203(71)90036-8
- Hay, S. I., Sinka, M. E., Okara, R. M., Kabaria, C. W., Mbithi, P. M., Tago, C. C., . . . Godfray, H. C. (2010). Developing global maps of the dominant anophelid vectors of human malaria. *PLoS Med*, 7(2), e1000209. doi:10.1371/journal.pmed.1000209
- Heath, I. B. (1980). Variant mitoses in lower eukaryotes: indicators of the evolution of mitosis. *Int Rev Cytol*, 64, 1-80. doi:10.1016/s0074-7696(08)60235-1
- Heiber, A., Kruse, F., Pick, C., Gruring, C., Flemming, S., Oberli, A., . . . Spielmann, T. (2013). Identification of new PNEPs indicates a substantial non-PEXEL exportome and underpins common features in *Plasmodium falciparum* protein export. *PLoS Pathog*, 9(8), e1003546. doi:10.1371/journal.ppat.1003546
- Helgeson, L. A., Zelter, A., Riffle, M., MacCoss, M. J., Asbury, C. L., & Davis, T. N. (2018). Human Ska complex and Ndc80 complex interact to form a load-bearing assembly that strengthens kinetochore-microtubule attachments. *Proc Natl Acad Sci U S A*, 115(11), 2740-2745. doi:10.1073/pnas.1718553115
- Hiller, N. L., Bhattacharjee, S., van Ooij, C., Liolios, K., Harrison, T., Lopez-Estrano, C., & Haldar, K. (2004). A host-targeting signal in virulence proteins reveals a secretome in malarial infection. *Science*, 306(5703), 1934-1937. doi:10.1126/science.1102737
- Hillier, C., Pardo, M., Yu, L., Bushell, E., Sanderson, T., Metcalf, T., . . . Choudhary, J. S. (2019). Landscape of the *Plasmodium* Interactome Reveals Both Conserved and Species-Specific Functionality. *Cell Rep*, 28(6), 1635-1647.e1635. doi:10.1016/j.celrep.2019.07.019
- Hirokawa, N. (1998). Kinesin and dynein superfamily proteins and the mechanism of organelle transport. *Science*, 279(5350), 519-526. doi:10.1126/science.279.5350.519

- Hori, Y., Kikuchi, A., Isomura, M., Katayama, M., Miura, Y., Fujioka, H., . . . Takai, Y. (1991). Post-translational modifications of the C-terminal region of the rho protein are important for its interaction with membranes and the stimulatory and inhibitory GDP/GTP exchange proteins. *Oncogene*, 6(4), 515-522.
- Hrycyna, C. A., & Clarke, S. (1993). Modification of eukaryotic signaling proteins by C-terminal methylation reactions. *Pharmacol Ther*, 59(3), 281-300. doi:https://doi.org/10.1016/0163-7258(93)90071-K
- Huang, J., Koide, A., Makabe, K., & Koide, S. (2008). Design of protein function leaps by directed domain interface evolution. *Proceedings of the National Academy of Sciences of the United States of America*, 105(18), 6578-6583. doi:10.1073/pnas.0801097105
- Huh, W. K., Falvo, J. V., Gerke, L. C., Carroll, A. S., Howson, R. W., Weissman, J. S., & O'Shea, E. K. (2003). Global analysis of protein localization in budding yeast. *Nature*, 425(6959), 686-691. doi:10.1038/nature02026
- Hulden, L., Hulden, L., & Heliövaara, K. (2005). Endemic malaria: an 'indoor' disease in northern Europe. Historical data analysed. *Malar J*, 4, 19. doi:10.1186/1475-2875-4-19
- Hunsicker, A., Steber, M., Mayer, G., Meitert, J., Klotzsche, M., Blind, M., . . . Süss, B. (2009). An RNA aptamer that induces transcription. *Chem Biol*, 16(2), 173-180. doi:10.1016/j.chembiol.2008.12.008
- Huotari, J., & Helenius, A. (2011). Endosome maturation. *The EMBO journal*, 30(17), 3481-3500. doi:10.1038/emboj.2011.286
- Inoue, H., Nojima, H., & Okayama, H. (1990). High efficiency transformation of *Escherichia coli* with plasmids. *Gene*, 96(1), 23-28. doi:10.1016/0378-1119(90)90336-p
- Ishiyama, A., Otoguro, K., Namatame, M., Nishihara, A., Furusawa, T., Takahashi, Y., . . . Ōmura, S. (2008). Simaomicin α : Effects on the Cell Cycle of Synchronized, Cultured *Plasmodium falciparum*. *The Journal of Antibiotics*, 61(4), 254-257. doi:10.1038/ja.2008.38
- Itsara, L. S., Zhou, Y., Do, J., Grieser, A. M., Vaughan, A. M., & Ghosh, A. K. (2018). The Development of Whole Sporozoite Vaccines for *Plasmodium falciparum* Malaria. *Frontiers in immunology*, 9, 2748-2748. doi:10.3389/fimmu.2018.02748
- Iwamoto, M., Bjorklund, T., Lundberg, C., Kirik, D., & Wandless, T. J. (2010). A general chemical method to regulate protein stability in the mammalian central nervous system. *Chem Biol*, 17(9), 981-988. doi:10.1016/j.chembiol.2010.07.009
- Jacobberger, J. W., Horan, P. K., & Hare, J. D. (1992). Cell cycle analysis of asexual stages of erythrocytic malaria parasites. *Cell Prolif*, 25(5), 431-445. doi:10.1111/j.1365-2184.1992.tb01452.x
- Janes, J. H., Wang, C. P., Levin-Edens, E., Vigan-Womas, I., Guillotte, M., Melcher, M., . . . Smith, J. D. (2011). Investigating the host binding signature on the *Plasmodium falciparum* PfEMP1 protein family. *PLoS Pathog*, 7(5), e1002032. doi:10.1371/journal.ppat.1002032
- Janouskovec, J., Horak, A., Obornik, M., Lukes, J., & Keeling, P. J. (2010). A common red algal origin of the apicomplexan, dinoflagellate, and heterokont plastids. *Proc Natl Acad Sci U S A*, 107(24), 10949-10954. doi:10.1073/pnas.1003335107
- Jeyaprasanth, A. A., Santamaria, A., Jayachandran, U., Chan, Y. W., Benda, C., Nigg, E. A., & Conti, E. (2012). Structural and functional organization of the Ska complex, a key component of the kinetochore-microtubule interface. *Mol Cell*, 46(3), 274-286. doi:10.1016/j.molcel.2012.03.005
- Jin, Y., Kebaier, C., & Vanderberg, J. (2007). Direct microscopic quantification of dynamics of *Plasmodium berghei* sporozoite transmission from mosquitoes to mice. *Infection and Immunity*, 75(11), 5532-5539. doi:10.1128/IAI.00600-07
- Jinek, M., East, A., Cheng, A., Lin, S., Ma, E., & Doudna, J. (2013). RNA-programmed genome editing in human cells. *Elife*, 2, e00471. doi:10.7554/eLife.00471
- Jonscher, E., Flemming, S., Schmitt, M., Sabitzki, R., Reichard, N., Birnbaum, J., . . . Spielmann, T. (2019). PfVPS45 Is Required for Host Cell Cytosol Uptake by Malaria Blood Stage Parasites. *Cell Host Microbe*, 25(1), 166-173 e165. doi:10.1016/j.chom.2018.11.010
- Jorgensen, R. (1990). Altered gene expression in plants due to trans interactions between homologous genes. *Trends Biotechnol*, 8(12), 340-344. doi:10.1016/0167-7799(90)90220-r

- Josling, G. A., & Llinas, M. (2015). Sexual development in Plasmodium parasites: knowing when it's time to commit. *Nat Rev Microbiol*, *13*(9), 573-587. doi:10.1038/nrmicro3519
- Jullien, N., Goddard, I., Selmi-Ruby, S., Fina, J. L., Cremer, H., & Herman, J. P. (2007). Conditional transgenesis using Dimerizable Cre (DiCre). *PLoS One*, *2*(12), e1355. doi:10.1371/journal.pone.0001355
- Jullien, N., Sampieri, F., Enjalbert, A., & Herman, J. P. (2003). Regulation of Cre recombinase by ligand-induced complementation of inactive fragments. *Nucleic Acids Res*, *31*(21), e131. doi:10.1093/nar/gng131
- Kafsack, B. F., Rovira-Graells, N., Clark, T. G., Bancells, C., Crowley, V. M., Campino, S. G., . . . Llinas, M. (2014). A transcriptional switch underlies commitment to sexual development in malaria parasites. *Nature*, *507*(7491), 248-252. doi:10.1038/nature12920
- Kaksonen, M., & Roux, A. (2018). Mechanisms of clathrin-mediated endocytosis. *Nature Reviews Molecular Cell Biology*, *19*, 313. doi:10.1038/nrm.2017.132
- Kantele, A., & Jokiranta, T. S. (2011). Review of cases with the emerging fifth human malaria parasite, Plasmodium knowlesi. *Clin Infect Dis*, *52*(11), 1356-1362. doi:10.1093/cid/cir180
- Kaushansky, A., Douglass, A. N., Arang, N., Vigdorovich, V., Dambrauskas, N., Kain, H. S., . . . Kappe, S. H. I. (2015). Malaria parasites target the hepatocyte receptor EphA2 for successful host infection. *Science*, *350*(6264), 1089-1092. doi:10.1126/science.aad3318
- Kehrer, J., Kuss, C., Andres-Pons, A., Reustle, A., Dahan, N., Devos, D., . . . Frischknecht, F. (2018). Nuclear Pore Complex Components in the Malaria Parasite Plasmodium berghei. *Sci Rep*, *8*(1), 11249. doi:10.1038/s41598-018-29590-5
- Khoury, D. S., Cromer, D., Best, S. E., James, K. R., Kim, P. S., Engwerda, C. R., . . . Davenport, M. P. (2014). Effect of mature blood-stage Plasmodium parasite sequestration on pathogen biomass in mathematical and in vivo models of malaria. *Infection and Immunity*, *82*(1), 212-220. doi:10.1128/IAI.00705-13
- Kilejian, A., Rashid, M. A., Aikawa, M., Aji, T., & Yang, Y. F. (1991). Selective association of a fragment of the knob protein with spectrin, actin and the red cell membrane. *Mol Biochem Parasitol*, *44*(2), 175-181. doi:10.1016/0166-6851(91)90003-o
- Kim, D. I., Jensen, S. C., Noble, K. A., Kc, B., Roux, K. H., Motamedchaboki, K., & Roux, K. J. (2016). An improved smaller biotin ligase for BioID proximity labeling. *Mol Biol Cell*, *27*(8), 1188-1196. doi:10.1091/mbc.E15-12-0844
- Kirkman, L. A., Lawrence, E. A., & Deitsch, K. W. (2014). Malaria parasites utilize both homologous recombination and alternative end joining pathways to maintain genome integrity. *Nucleic Acids Res*, *42*(1), 370-379. doi:10.1093/nar/gkt881
- Kiseleva, E., Rutherford, S., Cotter, L. M., Allen, T. D., & Goldberg, M. W. (2001). Steps of nuclear pore complex disassembly and reassembly during mitosis in early *Drosophila* embryos. *Journal of Cell Science*, *114*(20), 3607-3618.
- Klonis, N., Xie, S. C., McCaw, J. M., Crespo-Ortiz, M. P., Zaloumis, S. G., Simpson, J. A., & Tilley, L. (2013). Altered temporal response of malaria parasites determines differential sensitivity to artemisinin. *Proc Natl Acad Sci U S A*, *110*(13), 5157-5162. doi:10.1073/pnas.1217452110
- Knowles, R., & Gupta, B. M. D. (1932). A Study of Monkey-Malaria, and Its Experimental Transmission to Man. *The Indian medical gazette*, *67*(6), 301-320.
- Koblentz, B., Schoppmeier, J., Grunow, A., & Lechtreck, K. F. (2003). Centrin deficiency in Chlamydomonas causes defects in basal body replication, segregation and maturation. *J Cell Sci*, *116*(Pt 13), 2635-2646. doi:10.1242/jcs.00497
- Koch, M., & Baum, J. (2016). The mechanics of malaria parasite invasion of the human erythrocyte - towards a reassessment of the host cell contribution. *Cell Microbiol*, *18*(3), 319-329. doi:10.1111/cmi.12557
- Kono, M., Heincke, D., Wilcke, L., Wong, T. W., Bruns, C., Herrmann, S., . . . Gilberger, T. W. (2016). Pellicle formation in the malaria parasite. *J Cell Sci*, *129*(4), 673-680. doi:10.1242/jcs.181230
- Kono, M., Herrmann, S., Loughran, N. B., Cabrera, A., Engelberg, K., Lehmann, C., . . . Gilberger, T. W. (2012). Evolution and architecture of the inner membrane complex in asexual and sexual stages of the malaria parasite. *Mol Biol Evol*, *29*(9), 2113-2132. doi:10.1093/molbev/mss081

- Korochkina, S., Barreau, C., Pradel, G., Jeffery, E., Li, J., Natarajan, R., . . . Vernick, K. D. (2006). A mosquito-specific protein family includes candidate receptors for malaria sporozoite invasion of salivary glands. *Cell Microbiol*, 8(1), 163-175. doi:10.1111/j.1462-5822.2005.00611.x
- Kosh-Naucke, M. (2018). *Identification of novel parasitophorous vacuole proteins in P. falciparum parasites using BioID* Universität Hamburg.
- Kouznetsov, R. L. (1977). Malaria Control by Application of Indoor Spraying of Residual Insecticides in Tropical Africa and Its Impact on Community Health. *Tropical Doctor*, 7(2), 81-91. doi:10.1177/004947557700700216
- Kreidenweiss, A., Hopkins, A. V., & Mordmuller, B. (2013). 2A and the auxin-based degron system facilitate control of protein levels in Plasmodium falciparum. *PLoS One*, 8(11), e78661. doi:10.1371/journal.pone.0078661
- Krugliak, M., Zhang, J., & Ginsburg, H. (2002). Intraerythrocytic Plasmodium falciparum utilizes only a fraction of the amino acids derived from the digestion of host cell cytosol for the biosynthesis of its proteins. *Mol Biochem Parasitol*, 119(2), 249-256.
- Kulzer, S., Gehde, N., & Przyborski, J. M. (2009). Return to sender: use of Plasmodium ER retrieval sequences to study protein transport in the infected erythrocyte and predict putative ER protein families. *Parasitol Res*, 104(6), 1535-1541. doi:10.1007/s00436-009-1397-x
- LaCount, D. J., Schoenfeld, L. W., & Fields, S. (2009). Selection of yeast strains with enhanced expression of Plasmodium falciparum proteins. *Mol Biochem Parasitol*, 163(2), 119-122. doi:10.1016/j.molbiopara.2008.10.003
- LaCount, D. J., Vignali, M., Chettier, R., Phansalkar, A., Bell, R., Hesselberth, J. R., . . . Hughes, R. E. (2005). A protein interaction network of the malaria parasite Plasmodium falciparum. *Nature*, 438(7064), 103-107. doi:10.1038/nature04104
- Lacroix, C., Giovannini, D., Combe, A., Bargieri, D. Y., Späth, S., Panchal, D., . . . Ménard, R. (2011). FLP/FRT-mediated conditional mutagenesis in pre-erythrocytic stages of Plasmodium berghei. *Nature Protocols*, 6(9), 1412-1428. doi:10.1038/nprot.2011.363
- Langsley, G., van Noort, V., Carret, C., Meissner, M., de Villiers, E. P., Bishop, R., & Pain, A. (2008). Comparative genomics of the Rab protein family in Apicomplexan parasites. *Microbes Infect*, 10(5), 462-470. doi:10.1016/j.micinf.2008.01.017
- Laveran, A. (1881). *Nature parasitaire des accidents de l'impaludisme: description d'un nouveau parasite trouvé dans le sang des malades atteints de fièvre palustre*: J.-B. Baillière.
- Lazarus, M. D., Schneider, T. G., & Taraschi, T. F. (2008). A new model for hemoglobin ingestion and transport by the human malaria parasite Plasmodium falciparum. *J Cell Sci*, 121(11), 1937-1949. doi:10.1242/jcs.023150
- Le Bras, J., & Durand, R. (2003). The mechanisms of resistance to antimalarial drugs in Plasmodium falciparum. *Fundam Clin Pharmacol*, 17(2), 147-153. doi:10.1046/j.1472-8206.2003.00164.x
- Le Roch, K. G., Zhou, Y., Blair, P. L., Grainger, M., Moch, J. K., Haynes, J. D., . . . Winzeler, E. A. (2003). Discovery of Gene Function by Expression Profiling of the Malaria Parasite Life Cycle. *Science*, 301(5639), 1503-1508. doi:10.1126/science.1087025
- Lee, M. C., Moura, P. A., Miller, E. A., & Fidock, D. A. (2008). Plasmodium falciparum Sec24 marks transitional ER that exports a model cargo via a diacidic motif. *Mol Microbiol*, 68(6), 1535-1546. doi:10.1111/j.1365-2958.2008.06250.x
- Leirião, P., Rodrigues, C. D., Albuquerque, S. S., & Mota, M. M. (2004). Survival of protozoan intracellular parasites in host cells. *EMBO Rep*, 5(12), 1142-1147. doi:10.1038/sj.embor.7400299
- Li, J., & Zhou, B. (2010). Biological actions of artemisinin: insights from medicinal chemistry studies. *Molecules*, 15(3), 1378-1397. doi:10.3390/molecules15031378
- Liang, J., Choi, J., & Clardy, J. (1999). Refined structure of the FKBP12-rapamycin-FRB ternary complex at 2.2 Å resolution. *Acta Crystallogr D Biol Crystallogr*, 55(Pt 4), 736-744. doi:10.1107/s0907444998014747
- Liehl, P., Zuzarte-Luis, V., Chan, J., Zillinger, T., Baptista, F., Carapau, D., . . . Mota, M. M. (2014). Host-cell sensors for Plasmodium activate innate immunity against liver-stage infection. *Nat Med*, 20(1), 47-53. doi:10.1038/nm.3424

- Lines, J. D., & Nissor, N. S. (1991). DDT resistance in *Anopheles gambiae* declines with mosquito age. *Med Vet Entomol*, *5*(3), 261-265. doi:10.1111/j.1365-2915.1991.tb00550.x
- Luse, S. A., & Miller, L. H. (1971). Plasmodium falciparum malaria. Ultrastructure of parasitized erythrocytes in cardiac vessels. *Am J Trop Med Hyg*, *20*(5), 655-660.
- Lyko, B., Hammershaimb, E. A., Nguitragool, W., Wellems, T. E., & Desai, S. A. (2012). A high-throughput method to detect Plasmodium falciparum clones in limiting dilution microplates. *Malar J*, *11*, 124. doi:10.1186/1475-2875-11-124
- Machado, J. P., Johnson, W. E., Gilbert, M. T. P., Zhang, G., Jarvis, E. D., O'Brien, S. J., & Antunes, A. (2016). Bone-associated gene evolution and the origin of flight in birds. *BMC genomics*, *17*, 371-371. doi:10.1186/s12864-016-2681-7
- MacPherson, G. G., Warrell, M. J., White, N. J., Looareesuwan, S., & Warrell, D. A. (1985). Human cerebral malaria. A quantitative ultrastructural analysis of parasitized erythrocyte sequestration. *Am J Pathol*, *119*(3), 385-401.
- Mahajan, B., Selvapandiyani, A., Gerald, N. J., Majam, V., Zheng, H., Wickramarachchi, T., . . . Kumar, S. (2008). Centrins, cell cycle regulation proteins in human malaria parasite Plasmodium falciparum. *J Biol Chem*, *283*(46), 31871-31883. doi:10.1074/jbc.M800028200
- Mahmoudi, S., & Keshavarz, H. (2018). Malaria Vaccine Development: The Need for Novel Approaches: A Review Article. *Iranian journal of parasitology*, *13*(1), 1-10.
- Maier, A. G., Rug, M., O'Neill, M. T., Brown, M., Chakravorty, S., Szestak, T., . . . Cowman, A. F. (2008). Exported proteins required for virulence and rigidity of Plasmodium falciparum-infected human erythrocytes. *Cell*, *134*(1), 48-61. doi:10.1016/j.cell.2008.04.051
- Makhnevych, T., Lusk, C. P., Anderson, A. M., Aitchison, J. D., & Wozniak, R. W. (2003). Cell cycle regulated transport controlled by alterations in the nuclear pore complex. *Cell*, *115*(7), 813-823. doi:10.1016/s0092-8674(03)00986-3
- Mali, P., Yang, L., Esvelt, K. M., Aach, J., Guell, M., DiCarlo, J. E., . . . Church, G. M. (2013). RNA-guided human genome engineering via Cas9. *Science*, *339*(6121), 823-826. doi:10.1126/science.1232033
- Malleret, B., Claser, C., Ong, A. S., Suwanarusk, R., Sriprawat, K., Howland, S. W., . . . Renia, L. (2011). A rapid and robust tri-color flow cytometry assay for monitoring malaria parasite development. *Sci Rep*, *1*, 118. doi:10.1038/srep00118
- Mantel, P. Y., Hoang, A. N., Goldowitz, I., Potashnikova, D., Hamza, B., Vorobjev, I., . . . Marti, M. (2013). Malaria-infected erythrocyte-derived microvesicles mediate cellular communication within the parasite population and with the host immune system. *Cell Host Microbe*, *13*(5), 521-534. doi:10.1016/j.chom.2013.04.009
- Marat, A. L., & Haucke, V. (2016). Phosphatidylinositol 3-phosphates-at the interface between cell signalling and membrane traffic. *EMBO J*, *35*(6), 561-579. doi:10.15252/embj.201593564
- Marti, M., Good, R. T., Rug, M., Knuepfer, E., & Cowman, A. F. (2004). Targeting malaria virulence and remodeling proteins to the host erythrocyte. *Science*, *306*(5703), 1930-1933. doi:10.1126/science.1102452
- Matthews, H., Duffy, C. W., & Merrick, C. J. (2018). Checks and balances? DNA replication and the cell cycle in Plasmodium. *Parasites & Vectors*, *11*(1), 216. doi:10.1186/s13071-018-2800-1
- McFadden, G. I., Reith, M. E., Munholland, J., & Lang-Unnasch, N. (1996). Plastid in human parasites. *Nature*, *381*(6582), 482. doi:10.1038/381482a0
- McFadden, G. I., & Roos, D. S. (1999). Apicomplexan plastids as drug targets. *Trends Microbiol*, *7*(8), 328-333. doi:10.1016/s0966-842x(99)01547-4
- McKeage, K., & Scott, L. (2003). Atovaquone/proguanil: a review of its use for the prophylaxis of Plasmodium falciparum malaria. *Drugs*, *63*(6), 597-623. doi:10.2165/00003495-200363060-00006
- McLauchlan, H., Newell, J., Morrice, N., Osborne, A., West, M., & Smythe, E. (1998). A novel role for Rab5-GDI in ligand sequestration into clathrin-coated pits. *Curr Biol*, *8*(1), 34-45. doi:10.1016/s0960-9822(98)70018-1
- McNamara, C. W., Lee, M. C., Lim, C. S., Lim, S. H., Roland, J., Simon, O., . . . Winzeler, E. A. (2013). Targeting Plasmodium PI(4)K to eliminate malaria. *Nature*, *504*(7479), 248-253. doi:10.1038/nature12782

- Meissner, M., Krejany, E., Gilson, P. R., de Koning-Ward, T. F., Soldati, D., & Crabb, B. S. (2005). Tetracycline analogue-regulated transgene expression in *Plasmodium falciparum* blood stages using *Toxoplasma gondii* transactivators. *Proc Natl Acad Sci U S A*, *102*(8), 2980-2985. doi:10.1073/pnas.0500112102
- Meister, S., Plouffe, D. M., Kuhen, K. L., Bonamy, G. M., Wu, T., Barnes, S. W., . . . Winzeler, E. A. (2011). Imaging of *Plasmodium* liver stages to drive next-generation antimalarial drug discovery. *Science*, *334*(6061), 1372-1377. doi:10.1126/science.1211936
- Mendis, K., Sina, B. J., Marchesini, P., & Carter, R. (2001). The neglected burden of *Plasmodium vivax* malaria. *Am J Trop Med Hyg*, *64*(1-2 Suppl), 97-106.
- Merckx, A., Le Roch, K., Nivez, M. P., Dorin, D., Alano, P., Gutierrez, G. J., . . . Doerig, C. (2003). Identification and initial characterization of three novel cyclin-related proteins of the human malaria parasite *Plasmodium falciparum*. *J Biol Chem*, *278*(41), 39839-39850. doi:10.1074/jbc.M301625200
- Mesén-Ramírez, P., Bergmann, B., Tran, T. T., Garten, M., Stäcker, J., Naranjo-Prado, I., . . . Spielmann, T. (2019). EXP1 is critical for nutrient uptake across the parasitophorous vacuole membrane of malaria parasites. *PLOS Biology*, *17*(9), e3000473. doi:10.1371/journal.pbio.3000473
- Meshnick, S. R., Thomas, A., Ranz, A., Xu, C. M., & Pan, H. Z. (1991). Artemisinin (qinghaosu): the role of intracellular hemin in its mechanism of antimalarial action. *Mol Biochem Parasitol*, *49*(2), 181-189.
- Meshnick, S. R., Tsang, T. W., Lin, F. B., Pan, H. Z., Chang, C. N., Kuypers, F., . . . Lubin, B. (1989). Activated oxygen mediates the antimalarial activity of qinghaosu. *Prog Clin Biol Res*, *313*, 95-104.
- Meshnick, S. R., Yang, Y. Z., Lima, V., Kuypers, F., Kamchonwongpaisan, S., & Yuthavong, Y. (1993). Iron-dependent free radical generation from the antimalarial agent artemisinin (qinghaosu). *Antimicrob Agents Chemother*, *37*(5), 1108-1114. doi:10.1128/aac.37.5.1108
- Meunier, B., & Robert, A. (2010). Heme as trigger and target for trioxane-containing antimalarial drugs. *Acc Chem Res*, *43*(11), 1444-1451. doi:10.1021/ar100070k
- Milani, K. J., Schneider, T. G., & Taraschi, T. F. (2015). Defining the morphology and mechanism of the hemoglobin transport pathway in *Plasmodium falciparum*-infected erythrocytes. *Eukaryot Cell*, *14*(4), 415-426. doi:10.1128/EC.00267-14
- Miller, J. L., Sack, B. K., Baldwin, M., Vaughan, A. M., & Kappe, S. H. I. (2014). Interferon-mediated innate immune responses against malaria parasite liver stages. *Cell Rep*, *7*(2), 436-447. doi:10.1016/j.celrep.2014.03.018
- Miller, L. H., Ackerman, H. C., Su, X. Z., & Wellems, T. E. (2013). Malaria biology and disease pathogenesis: insights for new treatments. *Nat Med*, *19*(2), 156-167. doi:10.1038/nm.3073
- Miller, L. H., Mason, S. J., Clyde, D. F., & McGinniss, M. H. (1976). The resistance factor to *Plasmodium vivax* in blacks. The Duffy-blood-group genotype, FyFy. *N Engl J Med*, *295*(6), 302-304. doi:10.1056/nejm197608052950602
- Miller, L. H., Mason, S. J., Dvorak, J. A., McGinniss, M. H., & Rothman, I. K. (1975). Erythrocyte receptors for (*Plasmodium knowlesi*) malaria: Duffy blood group determinants. *Science*, *189*(4202), 561-563. doi:10.1126/science.1145213
- Mitchison, T. J., & Salmon, E. D. (2001). Mitosis: a history of division. *Nat Cell Biol*, *3*(1), E17-21. doi:10.1038/35050656
- Muller, I. B., & Hyde, J. E. (2010). Antimalarial drugs: modes of action and mechanisms of parasite resistance. *Future Microbiol*, *5*(12), 1857-1873. doi:10.2217/fmb.10.136
- Mundwiler-Pachlatko, E., & Beck, H. P. (2013). Maurer's clefts, the enigma of *Plasmodium falciparum*. *Proc Natl Acad Sci U S A*, *110*(50), 19987-19994. doi:10.1073/pnas.1309247110
- Munro, S., & Nichols, B. J. (1999). The GRIP domain - a novel Golgi-targeting domain found in several coiled-coil proteins. *Curr Biol*, *9*(7), 377-380. doi:10.1016/s0960-9822(99)80166-3
- Muralidharan, V., Oksman, A., Iwamoto, M., Wandless, T. J., & Goldberg, D. E. (2011). Asparagine repeat function in a *Plasmodium falciparum* protein assessed via a regulatable fluorescent affinity tag. *Proc Natl Acad Sci U S A*, *108*(11), 4411-4416. doi:10.1073/pnas.1018449108
- Murzin, A. G. (1998). How far divergent evolution goes in proteins. *Curr Opin Struct Biol*, *8*(3), 380-387. doi:10.1016/s0959-440x(98)80073-0

- Nabarro, D. (1999). Roll Back Malaria. *Parassitologia*, 41(1-3), 501-504.
- Nagano, M., Toshima, J. Y., & Toshima, J. (2015). [Rab GTPases networks in membrane traffic in *Saccharomyces cerevisiae*]. *Yakugaku Zasshi*, 135(3), 483-492. doi:10.1248/yakushi.14-00246
- Neghina, R., Neghina, A. M., Marincu, I., & Iacobiciu, I. (2010). Malaria, a journey in time: in search of the lost myths and forgotten stories. *Am J Med Sci*, 340(6), 492-498. doi:10.1097/MAJ.0b013e3181e7fe6c
- Netz, D. J., Pierik, A. J., Stumpfig, M., Bill, E., Sharma, A. K., Pallesen, L. J., . . . Lill, R. (2012). A bridging [4Fe-4S] cluster and nucleotide binding are essential for function of the Cfd1-Nbp35 complex as a scaffold in iron-sulfur protein maturation. *J Biol Chem*, 287(15), 12365-12378. doi:10.1074/jbc.M111.328914
- Netz, D. J., Pierik, A. J., Stumpfig, M., Muhlenhoff, U., & Lill, R. (2007). The Cfd1-Nbp35 complex acts as a scaffold for iron-sulfur protein assembly in the yeast cytosol. *Nat Chem Biol*, 3(5), 278-286. doi:10.1038/nchembio872
- Nicholls, A. (2012). Fenland ague in the nineteenth century. *Medical History*, 44(4), 513-530. doi:10.1017/S0025727300067107
- Nielsen, E., Christoforidis, S., Uttenweiler-Joseph, S., Miaczynska, M., Dewitte, F., Wilm, M., . . . Zerial, M. (2000). Rabenosyn-5, a novel Rab5 effector, is complexed with hVPS45 and recruited to endosomes through a FYVE finger domain. *J Cell Biol*, 151(3), 601-612. doi:10.1083/jcb.151.3.601
- Niles, J. C., Derisi, J. L., & Marletta, M. A. (2009). Inhibiting *Plasmodium falciparum* growth and heme detoxification pathway using heme-binding DNA aptamers. *Proc Natl Acad Sci U S A*, 106(32), 13266-13271. doi:10.1073/pnas.0906370106
- Nobel-Media. (2015). The Nobel Prize in Physiology or Medicine 2015 Retrieved from <https://www.nobelprize.org/prizes/medicine/2015/press-release/>
- Nosten, F., & Brasseur, P. (2002). Combination therapy for malaria: the way forward? *Drugs*, 62(9), 1315-1329. doi:10.2165/00003495-200262090-00003
- Nussenzweig, R. S., Vanderberg, J., Most, H., & Orton, C. (1967). Protective immunity produced by the injection of x-irradiated sporozoites of *Plasmodium berghei*. *Nature*, 216(5111), 160-162. doi:10.1038/216160a0
- Nussenzweig, R. S., Vanderberg, J. P., Most, H., & Orton, C. (1969). Specificity of protective immunity produced by x-irradiated *Plasmodium berghei* sporozoites. *Nature*, 222(5192), 488-489. doi:10.1038/222488a0
- O'Donnell, R. A., Saul, A., Cowman, A. F., & Crabb, B. S. (2000). Functional conservation of the malaria vaccine antigen MSP-119 across distantly related *Plasmodium* species. *Nat Med*, 6(1), 91-95. doi:10.1038/71595
- O'Neill, P. M., & Posner, G. H. (2004). A medicinal chemistry perspective on artemisinin and related endoperoxides. *J Med Chem*, 47(12), 2945-2964. doi:10.1021/jm030571c
- Oberli, A., Slater, L. M., Cutts, E., Brand, F., Mundwiler-Pachlatko, E., Rusch, S., . . . Vakonakis, I. (2014). A *Plasmodium falciparum* PHIST protein binds the virulence factor PfEMP1 and comigrates to knobs on the host cell surface. *FASEB J*, 28(10), 4420-4433. doi:10.1096/fj.14-256057
- Oehring, S. C., Woodcroft, B. J., Moes, S., Wetzel, J., Dietz, O., Pulfer, A., . . . Voss, T. S. (2012). Organellar proteomics reveals hundreds of novel nuclear proteins in the malaria parasite *Plasmodium falciparum*. *Genome Biol*, 13(11), R108. doi:10.1186/gb-2012-13-11-r108
- Ogutu, B. R., Apollo, O. J., McKinney, D., Okoth, W., Siangla, J., Dubovsky, F., . . . for the, M. S. P. M. V. W. G. (2009). Blood Stage Malaria Vaccine Eliciting High Antigen-Specific Antibody Concentrations Confers No Protection to Young Children in Western Kenya. *PLOS ONE*, 4(3), e4708. doi:10.1371/journal.pone.0004708
- Ohta, S., Bukowski-Wills, J. C., Wood, L., de Lima Alves, F., Chen, Z., Rappsilber, J., & Earnshaw, W. C. (2010). Proteomics of isolated mitotic chromosomes identifies the kinetochore protein Ska3/RamA1. *Cold Spring Harb Symp Quant Biol*, 75, 433-438. doi:10.1101/sqb.2010.75.022
- Olotu, A., Fegan, G., Wambua, J., Nyangweso, G., Awuondo, K. O., Leach, A., . . . Bejon, P. (2013). Four-year efficacy of RTS,S/AS01E and its interaction with malaria exposure. *N Engl J Med*, 368(12), 1111-1120. doi:10.1056/NEJMoal207564

- Olotu, A., Fegan, G., Wambua, J., Nyangweso, G., Leach, A., Lievens, M., . . . Bejon, P. (2016). Seven-Year Efficacy of RTS,S/AS01 Malaria Vaccine among Young African Children. *N Engl J Med*, 374(26), 2519-2529. doi:10.1056/NEJMoa1515257
- Ouattara, A., & Laurens, M. B. (2015). Vaccines against malaria. *Clin Infect Dis*, 60(6), 930-936. doi:10.1093/cid/ciu954
- Pagni, M., Ioannidis, V., Cerutti, L., Zahn-Zabal, M., Jongeneel, C. V., & Falquet, L. (2004). MyHits: a new interactive resource for protein annotation and domain identification. *Nucleic Acids Res*, 32(Web Server issue), W332-W335. doi:10.1093/nar/gkh479
- Payne, D. (1987). Spread of chloroquine resistance in *Plasmodium falciparum*. *Parasitol Today*, 3(8), 241-246.
- Pehrson, C., Salanti, A., Theander, T. G., & Nielsen, M. A. (2017). Pre-clinical and clinical development of the first placental malaria vaccine. *Expert Review of Vaccines*, 16(6), 613-624. doi:10.1080/14760584.2017.1322512
- Pfeffer, S. R. (1992). GTP-binding proteins in intracellular transport. *Trends Cell Biol*, 2(2), 41-46. doi:10.1016/0962-8924(92)90161-f
- Philip, N., & Waters, A. P. (2015). Conditional Degradation of *Plasmodium* Calcineurin Reveals Functions in Parasite Colonization of both Host and Vector. *Cell Host Microbe*, 18(1), 122-131. doi:10.1016/j.chom.2015.05.018
- Pines, J., & Rieder, C. L. (2001). Re-staging mitosis: a contemporary view of mitotic progression. *Nat Cell Biol*, 3(1), E3-6. doi:10.1038/35050676
- Pino, P., Sebastian, S., Kim, E. A., Bush, E., Brochet, M., Volkmann, K., . . . Soldati-Favre, D. (2012). A tetracycline-repressible transactivator system to study essential genes in malaria parasites. *Cell host & microbe*, 12(6), 824-834. doi:10.1016/j.chom.2012.10.016
- Pinzon-Ortiz, C., Friedman, J., Esko, J., & Sinnis, P. (2001). The binding of the circumsporozoite protein to cell surface heparan sulfate proteoglycans is required for *Plasmodium* sporozoite attachment to target cells. *J Biol Chem*, 276(29), 26784-26791. doi:10.1074/jbc.M104038200
- Pongvongsa, T., Culleton, R., Ha, H., Thanh, L., Phongmany, P., Marchand, R. P., . . . Maeno, Y. (2018). Human infection with *Plasmodium knowlesi* on the Laos-Vietnam border. *Tropical Medicine and Health*, 46(1), 33. doi:10.1186/s41182-018-0116-7
- Posner, G. H., & Oh, C. H. (1992). Regiospecifically oxygen-18 labeled 1,2,4-trioxane: a simple chemical model system to probe the mechanism(s) for the antimalarial activity of artemisinin (qinghaosu). *Journal of the American Chemical Society*, 114(21), 8328-8329. doi:10.1021/ja00047a076
- Pradel, G. (2007). Proteins of the malaria parasite sexual stages: expression, function and potential for transmission blocking strategies. *Parasitology*, 134(Pt.14), 1911-1929. doi:10.1017/s0031182007003381
- Prensier, G., & Slomianny, C. (1986). The karyotype of *Plasmodium falciparum* determined by ultrastructural serial sectioning and 3D reconstruction. *J Parasitol*, 72(5), 731-736.
- Prommana, P., Uthapibull, C., Wongsombat, C., Kamchonwongpaisan, S., Yuthavong, Y., Knuepfer, E., . . . Shaw, P. J. (2013). Inducible knockdown of *Plasmodium* gene expression using the glmS ribozyme. *PLOS ONE*, 8(8), e73783. doi:10.1371/journal.pone.0073783
- Prudêncio, M., Rodriguez, A., & Mota, M. M. (2006). The silent path to thousands of merozoites: the *Plasmodium* liver stage. *Nature Reviews Microbiology*, 4, 849. doi:10.1038/nrmicro1529
- Pulcini, S., Staines, H. M., Lee, A. H., Shafik, S. H., Bouyer, G., Moore, C. M., . . . Krishna, S. (2015). Mutations in the *Plasmodium falciparum* chloroquine resistance transporter, PfCRT, enlarge the parasite's food vacuole and alter drug sensitivities. *Sci Rep*, 5, 14552. doi:10.1038/srep14552
- Quevillon, E., Spielmann, T., Brahimi, K., Chattopadhyay, D., Yeramian, E., & Langsley, G. (2003). The *Plasmodium falciparum* family of Rab GTPases. *Gene*, 306, 13-25. doi:10.1016/s0378-1119(03)00381-0
- Raaijmakers, J. A., Tanenbaum, M. E., Maia, A. F., & Medema, R. H. (2009). RAMA1 is a novel kinetochore protein involved in kinetochore-microtubule attachment. *J Cell Sci*, 122(Pt 14), 2436-2445. doi:10.1242/jcs.051912
- Rabinowitz, M. (1941). Studies on the cytology and early embryology of the egg of *Drosophila melanogaster*. *Journal of Morphology*, 69(1), 1-49. doi:10.1002/jmor.1050690102

- Rahajeng, J., Caplan, S., & Naslavsky, N. (2010). Common and distinct roles for the binding partners Rabenosyn-5 and Vps45 in the regulation of endocytic trafficking in mammalian cells. *Experimental cell research*, *316*(5), 859-874. doi:10.1016/j.yexcr.2009.11.007
- Ralph, S. A., van Dooren, G. G., Waller, R. F., Crawford, M. J., Fraunholz, M. J., Foth, B. J., . . . McFadden, G. I. (2004). Tropical infectious diseases: metabolic maps and functions of the *Plasmodium falciparum* apicoplast. *Nat Rev Microbiol*, *2*(3), 203-216. doi:10.1038/nrmicro843
- Rastogi, R., Verma, J. K., Kapoor, A., Langsley, G., & Mukhopadhyay, A. (2016). Rab5 Isoforms Specifically Regulate Different Modes of Endocytosis in *Leishmania*. *The Journal of biological chemistry*, *291*(28), 14732-14746. doi:10.1074/jbc.M116.716514
- Read, M., Sherwin, T., Holloway, S. P., Gull, K., & Hyde, J. E. (1993). Microtubular organization visualized by immunofluorescence microscopy during erythrocytic schizogony in *Plasmodium falciparum* and investigation of post-translational modifications of parasite tubulin. *Parasitology*, *106* (Pt 3), 223-232. doi:10.1017/s0031182000075041
- Regev-Rudzki, N., Wilson, D. W., Carvalho, T. G., Sisquella, X., Coleman, B. M., Rug, M., . . . Cowman, A. F. (2013). Cell-cell communication between malaria-infected red blood cells via exosome-like vesicles. *Cell*, *153*(5), 1120-1133. doi:10.1016/j.cell.2013.04.029
- Retief, F., & Cilliers, L. (2006). Periodic pyrexia and malaria in antiquity. *S Afr Med J*, *96*(8), 684, 686-688.
- Risco-Castillo, V., Topcu, S., Marinach, C., Manzoni, G., Bigorgne, A. E., Briquet, S., . . . Silvie, O. (2015). Malaria Sporozoites Traverse Host Cells within Transient Vacuoles. *Cell Host Microbe*, *18*(5), 593-603. doi:10.1016/j.chom.2015.10.006
- Roberts, A. D., Nair, S. C., Guerra, A. J., & Prigge, S. T. (2019). Development of a conditional localization approach to control apicoplast protein trafficking in malaria parasites. *Traffic*, *20*(8), 571-582. doi:10.1111/tra.12656
- Robinson, M. S., Sahlender, D. A., & Foster, S. D. (2010). Rapid inactivation of proteins by rapamycin-induced rerouting to mitochondria. *Dev Cell*, *18*(2), 324-331. doi:10.1016/j.devcel.2009.12.015
- Robson, K. J., Frevert, U., Reckmann, I., Cowan, G., Beier, J., Scragg, I. G., . . . et al. (1995). Thrombospondin-related adhesive protein (TRAP) of *Plasmodium falciparum*: expression during sporozoite ontogeny and binding to human hepatocytes. *EMBO J*, *14*(16), 3883-3894.
- Roland, J., Soulard, V., Sellier, C., Drapier, A. M., Di Santo, J. P., Cazenave, P. A., & Pied, S. (2006). NK cell responses to *Plasmodium* infection and control of intrahepatic parasite development. *J Immunol*, *177*(2), 1229-1239. doi:10.4049/jimmunol.177.2.1229
- Roques, M., Wall, R. J., Douglass, A. P., Ramaprasad, A., Ferguson, D. J., Kaindama, M. L., . . . Tewari, R. (2015). *Plasmodium* P-Type Cyclin CYC3 Modulates Endomitotic Growth during Oocyst Development in Mosquitoes. *PLoS Pathog*, *11*(11), e1005273. doi:10.1371/journal.ppat.1005273
- Rosano, G. L., & Ceccarelli, E. A. (2014). Recombinant protein expression in *Escherichia coli*: advances and challenges. *Frontiers in microbiology*, *5*, 172-172. doi:10.3389/fmicb.2014.00172
- Rosenberg, R., & Rungsiwongse, J. (1991). The number of sporozoites produced by individual malaria oocysts. *Am J Trop Med Hyg*, *45*(5), 574-577. doi:10.4269/ajtmh.1991.45.574
- Rosenfeld, J. L., Moore, R. H., Zimmer, K. P., Alpizar-Foster, E., Dai, W., Zarka, M. N., & Knoll, B. J. (2001). Lysosome proteins are redistributed during expression of a GTP-hydrolysis-defective rab5a. *J Cell Sci*, *114*(Pt 24), 4499-4508.
- Ross, R. (2002). The role of the mosquito in the evolution of the malarial parasite: the recent researches of Surgeon-Major Ronald Ross, I.M.S. 1898. *The Yale journal of biology and medicine*, *75*(2), 103-105.
- RTS, S. C. T. P. (2015). Efficacy and safety of RTS,S/AS01 malaria vaccine with or without a booster dose in infants and children in Africa: final results of a phase 3, individually randomised, controlled trial. *The Lancet*, *386*(9988), 31-45. doi:https://doi.org/10.1016/S0140-6736(15)60721-8
- Rudzinska, M. A., & Trager, W. (1958). [The mechanism of feeding of *Plasmodium* malariae; electron-microscopic studies]. *Wiad Parazytol*, *4*(5-6), 617-618; English transl 618-619.

- Russell, P. F. (1968). The United States and malaria: debits and credits. *Bulletin of the New York Academy of Medicine*, 44(6), 623-653.
- Sabharanjak, S., Sharma, P., Parton, R. G., & Mayor, S. (2002). GPI-anchored proteins are delivered to recycling endosomes via a distinct cdc42-regulated, clathrin-independent pinocytotic pathway. *Dev Cell*, 2(4), 411-423. doi:10.1016/s1534-5807(02)00145-4
- Sachs, J., & Malaney, P. (2002). The economic and social burden of malaria. *Nature*, 415(6872), 680-685. doi:10.1038/415680a
- Sagara, I., Dicko, A., Ellis, R. D., Fay, M. P., Diawara, S. I., Assadou, M. H., . . . Saul, A. (2009). A randomized controlled phase 2 trial of the blood stage AMA1-C1/Alhydrogel malaria vaccine in children in Mali. *Vaccine*, 27(23), 3090-3098. doi:10.1016/j.vaccine.2009.03.014
- Salisbury, J. L., Suino, K. M., Busby, R., & Springett, M. (2002). Centrin-2 is required for centriole duplication in mammalian cells. *Curr Biol*, 12(15), 1287-1292. doi:10.1016/s0960-9822(02)01019-9
- Sallares, R. (2009). *Malaria and Rome : a history of malaria in ancient Italy*. Oxford: Oxford Univ. Press.
- Salminen, A., & Novick, P. J. (1987). A ras-like protein is required for a post-Golgi event in yeast secretion. *Cell*, 49(4), 527-538. doi:https://doi.org/10.1016/0092-8674(87)90455-7
- Sampson, F. B. (1981). Synchronous versus Asynchronous Mitosis within Permanent Pollen Tetrads of the Winteraceae. *Grana*, 20(1), 19-23. doi:10.1080/00173138109436732
- Sanders, M. A., & Salisbury, J. L. (1994). Centrin plays an essential role in microtubule severing during flagellar excision in *Chlamydomonas reinhardtii*. *J Cell Biol*, 124(5), 795-805. doi:10.1083/jcb.124.5.795
- Satori, C. P., Henderson, M. M., Krautkramer, E. A., Kostal, V., Distefano, M. D., & Arriaga, E. A. (2013). Bioanalysis of eukaryotic organelles. *Chemical reviews*, 113(4), 2733-2811. doi:10.1021/cr300354g
- Sauer, B. (1987). Functional expression of the cre-lox site-specific recombination system in the yeast *Saccharomyces cerevisiae*. *Molecular and Cellular Biology*, 7(6), 2087-2096. doi:10.1128/mcb.7.6.2087
- Schlagenhauf, P. (2004). Malaria: from prehistory to present. *Infect Dis Clin North Am*, 18(2), 189-205, table of contents. doi:10.1016/j.idc.2004.01.002
- Schmid, E. M., & McMahon, H. T. (2007). Integrating molecular and network biology to decode endocytosis. *Nature*, 448(7156), 883-888. doi:10.1038/nature06031
- Schmitt, H. D., Wagner, P., Pfaff, E., & Gallwitz, D. (1986). The ras-related YPT1 gene product in yeast: a GTP-binding protein that might be involved in microtubule organization. *Cell*, 47(3), 401-412. doi:10.1016/0092-8674(86)90597-0
- Schrevel, J., Asfaux-Foucher, G., & Bafort, J. M. (1977). [Ultrastructural study of multiple mitoses during sporogony of *Plasmodium b. berghei*]. *J Ultrastruct Res*, 59(3), 332-350. doi:10.1016/s0022-5320(77)90043-0
- Seeber, F., & Soldati-Favre, D. (2010). Metabolic pathways in the apicoplast of apicomplexa. *Int Rev Cell Mol Biol*, 281, 161-228. doi:10.1016/S1937-6448(10)81005-6
- Sekar, R. B., & Periasamy, A. (2003). Fluorescence resonance energy transfer (FRET) microscopy imaging of live cell protein localizations. *The Journal of cell biology*, 160(5), 629-633. doi:10.1083/jcb.200210140
- Sérandour, J., Girel, J., Boyer, S., Ravanel, P., Lemperière, G., & Raveton, M. (2007). How human practices have affected vector-borne diseases in the past: a study of malaria transmission in Alpine valleys. *Malaria journal*, 6, 115-115. doi:10.1186/1475-2875-6-115
- Sherman, I. W. (1998). *Malaria: Parasite Biology, Pathogenesis, and Protection*: ASM Press.
- Sibley, C. H., Brophy, V. H., Cheesman, S., Hamilton, K. L., Hankins, E. G., Wooden, J. M., & Kilbey, B. (1997). Yeast as a model system to study drugs effective against apicomplexan proteins. *Methods*, 13(2), 190-207. doi:10.1006/meth.1997.0511
- Sijwali, P. S., & Rosenthal, P. J. (2004). Gene disruption confirms a critical role for the cysteine protease falcipain-2 in hemoglobin hydrolysis by *Plasmodium falciparum*. *Proc Natl Acad Sci U S A*, 101(13), 4384-4389. doi:10.1073/pnas.0307720101

- Silvie, O., Rubinstein, E., Franetich, J. F., Prenant, M., Belnoue, E., Renia, L., . . . Mazier, D. (2003). Hepatocyte CD81 is required for *Plasmodium falciparum* and *Plasmodium yoelii* sporozoite infectivity. *Nat Med*, *9*(1), 93-96. doi:10.1038/nm808
- Simon, N., Scholz, S. M., Moreira, C. K., Templeton, T. J., Kuehn, A., Dude, M.-A., & Pradel, G. (2009). Sexual stage adhesion proteins form multi-protein complexes in the malaria parasite *Plasmodium falciparum*. *The Journal of biological chemistry*, *284*(21), 14537-14546. doi:10.1074/jbc.M808472200
- Sinden, R. E. (2009). Malaria, sexual development and transmission: retrospect and prospect. *Parasitology*, *136*(12), 1427-1434. doi:10.1017/S0031182009990667
- Sinden, R. E. (2015). The cell biology of malaria infection of mosquito: advances and opportunities. *Cellular Microbiology*, *17*(4), 451-466. doi:10.1111/cmi.12413
- Sinden, R. E., Butcher, G. A., Billker, O., & Fleck, S. L. (1996). Regulation of infectivity of *Plasmodium* to the mosquito vector. *Adv Parasitol*, *38*, 53-117. doi:10.1016/s0065-308x(08)60033-0
- Sinden, R. E., Hartley, R. H., & Winger, L. (1985). The development of *Plasmodium* ookinetes in vitro: an ultrastructural study including a description of meiotic division. *Parasitology*, *91* (Pt 2), 227-244. doi:10.1017/s0031182000057334
- Singer, M., Marshall, J., Heiss, K., Mair, G. R., Grimm, D., Mueller, A. K., & Frischknecht, F. (2015). Zinc finger nuclease-based double-strand breaks attenuate malaria parasites and reveal rare microhomology-mediated end joining. *Genome Biol*, *16*, 249. doi:10.1186/s13059-015-0811-1
- Singh, B., & Daneshvar, C. (2013). Human infections and detection of *Plasmodium knowlesi*. *Clin Microbiol Rev*, *26*(2), 165-184. doi:10.1128/CMR.00079-12
- Singh, B., Kim Sung, L., Matusop, A., Radhakrishnan, A., Shamsul, S. S., Cox-Singh, J., . . . Conway, D. J. (2004). A large focus of naturally acquired *Plasmodium knowlesi* infections in human beings. *Lancet*, *363*(9414), 1017-1024. doi:10.1016/S0140-6736(04)15836-4
- Sinha, A., Hughes, K. R., Modrzynska, K. K., Otto, T. D., Pfander, C., Dickens, N. J., . . . Waters, A. P. (2014). A cascade of DNA-binding proteins for sexual commitment and development in *Plasmodium*. *Nature*, *507*(7491), 253-257. doi:10.1038/nature12970
- Sinka, M. E., Bangs, M. J., Manguin, S., Chareonviriyaphap, T., Patil, A. P., Temperley, W. H., . . . Hay, S. I. (2011). The dominant *Anopheles* vectors of human malaria in the Asia-Pacific region: occurrence data, distribution maps and bionomic precis. *Parasit Vectors*, *4*, 89. doi:10.1186/1756-3305-4-89
- Sinka, M. E., Bangs, M. J., Manguin, S., Coetzee, M., Mbogo, C. M., Hemingway, J., . . . Hay, S. I. (2010). The dominant *Anopheles* vectors of human malaria in Africa, Europe and the Middle East: occurrence data, distribution maps and bionomic precis. *Parasit Vectors*, *3*, 117. doi:10.1186/1756-3305-3-117
- Sinnis, P., & Nardin, E. (2002). Sporozoite antigens: biology and immunology of the circumsporozoite protein and thrombospondin-related anonymous protein. *Chem Immunol*, *80*, 70-96. doi:10.1159/000058840
- Sinton, J. A., & Mulligan, H. W. (1932). A Critical Review of the Literature relating to the Identification of the Malarial Parasites recorded from Monkeys of the Families Cercopithecidae and Colobidae. *Records of the Malaria Survey of India*, *3*(2), 357-380 pp.
- Smythe, W. A., Joiner, K. A., & Hoppe, H. C. (2008). Actin is required for endocytic trafficking in the malaria parasite *Plasmodium falciparum*. *Cell Microbiol*, *10*(2), 452-464. doi:10.1111/j.1462-5822.2007.01058.x
- Snow, R. W., Guerra, C. A., Noor, A. M., Myint, H. Y., & Hay, S. I. (2005). The global distribution of clinical episodes of *Plasmodium falciparum* malaria. *Nature*, *434*(7030), 214-217. doi:10.1038/nature03342
- Snowden, F. M. (2006). *The Conquest of Malaria Italy, 1900-1962*: Yale University Press.
- Sommer, M. S., Gould, S. B., Lehmann, P., Gruber, A., Przyborski, J. M., & Maier, U. G. (2007). Der1-mediated preprotein import into the periplastid compartment of chromalveolates? *Mol Biol Evol*, *24*(4), 918-928. doi:10.1093/molbev/msm008

- Spielmann, T., & Gilberger, T. W. (2010). Protein export in malaria parasites: do multiple export motifs add up to multiple export pathways? *Trends Parasitol*, 26(1), 6-10. doi:10.1016/j.pt.2009.10.001
- Spielmann, T., Hawthorne, P. L., Dixon, M. W., Hannemann, M., Klotz, K., Kemp, D. J., . . . Gardiner, D. L. (2006). A cluster of ring stage-specific genes linked to a locus implicated in cytoadherence in *Plasmodium falciparum* codes for PEXEL-negative and PEXEL-positive proteins exported into the host cell. *Mol Biol Cell*, 17(8), 3613-3624. doi:10.1091/mbc.e06-04-0291
- Spork, S., Hiss, J. A., Mandel, K., Sommer, M., Kooij, T. W., Chu, T., . . . Przyborski, J. M. (2009). An unusual ERAD-like complex is targeted to the apicoplast of *Plasmodium falciparum*. *Eukaryot Cell*, 8(8), 1134-1145. doi:10.1128/ec.00083-09
- Srinivasan, P., Beatty, W. L., Diouf, A., Herrera, R., Ambroggio, X., Moch, J. K., . . . Miller, L. H. (2011). Binding of *Plasmodium* merozoite proteins RON2 and AMA1 triggers commitment to invasion. *Proc Natl Acad Sci U S A*, 108(32), 13275-13280. doi:10.1073/pnas.1110303108
- Staines, H. M., Alkhalil, A., Allen, R. J., De Jonge, H. R., Derbyshire, E., Egee, S., . . . Desai, S. A. (2007). Electrophysiological studies of malaria parasite-infected erythrocytes: current status. *Int J Parasitol*, 37(5), 475-482. doi:10.1016/j.ijpara.2006.12.013
- Staines, H. M., Ashmore, S., Felgate, H., Moore, J., Powell, T., & Ellory, J. C. (2006). Solute transport via the new permeability pathways in *Plasmodium falciparum*-infected human red blood cells is not consistent with a simple single-channel model. *Blood*, 108(9), 3187-3194. doi:10.1182/blood-2006-02-001693
- Stenmark, H. (2009). Rab GTPases as coordinators of vesicle traffic. *Nat Rev Mol Cell Biol*, 10(8), 513-525. doi:10.1038/nrm2728
- Stenmark, H., & Olkkonen, V. M. (2001). The Rab GTPase family. *Genome Biol*, 2(5), Reviews3007. doi:10.1186/gb-2001-2-5-reviews3007
- Stenmark, H., Parton, R. G., Steele-Mortimer, O., Lutcke, A., Gruenberg, J., & Zerial, M. (1994a). Inhibition of rab5 GTPase activity stimulates membrane fusion in endocytosis. *EMBO J*, 13(6), 1287-1296.
- Stenmark, H., Parton, R. G., Steele-Mortimer, O., Lütcke, A., Gruenberg, J., & Zerial, M. (1994b). Inhibition of rab5 GTPase activity stimulates membrane fusion in endocytosis. *The EMBO journal*, 13(6), 1287-1296.
- Straimer, J., Lee, M. C., Lee, A. H., Zeitler, B., Williams, A. E., Pearl, J. R., . . . Fidock, D. A. (2012). Site-specific genome editing in *Plasmodium falciparum* using engineered zinc-finger nucleases. *Nat Methods*, 9(10), 993-998. doi:10.1038/nmeth.2143
- Struck, N. S., de Souza Dias, S., Langer, C., Marti, M., Pearce, J. A., Cowman, A. F., & Gilberger, T. W. (2005). Re-defining the Golgi complex in *Plasmodium falciparum* using the novel Golgi marker PfGRASP. *J Cell Sci*, 118(Pt 23), 5603-5613. doi:10.1242/jcs.02673
- Struck, N. S., Herrmann, S., Langer, C., Krueger, A., Foth, B. J., Engelberg, K., . . . Gilberger, T. W. (2008a). *Plasmodium falciparum* possesses two GRASP proteins that are differentially targeted to the Golgi complex via a higher- and lower-eukaryote-like mechanism. *J Cell Sci*, 121(Pt 13), 2123-2129. doi:10.1242/jcs.021154
- Struck, N. S., Herrmann, S., Schmuck-Barkmann, I., de Souza Dias, S., Haase, S., Cabrera, A. L., . . . Gilberger, T. W. (2008b). Spatial dissection of the cis- and trans-Golgi compartments in the malaria parasite *Plasmodium falciparum*. *Mol Microbiol*, 67(6), 1320-1330. doi:10.1111/j.1365-2958.2008.06125.x
- Sturm, A., Amino, R., van de Sand, C., Regen, T., Retzlaff, S., Rennenberg, A., . . . Heussler, V. T. (2006). Manipulation of Host Hepatocytes by the Malaria Parasite for Delivery into Liver Sinusoids. *Science*, 313(5791), 1287-1290. doi:10.1126/science.1129720
- Su, X., Lodhi, I. J., Saltiel, A. R., & Stahl, P. D. (2006). Insulin-stimulated Interaction between insulin receptor substrate 1 and p85alpha and activation of protein kinase B/Akt require Rab5. *J Biol Chem*, 281(38), 27982-27990. doi:10.1074/jbc.M602873200
- Su, X. Z., Heatwole, V. M., Wertheimer, S. P., Guinet, F., Herrfeldt, J. A., Peterson, D. S., . . . Wellems, T. E. (1995). The large diverse gene family var encodes proteins involved in cytoadherence and antigenic variation of *Plasmodium falciparum*-infected erythrocytes. *Cell*, 82(1), 89-100. doi:10.1016/0092-8674(95)90055-1

- Sullivan, D. J. (2002). Theories on malarial pigment formation and quinoline action. *Int J Parasitol*, 32(13), 1645-1653.
- Sullivan, D. J., Jr., Gluzman, I. Y., & Goldberg, D. E. (1996). Plasmodium hemozoin formation mediated by histidine-rich proteins. *Science*, 271(5246), 219-222. doi:10.1126/science.271.5246.219
- Sultan, A. A., Thathy, V., Frevert, U., Robson, K. J., Crisanti, A., Nussenzweig, V., . . . Menard, R. (1997). TRAP is necessary for gliding motility and infectivity of plasmodium sporozoites. *Cell*, 90(3), 511-522.
- Suvorova, E. S., Radke, J. B., Ting, L. M., Vinayak, S., Alvarez, C. A., Kratzer, S., . . . White, M. W. (2013). A nucleolar AAA-NTPase is required for parasite division. *Mol Microbiol*, 90(2), 338-355. doi:10.1111/mmi.12367
- Szymczak, A. L., Workman, C. J., Wang, Y., Vignali, K. M., Dilioglou, S., Vanin, E. F., & Vignali, D. A. (2004). Correction of multi-gene deficiency in vivo using a single 'self-cleaving' 2A peptide-based retroviral vector. *Nat Biotechnol*, 22(5), 589-594. doi:10.1038/nbt957
- Tall, G. G., Hama, H., DeWald, D. B., & Horazdovsky, B. F. (1999). The phosphatidylinositol 3-phosphate binding protein Vac1p interacts with a Rab GTPase and a Sec1p homologue to facilitate vesicle-mediated vacuolar protein sorting. *Mol Biol Cell*, 10(6), 1873-1889. doi:10.1091/mbc.10.6.1873
- Taraschi, T. F., Trelka, D., Schneider, T., & Matthews, I. (1998). Plasmodium falciparum: characterization of organelle migration during merozoite morphogenesis in asexual malaria infections. *Exp Parasitol*, 88(3), 184-193. doi:10.1006/expr.1998.4254
- Taylor, W. R., Canon, V., & White, N. J. (2006). Pulmonary manifestations of malaria : recognition and management. *Treat Respir Med*, 5(6), 419-428. doi:10.2165/00151829-200605060-00007
- Tewari, R., Spaccapelo, R., Bistoni, F., Holder, A. A., & Crisanti, A. (2002). Function of region I and II adhesive motifs of Plasmodium falciparum circumsporozoite protein in sporozoite motility and infectivity. *J Biol Chem*, 277(49), 47613-47618. doi:10.1074/jbc.M208453200
- Thomas, J. A., Tan, M. S. Y., Bisson, C., Borg, A., Umrekar, T. R., Hackett, F., . . . Blackman, M. J. (2018). A protease cascade regulates release of the human malaria parasite Plasmodium falciparum from host red blood cells. *Nat Microbiol*, 3(4), 447-455. doi:10.1038/s41564-018-0111-0
- Tilley, L., Dixon, M. W., & Kirk, K. (2011). The Plasmodium falciparum-infected red blood cell. *Int J Biochem Cell Biol*, 43(6), 839-842. doi:10.1016/j.biocel.2011.03.012
- Tisdale, E. J., Bourne, J. R., Khosravi-Far, R., Der, C. J., & Balch, W. E. (1992). GTP-binding mutants of rab1 and rab2 are potent inhibitors of vesicular transport from the endoplasmic reticulum to the Golgi complex. *J Cell Biol*, 119(4), 749-761. doi:10.1083/jcb.119.4.749
- Tomii, K., Sawada, Y., & Honda, S. (2012). Convergent evolution in structural elements of proteins investigated using cross profile analysis. *BMC Bioinformatics*, 13(1), 11. doi:10.1186/1471-2105-13-11
- Touchot, N., Chardin, P., & Tavitian, A. (1987). Four additional members of the ras gene superfamily isolated by an oligonucleotide strategy: molecular cloning of YPT-related cDNAs from a rat brain library. *Proceedings of the National Academy of Sciences*, 84(23), 8210-8214. doi:10.1073/pnas.84.23.8210
- Trager, W., & Jensen, J. B. (1976). Human malaria parasites in continuous culture. *Science*, 193(4254), 673-675.
- Trampuz, A., Jereb, M., Muzlovic, I., & Prabhu, R. M. (2003). Clinical review: Severe malaria. *Crit Care*, 7(4), 315-323. doi:10.1186/cc2183
- Tu, Y. (2011). The discovery of artemisinin (qinghaosu) and gifts from Chinese medicine. *Nat Med*, 17(10), 1217-1220. doi:10.1038/nm.2471
- Tu, Y. Y., Ni, M. Y., Zhong, Y. R., Li, L. N., Cui, S. L., Zhang, M. Q., . . . Liang, X. T. (1981). [Studies on the constituents of Artemisia annua L. (author's transl)]. *Yao Xue Xue Bao*, 16(5), 366-370.
- Tunstad, E. (2013). *Darwins teori - Evolusjon gjennom 400 år*: Humanist forlag As.
- Vale, R. D. (2003). The molecular motor toolbox for intracellular transport. *Cell*, 112(4), 467-480. doi:10.1016/s0092-8674(03)00111-9

- van den Berg, H. (2009). Global status of DDT and its alternatives for use in vector control to prevent disease. *Environmental health perspectives*, 117(11), 1656-1663. doi:10.1289/ehp.0900785
- van Dooren, G. G., Marti, M., Tonkin, C. J., Stimmler, L. M., Cowman, A. F., & McFadden, G. I. (2005). Development of the endoplasmic reticulum, mitochondrion and apicoplast during the asexual life cycle of *Plasmodium falciparum*. *Mol Microbiol*, 57(2), 405-419. doi:10.1111/j.1365-2958.2005.04699.x
- van Dooren, G. G., & Striepen, B. (2013). The algal past and parasite present of the apicoplast. *Annu Rev Microbiol*, 67, 271-289. doi:10.1146/annurev-micro-092412-155741
- Van Wye, J., Ghorri, N., Webster, P., Mitschler, R. R., Elmendorf, H. G., & Haldar, K. (1996). Identification and localization of rab6, separation of rab6 from ERD2 and implications for an 'unstacked' Golgi, in *Plasmodium falciparum*. *Mol Biochem Parasitol*, 83(1), 107-120. doi:10.1016/s0166-6851(96)02759-4
- Vander Jagt, D. L., Hunsaker, L. A., & Campos, N. M. (1986). Characterization of a hemoglobin-degrading, low molecular weight protease from *Plasmodium falciparum*. *Mol Biochem Parasitol*, 18(3), 389-400. doi:10.1016/0166-6851(86)90095-2
- Varma, D., & Salmon, E. D. (2012). The KMN protein network--chief conductors of the kinetochore orchestra. *Journal of Cell Science*, 125(Pt 24), 5927-5936. doi:10.1242/jcs.093724
- Vaughan, A. M., Mikolajczak, S. A., Wilson, E. M., Grompe, M., Kaushansky, A., Camargo, N., . . . Kappe, S. H. (2012). Complete *Plasmodium falciparum* liver-stage development in liver-chimeric mice. *J Clin Invest*, 122(10), 3618-3628. doi:10.1172/jci62684
- Venkatesan, M., Alifrangis, M., Roper, C., & Plowe, C. V. (2013). Monitoring antifolate resistance in intermittent preventive therapy for malaria. *Trends Parasitol*, 29(10), 497-504. doi:10.1016/j.pt.2013.07.008
- Verhey, K. J., & Gaertig, J. (2007). The tubulin code. *Cell Cycle*, 6(17), 2152-2160. doi:10.4161/cc.6.17.4633
- Voller, A., Meuwissen, J. H. E., & Verhave, J. P. (1980). 2 - Methods for Measuring the Immunological Response to Plasmodia. In J. P. Kreier (Ed.), *Malaria* (pp. 67-109): Academic Press.
- von Heijne, G. (1990). The signal peptide. *J Membr Biol*, 115(3), 195-201. doi:10.1007/bf01868635
- Vorburger, K., Kitten, G. T., & Nigg, E. A. (1989). Modification of nuclear lamin proteins by a mevalonic acid derivative occurs in reticulocyte lysates and requires the cysteine residue of the C-terminal CXXM motif. *The EMBO Journal*, 8(13), 4007-4013. doi:10.1002/j.1460-2075.1989.tb08583.x
- Wagner, J. C., Platt, R. J., Goldfless, S. J., Zhang, F., & Niles, J. C. (2014). Efficient CRISPR-Cas9-mediated genome editing in *Plasmodium falciparum*. *Nat Methods*, 11(9), 915-918. doi:10.1038/nmeth.3063
- Walk, J., Reuling, I. J., Behet, M. C., Meerstein-Kessel, L., Graumans, W., van Gemert, G.-J., . . . Sauerwein, R. W. (2017). Modest heterologous protection after *Plasmodium falciparum* sporozoite immunization: a double-blind randomized controlled clinical trial. *BMC medicine*, 15(1), 168-168. doi:10.1186/s12916-017-0923-4
- Walliker, D., Quakyi, I. A., Wellems, T. E., McCutchan, T. F., Szarfman, A., London, W. T., . . . Carter, R. (1987). Genetic analysis of the human malaria parasite *Plasmodium falciparum*. *Science*, 236(4809), 1661-1666. doi:10.1126/science.3299700
- Walworth, N. C., Brennwald, P., Kabcenell, A. K., Garrett, M., & Novick, P. (1992). Hydrolysis of GTP by Sec4 protein plays an important role in vesicular transport and is stimulated by a GTPase-activating protein in *Saccharomyces cerevisiae*. *Mol Cell Biol*, 12(5), 2017-2028. doi:10.1128/mcb.12.5.2017
- Walworth, N. C., Goud, B., Kabcenell, A. K., & Novick, P. J. (1989). Mutational analysis of SEC4 suggests a cyclical mechanism for the regulation of vesicular traffic. *EMBO J*, 8(6), 1685-1693.
- Wang, J., Zhang, C. J., Chia, W. N., Loh, C. C., Li, Z., Lee, Y. M., . . . Lin, Q. (2015). Haem-activated promiscuous targeting of artemisinin in *Plasmodium falciparum*. *Nat Commun*, 6, 10111. doi:10.1038/ncomms10111

- Wang, Y., Wei, J.-H., Bisel, B., Tang, D., & Seemann, J. (2008). Golgi cisternal unstacking stimulates COPI vesicle budding and protein transport. *PLOS ONE*, 3(2), e1647-e1647. doi:10.1371/journal.pone.0001647
- Webster, W. A., & McFadden, G. I. (2014). From the genome to the phenome: tools to understand the basic biology of *Plasmodium falciparum*. *J Eukaryot Microbiol*, 61(6), 655-671. doi:10.1111/jeu.12176
- Weiner, A., Dahan-Pasternak, N., Shimoni, E., Shinder, V., von Huth, P., Elbaum, M., & Dzikowski, R. (2011). 3D nuclear architecture reveals coupled cell cycle dynamics of chromatin and nuclear pores in the malaria parasite *Plasmodium falciparum*. *Cellular Microbiology*, 13(7), 967-977. doi:10.1111/j.1462-5822.2011.01592.x
- Weiss, G. E., Crabb, B. S., & Gilson, P. R. (2016). Overlaying Molecular and Temporal Aspects of Malaria Parasite Invasion. *Trends Parasitol*, 32(4), 284-295. doi:10.1016/j.pt.2015.12.007
- Welburn, J. P., Grishchuk, E. L., Backer, C. B., Wilson-Kubalek, E. M., Yates, J. R., 3rd, & Cheeseman, I. M. (2009). The human kinetochore Skal complex facilitates microtubule depolymerization-coupled motility. *Dev Cell*, 16(3), 374-385. doi:10.1016/j.devcel.2009.01.011
- Westermann, S., & Weber, K. (2003). Post-translational modifications regulate microtubule function. *Nat Rev Mol Cell Biol*, 4(12), 938-947. doi:10.1038/nrm1260
- White, N. J. (2011). Determinants of relapse periodicity in *Plasmodium vivax* malaria. *Malar J*, 10, 297. doi:10.1186/1475-2875-10-297
- Wideman, J. G., Leung, K. F., Field, M. C., & Dacks, J. B. (2014). The cell biology of the endocytic system from an evolutionary perspective. *Cold Spring Harb Perspect Biol*, 6(4), a016998. doi:10.1101/cshperspect.a016998
- Wieffer, M., Maritzen, T., & Haucke, V. (2009). SnapShot: endocytic trafficking. *Cell*, 137(2), 382.e381-383. doi:10.1016/j.cell.2009.04.012
- Wilson, D. B., & Wilson, M. P. (1992). Identification and subcellular localization of human rab5b, a new member of the ras-related superfamily of GTPases. *J Clin Invest*, 89(3), 996-1005. doi:10.1172/jci115683
- Wilson, R. J., Denny, P. W., Preiser, P. R., Rangachari, K., Roberts, K., Roy, A., . . . Williamson, D. H. (1996). Complete gene map of the plastid-like DNA of the malaria parasite *Plasmodium falciparum*. *J Mol Biol*, 261(2), 155-172. doi:10.1006/jmbi.1996.0449
- Wolfrum, U. (1995). Centrin in the photoreceptor cells of mammalian retinae. *Cell Motility*, 32(1), 55-64. doi:10.1002/cm.970320107
- Wong, W., Bai, X.-C., Sleebbs, B. E., Triglia, T., Brown, A., Thompson, J. K., . . . Baum, J. (2017). Mefloquine targets the *Plasmodium falciparum* 80S ribosome to inhibit protein synthesis. *Nature Microbiology*, 2, 17031-17031. doi:10.1038/nmicrobiol.2017.31
- World-Health-Organisation. (2017, 29.11.2017). World Malaria Report. Retrieved from <http://www.who.int/malaria/media/world-malaria-report-2017/en/>
- World-Health-Organisation. (2018a, 18.01.2018). Overview of malaria treatment. Retrieved from <https://www.who.int/malaria/areas/treatment/overview/en/>
- World-Health-Organisation. (2018b, 19.11.2018). WHO Malaria Key facts. Retrieved from <https://www.who.int/en/news-room/fact-sheets/detail/malaria>
- World-Health-Organisation. (2018c). World Malaria Report 2018. Retrieved from <https://www.who.int/gho/malaria/en/>
- World-Health-Organisation. (2020). Q&A on the malaria vaccine implementation programme (MVIP). Retrieved from <https://www.who.int/malaria/media/malaria-vaccine-implementation-qa/en/>
- Wright, G. J., & Rayner, J. C. (2014). *Plasmodium falciparum* erythrocyte invasion: combining function with immune evasion. *PLoS Pathog*, 10(3), e1003943. doi:10.1371/journal.ppat.1003943
- Xie, S. C., Dogovski, C., Hanssen, E., Chiu, F., Yang, T., Crespo, M. P., . . . Tilley, L. (2016). Haemoglobin degradation underpins the sensitivity of early ring stage *Plasmodium falciparum* to artemisinins. *J Cell Sci*, 129(2), 406-416. doi:10.1242/jcs.178830

-
- Yamauchi, L. M., Coppi, A., Snounou, G., & Sinnis, P. (2007). Plasmodium sporozoites trickle out of the injection site. *Cellular Microbiology*, 9(5), 1215-1222. doi:10.1111/j.1462-5822.2006.00861.x
- Yang, M., Coppens, I., Wormsley, S., Baevova, P., Hoppe, H. C., & Joiner, K. A. (2004). The Plasmodium falciparum Vps4 homolog mediates multivesicular body formation. *J Cell Sci*, 117(Pt 17), 3831-3838. doi:10.1242/jcs.01237
- Yarunin, A., Panse, V. G., Petfalski, E., Dez, C., Tollervey, D., & Hurt, E. C. (2005). Functional link between ribosome formation and biogenesis of iron-sulfur proteins. *EMBO J*, 24(3), 580-588. doi:10.1038/sj.emboj.7600540
- Yayon, A., Timberg, R., Friedman, S., & Ginsburg, H. (1984). Effects of chloroquine on the feeding mechanism of the intraerythrocytic human malarial parasite Plasmodium falciparum. *J Protozool*, 31(3), 367-372. doi:10.1111/j.1550-7408.1984.tb02981.x
- Yeh, E., & DeRisi, J. L. (2011). Chemical rescue of malaria parasites lacking an apicoplast defines organelle function in blood-stage Plasmodium falciparum. *PLoS Biol*, 9(8), e1001138. doi:10.1371/journal.pbio.1001138
- Yuthavong, Y. (2002). Basis for antifolate action and resistance in malaria. *Microbes Infect*, 4(2), 175-182.
- Zaw, M. T., & Lin, Z. (2019). Human Plasmodium knowlesi infections in South-East Asian countries. *Journal of Microbiology, Immunology and Infection*, 52(5), 679-684. doi:https://doi.org/10.1016/j.jmii.2019.05.012
- Zhang, G., Kelstrup, C. D., Hu, X. W., Kaas Hansen, M. J., Singleton, M. R., Olsen, J. V., & Nilsson, J. (2012). The Ndc80 internal loop is required for recruitment of the Ska complex to establish end-on microtubule attachment to kinetochores. *J Cell Sci*, 125(Pt 13), 3243-3253. doi:10.1242/jcs.104208
- Zhang, M., Wang, C., Otto, T. D., Oberstaller, J., Liao, X., Adapa, S. R., . . . Adams, J. H. (2018). Uncovering the essential genes of the human malaria parasite Plasmodium falciparum by saturation mutagenesis. *Science*, 360(6388). doi:10.1126/science.aap7847
- Zhang, Q., Sivakumar, S., Chen, Y., Gao, H., Yang, L., Yuan, Z., . . . Liu, H. (2017). Ska3 Phosphorylated by Cdk1 Binds Ndc80 and Recruits Ska to Kinetochores to Promote Mitotic Progression. *Curr Biol*, 27(10), 1477-1484.e1474. doi:10.1016/j.cub.2017.03.060
- Zhang, X., Li, F., Lu, X.-W., & Liu, C.-F. (2009). Protein C-Terminal Modification through Thioacid/Azide Amidation. *Bioconjugate Chemistry*, 20(2), 197-200. doi:10.1021/bc800488n
- Zhou, H. C., Gao, Y. H., Zhong, X., & Wang, H. (2009). Dynamin like protein 1 participated in the hemoglobin uptake pathway of Plasmodium falciparum. *Chin Med J (Engl)*, 122(14), 1686-1691.
- Zhu, G., Marchewka, M. J., & Keithly, J. S. (2000). Cryptosporidium parvum appears to lack a plastid genome. *Microbiology*, 146 (Pt 2), 315-321. doi:10.1099/00221287-146-2-315
- Zhu, X. D., & Sadowski, P. D. (1995). Cleavage-dependent ligation by the FLP recombinase. Characterization of a mutant FLP protein with an alteration in a catalytic amino acid. *J Biol Chem*, 270(39), 23044-23054. doi:10.1074/jbc.270.39.23044
- Zimmermann, L., Stephens, A., Nam, S. Z., Rau, D., Kubler, J., Lozajic, M., . . . Alva, V. (2018). A Completely Reimplemented MPI Bioinformatics Toolkit with a New HHpred Server at its Core. *J Mol Biol*, 430(15), 2237-2243. doi:10.1016/j.jmb.2017.12.007

Publications

PfVPS45 Is Required for Host Cell Cytosol Uptake by Malaria Blood Stage Parasites.

Jonscher, E., **Schmitt, M.**, Flemming, S., Sabitzki, R., Reichard, N., Birnbaum, J., Spielmann, T.
Cell Host Microbe (2019), 25(1), 166-173 e165. doi:10.1016/j.chom.2018.11.010

A Kelch13-defined endocytosis pathway mediates artemisinin resistance in malaria parasites.

Jakob Birnbaum, Sarah Scharf, Sabine Schmidt, Ernst Jonscher, Wieteke Anna Maria Hoeijmakers, Sven Flemming¹, Christa Geeke Toenhake, **Marius Schmitt**, Ricarda Sabitzki, Bärbel Bergmann, Ulrike Fröhlke, Paolo Mesén-Ramírez, Alexandra Blancke Soares, Hendrik Herrmann, Richárd Bártfai, Tobias Spielmann,
Science. (2020), 367(6473), 51-59. doi:10.1126/science.aax4735

Danksagung

An dieser Stelle möchte ich mich in erster Linie bei Dr. Tobias Spielmann bedanken, der es mir ermöglicht hat, meine Doktorarbeit in seiner Arbeitsgruppe am Bernhard-Nocht-Institut für Tropenmedizin durchzuführen. Vielen Dank für die exzellente Betreuung, die vielen wertvollen Ideen und die stetige Verfügbarkeit bei jeglichen Fragen. Das Projekt und die sehr gute Arbeitsatmosphäre haben mir viel Freude bereitet. Ich habe in dieser Zeit viel gelernt und konnte mich wissenschaftlich erheblich weiterentwickeln. Vielen Dank dafür!

Zudem möchte ich mich bei Prof. Dr. Tim-Wolf Gilberger und Dr. Tobias Spielmann für die Erstellung des Dissertationsgutachtens bedanken. Auch möchte ich mich bei Frau Prof. Julia Kehr und Prof. Dr. Iris Bruchhaus für die Aufstellung als Prüfungskommission bedanken.

Ein weiterer Dank gilt an dieser Stelle der Jürgen-Manchot-Stiftung, die mir die Finanzierung meiner Doktorarbeit und eines Teils des Projekts ermöglicht hat.

Darüber hinaus möchte ich mich sehr herzlich bei der Arbeitsgruppe Spielmann und der Arbeitsgruppe Gilberger bedanken, die mir bei fachlichen Fragen immer geholfen haben und zu einer produktiven und freundlichen Arbeitsatmosphäre beigetragen haben.

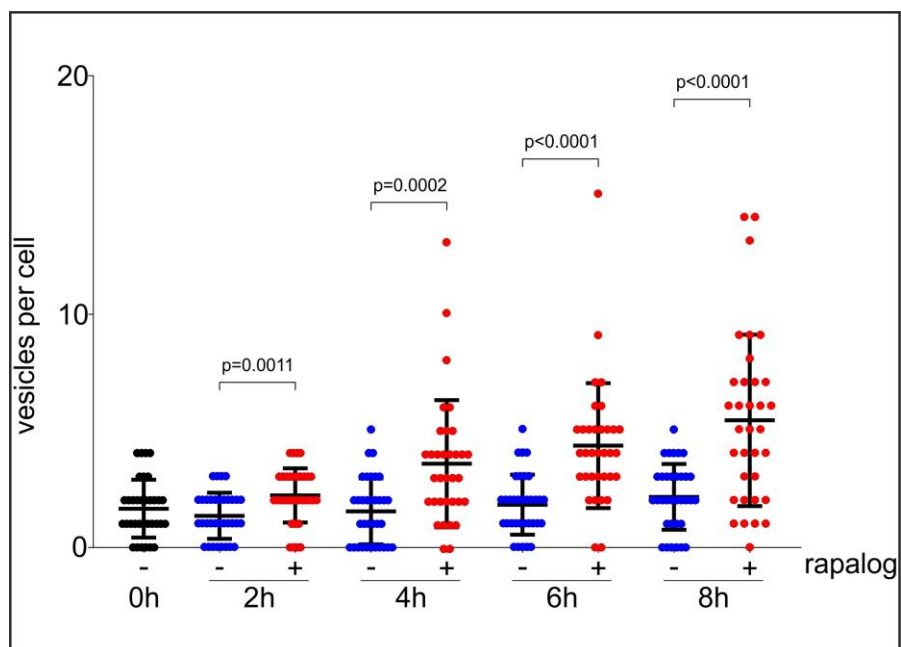
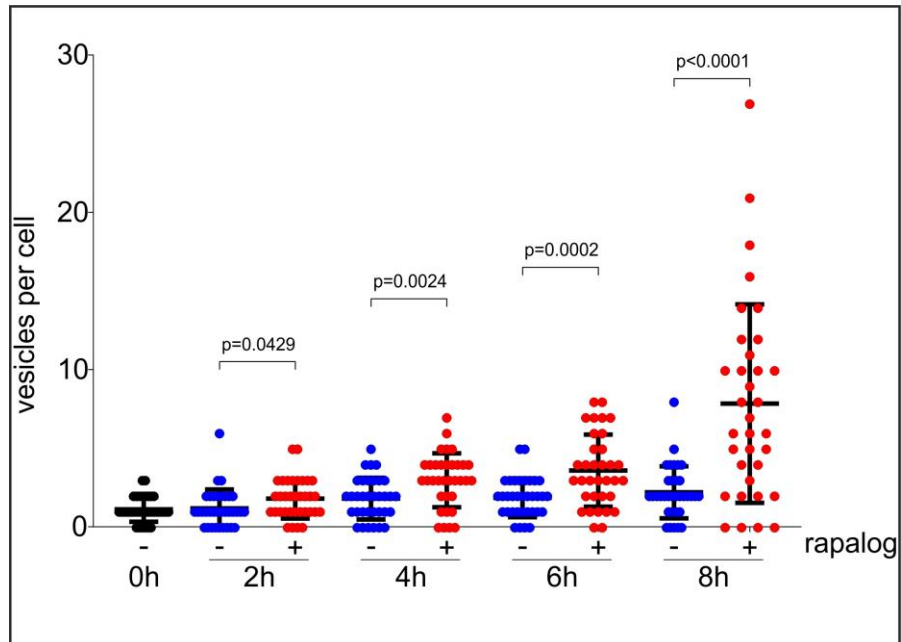
Im Besonderen möchte ich mich bei Dr. Paolo Mesén-Ramírez, Stephan Wichers, Paul Burda, Paul Hughes und Bärbel Strothmann-Schmitt für das Korrekturlesen meiner Doktorarbeit bedanken.

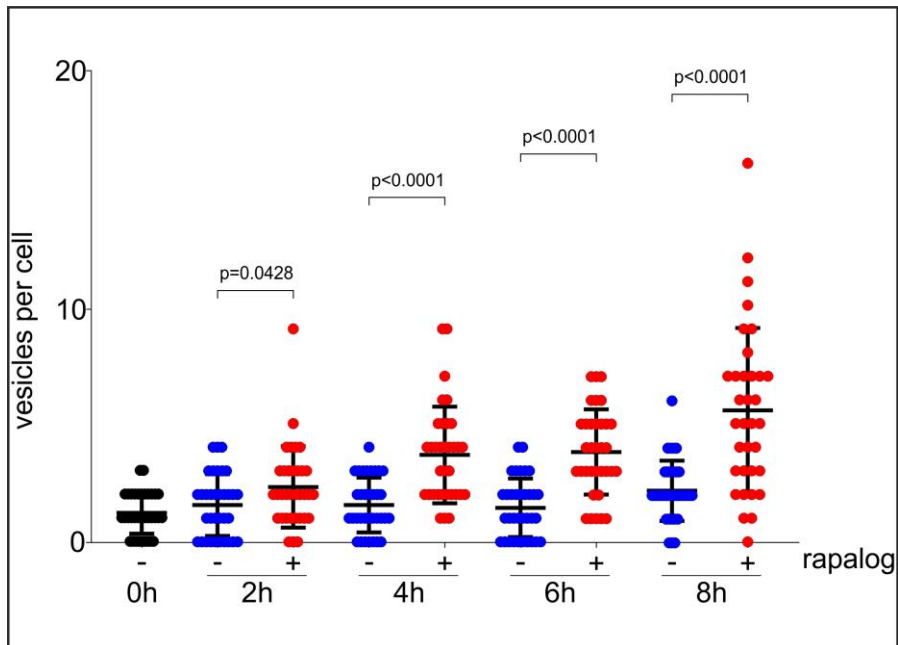
Abschließend möchte ich mich bei meiner Familie und meinen Freunden bedanken, die mir während der gesamten Zeit stets den Rücken gestärkt haben. Im Besonderen bedanke ich mich bei meiner Frau Sabrina Schmitt, die mich in all den Jahren immer unterstützt hat. Ich bin sehr froh und dankbar, dass wir so ein tolles Team sind und auch diese Zeit so gut gemeistert haben.

Appendix

Appendix 1

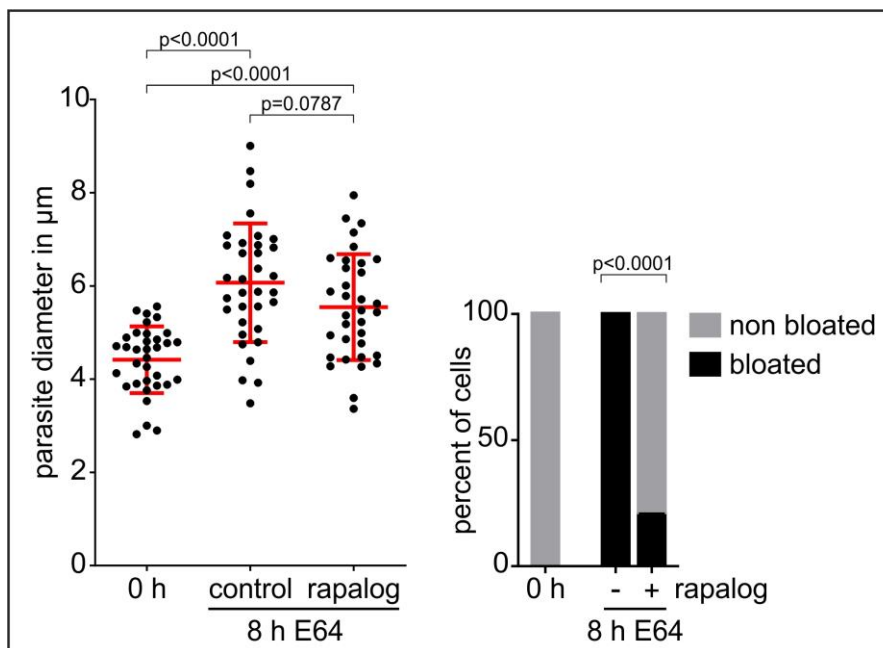
*Pf*Rab5b vesicle accumulation assay of independent experiments

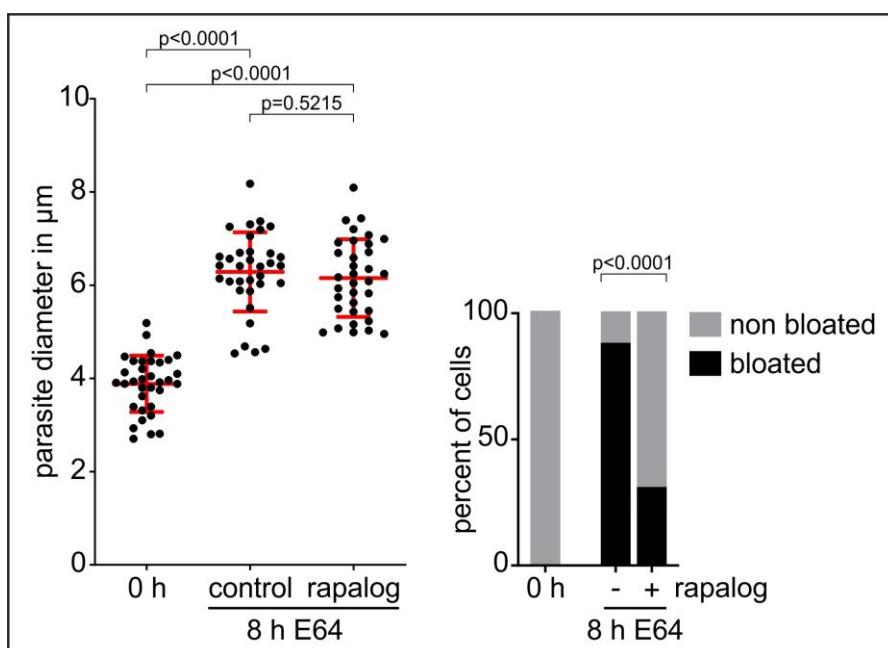
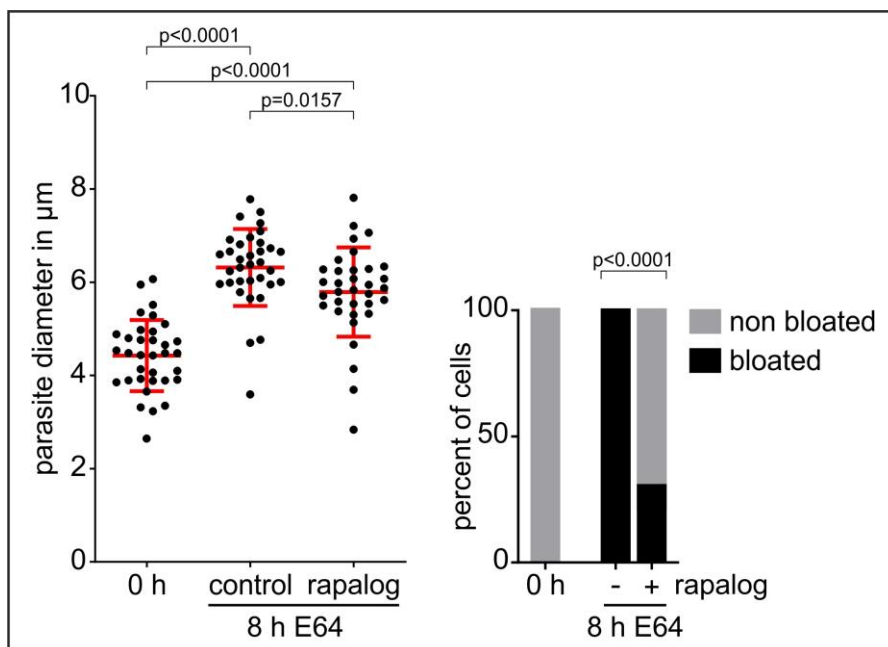




Appendix 2

*Pf*Rab5b bloated food vacuole assay of independent experiments





Appendix 3

Alignments of *PfRab5b*-GTPase mutants

Query = human Rab5b

Sbjct = *P. falciparum* Rab5b

Red squares = mutation sites

Sequence ID: Query_82447 Length: 207 Number of Matches: 1

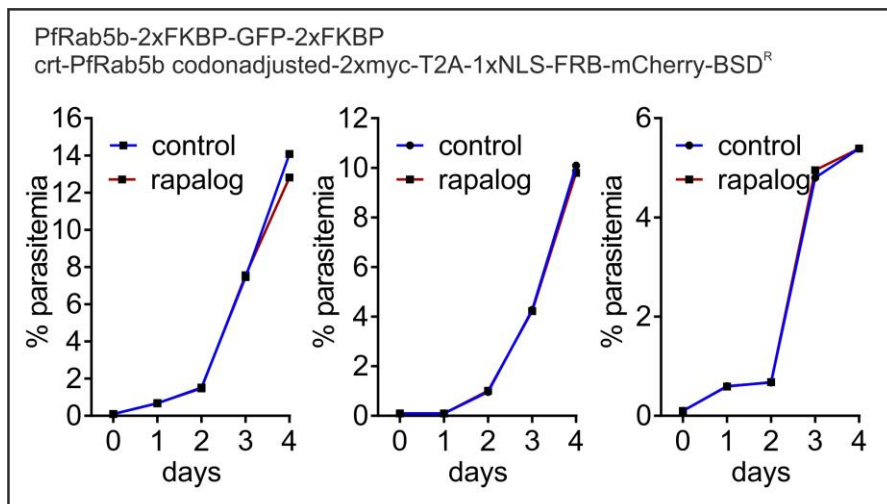
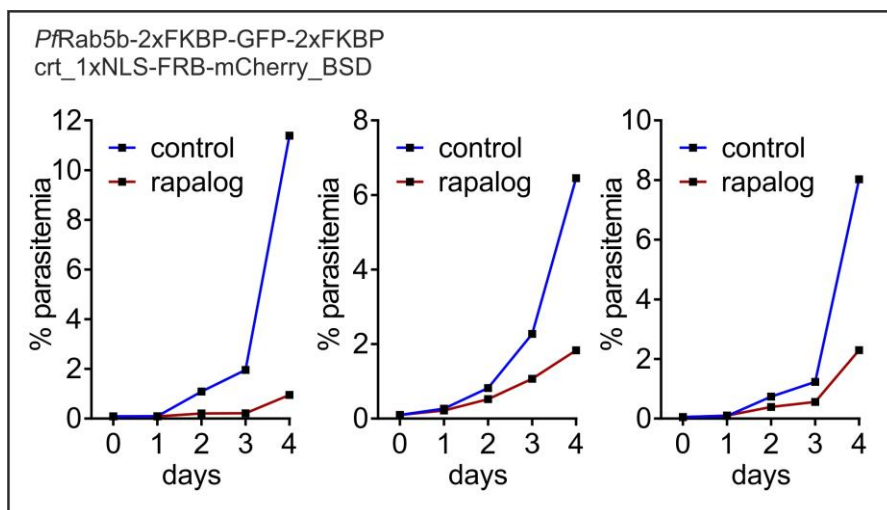
Range 1: 34 to 194 [Graphics](#)

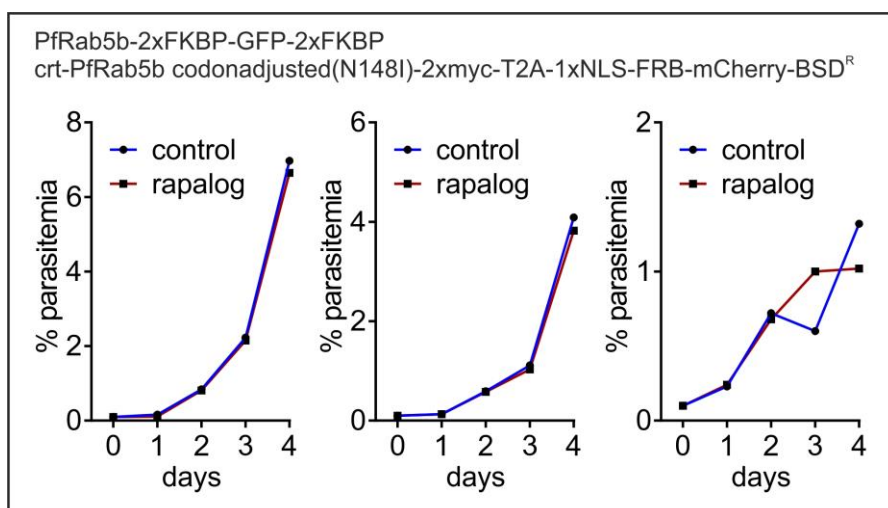
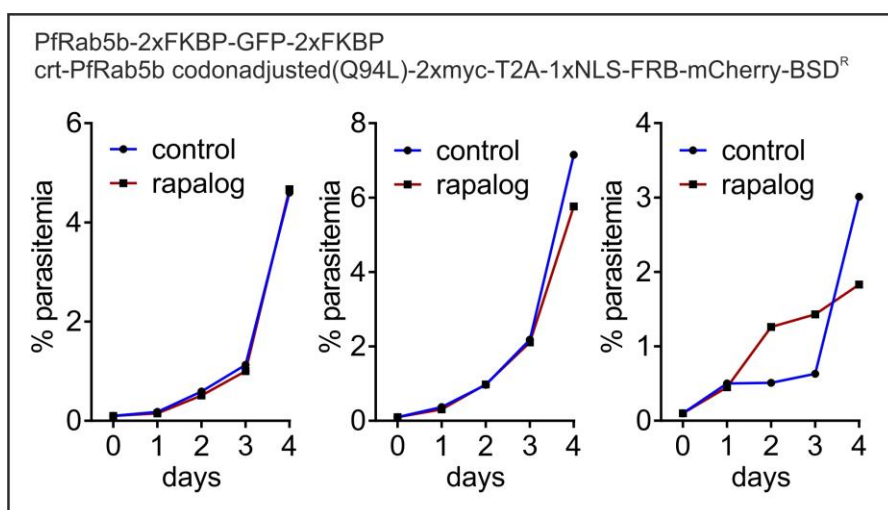
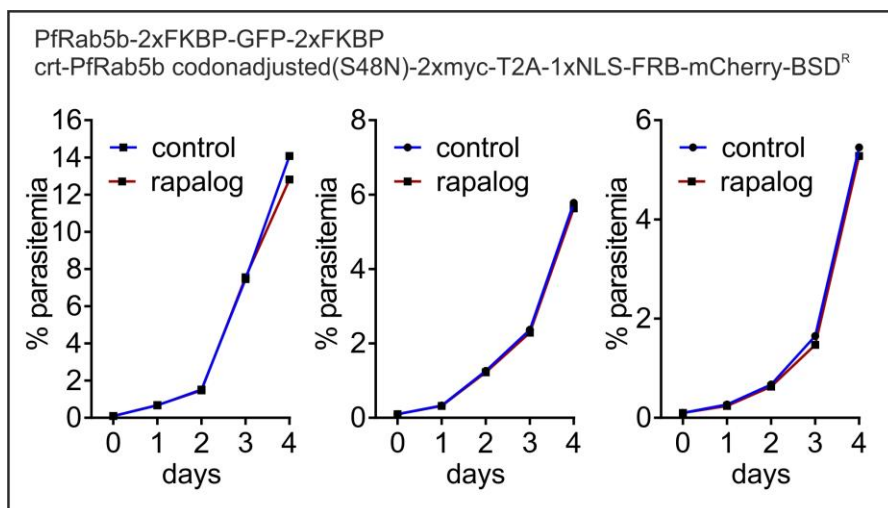
▼ Next Match ▲ Previous Match

Score	Expect	Method	Identities	Positives	Gaps
134 bits(338)	2e-44	Compositional matrix adjust.	67/163(41%)	98/163(60%)	3/163(1%)
Query 20	QFELVLLGESAVGH	S	SLVLRVFKGQFHEYQESTIGAAFLTQSVCLDD-TTVKFEIWDTAG		78
	+ ++VLLG+S VGH	SS+ L	G+F E + IIGAAFL ++ L + I+K IWDI G		
Sbjct 34	KVKIVLLGDSGVGH	S	SIALYLCHGRFSEKHQVTIGAAFLHNNIELKNGATMKLHIWDTGG		93
Query 79	QIRYHSLAPMYRGAQAAI	V	VYDITNQETFARAKTWVKELQRQASPSIVIALAGN	KADLA	138
	QIR+ S+AP+YYR A	A	A+VVD N E+F K W+ E++ + I + NK DL		
Sbjct 94	QIRFRSMAPLYYRDAYGAV	V	VYDSNNVESFDSLKYWINEIKSNGPRNCCIMVVA	N	153
Query 139	NKRMVEYEEAQAYADDNS	L	LFMETSAKTAMNVNDLFLAIAKKL		181
	K + E + + ++ F+E	SAKT	N+ LF +A ++		
Sbjct 154	QK--LNSEMVMKFCQENVS	F	IECSAKTGENITTLFEKLASRI		194

Appendix 4

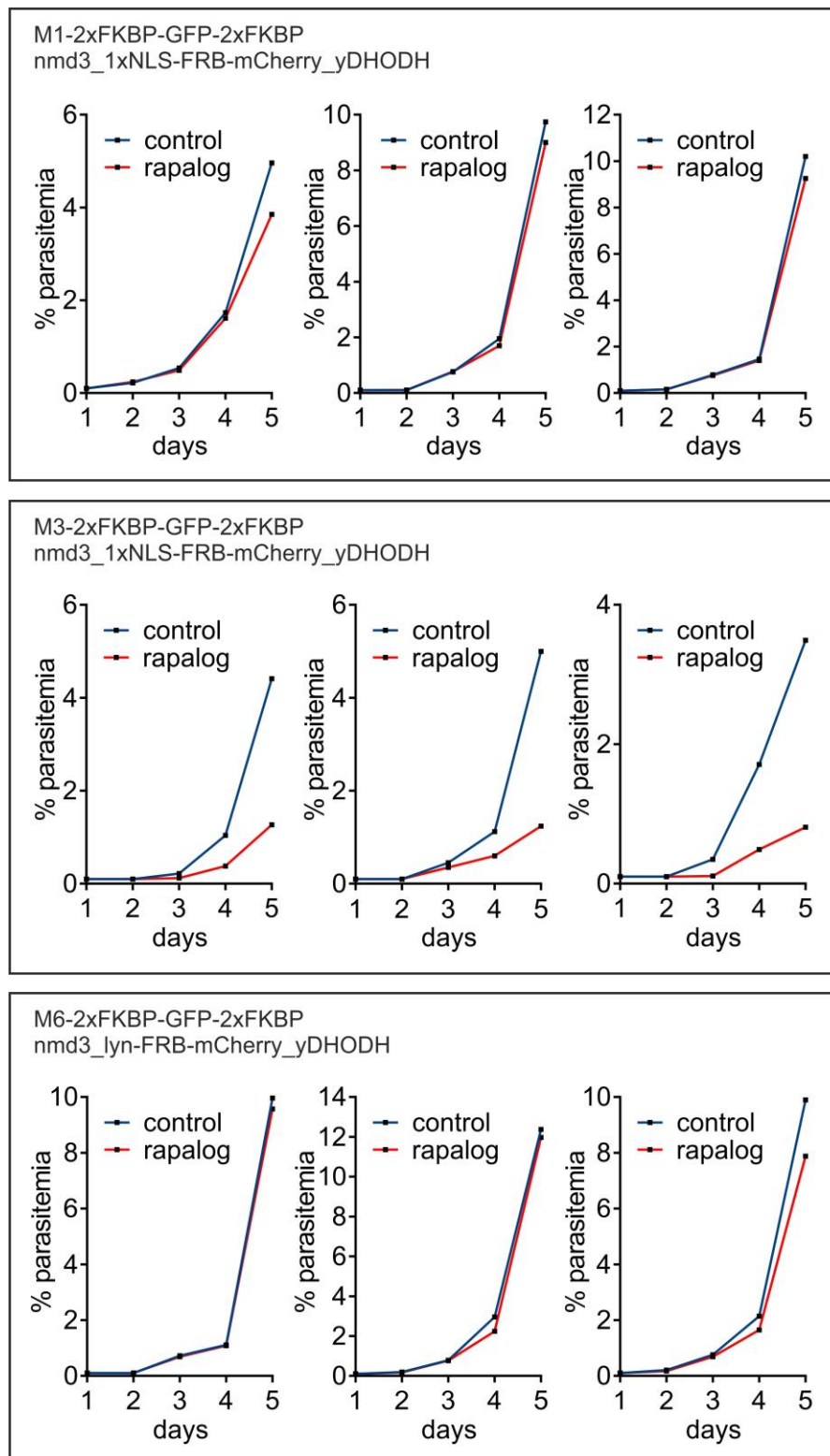
Flow cytometry growth curves for *PfRab5b* and complementations of independent experiments

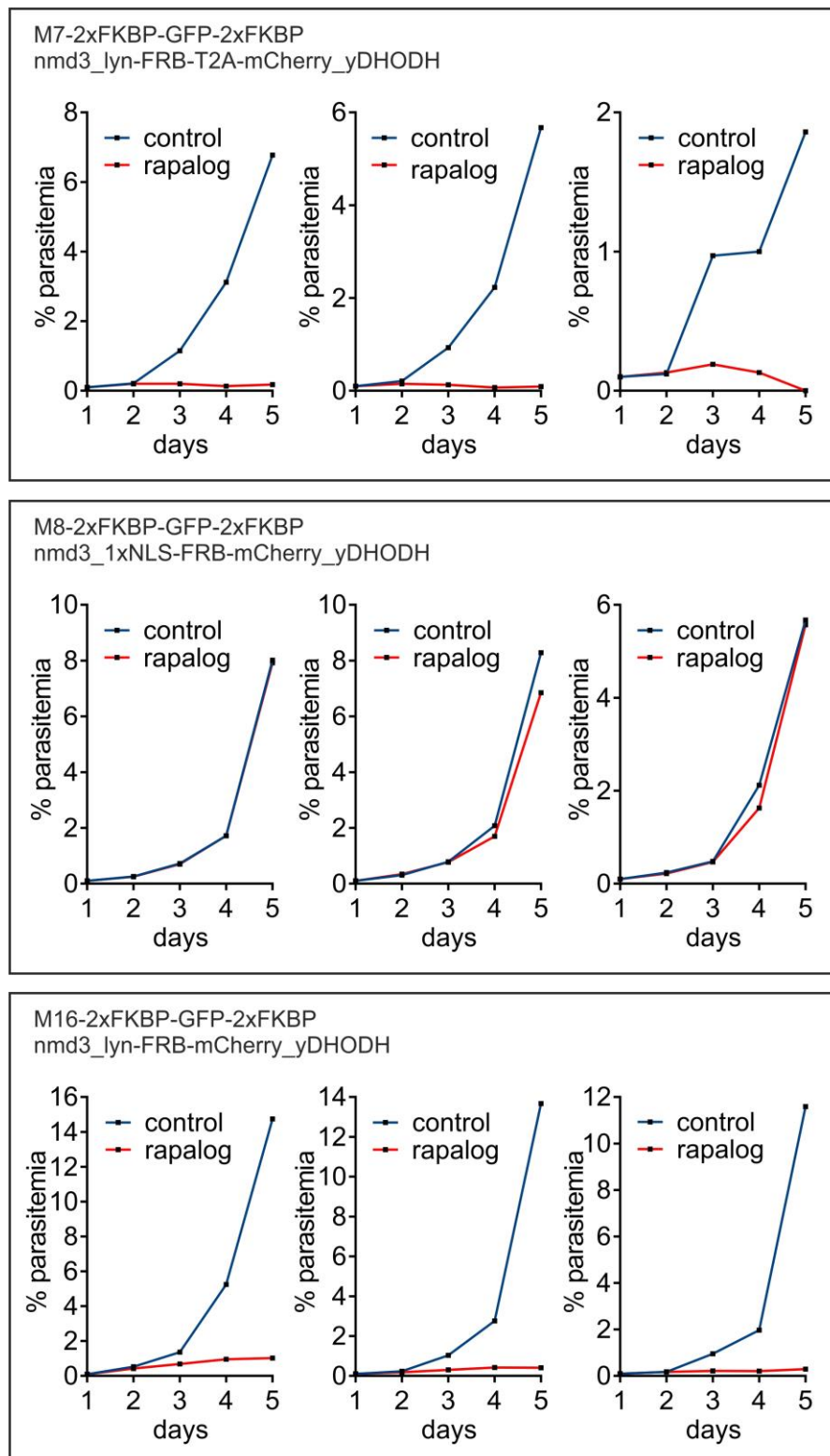


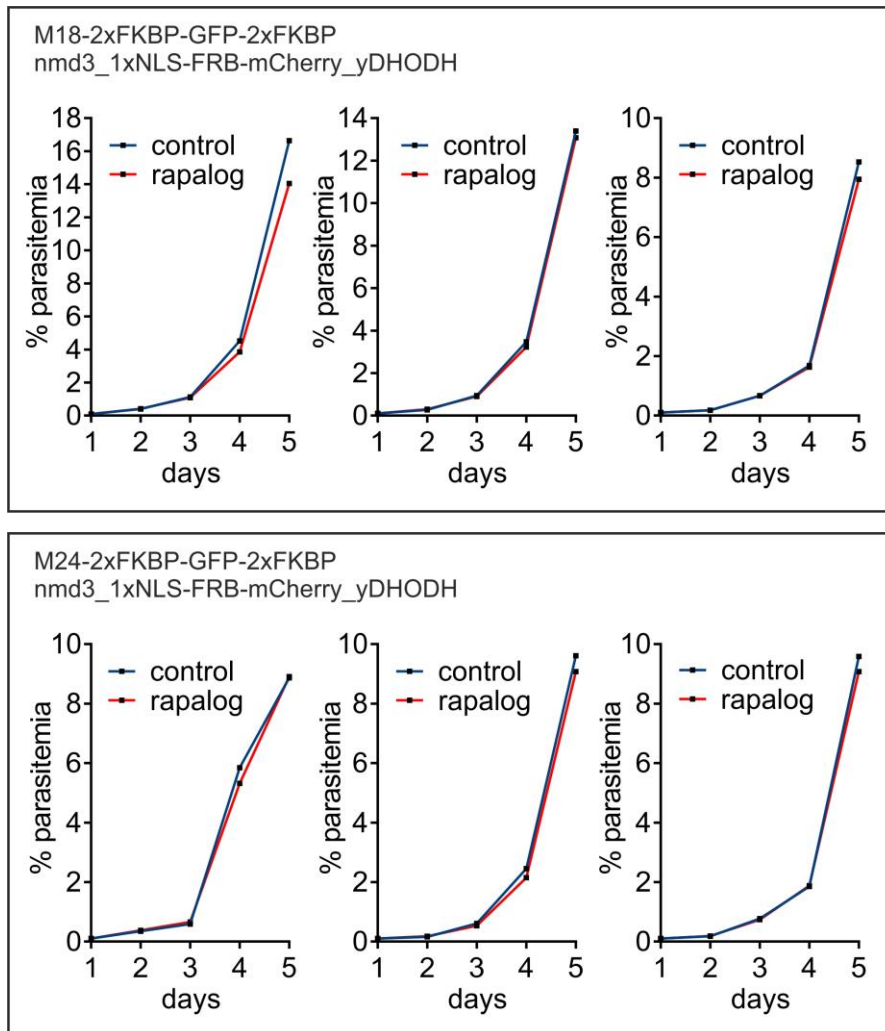


Appendix 5

Flow cytometry growth curves for the candidates of independent experiments

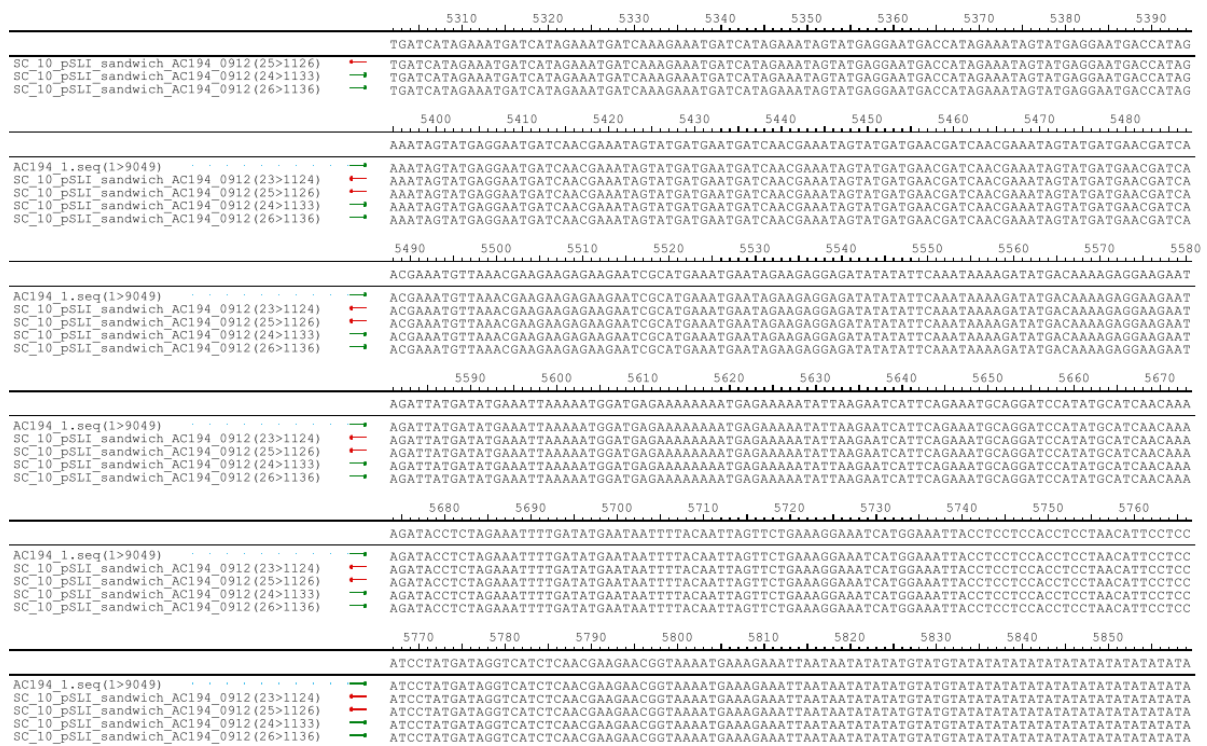
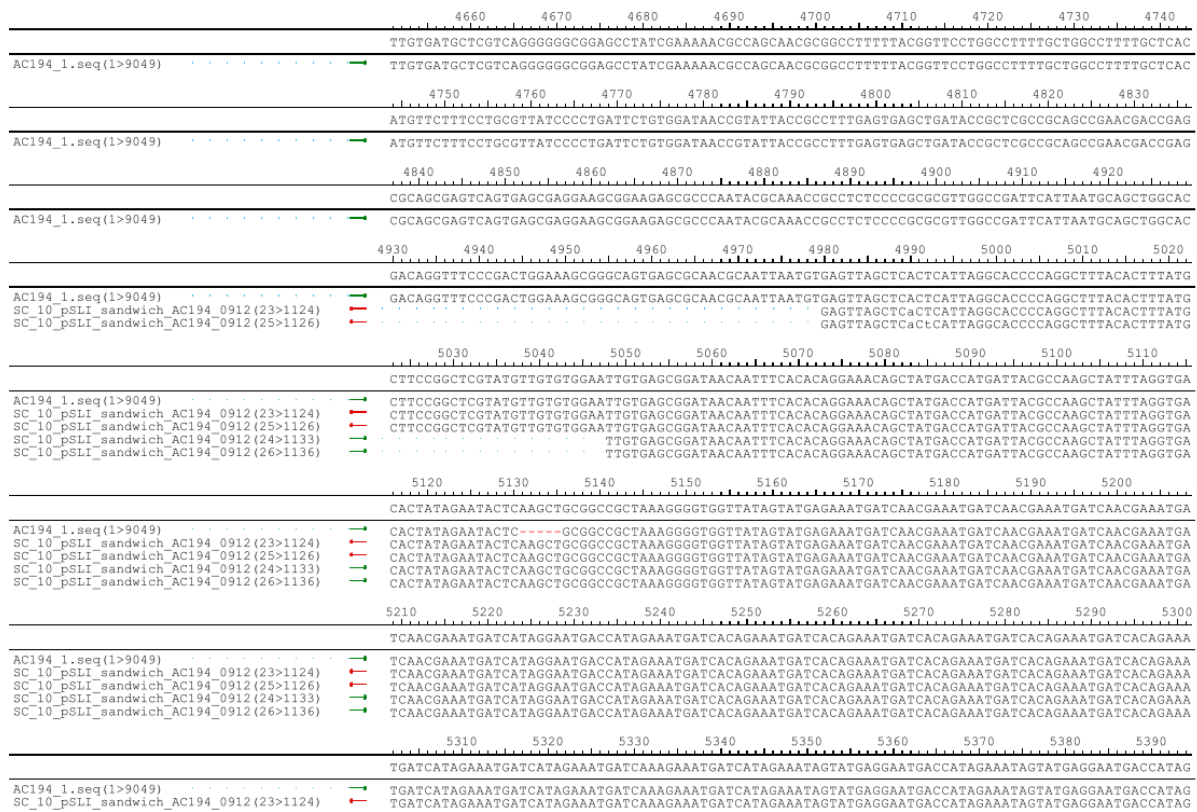


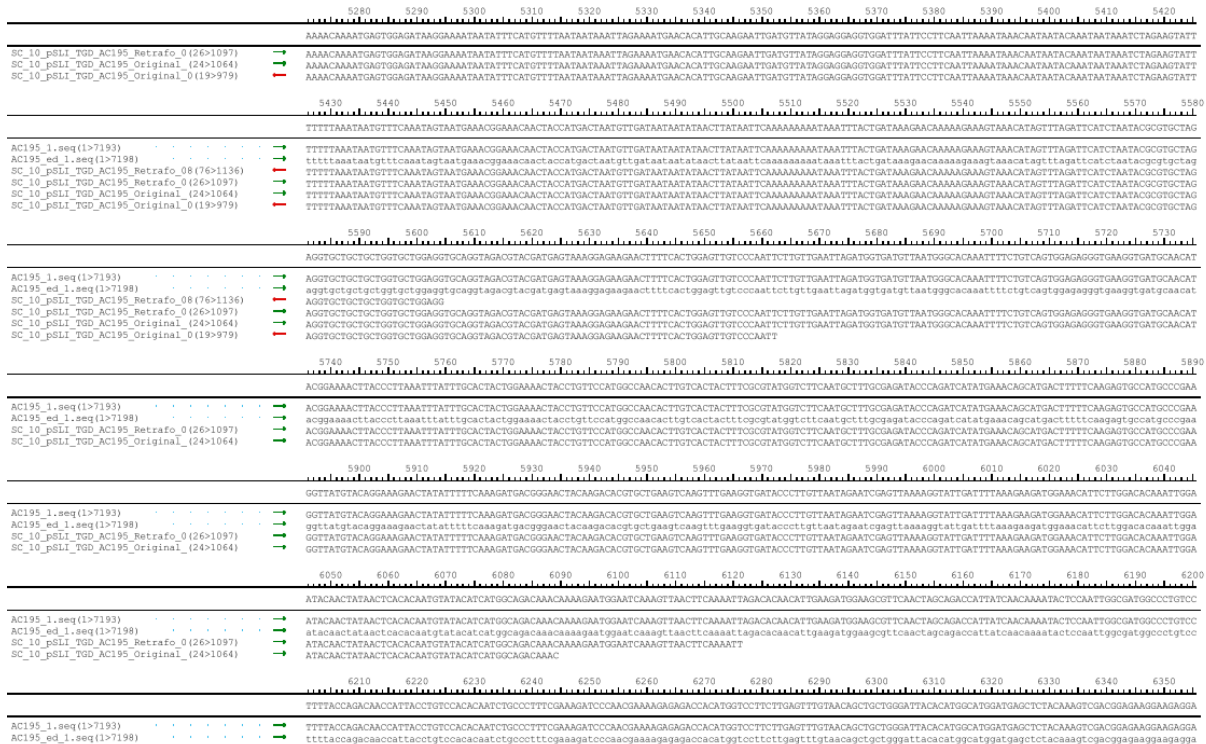




Appendix 6

Sequencing pSLI-sandwich from Life technologies (Darmstadt)



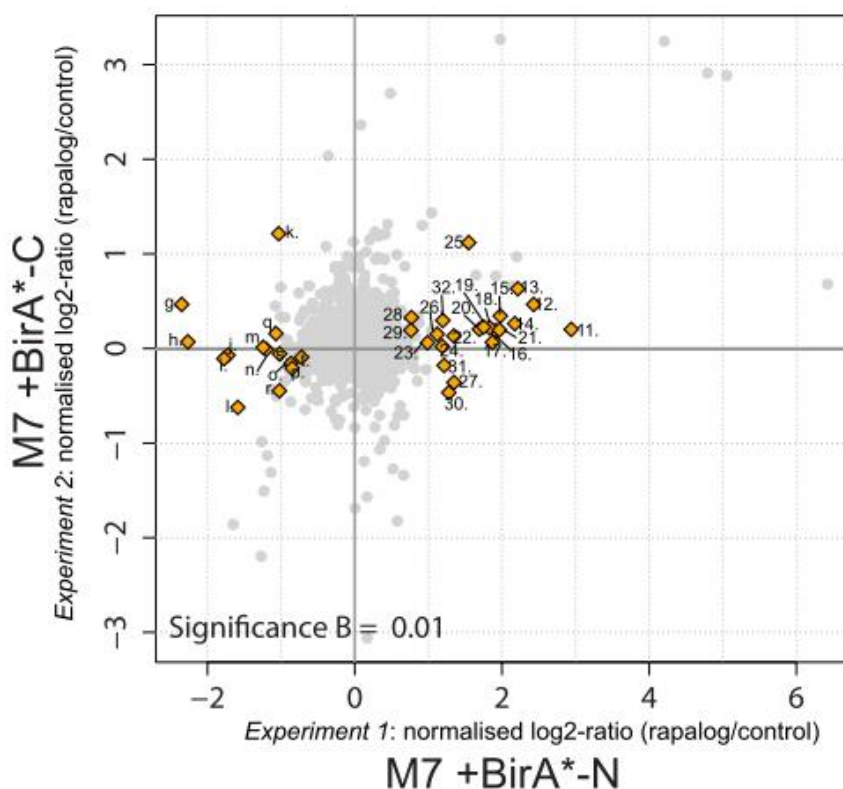


Appendix 7

Individual DIQ-BioID experiments of Candidate M7 (PF3D7_0307500)

Only significant in experiment 1

11	PF3D7_0915400	ATP-dependent 6-phosphofructokinase	PFK9
12	PF3D7_0513600	deoxyribodipyrimidine photo-lyase, putative	-
13	PF3D7_0316500	kinetochore protein NUF2, putative	NUF2
14	PF3D7_0723800	conserved Plasmodium protein, unknown function	-
15	PF3D7_1245100	kinesin-13, putative	KLP6
16	PF3D7_0111400	conserved Plasmodium protein, unknown function	GEXP19
17	PF3D7_0825000	conserved Plasmodium protein, unknown function	-
18	PF3D7_0729100	conserved Plasmodium protein, unknown function	-
19	PF3D7_1322200	conserved Plasmodium protein, unknown function	-
20	PF3D7_1207000	conserved Plasmodium protein, unknown function	-
21	PF3D7_1250800	DNA repair protein rhp16, putative	-
22	PF3D7_1116100	serine esterase, putative	-
23	PF3D7_0518500	ATP-dependent RNA helicase DDX23, putative	DDX23
24	PF3D7_0319400	kinesin-8, putative	-
25	PF3D7_1466800	conserved Plasmodium protein, unknown function	-
26	PF3D7_0317500	kinesin-5	EG5
27	PF3D7_0103500	conserved Plasmodium protein, unknown function	-
28	PF3D7_0410800	conserved Plasmodium protein, unknown function	-
29	PF3D7_0529400	conserved Plasmodium protein, unknown function	-
30	PF3D7_1247500	serine/threonine protein kinase, putative	-
31	PF3D7_1449700	exosome complex exonuclease RRP6	RRP6
32	PF3D7_1228400	conserved Plasmodium protein, unknown function	-

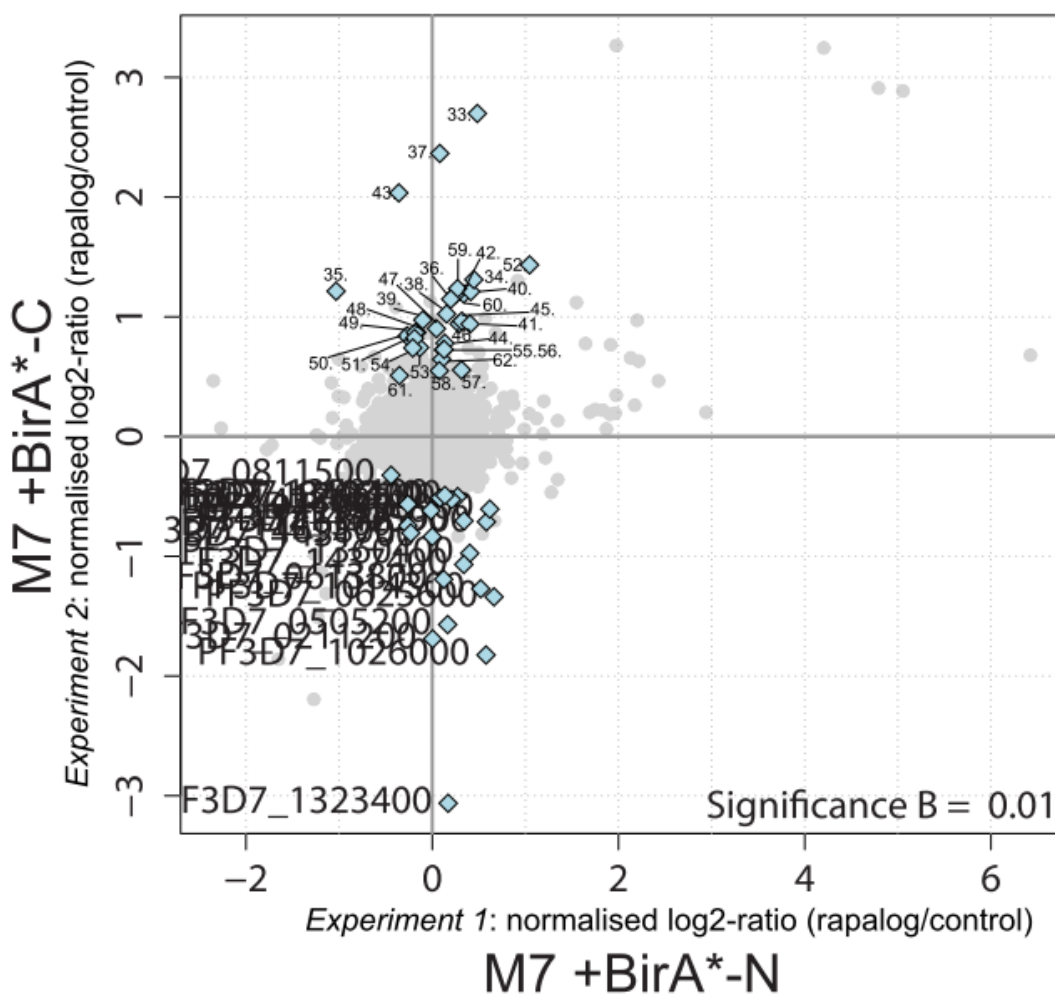


g	PF3D7_0317800	26S proteasome non-ATPase regulatory subunit 9	-
h	PF3D7_1458800	DNA-directed RNA polymerase III subunit RPC5, pu	-
i	PF3D7_1132000	ubiquitin-like protein, putative	-
j	PF3D7_0305100	conserved Plasmodium protein, unknown function	-
k	PF3D7_0503800	60S ribosomal protein L31	RPL31
l	PF3D7_0812100	conserved protein, unknown function	-
m	PF3D7_1346300	DNA/RNA-binding protein Alba 2	ALBA2
n	PF3D7_1233900	sentrin-specific protease 1	SEN1
o	PF3D7_0629400	RNA-binding protein, putative	-
p	PF3D7_0704300	conserved Plasmodium membrane protein, unknow	-
q	PF3D7_0703000	conserved Plasmodium protein, unknown function	-
r	PF3D7_1002700	conserved Plasmodium protein, unknown function	-
s	PF3D7_0218200	conserved Plasmodium protein, unknown function	-
t	PF3D7_0108700	secreted ookinete protein, putative	PSOP24

	A	B	C	D	E	F	G	H	I	J	K	L	M
1	Protein.IDs	Ratio.H.L.normalized d.M7_exp1	Ratio.H.L.normalized d.M7_exp1.Significa nce.B	Ratio.H.L.normalized d.M7_exp2	Ratio.H.L.normalized d.M7_exp2.Significa nce.B	plotr	Product Description	Gene Name or Symbol					
2	PF3D7_0915400	2,940562	5,29E-31	-0,2018748	3,09E-01	11	ATP-dependent 6-phosphofructokinase	PFK9					
3	PF3D7_0513600	2,430847	1,00E-21	-0,4650818	1,50E-02	12	deoxyribodipyrimidine photo-lyase, putative	null					
4	PF3D7_0316500	2,215171	2,51E-18	-0,6315557	1,02E-02	13	kinetochore protein NUF2, putative	NUF2					
5	PF3D7_0723800	2,174694	1,03E-17	-0,2625729	1,79E-01	14	conserved Plasmodium protein, unknown function	null					
6	PF3D7_1245100	1,976987	6,50E-15	-0,344117	1,74E-01	15	kinesin-13, putative	KLP8					
7	PF3D7_0111400	1,910618	4,95E-14	-0,1866395	3,50E-01	16	conserved Plasmodium protein, unknown function	GEXP19					
8	PF3D7_0825000	1,869556	1,68E-13	-0,06420836	7,82E-01	17	conserved Plasmodium protein, unknown function	null					
9	PF3D7_0729100	1,83374	4,79E-13	-0,2192027	2,67E-01	18	conserved Plasmodium protein, unknown function	null					
10	PF3D7_1322200	1,752235	4,81E-12	-0,2270502	2,49E-01	19	conserved Plasmodium protein, unknown function	null					
11	PF3D7_1207000	1,692784	2,43E-11	-0,2027047	3,07E-01	20	conserved Plasmodium protein, unknown function	null					
12	PF3D7_1250800	1,965286	5,93E-09	-0,1958968	7,55E-01	21	DNA repair protein rhp16, putative	null					
13	PF3D7_1116100	1,347155	6,21E-05	-0,1315345	8,74E-01	22	serine esterase, putative	null					
14	PF3D7_0518500	0,9886302	9,16E-05	-0,06062292	7,97E-01	23	ATP-dependent RNA helicase DDX23, putative	DDX23					
15	PF3D7_0319400	1,189601	3,97E-04	-0,02218521	9,14E-01	24	kinesin-8, putative	null					
16	PF3D7_1466800	1,548239	4,09E-04	-1,118664	1,19E-02	25	conserved Plasmodium protein, unknown function	null					
17	PF3D7_0317500	1,120816	8,37E-04	-0,1506733	5,84E-01	26	kinesin-5	EG5					
18	PF3D7_0103500	1,348402	1,98E-03	0,3586213	2,84E-01	27	conserved Plasmodium protein, unknown function	null					
19	PF3D7_0410800	0,7698564	2,27E-03	-0,3271312	1,97E-01	28	conserved Plasmodium protein, unknown function	null					
20	PF3D7_1247500	0,7636666	2,46E-03	-0,1918045	3,35E-01	29	conserved Plasmodium protein, unknown function	null					
21	PF3D7_1247500	1,277925	3,31E-03	0,4665489	1,79E-01	30	serine/threonine protein kinase, putative	null					
22	PF3D7_1449700	1,214373	5,16E-03	0,1790014	5,37E-01	31	exosome complex exonuclease RRP6	RRP6					
23	PF3D7_1228400	1,196418	5,83E-03	-0,2965803	5,81E-01	32	conserved Plasmodium protein, unknown function	null					
24													
25	PF3D7_0317800	-2,35078	5,17E-08	-0,4655598	3,39E-01	g	26S proteasome non-ATPase regulatory subunit 9, putative	null					
26	PF3D7_1458800	-2,266941	1,55E-07	-0,07029985	8,34E-01	h	DNA-directed RNA polymerase III subunit RPC5, putative	null					
27	PF3D7_1132000	-1,776948	4,38E-05	0,1083571	5,15E-01	i	ubiquitin-like protein, putative	null					
28	PF3D7_0305100	-1,722039	7,61E-05	0,07107621	7,31E-01	j	conserved Plasmodium protein, unknown function	null					
29	PF3D7_0503800	-1,032595	2,18E-04	-1,213772	1,05E-10	k	60S ribosomal protein L31	RPL31					
30	PF3D7_0812100	-1,58814	2,73E-04	0,623024	8,22E-02	l	conserved protein, unknown function	null					
31	PF3D7_1346300	-1,243182	8,56E-04	-0,01184981	9,65E-01	m	DNA/RNA-binding protein Alba 2	ALBA2					
32	PF3D7_1233900	-1,200979	1,29E-03	0,009633875	8,50E-01	n	sentrin-specific protease 1	SEN1					
33	PF3D7_0629400	-0,8678837	1,92E-03	0,158854	3,65E-01	o	RNA-binding protein, putative	null					
34	PF3D7_0704300	-0,8514434	2,34E-03	0,2088917	8,70E-02	p	conserved Plasmodium membrane protein, unknown function	null					
35	PF3D7_0703000	-1,070572	4,18E-03	-0,1571096	5,66E-01	q	conserved Plasmodium protein, unknown function	null					
36	PF3D7_1002700	-1,02415	6,18E-03	0,447103	1,82E-02	r	conserved Plasmodium protein, unknown function	null					
37	PF3D7_0218200	-1,020575	6,36E-03	0,05810868	7,56E-01	s	conserved Plasmodium protein, unknown function	null					
38	PF3D7_0108700	-0,7217298	9,99E-03	0,09247811	4,17E-01	t	secreted ookinete protein, putative	PSOP24					

Only significant in experiment 2

33	PF3D7_0708400	heat shock protein 90	HSP90
34	PF3D7_1109900	60S ribosomal protein L36	RPL36
35	PF3D7_0503800	60S ribosomal protein L31	RPL31
36	PF3D7_1410600	eukaryotic translation initiation factor 2 subunit gamma, putative	eIF2gamma
37	PF3D7_1223500	conserved Plasmodium protein, unknown function	-
38	PF3D7_1149400	Plasmodium exported protein, unknown function	-
39	PF3D7_1416900	prefoldin subunit 2, putative	-
40	PF3D7_0803000	peptidyl-prolyl cis-trans isomerase	CYP81
41	PF3D7_1453700	co-chaperone p23	P23
42	PF3D7_0723900	RNA-binding protein, putative	-
43	PF3D7_1141800	EELM2 domain-containing protein, putative	-
44	PF3D7_0312400	glycogen synthase kinase 3	GSK3
45	PF3D7_1367100	U1 small nuclear ribonucleoprotein, putative	-
46	PF3D7_0107800	double-strand break repair protein MRE11	MRE11
47	PF3D7_0605800	DNA repair protein RAD50, putative	RAD50
48	PF3D7_0314700	zinc finger protein, putative	-
49	PF3D7_1251500	ATP-dependent RNA helicase DRS1, putative	DRS1
50	PF3D7_0728000	eukaryotic translation initiation factor 2 subunit alpha, putative	-
51	PF3D7_1317700	conserved Plasmodium protein, unknown function	-
52	PF3D7_0509100	structural maintenance of chromosomes protein 4, putative	SMC4
53	PF3D7_0528200	eukaryotic translation initiation factor 3 subunit E, putative	EIF3E
54	PF3D7_1355700	NLI interacting factor-like phosphatase, putative	NIF3
55	PF3D7_1034900	methionine--tRNA ligase	MRSct
56	PF3D7_0514900	conserved Plasmodium protein, unknown function	-
57	PF3D7_1345800	conserved Plasmodium protein, unknown function	-
58	PF3D7_1134700	DNA-directed RNA polymerase I subunit RPA2, putative	RPA2
59	PF3D7_1140700	conserved Plasmodium protein, unknown function	-
60	PF3D7_0709700	prodrug activation and resistance esterase	PARE
61	PF3D7_1423800	vacuolar protein sorting-associated protein 3, putative	VPS3
62	PF3D7_0711000	AAA family ATPase, CDC48 subfamily	CDC48



	A	B	C	D	E	F	G	H	I	J	K	L	M	N
1	Protein IDs	Ratio.H.L normalized MT_exp1	Ratio.H.L no normalized MT_exp1	Signifi d	Ratio.H.L normalized MT_exp2	Ratio.H.L normalized MT_exp2	plomr	Product Description	Gene Name or Sybm					
2	PF307_0107800	0.2887	0.3690308	-0.94087	0.9408664	1.09E-04	46	double-strand break repair protein MRE11	MRE11					
3	PF307_0312400	0.1955	0.6534729	-0.779	0.7790015	3.77E-05	44	glycogen synthase kinase 3	GSK3					
4	PF307_0314700	-0.165	0.688973	-0.86949	0.8694909	3.58E-04	48	zinc finger protein, putative	null					
5	PF307_0503800	-1.033	0.0002182	-1.21377	1.213772	1.05E-10	35	60S ribosomal protein L31	RPL31					
6	PF307_0509100	1.0449	0.0194237	-1.43362	1.433623	1.09E-03	52	structural maintenance of chromosomes protein 4, putative	SMC4					
7	PF307_0514900	0.1206	0.6154306	-0.72249	0.7224913	3.16E-03	56	conserved Plasmodium protein, unknown function	null					
8	PF307_0528200	-0.135	0.7498467	-0.74342	0.743424	2.37E-03	53	eukaryotic translation initiation factor 3 subunit E, putative	EIF3E					
9	PF307_0605800	0.0449	0.8546846	-0.90136	0.9013649	2.13E-04	47	DNA repair protein RAD50, putative	RAD50					
10	PF307_0708400	0.4839	0.0537706	-2.69816	2.698155	2.74E-47	33	heat shock protein 90	HSP90					
11	PF307_0709700	0.3372	0.2979931	-1.1911	1.191096	7.20E-03	60	produg activation and resistance esterase	PAPE					
12	PF307_0711000	0.1006	0.7230831	-0.6448	0.6446002	8.69E-03	62	AAA family ATPase, CDC48 subfamily	CDC48					
13	PF307_0723900	0.2531	0.4271909	-1.18932	1.189318	8.91E-07	42	RNA-binding protein, putative	null					
14	PF307_0728000	-0.27	0.6054314	-0.84084	0.8408359	5.62E-04	50	eukaryotic translation initiation factor 2 subunit alpha, putative	CYP81					
15	PF307_0803000	0.4133	0.2062338	-1.21106	1.211064	5.57E-07	40	peptidyl-prolyl cis-trans isomerase	MRSocyt					
16	PF307_1034900	0.1276	0.6702868	-0.72726	0.7272602	2.36E-03	55	methionine--tRNA ligase	RPL36					
17	PF307_1109900	0.4466	0.0746464	-1.31079	1.31079	2.92E-12	34	60S ribosomal protein L36	RPA2					
18	PF307_1134700	0.0759	0.78419	-0.54839	0.5489868	3.92E-03	58	DNA-directed RNA polymerase I subunit RPA2, putative	null					
19	PF307_1140700	0.2763	0.4630171	-1.23301	1.233006	5.31E-03	59	conserved Plasmodium protein, unknown function	null					
20	PF307_1141800	-0.359	0.4661882	-2.03511	2.035106	2.58E-06	43	EELM2 domain-containing protein, putative	null					
21	PF307_1143400	0.1545	0.6139365	-1.02403	1.024032	5.35E-08	38	Plasmodium exported protein, unknown function	DRS1					
22	PF307_1223500	0.0812	0.7721992	-2.36431	2.364311	4.07E-08	37	conserved Plasmodium protein, unknown function	null					
23	PF307_1251500	-0.161	0.7598964	-0.86752	0.8675153	3.69E-04	49	ATP-dependent RNA helicase DRS1, putative	DRS1					
24	PF307_1317700	-0.19	0.7416886	-0.81988	0.8198776	7.77E-04	51	conserved Plasmodium protein, unknown function	null					
25	PF307_1345800	0.3142	0.3304621	-0.55544	0.5554369	3.51E-03	57	conserved Plasmodium protein, unknown function	NIIF3					
26	PF307_1355700	-0.209	0.6024211	-0.73959	0.7395889	2.50E-03	54	ML interacting factor-like phosphatase, putative	eIF2gamma					
27	PF307_1367700	0.3183	0.3244155	-0.96409	0.9640946	7.27E-05	45	U1 small nuclear ribonucleoprotein, putative	null					
28	PF307_1410600	0.1984	0.5265143	-1.14714	1.147138	1.05E-09	36	eukaryotic translation initiation factor 2 subunit gamma, putative	VPS3					
29	PF307_1416900	-0.102	0.8188533	-0.97344	0.9734408	2.38E-07	39	preludin subunit 2, putative	P23					
30	PF307_1423800	-0.352	0.3622255	-0.50982	0.509862	7.50E-03	61	vacuolar protein sorting-associated protein 3, putative	RPL23					
31	PF307_1453700	0.4057	0.214356	-0.93904	0.9390396	6.29E-07	41	co-chaperone p23	null					
32	PF307_1323400	0.1706	0.4846468	3.062726	-3.062726	1.14E-124	u	60S ribosomal protein L23	RPL23					
34	PF307_1026000	0.5773	0.164767	1.824279	-1.824279	1.17E-20	v	conserved Plasmodium protein, unknown function	null					
35	PF307_1431700	-3E-04	0.9780172	0.835762	-0.835762	5.68E-11	w	60S ribosomal protein L14, putative	PANK2					
36	PF307_1437400	0.3387	0.2959376	1.068602	-1.068602	3.76E-08	x	panthothenate kinase 2, putative	RAB5a					
37	PF307_1360400	0.4023	0.3161443	0.975043	-0.975043	4.32E-07	y	conserved Plasmodium protein, unknown function	ALP2b					
38	PF307_0211200	0.0039	0.9027945	1.690149	-1.690149	9.27E-06	z	ras-related protein Rab-5A	null					
39	PF307_1469800	-0.231	0.5619687	0.805705	-0.805705	3.00E-05	aa	conserved Plasmodium protein, unknown function	null					
40	PF307_0505200	0.1656	0.6316907	1.570269	-1.570269	3.62E-05	ab	actin-like protein, putative	null					
41	PF307_1319400	0.0824	0.7245801	0.512682	-0.512682	4.37E-05	ac	conserved Plasmodium protein, unknown function	PGM2					
42	PF307_1413000	-0.262	0.5053252	0.744161	-0.744161	1.12E-04	ad	conserved Plasmodium protein, unknown function	ApiAP2					
43	PF307_1425900	0.5819	0.0786108	0.72464	-0.72464	2.13E-04	ae	conserved Plasmodium protein, unknown function	null					
44	PF307_1451500	0.3405	0.3865422	0.704341	-0.704341	2.51E-04	af	pre-mRNA-splicing factor CwF18, putative	null					
45	PF307_0625600	0.6632	0.1143503	1.338966	-1.338966	3.90E-04	ag	poly(A) polymerase PAP, putative	null					
46	PF307_1014300	0.5199	0.2068093	1.271426	-1.271426	7.36E-04	ah	conserved protein, unknown function	null					
47	PF307_0413300	-0.013	0.3827789	0.617957	-0.617957	1.26E-03	ai	phosphoglucosyltransferase-2	AP2					
48	PF307_0613800	0.1225	0.6103113	1.920668	-1.920668	1.50E-03	aj	AP2 domain transcription factor, putative	null					
49	PF307_1453900	0.6182	0.0621115	0.606253	-0.606253	1.54E-03	ak	conserved Plasmodium protein, unknown function	null					
50	PF307_1436600	-0.281	0.3539485	0.565597	-0.565597	3.07E-03	al	conserved protein, unknown function	null					
51	PF307_1205500	0.2081	0.5079586	0.526369	-0.526369	5.73E-03	am	zinc finger protein, putative	null					
52	PF307_0403200	0.2723	0.3952214	0.501516	-0.501516	8.36E-03	an	conserved Plasmodium protein, unknown function	CARM1					
53	PF307_0811500	-0.442	0.1688335	0.322967	-0.322967	9.53E-03	ao	histone-arginine methyltransferase CARM1, putative	null					
54	PF307_1358100	0.1362	0.678537	0.491802	-0.491802	9.65E-03	ap	Sas10 domain-containing protein, putative	null					

Appendix 8

Oligonucleotides

Primer

Sequence

mCherry 620 fw

ctcccacaacgaggactacacc

mCherry 88 rv	ggccggttcacggagcctcc
GFP 633 fw	gccctttcgaaagatccc
GFP 272 as	ccttcgggcatggcactc
GFP 85 rv	accttcaccctctccactgac
pARLminus rv	cagttataaatacaatcaattgg
pArl 128 rv	agctatttacatgcatgtgcatgcac
pArl sense 55	ggaattgtgagcggataacaatttcacacagg
Crt fw	ccgtaataataaatacacgcagtc
crt 131 s	cacatatatgacataaataattttaaaatcg
linker-fkbp_rev	ttgtactcctctctgcagagc
FKBP 304_fw	tgcaacttttagtattcgacg
FRB 42 rv	aaacgagatgcctcttccag
FKBP 276_fw	caggccatcctggcatcatc
Neo 40 rv	cgaatagcctctccaccaag
Neo 746 fw	tgctttacggatcgcgcgctcc
FKBP 39 rv	ttgacctctttttggaaatgtacg
FRB 251 fw	gaatgtcaaggacctctccaagc
FRB 76 rv	tcaaacatgcctttcacgttcc
FRB 216 fw	ccaagagtggcaggaagtac
FKBP 82 rv	ctttccatcttcaagcattccag
FKBP 253 fw	tcaccagattatgcatacggtg
Neo 75 rv	cagagcagccgattgtctgttg
Neo 693 fw	cttggcggcgaatgggctgacc
HA rv(allg)	agcataatctggaacatcatatg
3xHA rv (Ricarda)	catcgtagcgtaatctggaacatcg
nmd3_1051_fw	gaggaaatttatatttctttaacaac
M1-loc intcheck	5' fw: agcattacgaatgataccatggatg 3' rev: acatattatttttatccaaacattc
M1-TGD intcheck	5' fw: tattatacagaatgtacgattcttg 3' rev: ctttacattattaacattttaaagct
M3-loc intcheck	5' fw: gaggaaatgaataattataaagaag 3' rev: ttttaacatgtcatagctttatttg
M3-TGD intcheck	5' fw: gtaaatatatacacaattatattac 3' rev: gaattatctgtataattaatagacg
M4-TGD intcheck	5' fw: gcataagtaaccagatataaaaaga 3' rev: gccgtttattaaattgagcattgac
M5-TGD intcheck	5' fw: gacgacgtatggaattgatatgttag 3' rev: catacgcaaataatagacattttc
M6-loc intcheck	5' fw: aaataaaattaaaaggaaaatag 3' rev: catatttatataatttcataaatcc
M6-TGD intcheck	5' fw: ctgttttaagaatgaaaagaaaatg 3' rev: cattaataaaattattattaaattc
M7-loc intcheck	5' fw: gaataatacgaataaatgaataatag 3' rev: cacataattataatttctctctctc
M7-TGD intcheck	5' fw: catacagataaatacacaacattgttg 3' rev: gttccttatgtatattctctaaatc
M8-loc intcheck	5' fw: actcatcaatataaataattatatac 3' rev: atatttatgttatgataatttatgc
M8-TGD intcheck	5' fw: gtacttgaagtataaaaagtacc 3' rev: acctagtctttcatatgttgtttg

M9-loc intcheck	5' fw: ctagagaggagaataaaaagtgatcc 3' rev: gtggtacactttataaaattggcagc
M9-TGD intcheck	5' fw: ctcccctgtccattatatttttc 3' rev: ctaaaattaaggctctcattgttttc
M10-loc intcheck	5' fw: ttaaatcatatcaaaaatataatag 2. 5' fw: gaaatgtaaaataactgacgatattg 3' rev: atatatttacatatttacatatttg
M10-TGD intcheck	5' fw: ttccatgtacattagatgtatagag 3' rev: gttggtgtccatataatcgataattc
M2-TGD intcheck	5' fw: gtcataaaataaataccccatatag 3' rev: cattataattattattattattgc
M11-loc intcheck	5' fw: gaagaaatgtacacataatgatgtc 3' rev: ctatacacatacatatattgtac
M11-TGD intcheck	5' fw: cttttcatttttcatttttgtgtgg 3' rev: catggtgcggtatgattaatattaac
M12-loc intcheck	5' fw: gtcaaaatcatatgaataaaaaataag 3' rev: catttatatgtaattcaattaatac
M12-TGD intcheck	5' fw: cttttcatttttcatttttgtgtgg 3' rev: cttatttttattcatatgattttgac
M13-loc intcheck	5' fw: gaatccatttttaaatctaaattgg 2. 5' fw: gataaatatgaagtaagataacg 3' rev: cacatatatgtaccatataaaatag
M13-TGD intcheck	5' fw: gaaaggtagcacaaaaattccactc 3' rev: ctcttaaacattttcttaacatttc
M14-loc (pSLI) / M14-TGD	5' fw: gtttaataataagtttatagaaaag 3' rev: gttttataattttctatgtgttccc
M15-TGD	5' fw: caatgaagttaaaaaggacagagac 3' rev: cttttctgttttcaatttattcaag
M16-loc intcheck	5' fw: cttattattaaatccacaaaacgtg 3' rev: gcaaaaaaattaatgctccacataac
M16-TGD intcheck	5' fw: ctattgaaactagattattataatg 3' rev: catcattttttgtttgtgcattctc
M17-TGD intcheck	5' fw: caaattaatagacagaagaaggaag 3' rev: gtttgatgtcctacctacagttttg
M18-loc intcheck	5' fw: gaacaaagacataaatgaacagatg 3' rev: catatattcgtgtgtatagttaaatc
M18-TGD intcheck	5' fw: aagatggacaacgaatgtaataatg 3' rev: cttgtaattttttatagtattc
M19-loc intcheck	5'fw:cttttatataatattataatgtttatg aslo tgd fw 2.5'fw:gatagaaaatttttatcaacataacaaag 3' rev: cgtgttctccgtttttatgttaac
M19-TGD intcheck	3' rev: gaattcctcaaaattattagaagaatg
M20-loc intcheck	5' fw: ctatatacatatagtaaaacttgaatac 3' rev: gtgtttgtgtttatgtttatgttg
M20-TGD intcheck	5' fw: ctaattatcgtaagaatgaaaaaac 3' rev: ctttttttcattttctacatttttttc
M24-loc intcheck	5' fw: caataacactaacgaatcttctg 3' rev: gattagaaatttattattttatttctg
M24-TGD intcheck	5' fw: gtttattacaaatggctcataaaag 3' rev: gaagcttctattttcgttatgttc
Rab5b_codonadj_myc_2TA Gibson fw:	gttttttttaattttcttacatataactcgagggtcgacatgggttgcagtagttcaacag agc

Gibson rev for crt1xNLS	cttgttgatcacgcgtaacttttcttttttttttttgggtcgctcactggacctggatt ttcttcaacatcac
Gibson rev for crt VPS45	ctgatattaacttctgctccctagtggttattgtagtaaagtacctcc
MutationS48N locked: Gibson fw	cttgagattcaggagtagtaagaattcaatagcactttacctttgccac
MutationS48N(locked):Gibson rv	cttacctactcctgaatctccaagaagtacaatcttaacctttgtgtcctg
Mutation N148I (locked): Gibson fw	ctgctgcataatggttgtagcaatcaagaagatcttccacagaagttaaac
Mutation N148I (locked): Gibson rv	tgctacaaccattatgcagcagttacgaggtccgttactcttaatctc
Mutation Q94L (aktiv): Gibson fw	gcttcacatatgggacacaggtggactggagcgtttcagaagtatggcaccac
Mutation Q94L (aktiv): Gibson rv	tccacctgtgtcccatatgtgaagcttcatagtagctccgttcttaagctc
Mutation I67M (aktiv): Gibson fw	gattcagcagagaagcaccaggttaacaatgggagctgcttctcaccacaac
Mutation I67M (aktiv): Gibson rv	tgttacctggtgcttctcgtcgtgaatcttccgtggcaaaggtaaagtgtattg
M6-loc fw NotI	cactgcgccgctaaggacagaatggtaaagatgattataatg
M6-loc rv AvrII	gactcctaggtaaatccacgacctctttatgttgcg
M7-loc fw NotI	cactgcgccgctaagaacatgatgatctaagaaatgatgatg
M7-loc rv AvrII	tcctcctaggttttctctatgcatgtttttttttctttttttcttttttaagc
M9-loc fw NotI	cactgcgccgctaaggatattcaacttttattgatgaaaataataagac
M9-loc rv AvrII	tcctcctaggttttaggtaacaaaacataaaaaatatttttagcggacc
M32-TGD fw NotI	cactgcgccgctaagatgggaatgaatatacatacagcgg
M32-TGD rv Mull	tcctacgcgatgcttaaactttttcaaacctac
M2-loc fw	gctatttaggtgacactatagaatactcgcggccgctaataataatcataatccaattca tataaac
M2-loc rv AvrII reverse	cagcagatcttgatctcaatcctgacctaggattttttttcaataatgctttaaat c
M4-loc fw	gctatttaggtgacactatagaatactcgcggccgctaacataaaaaatattatgaataa ttataata
M4-loc rv	gcagcagatcttgatctcaatcctgacctaggcttgtgcttatagaaatgaggtacg
M12-loc fw	gctatttaggtgacactatagaatactcgcggccgctaataccgaaaatataaataatgt tattg
M12-loc rv	cagcagatcttgatctcaatcctgacctaggatttttgcttcatgcccactagc
M14-loc fw	gccaaactatttaggtgacactatagaatactcgcggccgctaagcaacaagttgttat ggcaatttttttattttg
M14-loc rv	gcagcagatcttgatctcaatcctgacctagggtcctgaaattcaacacggtgag
M20_TGD fw	ctatttaggtgacactatagaatactcgcggccgctaaaaagaaaacatttctattaat aag
M20_TGD rv	ccagcaccagcagcagcactctagcacgcgtatatttttctacatttttttc
M21_loc fw	ctatttaggtgacactatagaatactcgcggccgctaaaacctcaacggttaataaaaat gctg
M21_loc rv	cagcagatcttgatctcaatcctgacctaggatatttttaattttttcttc
M30_loc fw	ctatttaggtgacactatagaatactcgcggccgctaaccatattttgatttaacggaa attg
M30_loc rv	cagcagatcttgatctcaatcctgacctagggtgattgtatgagctaaaaataaaag
M32_loc fw	ggtagactatagaatactcgcggccgctaagccttctttgcttctttatatac
M32_loc rv	cagcagatcttgatctcaatcctgacctaggatattttataaattgttctttatc
M33_loc fw	ctatttaggtgacactatagaatactcgcggccgctaatacaatggttttagtgctccaa gaatc
M33_loc rv	gcagcagatcttgatctcaatcctgacctaggaaacaagttgtcttctgctttttctc